Quantum gauge theory simulation with ultracold atoms

Alejandro Zamora

PhD. Thesis

Supervisor: Prof. Maciej Lewenstein
Co-supervisor: Dr. Gergely Szirmai

Castelldefels, 2014.

Abstract

The study of ultracold atoms constitutes one of the hottest areas of atomic, molecular, and optical physics and quantum optics. The experimental and theoretical achievements in the last three decades in the control and manipulation of quantum matter at macroscopic scales lead to the so called third quantum revolution. Concretely, the recent advances in the studies of ultracold gases in optical lattices are particularly impressive. The very precise control of the diverse parameters of the ultracold gas samples in optical lattices provides a system that can be reshaped and adjusted to mimic the behaviour of other many-body systems: ultracold atomic gases in optical lattices act as genuine quantum simulators. The understanding of gauge theories is essential for the description of the fundamental interactions of our physical world. In particular, gauge theories describe one of the most important class of systems which can be addressed with quantum simulators. The main objective of the thesis is to study the implementation of quantum simulators for gauge theories with ultracold atomic gases in optical lattices.

First, we analyse a system composed of a non-interacting ultracold gas in a 2D lattice under the action of an exotic and external gauge field related to the Heisenberg-Weyl gauge group. We describe a novel method to simulate the gauge degree of freedom, which consists of mapping the gauge coordinate to a real and perpendicular direction with respect to the 2D space of positions. Thus, the system turns out to be a 3D insulator with a non-trivial topology, specifically, a quantum Hall insulator.

Next, we study an analog quantum simulation of dynamical gauge fields by considering spin-5/2 alkaline-earth atoms in a 2D honeycomb lattice. In the strongly repulsive regime with one particle per site, the ground state is a chiral spin liquid state with broken time reversal symmetry. The spin fluctuations

around this configuration are given in terms of an emergent U(1) gauge theory with a Chern-Simons topological term. We also address the stability of the three lowest lying states, showing a common critical temperature. We consider experimentally measurable signatures of the mean field states, which can also be key insights for revealing the gauge structure .

Then, we introduce the notion of constructive approach for the lattice gauge theories, which leads to a family of gauge theories, the gauge magnets. This family corresponds to quantum link models for the U(1) gauge theory, which consider a truncated dimensional representation of the gauge group. First of all, we (re)discover the phase diagram of the gauge magnet in 2+1 D. Then, we propose a realistic implementation of a digital quantum simulation of the U(1) gauge magnet by using Rydberg atoms, considering that the amount of resources needed for the simulation of link models is drastically reduced as the local Hilbert space shrinks from infinity to 2D (qubit).

Finally, motivated by the advances in the simulation of open quantum systems, we turn to consider some aspects concerning the dynamics of correlated quantum many body systems. Specifically we study the time evolution of a quench protocol that conserves the entanglement spectrum of a bipartition. We consider the splitting of a critical Ising chain in two independent chains, and compare it with the case of joining two chains, which does not conserve the entanglement spectrum. We show that both quenches are both locally and globally distinguishable. Our results suggest that this conservation plays a fundamental role in both the out-of-equilibrium dynamics and the subsequent equilibration mechanism.

Resum: Simulació quàntica de teories gauge amb atoms ultrafreds

L'estudi dels àtoms ultrafreds constitueix una de les àrees més actives de la física atòmica, molecular, òptica i de l'òptica quàntica. Els èxits teòrics i experimentals de les tres últimes dècades sobre el control i la manipulació de la matèria quàntica a escala macroscòpica condueixen a l'anomenada tercera revolució quàntica. Concretament, els recents avenços en els estudis dels àtoms ultrafred en xarxes òptiques proporcionen un sistema que es pot reajustar i reorganitzat per imitar el comportament d'altres sistemes de molts cossos: els gasos d'àtoms ultrafreds en xarxes òptiques actuen com a genuïns simuladors quàntics. La comprensió de les teories de gauge és clau per a la descripció de les interaccions fonamentals del nostre món físic. Particularment, les teories de gauge descriuen una de les més importants classes de sistemes que poden ser tractats amb simuladors quàntics. L'objectiu principal de la tesi és estudiar la implementació de simuladors quàntics de teories de gauge amb gasos d'àtoms ultrafreds en xarxes òptiques.

En primer lloc, analitzem un sistema format per un gas ultrafred no interaccionant en una xarxa 2D sota l'acció d'un camp de gauge exòtic i extern descrit pel grup de gauge de Heisenberg-Weyl. Descrivim un nou mètode per simular el grau de llibertat de gauge, que consisteix en associar la coordenada gauge a una coordenada real i perpendicular a l'espai 2D de les posicions. Així, el sistema resulta ser un aïllant en 3D amb una topologia no trivial, concretament un aïllant Hall quàntic.

Seguidament, estudiem un simulador quàntic analògic de camps de gauge dinàmics amb àtoms alcalinoterris en una xarxa hexagonal. En el régim fortament repulsiu i amb un àtom en cada lloc de la xarxa, l'estat fonamental és un líquid espinorial quiral amb la simetria d'inversió temporal trencada. Les fluctuacions d'espín al voltant d'aquesta configuració sÃşn descrites per una teoria gauge U(1) emergent amb un terme topològic de Chern-Simons. També tractem l'estabilitat dels tres estats amb mínima energia, tot observant una temperatura crítica comuna. Considerem indicis experimentals mesurables dels estats de camp mitj, que poden ser claus per revelar l'estructura gauge.

A continuació, introduïm un enfoc constructiu per a teories gauge en el reticle, la qual porta a una família de teories de gauge, els magnets de gauge. Aquesta família es correspon amb els models d'enllaços quàntics de la teoria gauge U(1). Primer, (re)descobrim el diagrama de fases del magnet de gauge en 2+1 D. Després, proposem una implementació realista d'un simulador quàntic digital del magnet de gauge U(1) amb àtoms de Rydberg, considerant que el nombre de recursos necessaris per a la simulació dels models d'enllaços es redueix dràsticament pel fet que l'espai d' Hilbert local disminueix de dimensió infinita a 2 (bit quàntic).

Finalment, motivats pels avenços en la simulació de sistemes quàntics oberts, considerem alguns aspectes de la dinàmica de sistemes quàntics correlacionats de molts cossos. Específicament, estudiem l'evolució temporal en un protocol de canvi sobtat que conserva l'espectre d'entrellaçament d'una bipartició. Considerem la ruptura d'una cadena d'Ising en dues cadenes independents i ho comparem amb la unió de dues cadenes, situació que no conserva l'espectre d'entrellaçament. Observem que aquests dos diferents escenaris són localment i globalment distingibles. El nostre resultat suggereix que l'esmentada conservació juga un paper fonamental en la dinàmica fora de l'equilibri i en el consegüent equilibri.

Resumen: Simulación cuántica de teorías gauge con átomos ultrafríos

El estudio de los átomos ultrafríos constituye una de las áreas mas activas de la física atómica, molecular, óptica y de la óptica cuántica. Los logros teóricos y experimentales de las tres últimas décadas sobre el control y la manipulación de la materia cuántica a escala macroscópica conducen a la denominada tercera revolución cuántica. Concretamente, los avances recientes en los estudios de átomos ultrafríos en redes ópticas proporcionan un sistema que puede ser reajustado y reorganizado para imitar el comportamiento de otros sistemas de muchos cuerpos: los gases de átomos ultrafríos en redes ópticas actúan como genuinos simuladores cuánticos. La comprensión de las teorías de gauge es clave para la descripción de la interacciones fundamentales de nuestro mundo físico. En particular, las teorías de gauge describen una de las mas importante clase de sistemas que pueden ser abordados con simuladores cuánticos. El objetivo principal de la tesis es estudiar la implementación de simuladores cuánticos de teorías de gauge con gases de átomos ultrafríos en redes ópticas.

En primer lugar, analizamos un sistema formado por un gas ultrafrío no interactuante en una red 2D, bajo la acción de un campo de gauge exótico y externo descrito por el grupo de gauge de Heisenberg-Weyl. Describimos un método novedoso para simular el grado de libertad gauge , que consiste en asociar la coordenada gauge a una coordenada real y perpendicular al espacio 2D de las posiciones. Así, el sistema resulta ser un aislante 3D con una topología no trivial, específicamente un aislante Hall cuántico.

Seguidamente, estudiamos un simulador cuántico analógico de campos de gauge dinámicos, considerando átomos alcalinotérreos en una red hexagonal. En el régimen fuertemente repulsivo con una átomo en cada sitio, el estado fundamental es un liquido espinorial quiral con la simetría de inversión temporal rota. Las fluctuaciones de espín alrededor de dicha configuración vienen dadas en términos de una teoría de gauge U(1) emergente con un término topológico de Chern-Simons. También tratamos la estabilidad de los tres estados con mínima energía, observando una temperatura crítica común. Consideramos indicios experimentales medibles de los estados de campo medio, que pueden claves para revelar la estructura de gauge.

A continuación, introducimos la noción del enfoque constructivo para teorías de gauge en el retículo, lo que conduce a una familia de teorías de gauge, los magnetos de gauge. Esta familia se corresponde con los modelos de enlaces cuánticos para la teoría de gauge U(1), los cuales consideran una representación dimensional truncada del grupo de gauge. Primeramente, (re)descubrimos el diagrama de fases del magneto de gauge en 2+1D. Seguidamente, proponemos un implementación realista de un simulador cuántico digital del magneto de gauge U(1) usando átomos de Rydberg, considerando que el número de recursos necesarios para la simulación de los modelos de enlace está drásticamente reducido debido a que el espacio de Hilbert local disminuye de infinitas dimensiones a 2 (bit cuántico).

Finalmente, motivados por los avances en la simulación de sistemas cuánticos abiertos, consideramos algunos aspectos sobre la dinámica de sistemas cuánticos correlacionados de muchos cuerpos . Específicamente, estudiamos la evolución temporal en un protocolo de cambio súbito que conserva el espectro de entrelazamiento de una bipartición. Consideramos la ruptura de una cadena de Ising en dos cadenas independientes y lo comparamos con la unión de dos cadenas, la cual no conserva el espectro de entrelazamiento. Estos dos cambios abruptos son localmente y globalmente distinguibles. Nuestro resultado sugiere que la mencionada conservación juega un papel fundamental en la dinámica fuera de equilibrio y en el consiguiente equilibrio.

Acknowledgements

The work which is presented in this thesis has been possible thanks the help and support of many people. First of all, I would like to thank Maciej Lewenstein, my supervisor, for giving me the opportunity of joining his group and for all his scientific support during these years. I appreciate the fact that he cares for the people in his group and he is optimistic when presented with results. I am also very grateful to Gergely Szirmai -my co-supervisor- and Luca Tagliacozzo for tutoring me during these years and for all the stimulating discussions about physical and *non physical* systems. They have taught me valuable lessons, both for my scientific career and for everyday life, as for instance, to break down a complex task into simpler problems.

It has been really a great experience to be part of the *Quantum Optics Theory* group at ICFO and to enjoy its warm environment. Especially, I thank to Alessio Celi and Javier Laguna for feedbacks in and conversations, and to Pietro Massignan -my officemate all these years- for having always *five minutes* for discussions about physics and life. My three stays in Budapest have been really fruitful thanks to the collaboration with Peter Sinkovicz, Edina Szirmai and my co-supervisor, and thanks to the facilities that I shared with the Group of Quantum Optics and Quantum Information, Wigner Research Centre in Budapest, led by Prof. Peter Domokos. I would also like to thank the Szirmai family for all the hospitality in the non-working time in Budapest.

This thesis has been possible thanks to the facilities and support received from all the people who work at ICFO, especially from the human resources and the information technology departments. It has been a pleasure for me to work with all the people in this institute.

I would like to thank all my *icfonian* friends I made during these years

working at ICFO, especially to Camila, Claudia, Rafa, Ramaiah, Roberto, Alberto, Jiri, Armand, Philipp, Nadia, Carmelo, Valeria, Mariale, Kenny, Luis, Isa, Yannick, Anaid, Ulrich, Gonzalo, Federica. I am very happy to have been sharing many days, nights, kebabs, salsa, laughters and happiness with all of them. I want to thank as well my *Hungarian friends*, Fabien and Yazbel for all the moments in Budapest and my *non-icfonian* friends for being there always, Isma, Raul, Gabriel, Ruben, David C., David A. Gerardo, Moises, Miquel, Ivan, Juanca.

Finally, I thank my parents and my sister. Without their emotional support, this thesis would not been possible.

Contents

Chapter 1

Introduction

The study of ultracold atoms constitutes one of the hottest areas of atomic, molecular, and optical physics and quantum optics [1, 2, 3]. The explosion of studies of weakly interacting, dilute and cold atomic gases stems back to more than one decade, to the experimental achievement of *Bose-Einstein condensation* (BEC) in gas samples of alkali atoms [4, 5, 6]. The original aim was to observe BEC and to study quantum mechanical effects on a macroscopic scale.

Our daily experiences indicate that the physical world which surrounds us can be described with classical physics. The effects of the temperature mask the quantum behaviour of the usual macroscopic systems. This effect can be read from the de Broglie relation $\lambda \sim \frac{1}{\sqrt{T}}$, where λ is the quantum wave length of a quantum object at temperature T. At room temperatures, the wave length for a normal gas is much smaller than the inter-particle distance, $d_{\rm at}$, and , consequently, the quantum regime remains hidden. Then, one strategy for finding evidences of the quantum world at macroscopic scales is to cool the physical system and/or to increase the density, i.e. to diminish $d_{\rm at}$. At sufficient low temperatures, the wave length λ for a bosonic gas start to be comparable with $d_{\rm at}$ and the system undergoes a genuine phase transition, where a macroscopic number of particles condense to the ground state, which is the BEC regime. This effect was originally predicted by A. Einstein [7], based on some ideas developed by Bose originally for photons [8]. It was first experimentally observed in the nineties in the above mentioned ultracold atomic system of alkali atoms.

The experimental and theoretical achievements of the atomic and optic physics community in the last three decades in the control and manipulation of

quantum matter at macroscopic scales lead to a quantum engineering era and to the so called *third quantum revolution* [2].

The current techniques in cooling, trapping and manipulating atoms, ions and molecules up to nanokelvin scales provide an ideal scenario to study macroscopic quantum many-body systems with a highly accurate level of control and tunability in the quantum system. Concretely, the recent advances in the studies of ultracold gases in *optical lattices* are particularly impressive. Optical lattices are composed of several laser beams arranged to produce standing wave configurations creating a periodic optical potential for polarize particles, such as atoms. They provide practically ideal, free of losses potentials, in which ultracold atoms may move and interact one with another. Nowadays it is routinely possible to create systems of ultracold bosonic or fermionic atoms, or their mixtures, on one, two or three dimensional optical lattices in strongly-correlated states. Genuine quantum correlations, such as entanglement extend over large distances in the system.

The very precise control of the diverse parameters of the ultracold gas samples in optical lattices, supported by atomic transitions in the optical range, provides not a just a unique quantum system, but also some sort of a meta system that can be reshaped and adjusted to mimic the behaviour of other many-body systems, such as: systems in periodic potentials, which are inevitably the foundation stone of solid-state physics [9, 10]; disordered systems, playing an important role in the transport and equilibrium properties of materials [11]; strongly coupled fermion systems, arising in high temperature superconductors [3]. Ultracold atomic gas systems in optical lattices thus act as genuine *quantum simulators*.

An inherent characteristic of generic quantum many-body systems is that the description of such systems requires a number of parameters which grows exponentially with the number of constituents. Therefore, the exact classical computation of these systems is possible only for systems with small numbers of constituents. The community has put in a great effort towards the development of techniques for the classical computation of many-body quantum systems. Thus, very powerful and successfully numerical tools and complementing analytical methods have been developed for characterising many-body systems with a large number of constituents. Within this category one can find *mean field* methods, *quantum Monte Carlo* algorithms and *tensor networks* tools. These methods, which are based in classical computations, do not consider the feature of the complexity of many body quantum systems completely.

R. P. Feynman suggested a solution for overcoming the problem of computing

complex many-body quantum systems. In his seminal work [12], he proposed to study the complex quantum system by performing a simulation with a *controllable* quantum machine, the *quantum simulator*. This machine mimics, emulates and encloses all the relevant physics of the system of interest. Since this simulator is a genuine quantum machine, it would to address the inherent exponential number of degrees of freedom in a controlled and, in principle, accurate manner.

For instance, let us consider that we are dealing with the time evolution of a quantum state $|\psi(0)\rangle$, with a given Hamiltonian H. A generic quantum simulation for such a scenario contains three well defined steps: i) The preparation of the initial state in the quantum simulator, i.e. $|\psi(0)\rangle_{\text{sim}}$, ii) time evolution of this state, iii) measurement of the evolved state $|\psi(t)\rangle_{\text{sim}}$. An implementation of a quantum simulator is deemded efficient if only polynomial resources are required for performing al three steps [13, 14].

One may distinguish two different types of quantum simulations:

- **Digital quantum simulator**. The time evolution of $|\psi(t)\rangle_{\text{sim}}$, which is expressed in a computational basis, is performed through a quantum circuit model [15] which is composed of the sequence of many small time-ordered sequence of gates U_l. These gates come from the Trotter expansion [16] of the time evolution operator. For real physical systems, the Hamiltonian is composed of the sum of local terms: $H = \sum_s H_s$. Therefore, the gates U_l can be described with a universal set of gates [17, 18, 15]

- **Analog quantum simulator**. The Hamiltonian H of the system of interest is mapped to a Hamiltonian H_{sim}: $H_{\text{sim}} = fHf^{-1}$ acting on the quantum simulator [14]. The time evolution of the state is performed continuously in the quantum simulator through H_{sim}. In some cases, it is possible to map exactly the Hamiltonian H into the quantum simulator. But in the most general case H_{sim} is an effective Hamiltonian of H, since it retains some specific features of H. The level of analogy between both systems is given by the map f.

Quantum simulators are getting a great and impressive impact on many areas of physics and chemistry, as condensed matter systems, high energy physics and atomic physics. They are changing our understanding about the quantum world, since they make accessible the study of quantum systems which are intractable classically, such as the study of some spin systems, topological matter, Hubbard-type systems, chemical properties of molecules, etc. Specifically, in this thesis we have focused on the quantum simulations of *gauge theories*.

All of the fundamental interactions in the known world can be expressed in terms of gauge-theories. These theories describe all of the phenomenology of high energy physics accessible in current experiments: from quantum electrodynamics, through the Weinberg-Salam model of weak interactions, to quantum chromodynamics describing strong interactions. All these theories are unified in the *Standard Model*, in which interactions between matter (leptons and quarks) are mediated by gauge bosons (e.g. photons). Gravity can also be derived from the gauge principle. Evidently, gauge theories provide an elegant and beautiful geometrical description of the fundamental interactions.

Moreover, gauge theories also play a fundamental role in other areas of physics. Thus, collective fluctuations in certain condensed matter systems can be described through the emergence of effective gauge theories [19, 20].

Quantum simulators for lattice gauge theories can provide understanding of very challenging problems, as the phase diagram of pure gauge theories, with the consequent confinement-deconfinement phase transition or the study of the phase diagram of a finite density of fermionic matter coupled to the SU(3) gauge fields, with the emergence of novel phases, as the color-superconductors [21].

Applying analog quantum simulators to study gauge theories is particularly challenging since, in general, their dynamics involve Hamiltonian with couplings among more than just two-body terms. This is the reason why, until recently, the main focus had been on simulating the effects of static and external non-trivial background gauge fields on the phases of matter. The interest in such studies ranges from Quantum Hall physics, where strong magnetic fluxes, very hard to obtain in condensed matter with real magnetic field, are needed, to the simulation of relativistic matter and topological insulators, or extra-dimensions [22, 23].

A natural step further towards the simulation of gauge theories is to include the dynamics of the gauge fields. Such aim, for instance in two dimensions, requires the engineering of at least four-body couplings in the most common square lattices. These kind of interactions are challenging to induce in quantum simulator platforms, as optical lattice or trapped ions.

The first quantum simulator for dynamical gauge fields was proposed by Buchler *et al.* [24]. The proposal considers a ring exchange interaction in a cold atomic gas between one type of bosons with a two particle or *molecular* state. In a certain regime, the molecular field can be integrated out leading to

an effective U(1) gauge theory for the bosons:

$$H_{\text{eff}} = k \sum_{P} (b_1^\dagger b_2 b_3^\dagger b_4 + b_1 b_2^\dagger b_3 b_4^\dagger - n_1 n_3 - n_2 n_4) \tag{1.1}$$

where the sum is done over the plaquettes P of the lattice and $b^\dagger$ (b) is the creation (annihilation) operator for the bosons and $n_i = b_i^\dagger b_i$.

Substantial progress towards the simulation of dynamical gauge theories in ultracold atomic systems has been achieved in the last years. In particular, proposals for the quantum simulation of relativistic matter fields [25], pure U(1) gauge theories [26, 27], compact U(1) gauge theory interacting with matter field [28, 29, 30] have been made. These methods have been extended to simulate pure non-Abelian gauge theories, as the 1+1 Yang-Mills SU(2) theory [31] or non-Abelian gauge fields interacting with matter fields [32, 33]. While these proposals correspond of analog quantum simulators, *hybrid-digital* quantum simulation of lattice gauge theories has also been considered [34, 35], which consider a finite dimensional representation of the gauge group. Recent studies also consider the formulation of lattice gauge theories in a *tensor network* language [36, 37, 38].

The simulation of many body quantum systems not only refers to the simulation of closed systems, as the quantum simulators of gauge theories. The engineering of quantum simulation can be applied to *open quantum* systems: the system of study is coupled to an environment in a controlled way [39]. This simulation can be done either by simulating an open system as part of a closed quantum system or by considering the natural decoherence of the quantum simulator [14].

Quantum simulations for open systems can address very challenging problems concerning to the dynamics of strongly correlated many body systems. One of them is the characterization the system in equilibrium regime. In the last years very meaningful studies of this topic have concluded that an isolated generic quantum many-body system relaxes to a equilibrium state well described by standard statistical methods, with a *generalized Gibbs* ensemble. This ensemble takes in account all the conserved quantities of the system during the evolution [40].

Interest in the out-of equilibrium quantum dynamics has increased recently due to the numerous theoretical studies and new experiments in this context using cold atomic gases and optical lattices [41, 42, 43, 44, 45]. One of the impressive phenomenon which appear in these far-from-equilibrium scenarios

is the so-called *pre-thermalization*. In such a situation, some properties of the many-body quantum system acquire their thermal values in a time scale much lower than the typical thermal scale of the system [46].

1.1 Objectives and overview of the thesis

The overall main objective of the thesis is to harvest the benefits of the high precision control and excellent detection and imaging techniques available for ultracold atomic gases in order to:

- study the implementation and phenomenology of quantum simulator for quantum systems subjected to external and exotic gauge fields.
- implement quantum simulators for dynamical pure gauge theories based on gauge link models and digital quantum simulations.
- understand the behaviour of high spin systems and their projection to effective gauge field theories.
- study the role of the conservation of the entanglement spectrum in the dynamics of strongly-many body systems.

The thesis is organized as follow:

- In **chapter 2**, we present a summary of the physics of gauge theories. First we introduce the notion of gauge symmetry in classical field theory on the continuum under the Lagrangian formulation. We also discuss the Hamiltonian formulation for such systems. Later on, we describe the quantum formulation of gauge field theory in the continuum. Finally, we summarize the formulation of gauge theories on a lattice, focusing on the lattice formulation of pure gauge theories, i.e. the *Wilson's formulation* and the *Kogut-Susskind's formulation* based on the Lagrangian and Hamiltonian description of the system respectively. More detailed discussions on these topics can be found in the literature. Particularly, we refer the reader to the excellent books by V. Rubakov [47], by I. Montvay and G. Münster [48] and by P. Ramond [49].
- In **chapter 3**, we present a summary on the quantum simulation of external gauge field in ultracold atomic gases placed in optical lattices. First, we describe the physics of ultracold gases in optical lattices, focusing in the tight binding approximation. We introduce the lattice formulation of

the system, arriving to a Hubbard-type description of the system. Then, we describe the consequent Mott insulator-Superfluid phase transition for such a system, which is a genuine pure quantum phase transition at T=0. Later on, we summarize different techniques for engineering, mimicking and emulating external gauge fields, both Abelian and non-Abelian, in optical lattices. Then, we focus on the study of a 2D quantum system subjected to an external and constant magnetic field. Since this system presents non-trivial topological properties due to the appearance of the quantum Hall effect, we finish this chapter describing the physics of this phenomenon.

- In **chapter 4**, motivated by the topics treated in the previous chapter, we analyse systems composed of a non-interacting ultracold gas placed on a 2D lattice under the action of an exotic gauge field. Specifically, we consider the action of an external magnetic field generated by the Heisenberg-Weyl gauge group, which is the simplest non-compact gauge group. We describe a novel method to simulate the gauge degree of freedom, which consists of mapping the gauge coordinate of the system to a the real and perpendicular direction with respect to the 2D space of positions. Thus, the system turns out to be a 3D insulator with a non-trivial topology, specifically, a quantum Hall insulator. We further show that non trivial combinations of quantized transverse Hall conductivities can be engineered with the help of a staggered potential. We investigate the robustness and topological nature of this conductivity and connect it to the surface modes of the system. We also propose a simple experimental realization with ultracold atoms in 3D confined to a 2D square lattice with the third dimension being mapped to the gauge coordinate.

- **Chapter 5** is devoted to present an experimentally feasible setup with ultracold alkaline earth atoms to simulate the dynamics of U(1) lattice gauge theories in 2+1 dimensions with a Chern-Simons term. To this end we consider the ground state properties of spin-5/2 alkaline earth fermions on a honeycomb lattice. We focus in the strong repulsive regime, where essentially the system fulfills the constraint of one fermion per site, i.e. 1/6 filling. First, we analyse the characteristic of the system at T=0 by a mean field approach. We show that the ground state of the system is a chiral spin liquid state with an emergent magnetic flux of $2\pi/3$ per plaquette, which spontaneously violates time reversal invariance. Thus, the system exhibits quantum Hall effect and chiral edge states. We also discuss the properties of the lowest energy competing orders. Later on, we study the stability

of the system at finite temperature, under a path integral formalism and saddle point approximation. We identify a critical temperature, where all the spin liquid phases melt and the system goes to the paramagnetic phase. We also show that the chiral spin liquid state is realized even at finite temperatures. We also determine the spin structure factor, which, in principle, is an experimentally measurable quantity and is the basic tool to map the spectrum of elementary excitations of the system. We relate the spin fluctuations of the system to an emerging gauge field and we identify the Lagrangian system, which describes a system composed of fermionic matter coupled to a dynamical U(1) gauge field.

- We continue the line of the study of quantum simulation for dynamical gauge theories. Thus, in **chapter 6** we present a family of gauge theories that can be efficiently simulated with ultracold atomic systems in optical lattice. This is the so-called family of *gauge magnets*, which corresponds to quantum link models for the U(1) gauge theory. The Kogut-Susskind formulation of lattice gauge theory considers that every site of the lattice contains a local Hilbert space with dimension equals to the dimension of the regular representation of the gauge group. For the U(1) gauge group, this dimension is infinite. However, link model formulation of gauge theories considers a truncated dimension of the local Hilbert space, preserving the total gauge symmetry. We present a *constructive approach* for lattice gauge theory where the links models come out in a natural way. We give the prescription for the construction of the different link models for Abelian gauge groups. As an example, we focus on the gauge magnets, which are link models for the U(1) gauge group with a truncated local Hilbert space of dimension 2, We re-derived the phase diagram of this system, which was already studied some years ago. Finally, we summarize the proposal developed by A. Celi, L. Tagliacozzo, M. Lewenstein and me related to the digital quantum simulation of the U(1) gauge magnet by using Rydberg atoms.

- In **chapter 7**, motivated by the advances in the simulation of open quantum systems, we turn to consider some aspects concerning the dynamics of strongly correlated quantum many body systems. Specifically we study the dynamics in a physical system produced by a quench protocol that conserves the entanglement spectrum of a bipartition of the strongly correlated system. Concretely we consider the splitting of a critical Ising chain in two chains, and compare it with the well studied case of joining

of two chains. We show that both the out of equilibrium and equilibrium regimes after the quench are different in the two scenarios. Since the two quenches only differ in the presence/absence of the conservation of the entanglement spectrum, our results suggest that this conservation plays a fundamental role in both the out-of-equilibrium dynamics and the subsequent equilibration mechanism.

- **Chapter 8** is devoted to the conclusions of the work which forms the thesis. We also present some open questions and future investigations related to the different topics treated in the thesis.

Chapters 4, 5, 6 and 7 contain original studies and results obtained during the doctoral period. The list of original publications which conform these investigations is:

- *Layered quantum Hall insulators with ultracold atoms.*

  A. Zamora, G. Szirmai and M. Lewenstein.

  Physical Review A, **84**, 053620 (2011).

  Chapter 4 of the thesis.

- *Gauge fields emerging from time-reversal symmetry breaking for spin-5/2 fermions in a honeycomb lattice.*

  G. Szirmai, E. Szirmai, A. Zamora, M. Lewenstein

  Physical Review A, **84**, 011611 (2011).

  Chapter 5 of the thesis.

- *Spin liquid phases of alkaline-earth-metal atoms at finite temperature.*

  P. Sinkovicz, A. Zamora, E. Szirmai, M. Lewenstein and G. Szirmai.

  Physical Review A, **88**, 043619 (2013).

  Chapter 5 of the thesis.

- *Optical Abelian lattice gauge theories.*

  L.Tagliacozzo, A. Celi, A. Zamora, M. Lewenstein

  Annals of Physics, **330** (2013).

  Chapter 6 of the thesis.

- *Splitting a critical spin chain.*
  A. Zamora, J. Rodríguez Laguna, M. Lewenstein and L. Tagliacozzo.
  Accepted in Journal of Statistical Mechanics: Theory and Experiment.
  Chapter 7 of the thesis.

Chapter 2

Gauge theories

Gauge theories describe fundamental interaction appearing in Nature. Moreover, gauge interactions appear as emergent phenomena in many low energy effective systems in condensed matter, such as frustrated quantum systems and high-temperature superconductors [21].

The gauge symmetry reflects a freedom in the description of the system through gauge fields. These fields contain degrees of freedom which are not physical. Therefore, infinitely many different configurations of the gauge field are gauge equivalent and provide the same physical results, which are gauge invariant quantities.

In the simplest and probably best known gauge-theory, the Abelian-gauge theory of electrodynamics, the field strengths can be expressed with the help of scalar ϕ and vector potentials $\mathbf{A}$:

$$\begin{aligned} \mathbf{E}(\mathbf{x},t) &= -\nabla\phi(\mathbf{x},t) - \frac{1}{c}\frac{\partial \mathbf{A}(\mathbf{x},t)}{\partial t}, \\ \mathbf{B}(\mathbf{x},t) &= \nabla \times \mathbf{A}(\mathbf{x},t), \end{aligned} \tag{2.1}$$

where c is the speed of light.

The field strengths $\mathbf{E}$ and $\mathbf{B}$ are physical fields, whereas the scalar and the vector potentials are non-physical, they can not be measured. This indicates the system has some kind of arbitrariness or freedom in the selection of these non physical fields. In fact, performing the following transformation:

$$\phi(\mathbf{x},t) \to \phi'(\mathbf{x},t) - \frac{1}{c}\frac{\partial\theta(\mathbf{x},t)}{\partial t},$$
$$\mathbf{A}(\mathbf{x},t) \to \mathbf{A}'(\mathbf{x},t) + \nabla\theta(\mathbf{x},t), \tag{2.2}$$

with an arbitrary scalar function $\theta(\mathbf{x},t)$ on space and time coordinates, it is easy to check that the equations (2.1) do not change, i.e. the field strengths $\mathbf{E}$ and $\mathbf{B}$ are invariant under this transformation. This transformation whose parameter χ depends on space and time is called *gauge transformation*, while the term *global transformation* refers to a transformation with a space-time independent parameter.

The main postulate for the gauge theories is that all the physical quantities should be invariant under local gauge transformations. Electromagnetism fulfils this condition, and it is in fact the most simple gauge theory.

2.1 Gauge symmetry in electrodynamics

The aim of this section is to study the gauge structure of the classical electromagnetism. The 4-vector of the electromagnetism is given by $A^\mu = (-\phi, \mathbf{A})$. Then, the gauge transformation introduced at Eq. (2.2) can be expressed as:

$$A^\mu \to A'^\mu = A^\mu + \partial^\mu\theta, \tag{2.3}$$

where $\partial^\mu = (\frac{1}{c}\partial_t, \nabla)$. The metric we use is $g_{\mu\nu} = \mathrm{diag}(-1,1,1,1)$. Then, $A_\mu = g_{\mu\nu}A^\nu = (-A_0, \mathbf{A})$, using the Einstein summation convention.

The action for the free electromagnetic field is:

$$S_{\mathrm{EM}} = \int d^4x \mathcal{L}_{\mathrm{EM}} = \int d^4x \left(-\frac{1}{4}F^{\mu\nu}F_{\mu\nu}\right), \tag{2.4}$$

with

$$F^{\mu\nu} = \partial^\mu A^\nu - \partial^\nu A^\mu. \tag{2.5}$$

The gauge transformation (2.3) leaves the action S_{EM} invariant:

$$S_{\mathrm{EM}} \to S'_{\mathrm{EM}} = S_{\mathrm{EM}}. \tag{2.6}$$

Let us now consider a system composed of an electromagnetic field interacting with a particle with electrical charge e. The action of the systems contains three terms:

$$S[A] = S_{\rm P} + S_{\rm EM} + S_{\rm int} = S_P + \int d^4x \left(-\frac{1}{4} F^{\mu\nu} F_{\mu\nu} + j^\mu A_\mu \right), \tag{2.7}$$

where $S_{\rm P}$ is the free action of the particle, $S_{\rm int} = \int d^4x j^\mu A_\mu$ is the action term corresponding to the interaction and $j^\mu = q\delta(x)(1, \mathbf{v})$ is the four current of the particle with charge q.

Considering the invariance of $S_{\rm EM}$ under the gauge transformation and the independence of $S_{\rm P}$ on the vector potential, the action of the gauge transformation (2.3) on this action is:

$$S[A] \to S'[A] = S[A'] = S_{\rm P} + S_{\rm EM}[A'] + S_{\rm int}[A'] = S[A] - \int d^4x (e j_\mu \partial^\mu \theta) =$$
$$= S[A] - \int d^4x \partial^\mu (q j_\mu \theta) + \int d^4x (q \partial^\mu j_\mu)\theta = S[A]. \tag{2.8}$$

The full action $S[A]$ of the system remains invariant. Since

- $\int d^4x \partial^\mu (q j_\mu \theta) = 0$, because it is the integral of the flux over an infinitely distant 4D surfacer where $\theta(x^\mu)$ vanishes.
- Conservation of the four current:

  $$\partial^\mu j_\mu = 0, \tag{2.9}$$

  which can be derived from the variation of the field equation

  $$\partial_\mu F^{\mu\nu} = q j^\nu. \tag{2.10}$$

Therefore, there is an intimate connection between the gauge invariance and the conservation of the current. This point will be treated later.

2.2 Gauge symmetry in classical field theory

In this section, we are going to construct a gauge invariant theory by imposing the gauge invariance principle in a system containing classical matter fields.

Let us start with a system composed of a free scalar complex field. The action is given by the integral of the Lagrangian density $\mathcal{L}_{\text{field}}$ over space-time:

$$S_{\text{field}} = \int d^4x \mathcal{L}_{\text{field}} = \int d^4x \left(\frac{1}{2} |\partial_\mu \varphi|^2 - V(\varphi) \right), \tag{2.11}$$

where $|\partial^\mu \varphi| = \partial^\mu \varphi \cdot \partial_\mu \varphi^*$ and $V(\varphi) = \frac{1}{2} m |\varphi|^2 + \lambda |\varphi|^4 + ...$, which can be a polynomial potential in powers of φ, containing a mass term (quadratic term) and interacting terms (hight order in φ) [47, 49].

The energy E for such a field is given by:

$$\begin{aligned} E &= \int d^3x \left(\frac{\partial \mathcal{L}_{\text{field}}}{\partial(\partial_t \varphi)} \partial_t \varphi + \frac{\partial \mathcal{L}_{\text{field}}}{\partial(\partial_t \varphi^*)} \partial_t \varphi^* - \mathcal{L}_{\text{field}} \right) \\ &= \int d^3x \left(\frac{1}{2} |\partial_t \varphi|^2 + \frac{1}{2} |\nabla \varphi|^2 + V(\varphi) \right). \end{aligned} \tag{2.12}$$

A stable physical theory requires an energy bounded from below. Considering $V(\varphi) = \frac{1}{2} m |\varphi|^2 + \lambda |\varphi|^4$, the stability requirement implies $\lambda \geq 0$. For $m > 0$ there is one minimum of the potential at $\varphi = 0$, while for $m < 0$ there is set of minima at $|\varphi| = +\sqrt{\frac{m}{2\lambda}}$ and an unstable (maximum) configuration $|\varphi| = 0$ (see Fig.2.1) . The theory given by $\lambda = 0$ and $m > 0$ describes a Klein-Gordon field.

The action (2.11) is invariant under the following *global gauge transformations*:

$$\begin{aligned} \varphi(x) &\to \varphi'(x) = e^{i\theta} \varphi(x), \\ \varphi^*(x) &\to \varphi^{*\prime}(x) = e^{-i\theta} \varphi^*(x), \end{aligned} \tag{2.13}$$

where the parameter θ does no depen on the space-time position. Following Noether's theorem [50], one obtains the conserved current associated to this transformation:

$$j^\nu = -i \left(\varphi^* \partial^\nu \varphi - \partial^\nu \varphi^* \varphi \right) \tag{2.14}$$

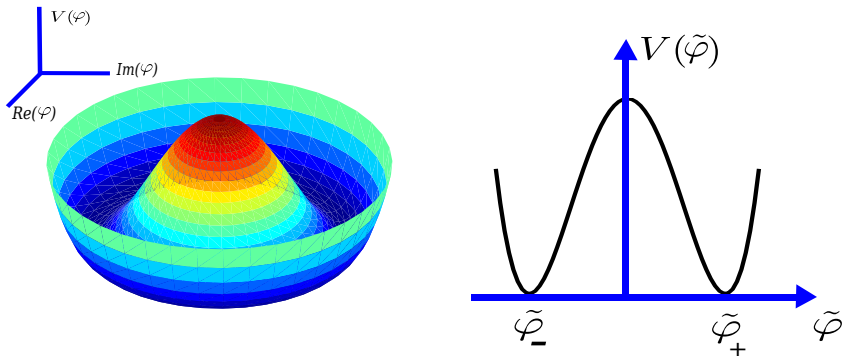

Figure 2.1: *Left panel*: Graphical representation of the potential $V(\varphi) = \frac{1}{2}m|\varphi|^2 + \lambda|\varphi|^4$ for $m < 0,\ \lambda > 0$ as a function of the complex field $\varphi = |\varphi|e^{i\theta}$. It is invariant with respect to the angle θ. There is an unstable physical configuration at $\varphi = 0$ and there are infinitely many degenerate stable configurations at $|\varphi| = \sqrt{\frac{m}{2\lambda}}$. *Right panel*: Section of the potential for an specific $\theta = \tilde{\theta}$, which determines $\tilde{\varphi} = \varphi|_{\tilde{\theta}}$. The potential exhibits two minima at $\tilde{\varphi}_\pm = \pm|\tilde{\varphi}|$.

Let us now consider *local gauge transformations*, where the parameter of the transformation depends on the space-time position $x = (t, \mathbf{r})$.

$$\begin{aligned} \varphi(x) &\to \varphi'(x) = e^{i\theta(x)}\varphi(x), \\ \varphi^*(x) &\to \varphi^{*\prime}(x) = e^{-i\theta(x)}\varphi^*(x). \end{aligned} \tag{2.15}$$

We observe that the term with derivatives in the action transforms as:

$$\partial_\mu\varphi \to \partial_\mu\varphi' = e^{i\theta(x)}\left(\partial_\mu + i(\partial_\mu\theta(x))\varphi\right), \tag{2.16}$$

The appearing $\partial_\mu\theta(x)$ term makes the action (2.11) non-invariant under such local transformations. The requirement of invariance under the local gauge transformation needs the introduction of a new field in the theory, the *gauge field* $A_\mu(x)$. This gauge field transforms under a gauge transformation in such way that compensates the $\partial_\mu\theta(x)$ term. The gauge field is introduced by replacing the usual derivative ∂_μ by the so-called *covariant derivative* D_μ:

$$\partial_\mu \to D_\mu = \partial_\mu - iqA_\mu. \tag{2.17}$$

By Doing such replacement, the action given at (2.11) becomes:

$$S_{\text{field}}[D_\mu] = \int d^4x \left(\frac{1}{2}|D_\mu\varphi|^2 - V(\varphi)\right) = \int d^4x \left(\frac{1}{2}|(\partial_\mu - iqA_\mu)\varphi|^2 - V(\varphi)\right), \tag{2.18}$$

which is the action of a matter scalar field φ coupled to a gauge field A_μ.

Under the local gauge transformation:

$$\begin{aligned}
&\varphi(x) \to \varphi'(x) = e^{i\theta(x)}\varphi(x), \\
&\varphi^*(x) \to \varphi^{*\prime}(x) = e^{-i\theta(x)}\varphi^*(x), \\
&A_\mu(x) \to A_\mu(x)' = A_\mu(x) + \frac{1}{q}\partial_\mu\theta(x),
\end{aligned} \tag{2.19}$$

the covariant derivative transforms as:

$$D_\mu\varphi \to D'_\mu\varphi' = e^{i\theta(x)}D_\mu\varphi. \tag{2.20}$$

Then, the action (2.18) is invariant under such local gauge transformation.

However, the systems described by (2.18) contains an external gauge field. Then, it is necessary to add a gauge invariant kinetic term for the gauge field to this action in order to consider dynamical gauge fields. In the last section we observed the action for the gauge field (2.4) is gauge invariant. Then, adding this term, we end up to the action for a complex matter field coupled to a dynamical gauge field:

$$\begin{aligned}
&S = S_{\text{field}}[D_\mu] + S_{\text{EM}} = S_{\text{field}}[\partial_\mu + ieA_\mu] + S_{\text{EM}} = \\
&= \int d^4x \left(\frac{1}{2}|D_\mu\varphi|^2 - V(\varphi) - \frac{1}{4}F^{\mu\nu}F_{\mu\nu}\right) = \\
&= \int d^4x \left(\frac{1}{2}|(\partial_\mu - ieA_\mu)\varphi|^2 - V(\varphi) - \frac{1}{4}F^{\mu\nu}F_{\mu\nu}\right).
\end{aligned} \tag{2.21}$$

It can be checked that this action in invariant under the gauge transformation expressed in (2.19).

The equations of motion for this system are obtained by the variational principle: $\frac{\delta S}{\delta\varphi} = 0$ and $\frac{\delta S}{\delta A_\mu} = 0$. Applying this principle, we obtain:

$$\partial_\mu F^{\mu\nu} = j^\nu,$$
$$|D^\mu|^2\varphi + m^2\varphi = 0, \tag{2.22}$$

where $j^\nu = -i\left(\varphi^* D^\nu\varphi - (D^\nu\varphi)^*\varphi\right)$ is the four-current of the matter field coupled to the gauge field. It can be obtained as well by the replacement with the covariant derivative in the expression appearing at Eq. (2.14). These equations of motion are also gauge invariant expressions. For instance:

$$|D^\mu|^2\varphi + m^2\varphi = 0 \;\rightarrow\; |D'^\mu|^2 e^{i\theta(x)}\varphi + m^2 e^{i\theta(x)}\varphi = 0 \;\rightarrow$$
$$e^{i\theta(x)}|D^\mu|^2\varphi + m^2 e^{i\theta(x)}\varphi = 0 \;\rightarrow\; |D^\mu|^2\varphi + m^2\varphi = 0 \tag{2.23}$$

2.3 Gauge principle and constrained Hamiltonian

The gauge symmetry indicates that the description of the physical system in terms of the gauge field A_μ contains non-physical degrees of freedom, i.e. there is a freedom in the choice of this field. In this section we will see the relation between this freedom and the appearance of constraints in the Hamiltonian formulation of gauge theories.

Let us consider an electromagnetic field interacting with external sources. The Lagrangian density for such a system is given by:

$$\mathcal{L} = j^\mu A_\mu - \frac{1}{4}F^{\mu\nu}F_{\mu\nu}. \tag{2.24}$$

The canonical Hamiltonian density reads as:

$$\mathcal{H}_c = \Pi^\mu(\partial_t A_\mu) - \mathcal{L} = \frac{1}{2}(\mathbf{E}^2 + \mathbf{B}^2) + \mathbf{E}\cdot\nabla A_0 - j^\mu A_\mu, \tag{2.25}$$

where $\Pi^\mu = \frac{\partial\mathcal{L}}{\partial(\partial_t A_\mu)} = -F^{0\mu}$ is the conjugate momentum, and the electric E_i and magnetic fields B_i read as:

$$E_i = -F_{0i} = \partial_i A_0 - \partial_t A_i,$$
$$B_i = -\frac{1}{2}\epsilon_{ijk}F_{jk} = -\frac{1}{2}\epsilon_{ijk}(\partial_j A_k - \partial_k A_j). \tag{2.26}$$

The momentum conjugate of A_0 vanishes due to A_0 has no time derivative in $\mathcal{L}$:

$$\Pi^0 = 0. \tag{2.27}$$

The introduction of this constraint in (2.25), and the integration over the space leads to the Hamiltonian of the system:

$$H = \int d^3x(\mathcal{H}_c + \lambda(x)\Pi_0) = \int d^3x \left(\frac{1}{2}(\mathbf{E}^2 + \mathbf{B}^2) + \lambda(x)\Pi_0 - A_0(\nabla \cdot \mathbf{E} + j^0) + \mathbf{j} \cdot \mathbf{A}\right), \tag{2.28}$$

where $\lambda(x)$ is a Lagrange multiplier and we have dropped out a surface term coming from the integration by parts of the term $\mathbf{E} \cdot \nabla A_0$.

Since the constraint (2.27) has to be fulfilled at every time t:

$$0 = \partial_t \Pi_0 = -\frac{\delta H}{\delta A_0} = -\frac{\partial \mathcal{H}_1}{\partial A_0} + \partial_i \frac{\partial \mathcal{H}_1}{\partial_i A_0} = \{H, \Pi_0\}, \tag{2.29}$$

where we have introduced the *Poisson bracket*:

$$\{M, N\} = \int d^3x \left(\frac{\delta M}{\delta A_\mu}\frac{\delta N}{\delta \Pi^\mu} - \frac{\delta M}{\delta \Pi^\mu}\frac{\delta N}{\delta A_\mu}\right). \tag{2.30}$$

Therefore, an additional constraint, the so-called *Gauss Law* G_G, is generated:

$$G_G = \nabla \mathbf{E} + j^0 = 0. \tag{2.31}$$

This constraint is already present in the Hamiltonian (2.28), with the field A_0 as a Lagrange multiplier. Since the time derivative of the field A_0 can be expressed as:

$$\partial_t A_0 = \frac{\delta H}{\delta \Pi_0} = \frac{\partial \mathcal{H}_1}{\partial \Pi_0} = \lambda(x), \tag{2.32}$$

finally we can write:

$$H = \int d^3x \left(\frac{1}{2}(\mathbf{E}^2 + \mathbf{B}^2) + (\partial_t A_0)\Pi_0 - A_0(\nabla \cdot \mathbf{E} + j^0) + \mathbf{j} \cdot \mathbf{A}\right), \tag{2.33}$$

which is the constrained Hamiltonian where the Lagrange multipliers are given in terms of the gauge field component A_0.

Since the *Gauss Law* has to be fulfilled at every time t, this leads to the conservation of the four current j^μ:

$$0 = \frac{\partial}{\partial_t}(\nabla \mathbf{E} + j^0) = \{H, \nabla \mathbf{E} + j^0\} = \partial_\mu j^\mu, \tag{2.34}$$

which was introduced already in (2.10). This equation is related to a symmetry of the system, i.e. the invariance of the physical quantities with respect to a certain transformations. This transformations are generated by the constraints appering at the Hamiltonian. (2.33):

$$G[\theta] = \int d^3x \big(\partial_t \theta(x) G_1(x) - \theta(x) G_{\mathrm{G}}(x)\big), \tag{2.35}$$

where $\theta(x)$ is the parameter of the transformation, $G_1(x) = \Pi_0(x)$ and $G_G(x)$ is the *Gauss law*.

The gauge field transforms under $G[\theta]$ as:

$$\delta A_\mu = A'_\mu - A_\mu = \{G[\theta], A_\mu\} = \partial_\mu \theta. \tag{2.36}$$

This result indicates that the transformation generated by $G[\theta]$ is the gauge transformation expressed in Eq. (2.2).

As we expect, the Hamiltonian (2.33) is invariant under the action of this transformation:

$$\delta H = H' - H = \{G[\theta], H\} = -\partial_\mu j^\mu = 0. \tag{2.37}$$

Thus, the dynamics of the system is invariant under such transformations. The systems related by these transformations are physically equivalent, they belong to the same equivalent class.

2.4 Gauge group and parallel transport

Considering that $g(x) \equiv e^{i\theta(x)} \in U(1)$, where $U(1)$ is the unitary group of dimension 1, i.e. the complex number of modulus 1 under the multiplication operation; the matter field appearing in Eq. (2.19) transforms under the action of the fundamental representation of such group:

$$\varphi \to \varphi' = g(x)\varphi. \tag{2.38}$$

It is natural to think of the extension of this transformation law considering other groups. First we notice that the action of N-component scalar fields:

$$\begin{aligned} S_{\text{field}} &= \int d^4x \left(\frac{1}{2} \sum_{a=1}^{n} \partial^\mu \varphi_a^* \partial_\mu \varphi_a + V(\varphi_a^* \varphi_a) \right) = \\ &= \int d^4x \left(\frac{1}{2} \partial^\mu \vec{\varphi}^\dagger \partial_\mu \vec{\varphi} + V(\vec{\varphi}^\dagger \vec{\varphi}) \right), \end{aligned} \tag{2.39}$$

is invariant under the global transformation:

$$\begin{aligned} \vec{\varphi} &\to \vec{\varphi}' = g\vec{\varphi}, \\ \vec{\varphi}^\dagger &\to \vec{\varphi}'^\dagger = \vec{\varphi}^\dagger g^\dagger, \end{aligned} \tag{2.40}$$

where g, is an element of a unitary group $\mathcal{G}$:

$$g \in \mathcal{G} \to g = e^{i \sum_a \theta_a T_a}. \tag{2.41}$$

Here G can be any semi-simple Lie group with N dimensional representation. The matrices T_a are the generators, due to the unitarity of the group, the generators are hermitian: $T_a = T_a^\dagger$. They satisfy the corresponding Lie algebra of the group:

$$[T_a, T_b] = i \sum_c f_{abc} T_c, \tag{2.42}$$

where f_{abc} are the antisymmetric structure constants of the group.

Here the gauge field is a linear combination of such generators:

$$A^\mu(x) = \sum_a A_a^\mu(x) T_a. \tag{2.43}$$

To construct the interacting theory between matter field and gauge fields we require the full action of the system to be invariant under the local gauge transformation $g(x) = e^{i \sum_a \theta_a(x) T_a}$. Then the procedure is:

- To replace the usual derivative ∂^μ by the covariant derivative $D^\mu = \partial^\mu + ie \sum_a A_a^\mu(x^\mu) T_a$ in the action (2.39). This gives the action for the matter field and the interaction between matter and gauge field.

- To add a gauge invariant action S_{gauge} for the gauge field. The best gauge invariant candidate is given by the Yang-Mills action [51]:

$$S_{\text{gauge}} = \int d^4x \mathcal{L}_{\text{gauge}} = \int d^4x \left(-\frac{1}{4} \text{Tr}(F^{\mu\nu} F_{\mu\nu}) \right), \tag{2.44}$$

with the *strength tensor* $F^{\mu\nu}$ constructed as:

$$\begin{aligned} F^{\mu\nu} &= [D^\mu, D^\nu] = \partial^\mu A^\nu - \partial^\nu A^\mu + i[A^\mu, A^\nu] = \sum_a F_a^{\mu\nu} T_a, \\ F_a^{\mu\nu} &= \partial^\mu A_a^\nu - \partial^\nu A_a^\mu - f_{abc} A_b^\mu A_c^\nu. \end{aligned} \tag{2.45}$$

We stress that $f_{abc} \neq 0$ for a non-Abelian gauge theory and this characteristic provides a self-interacting term for the gauge field.

Finally the total action of the system is:

$$S = \int d^4x \left(\frac{1}{2} (D^\mu \vec{\varphi})^\dagger D_\mu \vec{\varphi} + V(\vec{\varphi}^\dagger \vec{\varphi}) - \frac{1}{4} \text{Tr}(F^{\mu\nu} F_{\mu\nu}) \right). \tag{2.46}$$

This action is invariant under the local gauge transformations:

$$\begin{aligned} &\vec{\varphi} \to \vec{\varphi}' = g(x) \vec{\varphi}, \\ &\vec{\varphi}^\dagger \to \vec{\varphi}'^\dagger = \vec{\varphi}^\dagger g(x)^\dagger, \\ &ieA^\mu \to ieA'^\mu = ieg(x) A^\mu g^\dagger(x) + g(x) \partial^\mu g^\dagger(x), \\ &F_{\rho\sigma} \to F'_{\rho\sigma} = g(x) F_{\rho\sigma} g^\dagger(x), \end{aligned} \tag{2.47}$$

where the last equation can be derived from the previous ones by requiring $D^\mu \vec{\varphi}$ to transform under the fundamental representation of $\mathcal{G}$:

$$D^\mu \vec{\varphi} \to \partial^\mu \vec{\varphi}' + ieA'^\mu \vec{\varphi}' = g(x) D^\mu \vec{\varphi}. \tag{2.48}$$

The appearance of the covariant derivative in the formulation of gauge theories is a consequence of a general principle which consists of the independence of the physical laws with respect to the choice of a local basis. In gauge theories the coordinates we refer to are the N components of the vector $\vec{\varphi}(x)$ at a given site x, forming a basis which we call V_x. The gauge transformation $\vec{\varphi} \to \vec{\varphi}' = g(x^\mu) \vec{\varphi}$ can be viewed as a change of basis $V_x \to V'_x$. Since the gauge

transformation is local, the basis depends explicitly on the position x. Therefore, if we want to compare a vector $\varphi(x)$ at site x with a vector $\varphi(y)$ at site y it is necessary to parallel transport the vector from the first point to the next along some curve γ_{yx}:

$$\begin{aligned} U(\gamma_{yx}) : V_x &\to V_y \\ \varphi(x) &\to U(\gamma_{yx})\varphi(x) \in V_y, \end{aligned} \tag{2.49}$$

where $U(\gamma_{yx}) \in U(N)$ is the parallel transporter

As a parallel transport, this object $U(\gamma_{yx})$ fulfils the next properties:

- $U(\emptyset) = \mathbb{I}$, where $\emptyset$ is the curve zero length.
- $U(\gamma_1 \circ \gamma_2) = U(\gamma_1)U(\gamma_2)$ where the symbol $\circ$ denotes the composition of curves.
- $U(\gamma)^{-1} = U(-\gamma)$ where $-\gamma$ is the reversed curve γ

If we compare a vector at x with the corresponding one at $x + dx$, the parallel transport differs infinitesimally from the identity:

$$\begin{aligned} &D\varphi(x) = U(\gamma_{x,x+dx})\varphi(x + dx) - \varphi(x) = (\mathbb{I} + i\mathcal{A}dx)\varphi(x + dx) - \varphi(x) = \\ &= (\mathbb{I} + ieA_\mu(x)dx^\mu)\varphi(x + dx) - \varphi(x), \end{aligned} \tag{2.50}$$

where we have considered the expression (2.17) in the last step.

The *strength tensor* appering in Eq. (2.45) can be obtained by considering the parallel transport among a closed curve γ_{xx} which covers the perimeter of an infinitesimal parallelogram:

$$F_{\mu\nu}(x) = \mathbb{I} - U(\gamma_{xx}). \tag{2.51}$$

The parallel transporters are defined unequivocally by the specification of the gauge fields $A(x)$ and vice versa. With the help of the expression Eq. (2.50), the parallel transport can be reconstructed among a curve γ with the path ordered expression, the so-called *Dyson's formula* [52, 48]:

$$U(\gamma) = \mathbb{P}e^{-\int_\gamma A_\mu(x)dx^\mu}. \tag{2.52}$$

2.5 Gauge symmetry in quantum systems

Let us consider a charged particle coupled to an external electromagnetic field. The classical Hamiltonian for the system is given by:

$$H = \frac{1}{2m}(p - q\mathbf{A})^2 + q\phi, \tag{2.53}$$

where q is the charge of the particle.

The quantum Hamiltonian in the space position basis is obtained from the last expression, by replacing the canonical coordinates and momenta, x, p by the multiplicative operator x and the derivative operator $-i\nabla$, respectively:

$$H = -\frac{1}{2m}(\nabla - iq\mathbf{A})^2 + q\phi. \tag{2.54}$$

The Schrödinger equation for wave function $\varphi(\mathbf{x}, t)$ reads as:

$$\left(-\frac{1}{2m}(\nabla - iq\mathbf{A})^2 + q\phi\right)\varphi(\mathbf{x}, t) = i\frac{\partial\varphi(\mathbf{x}, t)}{\partial t}. \tag{2.55}$$

Using the covariant derivative defined in Eq. (2.17), we can rewrite the last equation as:

$$-\frac{1}{2m}\mathbf{D}^2\varphi(\mathbf{x}, t) = iD_0\varphi(\mathbf{x}, t), \tag{2.56}$$

where $D_\mu = (D_0, \mathbf{D}) = (\partial_t - iq\phi, \nabla - iq\mathbf{A})$. This equation remains invariant under the gauge transformation (2.2):

$$\begin{aligned}
&-\frac{1}{2m}\mathbf{D}^2\varphi(\mathbf{x}, t) = iD_0\varphi(\mathbf{x}, t) \;\rightarrow\; -\frac{1}{2m}(\mathbf{D}')^2 e^{i\theta(\mathbf{x},t)}\varphi(\mathbf{x}, t) = iD_0' e^{i\theta(\mathbf{x},t)}\varphi(\mathbf{x}, t) \;\rightarrow \\
&\rightarrow\; e^{i\theta(\mathbf{x},t)}\left(-\frac{1}{2m}\right)\mathbf{D}^2\varphi(\mathbf{x}, t) = e^{i\theta(\mathbf{x},t)}iD_0\varphi(\mathbf{r}, t) \;\rightarrow \\
&-\frac{1}{2m}\mathbf{D}^2\varphi(\mathbf{x}, t) = iD_0\varphi(\mathbf{x}, t).
\end{aligned} \tag{2.57}$$

Therefore, two different quantum systems, S_1 and S_2, characterized by the wave function and the vector potential:

$$\begin{aligned}
&S_1 : \{\varphi(\mathbf{x}, t), A_\mu(\mathbf{x}, t)\}, \\
&S_2 : \{\varphi'(\mathbf{x}, t), A'_\mu(\mathbf{x}, t)\},
\end{aligned} \tag{2.58}$$

are physically indistinguishable if they are related by a gauge transformation g:

$$g: \{\varphi(\mathbf{x},t), A_\mu(\mathbf{x},t)\} \to \{\varphi'(\mathbf{x},t), A'_\mu(\mathbf{x},t)\}. \tag{2.59}$$

As we have seen in the previous section for classical systems, the gauge principle can be extended to different gauge groups. This extension leads to a generalized Schrödinger equation:

$$\left(-\frac{1}{2m}(\nabla \cdot \mathbb{I}_N - iq\mathbf{A})^2 + e\phi)\right)\vec{\varphi}(\mathbf{x},t) = i\frac{\partial\vec{\varphi}(\mathbf{x},t)}{\partial t}, \tag{2.60}$$

with

$$\begin{aligned} \vec{\varphi} &= (\varphi_1, \varphi_2, ..., \varphi_N)^T, \\ \mathbf{A} &= \sum_a \mathbf{A}_a(\mathbf{x},t)\cdot T_a, \\ \phi &= \sum_a \phi_a(\mathbf{x},t)\cdot T_a, \end{aligned} \tag{2.61}$$

where $\mathbf{A}, \varphi$ are real fields and T_a are the generators of the gauge group $\mathcal{G}$. They obey the commutation relations appearing in Eq. (2.42) and generate the Lie algebra of the group.

It can be checked that the equation (2.60) is invariant under the gauge transformations appearing in Eq. (2.47).

2.5.1 Quantum field theory and gauge symmetry

We are interested in the study of a system composed of an atomic gas, which is a many-body quantum system. Then it is convenient to treat the system in the *second quantized* formalism, introducing non-relativistic quantum field matter $\hat{\vec{\varphi}}$. The Hamiltonian for a non-relativistic N-component quantum gas with two-body interaction reads as:

$$\hat{H}_{\text{field}} = \int d^3x \left[\hat{\vec{\varphi}}^\dagger\left(-\frac{1}{2m}\nabla^2 + V(\mathbf{x})\right)\hat{\vec{\varphi}} + g\hat{\vec{\varphi}}^\dagger\hat{\vec{\varphi}}^\dagger\hat{\vec{\varphi}}\hat{\vec{\varphi}}\right], \tag{2.62}$$

where $\hat{\vec{\varphi}}$ is the field operator for an atom at site $\mathbf{x}$, $V(\mathbf{x})$ is a time-independent external potential and g is the coupling of the interaction between the atoms, $g<0$ ($g>0$) for attractive (repulsive) interaction. Concretely, we are interested s-wave scattering processes, then $g = \frac{4\pi a}{m}$, where a the s-wave scattering length.

The Lagrangian density $\mathcal{L}_{\text{field}}$ is given in term of the matter field $\vec{\varphi}$ by:

$$\mathcal{L}_{\text{field}} = \vec{\varphi}^\dagger i\partial_t \vec{\varphi} + \vec{\varphi}^\dagger \left(\frac{1}{2m}\nabla^2 - V(\mathbf{x}) \right) \vec{\varphi} - g\vec{\varphi}^\dagger \vec{\varphi}^\dagger \vec{\varphi}\vec{\varphi}. \tag{2.63}$$

The theory which describes the quantum atomic gas coupled to a gauge field is obtained by introducing the covariant derivative (2.17) and by adding a dynamical term for the gauge field (see Eq. (2.44)):

$$\begin{aligned} &\mathcal{L} = \mathcal{L}_{\text{field}}[\partial_\mu \to D_\mu] + \mathcal{L}_{\text{gauge}} = \\ &\vec{\varphi}^\dagger i(\partial_t - iq\phi)\vec{\varphi} + \vec{\varphi}^\dagger \left(\frac{1}{2m}(\nabla - iq\mathbf{A})^2 - V(\mathbf{x}) \right) \vec{\varphi} - g\vec{\varphi}^\dagger \vec{\varphi}^\dagger \vec{\varphi}\vec{\varphi} - \frac{1}{4}\text{Tr}(F^{\mu\nu}F_{\mu\nu}), \end{aligned} \tag{2.64}$$

It can be checked that the action $S = \int d^4x \mathcal{L}$ for such a system is invariant under the gauge transformations appearing in (2.3).

The Hamiltonian of the system read as:

$$\hat{H} \;=\; \int d^3x \left[\hat{\vec{\varphi}}^\dagger \left(-\frac{1}{2m}(\nabla - iq\mathbf{A})^2 + V(\mathbf{x}) + \hat{\phi} \right) \hat{\vec{\varphi}} + g\hat{\vec{\varphi}}^\dagger \hat{\vec{\varphi}}^\dagger \hat{\vec{\varphi}}\hat{\vec{\varphi}} \right] \;+\; \hat{H}_{\text{field}}, \tag{2.65}$$

where $\hat{H}_{\text{field}}$ is the Hamiltonian for the gauge field. Specifically for the electromagnetic field, it is a function of the electric $\mathbf{E}$ and magnetic $\mathbf{B}$ field strengths:

$$\hat{H}_{\text{field}} = \int d^3x \, \frac{1}{2}(\mathbf{E}^2 + \mathbf{B}^2), \tag{2.66}$$

which is obtained from the classical Hamiltonian (2.28) without the constraints and replacing of the fields by operators and considering a free gauge field.

For the Hamiltonian formulation of the gauge theory it is convenient to work in the *temporal or Weyl gauge*, defined with the condition $A_0 = 0$. This choice does not fix the gauge completely, since there is a freedom for performing time-independent transformations [53].

As we indicated in Eq. (2.35), the time-independent gauge transformations are generated by the *Gauss law*, G_G, defined at (2.31). Then, it is necessary

to introduce this constraint in a quantum level. We notice that the *Gauss law*, which is enforced to vanish at a classical level, can not vanish on an operator level for the quantum system, since there are relations as:

$$[G_{\mathrm{G}}(x), G_{\mathrm{G}}(y)] = i\delta(x-y)\mathbb{I} \tag{2.67}$$

Then, in quantum field theory the constraint G_G, which generates the gauge symmetry, has to be implemented in a certain subspace $\mathcal{H}_{\mathrm{phys}}$ of the total Hilbert space. This subspace is composed of all the vectors which fulfil:

$$G_G|\psi\rangle_{\mathrm{phys}} = 0. \tag{2.68}$$

This condition is fulfilled during all the time evolution due to:

$$\big[H, G_G\big] = 0, \tag{2.69}$$

As we showed at Section 2.4, the gauge and the matter fields are not gauge invariant quantities. Therefore, at a quantum level, there is a certain unitary operator $V[g]$, whose generator is G_G, which implements the transformation law appearing at (2.3). Specifically for the U(1) gauge group:

$$\begin{aligned}
&\mathbf{A} \to \mathbf{A}' = V[g]\mathbf{A}V^\dagger[g] = g(x)\mathbf{A}g^\dagger(x) - ig(x)\nabla g^\dagger(x) = \\
&\mathbf{A} - \nabla\theta \to \delta\mathbf{A} = i\big[G_G[\theta], \mathbf{A}\big] = -\nabla\theta(x), \\
&\hat{\varphi} \to \hat{\varphi}' = V[g]\hat{\varphi}V^\dagger[g] = g(x)\hat{\varphi} = e^{i\theta(x)}\hat{\varphi} \to \delta\hat{\varphi} = i\big[G_G[\theta], \hat{\varphi}] = i\theta(x)\hat{\varphi},
\end{aligned} \tag{2.70}$$

and $g(x) = e^{i\theta(x)}$ is the element of the gauge group U(1).

Then, $V[g]$ takes the form:

$$V[g] = \exp\left(iG_G[\theta]\right) = \exp\left(i\int dx^3\ \theta(x)G_G(x)\right), \tag{2.71}$$

Since we work in the *temporal gauge*, we only consider time-independent gauge transformations.

2.6 Lattice formulation of the gauge theories

In the present thesis we focus on the quantum simulation of lattice gauge theories, therefore in this section we review an introduction to the formulation of gauge theories on a lattice. For simplicity we will consider a lattice in D dimensions with a constant lattice spacing a (square lattice in 2D, cubic lattice in 3D,...). The generalization of the results to other lattices is straightforward.

2.6.1 Covariant derivative on the lattice

The formulation of the lattice theory requires the replacement of the integrals to finite sums and the derivatives to finite differences. Therefore, some helpful relations are:

$$\int d^D x \varphi^\dagger(x)\varphi(x) \to \sum_x a^D \varphi_x^\dagger \varphi_x, \tag{2.72}$$

$$\int d^D x \varphi^\dagger(x)(-\nabla^2)\varphi(x) = -\int d^D x \nabla(\varphi^\dagger(x)\nabla\varphi(x)) + \int d^D x \nabla\varphi^\dagger(x)\cdot\nabla\varphi(x) =$$

$$= \int d^D x \nabla\varphi^\dagger(x)\cdot\nabla\varphi(x) \to a^D \sum_{<x,y>} \frac{1}{a^2}(\varphi_y^\dagger - \varphi_x^\dagger)\cdot(\varphi_y - \varphi_x) =$$

$$= a^D \sum_{\langle x,y\rangle} \frac{1}{a^2}(-\varphi_y^\dagger\varphi_x - \varphi_x^\dagger\varphi_y + 2\varphi_x^\dagger\varphi_x), \tag{2.73}$$

where x, y are lattice points and $\varphi_x \equiv \varphi(x)$. We have used the fact that the integral of the total derivative vanishes becuase we are considering fields which obey periodic boundary conditions:

$$\int d^D x \nabla(\varphi^\dagger(x)\nabla\varphi(x)) = 0. \tag{2.74}$$

To construct the covariant derivative let's go back to Eq. (2.50). In the continuum case, the covariant derivative is understood as the parallel transporter along a curve with infinitesimally small length. However, in the lattice formalism, the lattice spacing a is the shortest distance. Therefore the lattice version of the covariant derivative connects the point x with its nearest neighbour y via a parallel transporter $U(y,x) \in U(N)$ along the curve with finite length a over the link which connects the two points:

$$\int d^D x \varphi^\dagger(x)(-\mathbf{D}^2)\varphi(x) = -\int d^D x \varphi^\dagger(x)(\nabla - iq\mathbf{A})^2\varphi(x)$$
$$= \int d^D x((\nabla - iq\mathbf{A})\varphi)^\dagger(\nabla - iq\mathbf{A})\varphi =$$
$$= \int d^D x(\mathbf{D}\varphi)^\dagger(\mathbf{D}\varphi) \to a^D \sum_{\langle x,y\rangle} \frac{1}{a}(U\varphi_y - \varphi_x)^\dagger(U\varphi_y - \varphi_x) =$$
$$= a^D \sum_{\langle x,y\rangle} \frac{1}{a^2}(-\varphi_y^\dagger U_{xy}^\dagger \varphi_x - \varphi_x^\dagger U_{xy}\varphi_y + 2\varphi_x^\dagger \varphi_x), \tag{2.75}$$

with $U_{xy} = \exp(iqaA_{xy})$, the element of the gauge group $\mathcal{G}$ at the $\langle x, y\rangle$ link, and A_{xy} is the vector potential. Therefore, the relevant degrees of freedom for a gauge theory defined on the lattice are the parallel transporters, $\{U_{\langle x,y\rangle}\}$ defined on the links of the lattice.

Equation (2.75) is the basic ingredient of the lattice theory for the matter field. Introducing this expression in the Hamiltonian (2.65), we end up to the lattice Hamiltonian for a quantum matter field coupled to a gauge field:

$$\hat{H} = -\tilde{t}\sum_{\langle x,y\rangle}(\varphi_y^\dagger U_{xy}^\dagger \varphi_x + \varphi_x^\dagger U_{xy}\varphi_y - 2\varphi_x^\dagger\varphi_x) + \sum_x V_x\varphi_x^\dagger\varphi_x + \tilde{g}\sum_x \varphi_x^\dagger\varphi_x^\dagger\varphi_x\varphi_x + H_{\text{field}}, \tag{2.76}$$

where $\tilde{t} = a^D/2ma^2, \tilde{g} = ga^D/a^2$ and:

$$\sum_x V_x\varphi_x^\dagger\varphi_x \to \int d^D x V(x)\varphi^\dagger(x)\varphi(x), \tag{2.77}$$

in the continuum limit, where $V(x)$ is an external potential.

The lattice expression of the Hamiltonian for the gauge field, H_{field}, is obtained in the next section.

2.6.2 Pure gauge field on a lattice

As we have seen in the previous section, the lattice theory contains two ingredients: the matter field φ, which is defined on the vertices of the lattice, and the gauge variables U, which are defined on the links between nearest neighbour vertices. The last ones are the lattice version of the parallel transporter given

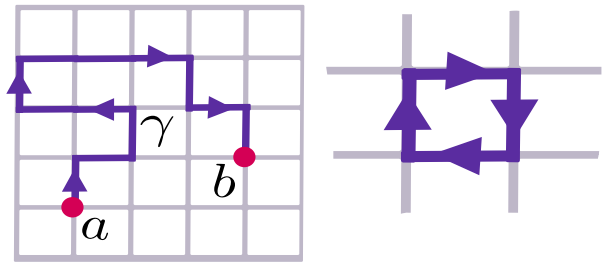

Figure 2.2: *Left panel* Two points a and b on the lattice connected trough a curve γ. The parallel transporter of the curve is given by the product of the parallel transporters at each link. *Right panel* Elementary plaquette with a given orientation, defined by the direction of the curve which encloses the plaquette.

in Eq. (2.49) and they fulfil the characteristics of parallel transporters. Under the gauge transformations (2.3), the link variable transforms as:

$$U_{xy} \to U'_{xy} = g(x) U_{xy} g^\dagger(y). \tag{2.78}$$

Consider two points on the lattice, namely a and b and a path γ which connects these two points through l links. The parallel transporter U_{ab} on the lattice associated to this curve is formed by the composition of the different link variables among the curve (see Fig 2.2):

$$U_{ab} = U_1 \circ U_2 \circ \cdots \circ U_l, \tag{2.79}$$

which is the lattice version of the object appearing in Eq. (2.52). It transforms under a gauge transformation as:

$$U_{ab} \to U'_{ab} = g(a)\, U_{ab}\, g^\dagger(b), \tag{2.80}$$

since the gauge transformations inside the curve are always cancelled. Then, the trace of the link variable associated to a closed path is a gauge invariant object:

$$\mathrm{Tr}(U_{aa}) \to \mathrm{Tr}(g(a)\, U_{aa}\, g^\dagger(a)) \to \mathrm{Tr}(U_{aa}) \tag{2.81}$$

Since the action of the pure gauge field has to be gauge invariant object, these traces over closed paths can act as building blocks for the action. Inspired by the Yang-Mills action (2.44) and the relation between the strength tensor $F_{\mu\nu}$

and the parallel transporter U (2.51), a suitable candidate for the pure gauge action on the lattice is given by the so-called Wilson's action S_W [54]:

$$S_W = a^D \sum_P \frac{1}{a^2 \tilde{g}^2} \left(\mathrm{Tr}(U_P + U_P^{-1}) \right) \tag{2.82}$$

where the sum is over the elementary plaquettes of the lattice (see Fig. 2.2), which define the shortest closed path on the lattice, U_P is the product of the link variables U over these plaquettes, and $\tilde{g}$ is a constant, whose value is determined by performing the continuum limit and recovering the result in the continuum. The sum considers the two different orientations of the plaquettes.

For instance, for the SU(N) gauge group, this action is reduced to:

$$S_W = a^D \sum_P \frac{1}{a^2 2\tilde{g}^2} \mathrm{Re}\ (\mathrm{Tr} U_P). \tag{2.83}$$

Let us now derive the Hamiltonian formulation of the lattice gauge theories. The quantum Hamiltonian for the gauge field in the continuum is given by Eq. (2.66), where the fields $\hat{\mathbf{E}}$ and $\hat{\mathbf{B}}$, rather than $\mathbb{C}$-numbers, they are operators. For the Hamiltonian formulation on the lattice we consider the gauge link variable $U_{xy} = e^{iqaA_{xy}}$ and the electric field $\hat{\mathbf{E}}$ as degrees of freedom. The commutation relations between these operators are given by [21]:

$$\begin{aligned} [E_{xy}, U_{x'y'}] &= \delta_{xx'}\delta_{yy'} U_{xy}, \\ [E_{xy}, U^\dagger_{x'y'}] &= -\delta_{xx'}\delta_{yy'} U^\dagger_{xy}. \end{aligned} \tag{2.84}$$

The *Gauss law* (2.31) on the lattice reads as:

$$G_x = \varphi^\dagger_x \varphi_x + \sum_{\hat{q}} (E_{x+\hat{q},x} - E_{x,x+\hat{q}}), \tag{2.85}$$

where $j_0 = \varphi^\dagger_x \varphi_x$ is the charge density of the matter field and $\hat{q}$ is the vector between neighboring sites.

This *Gauss law* generates the spatial gauge transformations (we remind that we are working in the *temporal gauge* and, therefore, we only consider time-independent gauge transformations). In the lattice, the transformations appearing in (2.70) take the form:

$$\begin{aligned} \varphi_x &\to \varphi'_x = V[g]\varphi_x V^\dagger[g] = g(x)\varphi_x, \\ U_{xy} &\to U'_{xy} = V[g] U_{xy} V^\dagger[g] = g(x) U_{xy} g^\dagger(y), \end{aligned} \tag{2.86}$$

where:

$$V[g] = \prod_x A_x(\theta_x) = \prod_x e^{iq\theta_x G_x}, \tag{2.87}$$

is the unitary operator on the lattice which implements the gauge transformations and $g(x)$ is the element of the gauge group.

A physical state $|\psi\rangle$ fulfils:

$$G_x|\psi\rangle = 0 \rightarrow V[g]|\psi\rangle = |\psi\rangle \;\; \forall g \in \mathcal{G} \tag{2.88}$$

This relation leads to the definition of the *physical* Hilbert space, $\mathcal{H}_{\text{phys}}$, as the set of those states in H that are gauge invariant,

$$\mathcal{H}_{\text{phys}} = \{|\psi\rangle\} \; s.t. \; V[g]|\psi\rangle = |\psi\rangle, \forall g \in \mathcal{G}, \tag{2.89}$$

which is the lattice version of the relation (2.68) in the continuum.

The lattice version of the quantum Hamiltonian for the pure gauge field expressed in (2.66) reads as:

$$\hat{H}_{\text{gauge}} = \frac{ag^2}{2} \sum_l E_l^2 + \frac{4}{ag^2} \sum_P (U_P + U_P^{-1}) \tag{2.90}$$

where a is the lattice spacing and g are constant, whose values are obtained by performing the continuum limit. The first term contains the magnitude of the electric field at every link l, while the second one contains the elementary plaquette terms U_P, which are the product of link variables through an elementary loop on the lattice (see Fig. 2.2 and Eq. (2.82)). This plaquette term encodes the magnetic field $\mathbf{B}$ appearing in (2.66).

This Hamiltonian was first derived by Kogut and Susskind [55]. It plays an important role in different topics treated in this thesis and we will refer to it as *Kogut-Susskind Hamiltoian*.

As in the continuum case (see Eq. (2.69)), the Hamiltonian $\hat{H}_{\text{gauge}}$ on the lattice commutes with the generator of the gauge transformations, i.e. G_x:

$$[\hat{H}_{\text{gauge}}, G_x] = 0. \tag{2.91}$$

Then, the condition (2.88), which defines the physical Hilbert space, is fulfilled during all the evolution of the system.

Chapter 3

Quantum simulation of external gauge fields in ultracold atomic systems

The very precise control of the diverse parameters of the ultracold gases in optical lattices provides a platform that can be reshaped and adjusted to mimic and simulate the behaviour of many other quantum many-body systems. This capability is supported by very particular and important features:

- It is possible to create systems of ultracold bosonic or fermionic atoms, or their mixtures in practically any **lattice configuration**, due to the high degree of control on the direction and polarization of the laser beams. The range of the different lattice configurations runs from cubic lattices in 1D, 2D and 3D, through triangular lattices, hexagonal lattices, kagomé lattices. Furthermore recently developed techniques facilitate the creation of more intricate lattices. For instance, the *superlattice* method adds an extra lattice on a top of an existing one, creating a final lattice with a double well potential per unit cell.

- The interaction between the atoms in a dilute ultracold gas is governed by the s-wave scattering because of the low range of temperatures (nanoKelvin). Therefore the interaction between the atoms can be described by an **on-site interaction** characterized by a scattering length a_g. This parameter can be very well controlled in the experiments by Feshbach resonances in

magnetic fields, achieving a vast range of values, from positive (repulsive interaction) to negative (attractive interaction) ones.

- The non zero overlap between the wave function of the atoms at different minima of the potential causes a **tunneling** between different sites. In many realistic situations it is only considered the tunnelling between neighbour sites, which is characterized by a parameter t. This parameter can be well controlled and tuned in current experiments.

- The standard optical lattice is a **phonon free system**, due to its robustness and rigidity.

- It is feasible to explore new phases of the matter related to the **long range interaction**, such as supersolids or dilute Mott insulators with crystal order in ultracold atomic systems, due to the recent developments in control and manipulation of polar molecules or magnetic dipolar gases.

This chapter contains an introduction to the physics of the ultracold atomic gas in optical lattice and a summary of the techniques for the quantum simulation of external gauge fields with the help of neutral atoms in optical lattices.

3.1 Optical lattices

The interaction between a neutral atom with a dipole moment $\mathbf{d}$ with an electromagnetic wave takes the form:

$$H_I = -\mathbf{d} \cdot \mathbf{E}, \tag{3.1}$$

where $\mathbf{E}$ is the electric field of the electric field.

Let us consider a two level atom coupled to a laser with frequency $\nu = \omega/2\pi$ largely detuned from any optical transition of the atom,. Due to the matter-field interaction, the atom experiences a spectral shift ΔE, which can be calculated perturbatively:

$$\Delta E \propto \frac{|\Omega(x)|^2}{\Delta} \propto \frac{I}{\Delta}, \tag{3.2}$$

where $\Delta = \omega - \omega_{\text{at}}$ is the detuning of the laser from the atomic transition $\hbar\omega_{\text{at}}$, $\Omega(x)$ is the Rabi-frequency ($\Omega(x) \propto e^{ikx}$ for plane waves) and I is the intensity of the laser beam. This energy shift is the so called *ac-Stark shift* [56].

Then, the Hamiltonian for the atom in a light field can be simplified to an expression which contains only two terms, the kinetic term H_{kin} and the energy shift, renamed as the *optical potential* $V_{\text{opt}}(x)$:

$$H = \frac{\mathbf{p}^2}{2m} + V_{\text{opt}}(x). \tag{3.3}$$

The superposition of two counter-propagating waves yields a Rabi frequency which is periodic in space. In this situation, the optical potential takes the form:

$$V_{\text{opt}} = V_0 \sin^2(kx), \tag{3.4}$$

where k=$2\pi/\lambda$ and λ is the wave length of the laser beam.

A sufficiently deep optical potential thus acts as a one dimensional 1D trap: the atoms tend to stay at the minima of these periodical potential. Thus, the laser beams create a 1D regular lattice, with lattice spacing $a = \lambda/2$ (the distance between the minima). Applying this configuration of counter-propagating lasers simultaneously in other spatial directions, one can engineer different lattices in 2D or 3D (see Fig. 3.1). For instance, a 3D cubic lattice with a constant lattice spacing $a = \lambda/2$ can be created with the use of counter-propagating waves in the x, y and z directions with laser beams of equal wave length:

$$V_{opt} = V_x \sin^2(kx) + V_y \sin^2(ky) + V_z \sin^2(kz). \tag{3.5}$$

Manipulating the wave lengths of the lasers, the direction of the beams, the intensity of the atom-light interaction and the polarizations, a vast number of different lattice configurations can be implemented in the laboratory, providing ideal scenarios for the study of quantum matter in various configurations.

3.2 Hubbard model

In this section we are going to consider the quantum simulation with ultracold atoms of a paradigmatic model, the *Hubbard model* [57]. Despite the simplicity of the this model, it is considered a key element for understanding very challenging phenomena in condensed matter systems, like high T_c superconductors.

Let us start from the time-independent Schrödinger equation for an atom placed on an optical potential:

$$\left(-\frac{1}{2m}\nabla^2 + V_{\text{opt}}(\mathbf{r})\right)\varphi(\mathbf{r}) = E\varphi(\mathbf{r}), \tag{3.6}$$

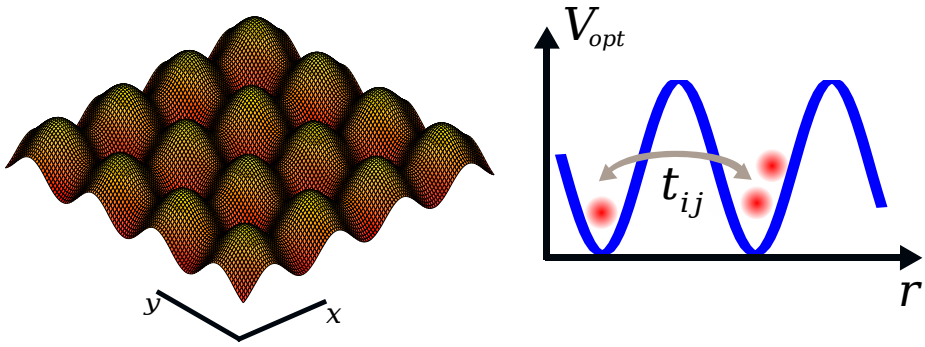

Figure 3.1: *Left panel*: A 2D optical potential created with two pairs of counter-propagating lasers. The maxima and the minima are separated by $\lambda/2$. *Right panel*: Ultracold atomic gas on a 1D optical lattice. The transition amplitude for the tunnelling between one site i and its neighbour j is given by t_{ij}.

where $\varphi(\mathbf{r})$ is the eigenfunction of the atom with energy E.

The optical potential is a perodic function:

$$V_{\text{opt}}(\mathbf{r}) = V_{\text{opt}}(\mathbf{r} + \mathbf{a}), \tag{3.7}$$

where:

$$\mathbf{a} = m_1\hat{a}_1 + m_2\hat{a}_2 + m_3\hat{a}_3 \tag{3.8}$$

is the translational vector in all the directions and m_1, m_2 and m_3 are integer numbers. For instance, for the 3D cubic lattice, these three directions correspond to the x, y and z-direction and the lattice spacing is $a_i = |a_i| = \lambda/2$.

Due to the periodicity of the potential, we can apply the Bloch theorem, which states that the wave function has a simple form containing two different factors: a function which has the periodicity of the potential times a plane wave:

$$\varphi(\mathbf{r}) \to \varphi_k^{(n)}(\mathbf{r}) = u^{(n)}(\mathbf{r}) \cdot e^{i\mathbf{kr}}, \tag{3.9}$$

with $u^{(n)}(\mathbf{r}) = u^{(n)}(\mathbf{r} + \mathbf{a})$ and $-\frac{\pi}{a_i} < k_i < \frac{\pi}{a_i}$ (i=1,2,3) is the quasimomentum, which lies in the first Brillouin zone. The *band* index n labels the different solutions for a given momentum k, which form the band structure.

Substituting the last expression in (3.6), we end up to:

$$\left(-\frac{1}{2m}\nabla^2 + V_{\text{opt}}(\mathbf{r})\right)\varphi_k^{(n)}(\mathbf{r}) = E_k^{(n)}\varphi_k^{(n)}(\mathbf{r}) \rightarrow \left(-\frac{1}{2m}(\nabla^2 + k^2) + V_{\text{opt}}(\mathbf{r})\right)u_k^{(n)}(\mathbf{r}) = E_k^{(n)}u_k^{(n)}(\mathbf{r}). \quad (3.10)$$

The solution of this equation leads to the band spectrum of a periodic quantum systems.

Let us turn to consider an ultracold atomic gas in an optical lattice. Since, this many body systems is composed of a large number of atoms, it is practical to describe the system under the second quantized formalism. Thus, the Hamiltonian is written in terms of the quantum field operator $\hat{\varphi}$, which is the matter field which characterizes the ultracold atomic gas:

$$\hat{H} = \int d^3x\hat{\varphi}^\dagger(\mathbf{x})\left(-\frac{\nabla^2}{2m} + V_{\text{opt}} + V_{\text{trap}}\right)\hat{\varphi}(\mathbf{x}) + \tilde{g}\int d^3x\hat{\varphi}^\dagger(\mathbf{x})\hat{\varphi}^\dagger(\mathbf{x})\hat{\varphi}(\mathbf{x})\hat{\varphi}(\mathbf{x}), \quad (3.11)$$

where V_{trap} denotes an external potential which confines the atoms in a trap (such as harmonic potential). The first integral contains the kinetic energy of the gas and the potential energy. The last term describes the interaction between the atom of the gas. Considering a s-wave scattering process between the atoms, the interaction is on-site and it is governed by the coupling $\tilde{g} = \frac{4\pi a}{m}$, where a is the s-wave scattering length.

The field operators $\hat{\varphi}^\dagger(\mathbf{x})$ ($\hat{\varphi}(\mathbf{x})$) are the creation (anihilation) operators of an atom at site $\mathbf{x}$. For a bosonic system, they obey the bosonic commutation relation:

$$\begin{aligned}&[\hat{\varphi}(\mathbf{x}), \hat{\varphi}^\dagger(\mathbf{x}')] = \delta(\mathbf{x} - \mathbf{x}'),\\ &[\hat{\varphi}(\mathbf{x}), \hat{\varphi}(\mathbf{x}')] = [\hat{\varphi}^\dagger(\mathbf{x}), \hat{\varphi}^\dagger(\mathbf{x}')] = 0, \quad \forall\, \mathbf{x}, \mathbf{x}',\end{aligned} \quad (3.12)$$

while the fields anticommute in a fermionic system:

$$\begin{aligned}&\{\hat{\varphi}(\mathbf{x}), \hat{\varphi}^\dagger(\mathbf{x}')\} = \delta(\mathbf{x} - \mathbf{x}'),\\ &\{\hat{\varphi}(\mathbf{x}), \hat{\varphi}(\mathbf{x}')\} = \{\hat{\varphi}^\dagger(\mathbf{x}), \hat{\varphi}^\dagger(\mathbf{x}')\} = 0, \quad \forall\, \mathbf{x}, \mathbf{x}',\end{aligned} \quad (3.13)$$

The vacuum $|\Omega\rangle$ of the systems contains no atoms: $\hat{\varphi}(\mathbf{x})|\Omega\rangle = 0,\ \forall\, \mathbf{x}$

Due to the periodicity of the optical potential V_{opt}, we can describe the system applying the Bloch functions introduced in Eq. (3.9), as we already did for the one particle case.

However, for our purpose, it is more practical to describe the fields in the space position. Thus, we introduce the *Wannier functions*: $w^{(n)}(\mathbf{x}-\mathbf{X_i})$, where $\mathbf{X_i}$ label the minima of the optical potential. The change of basis from the Bloch to the Wannier functions is given by:

$$w^{(n)}(\mathbf{x}-\mathbf{X_i}) = \frac{1}{\sqrt{N}} \sum_{\mathbf{k}} \varphi_k^{(n)} e^{-i\mathbf{k}\mathbf{X_i}}. \tag{3.14}$$

The Wannier functions form an orthonormal basis:

$$\int w^{*(n)}(\mathbf{x}-\mathbf{X_i}) \cdot w^{(m)}(\mathbf{x}-\mathbf{X_j}) = \delta_{ij}^{nm}. \tag{3.15}$$

Thus, the field operator can be written as:

$$\hat{\varphi}^{(n)}(\mathbf{x}) = \sum_j b_j^{(n)} w^{(n)}(\mathbf{x}-\mathbf{X_j}), \tag{3.16}$$

where $b_i^{(n)\dagger}$ $\left(b_i^{(n)}\right)$ is the atom creation (annihilation) field operator in the n band at site $\mathbf{X}_i$, which is a minimum of the optical potential. They obey the usual commutation (anticommutation) relation for bosons (fermions) appearing at (3.12) and (3.13).

By increasing the strength of the optical potential, the gaps between the different bands increase. Therefore, for sufficiently deep potentials, the atoms occupy basically the lowest band and the occupation of the other bands can be neglected. In such conditions, the Hamiltonian of the system takes the form:

$$\hat{H} = -\sum_{ij} t_{ij} b_i^\dagger b_j + g \sum_i b_i^\dagger b_i^\dagger b_i b_i, \tag{3.17}$$

where we have omitted the label of the first band and

$$t_{ij} = -\int d^3x \varphi^{*(1)}(\mathbf{x}-\mathbf{x_i}) \left(-\frac{\nabla^2}{2m} + V_{opt}\right) \varphi^{(1)}(\mathbf{x}-\mathbf{x_j}), \tag{3.18}$$

$$g = \tilde{g} \int d^3x \varphi^{*(1)}(\mathbf{x}-\mathbf{x_i}) \varphi^{*(1)}(\mathbf{x}-\mathbf{x_i}) \varphi^{(1)}(\mathbf{x}-\mathbf{x_i}) \varphi^{(1)}(\mathbf{x}-\mathbf{x_i}), \tag{3.19}$$

are the tunnelling and the interaction strengths respectively. The label (1) indicates that we are considering only the first band.

Numerical computation of t_{ij} indicates that the leading term is obtained for the tunnelling between nearest neighbours: $i, i+1$. Then, considering only tunnelling between nearest neighbours is significant, the Hamiltonian of the system reads as:

$$\hat{H} = -\sum_{\langle i,j \rangle} t_{ij} b_i^\dagger b_j + \sum_j v_j b_j^\dagger b_j + g \sum_i b_i^\dagger b_i^\dagger b_i b_i, \tag{3.20}$$

whith $v_j \equiv \int d^3x V_{trap}(\mathbf{x}) |\varphi^{(0)}(\mathbf{x} - \mathbf{x_j})|^2$.

Then, the ultracold atomic system in an optical lattice is a genuine system on a lattice, where the effect of the optical potential has been encoded in the tunnelling t between neighbour sites. The Hamiltonian was derived first by Jaksch *et al.* [58]. It takes the same form as the celebrated Hubbard model [57]. Due to its many-body nature, the complexity of its computation increases exponentially with the number of constituents. Therefore, some numerical methods have been developed for addressing this type of systems, as quantum Monte-Carlo techniques, mean field theory or tensor network methods [2].

As it was theoretically studied for bosonic systems (liquid helium systems) at $T = 0$, this Hubbard-type system can experience a phase transition between two different competing phases: the Mott insulator phase and a superfluid phase [59].

At zero temperature, the thermal fluctuations of the system are frozen out. Therefore the system, which is in the ground state, can not experience a phase transition mediated by thermal fluctuations. However, the system can support non-zero quantum fluctuations a $T = 0$. Depending on the regime where the system is at, these quantum fluctuations can be really important, driving the system from one phase to another phase. Thus, the system can experience a purely quantum phase transition at $T = 0$ between the superfluid phase and the Mott insulator phase.

The control parameter which governs this quantum phase transition is the ratio t/g. When $t \gg g$ the system is in the superfluid phase: the tunnelling between the sites dominates over the on site interaction and therefore the atoms are fully delocalised and the wave function is spread over the entire lattice. In this situation the wave function exhibits long range phase coherence and the system is in a Bose-Einstein condensate. However, when t decreases (for ex-

ample by making the optical lattice deeper) and/or by increasing the on-site interaction, the delocalization of the atoms start to diminish and the system can undergoes a transition to a regime where the minimization of the energy is achieved by a well defined number of atoms per site: the Mott insulator phase. In this phase, the long-range phase coherence is completely lost and the system exhibits a gap between the ground state and the excitations.

The wave function of a system with N atoms on a lattice with M sites can be written down in these two limiting cases:

$$\begin{aligned} &\text{Superfluid phase: } |\varphi_{\mathrm{SF}}\rangle_{g=0} \propto \left(\sum_{i=1}^{M} \hat{b}_i^\dagger\right)^N |\Omega\rangle, \\ &\text{Mott insulator phase: } |\varphi_{\mathrm{MI}}\rangle_{t=0} \propto \prod_{i=1}^{M} (\hat{b}_i^\dagger)^n |\Omega\rangle, \end{aligned} \tag{3.21}$$

where n is the numbeer of atoms per site.

This pure quantum phase transition was theoretically predicated for ultracold bosons in an optical lattice by Jaksch *et al.* [58]. It was successfully achieved experimentally driving a BEC condensate (Superfluid phase) composed by atoms ^{87}Rb, in a 3D cubic optical lattice, to the Mott insulator phase, by increasing the optical depth [60]. The detection of phase coherence was carried out by turning off the optical lattice, allowing the ultracold gas to expand freely and interfere with itself. The interference pattern changes drastically when the depth of the optical lattice is increased, indicating the quantum phase transition (see Fig. 3.2)

3.3 Ultracold atomic gas subjected to external gauge fields

In the recent years there has been a considerable development regarding to the simulation of quantum system subjected to external gauge fields in ultracold atomic platforms. The aim of this section is to review different techniques for this purpose, focusing in the simulation of external and classical gauge fields.

As we discussed in the last chapter in a usual system composed of matter, the substitution of the usual derivative by the covariant derivative (see Eq.

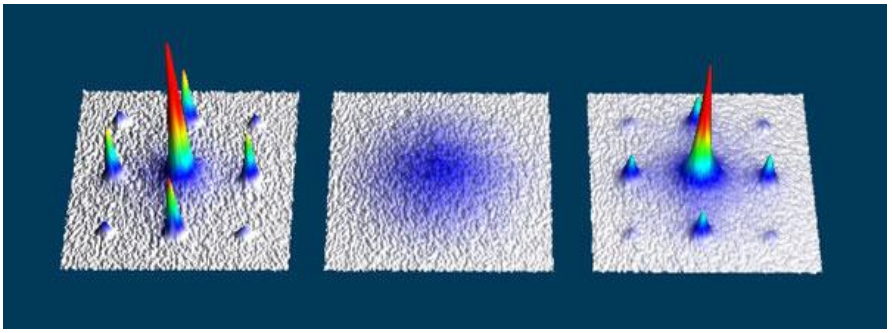

Figure 3.2: Mott insulator-Superfluid phase transit for an ultracold atomic system described by the Hubbard model. The transition goes from a fully coherent superfluid phase phase (left panel) to a fully non-coherent phase or Mott phase (central panel) and the return back to the superfluid phase (right panel). retirived from greiner.physics.harvard.edu/MottInsulator.html

(2.17)) leads to the appearance of the gauge field in the system. On a lattice, this prescription requires the introduction of the link variable U_l at the link l, which encodes the gauge degree of freedom (see Eq. (2.75)).

Then, by performing the next substitution:

$$t_{ij} \rightarrow t_{ij}\, U_{ij} \tag{3.22}$$

in the expression (3.20), we end up to the Hamiltonian for a ultracold atomic gas on a lattice coupled to a gauge field:

$$\hat{H} = -t \sum_{\langle i,j \rangle} U_{ij} b_i^\dagger b_j + \sum_j v_j b_j^\dagger b_j + g \sum_i b_i^\dagger b_i^\dagger b_i b_i, \tag{3.23}$$

where we have considered a homogeneous tunnelling: $t_{ij} = t \;\; \forall$ link i, j. Since in this chapter we focus on external gauge fields, we do not consider the Hamiltonian for the free gauge field in the expression (3.23)

The high level of tunability of the atomic neutral gas in an optical lattice provides mechanisms to *synthesise* the gauge link variable U_{ij} appearing in (3.23). Therefore, the ultracold gas experiences the action of an *artificial* gauge field and acts as a quantum simulator.

Moreover, the high level of control of the parameters of the system permits the simulation of a wide variety of gauge configurations: from standard configurations, as the electromagnetism to more exotic and sophisticate ones. Specifically, Chapther 4 is devoted to the description of the quantum simulation of the exotic gauge theory generated by the Heisenberg-Weyl group.

In the recent years there has been a considerable experimental development towards the simulation of external gauge fields in ultracold atomic setups, both considering optical lattices [61, 62, 63, 64, 65] and non optical lattices platforms [66, 67, 68, 69, 70, 71]. Moreover, recent experiments with spin orbit coupled atomic gas open the posibility of exploring spin Halls topological insulators [72, 70, 71, 73, 74, 75, 76, 77].

Next, we review some of the proposals for emulating the action of external gauge fields in optical lattice setups. We refer the reader to the excellent review about the subject by *N. Goldman et al.* [78] for details.

Artificial gauge fields by laser-assisted tunneling

In the original proposal by Jaksch and Zoller [79], it is considered a 2D optical lattice with an ultracold of one-specie atomic gas, with two different internal states, namely $|e\rangle$ and $|g\rangle$. The atoms are placed such that the rows in the lattice are alternating in state $|e\rangle$ and state $|g\rangle$ (see Fig. 3.3). The tunnelling in the $x-$ direction conserves the internal state and is gives a trivial link variable:

$$U_x = 1. \tag{3.24}$$

However, the tunnelling in the $y-$ direction is assisted by a Raman laser and produces a change in the internal state of the atom depending on the $x-$ coordinate:

$$U_y(x) = e^{i\frac{\sigma\lambda}{2\pi}x}, \tag{3.25}$$

where λ is the wavelength of the optical lattice and σ is given by the assisting laser.

Therefore, if an atom hops around a loop over a plaquette, it acquires a non-trivial phase:

$$\begin{aligned}\psi(x,y) \to \psi'(x,y) =& U_y^\dagger(x,y+1)U_x^\dagger U_y(x+1,y)U_x(x,y)\psi(x,y) = \\ &= e^{i2\pi\phi}\psi(x,y),\end{aligned} \tag{3.26}$$

where $\phi = \frac{\sigma\lambda}{4\pi}$ is the flux in the elementary plaquette created by the artificial gauge field. This flux can be tuned due to the controllability of the Raman

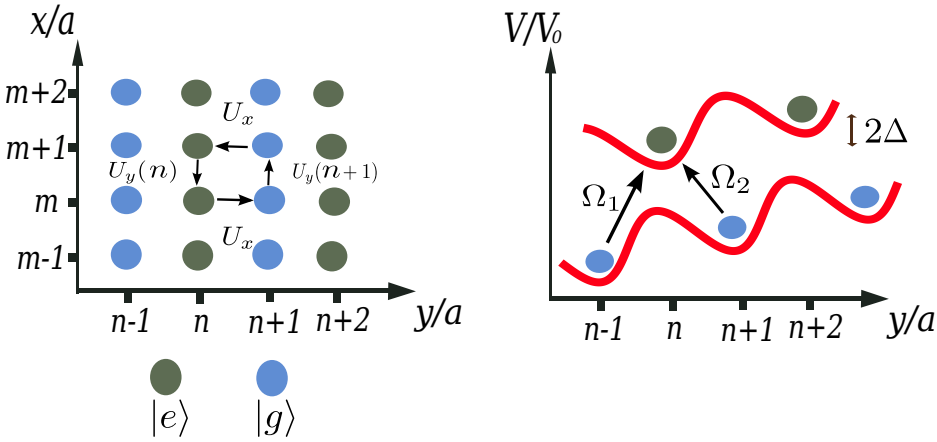

Figure 3.3: Jaksch and Zoller's scheme for the creation of an artificial U(1) gauge field on a 2D lattice. The tunnelling in the $y-$direction in laser assisted by two Raman lasers with Ω_1, Ω_2 frequencies. Due to the presence of an external electric field in the $y-$direction, there is a shift Δ in the energy for the adjacent points in this direction (*right panel*). A neutral atom picks up a non-trivial phase, when it performs an elementary loop on the lattice (*left panel*).

transitions.

This method was extended for the simulation of non-Abelian gauge groups [80], by considering a gas composed of one specie with two different states, $|e\rangle$ and $|g\rangle$, each of them contains two different hyperfine state, namely a and b. Thus, the atomic gas is composed of atoms in the states $|e\rangle_i$ and $|g\rangle_j$, where $i, j = a, b$ are the labels for the hyperfine state. The usual tunnelling in both directions is suppressed and it is allowed by laser assistance: the tunnelling in the $x-$ direction maintains the internal state but changes the hyperfine, while the tunnelling in the $y-$ direction changes the internal state and conserves the hyperfine state. This setup permits the simulation of non-Abelian gauge groups, as the U(2). For example, with a suitable combination of the parameter, one can obtain:

$$\begin{aligned} U_x &= \begin{pmatrix} 0 & e^{i\alpha} \\ e^{-i\alpha} & 0 \end{pmatrix}, \\ U_y(x) &= \begin{pmatrix} e^{i2\pi\beta_1 x} & 0 \\ 0 & e^{i2\pi\beta_2 x} \end{pmatrix}. \end{aligned} \tag{3.27}$$

In this particular case, the wave function $\vec{\psi}(x, y)$ of an atom transforms along a close path over a plaquette as:

$$\begin{aligned} \vec{\psi}(x,y) \to \vec{\psi}'(x,y) =& U_y^\dagger(x,y+1)U_x^\dagger U_y(x+1,y)U_x(x,y)\vec{\psi}(x,y) = \\ &= \begin{pmatrix} e^{i2\pi x(\beta_2-\beta_1)+i2\pi\beta_1} & 0 \\ 0 & e^{-i2\pi x(\beta_2-\beta_1)+i2\pi\beta_2} \end{pmatrix} \vec{\psi}(x,y), \end{aligned} \tag{3.28}$$

where $\vec{\psi} = (\psi_a, \psi_b)$.

This system can exhibit phases with non trivial topology, as quantum Hall insulators. Moreover, the system presents Dirac cones and it can act as a simulator of relativistic field theories [81, 82].

Rotating ultracold atomic systems

The similarity between the Coriolis and the Lorentz forces permets to describe a rotating neutral gas in a harmonic trap as charged atomic gas subjected to an external and perpendicular magnetic field [83, 84].

The Hamiltonian for a 2D rotating gas with angular velocity Ω reads as:

$$H = \frac{1}{2m}\mathbf{p}^2 + \frac{1}{2}m\omega_{\rm tr}^2\mathbf{r}^2 - \vec{\Omega}\cdot(\mathbf{r}\times\mathbf{p}), \tag{3.29}$$

where the last term is the angular momentum of the system and $\omega_{\rm tr}$ is the frequency of an external harmonic trap. This expression can be written as:

$$H = \frac{1}{2m}(\mathbf{p} - m\omega_{\rm tr}\cdot\mathbf{e}_z\times\mathbf{r})^2 + (\omega_{\rm tr}-\Omega)\mathbf{r}\times\mathbf{p}, \tag{3.30}$$

where we consider a rotation perpendicular with respect to the plane which contains $\mathbf{r}$ and $\mathbf{p}$. Thus, this system is equivalent to a system under the presence of a vector potential $\mathbf{A} = -m\omega_{\rm tr}\cdot\mathbf{e}_z\times\mathbf{r}$, with an additional term.

A rapidly rotating optical lattice can simulate the effect of an external vector potential $\mathbf{A}$. In the limit $\Omega\to\omega_{\rm tr}$, the last term of the Hamiltonian vanishes and the spectrum of the system recovers exactly the energies of the Landau Hamiltonian, which describes 2D charged particles coupled to a perpendicular magnetic field:

$$E_n = 2\hbar\omega_{\rm tr}(1/2+n). \tag{3.31}$$

Each value of n presents a degeneracy corresponding to the values of the angular momentum l.

By considering interaction between the atoms, rich phenomena emerge in the system, as crystal-type structures for the Laughlin state [85, 86, 87].

Artificial gauge field by geometric phase

Let us consider a system composed of an ultracold atomic gas of two-level atoms, $|e\rangle$ and $|g\rangle$, interacting with a field which couples those internal states. This external field can be a laser field with frequency near the resonance frequency ω_S of the internal states, a microwave or a static electric or magnetic field interacting with the dipole moment of the atom [88]. The Hamiltonian for the atoms in the basis $\{|e\rangle,|g\rangle\}$ reads as:

$$H = (\frac{\mathbf{p}^2}{2m} + V)\cdot\mathbb{I}_{2\times2} + H_{\rm eg}, \tag{3.32}$$

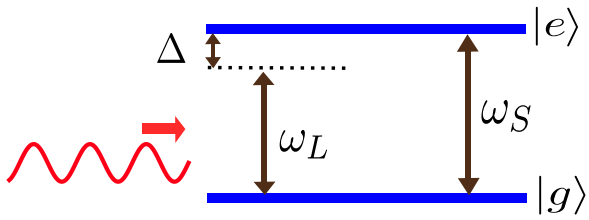

Figure 3.4: A two level atom coupled to a laser beam with a frequency which differs from the atomic resonance by Δ.

where the first term contains dynamics of the atoms (kinetic terms and trapping potential V) and H_{eg} is the coupling between the two internal states:

$$H_{\text{eg}} = \frac{\hbar\Omega}{2}\begin{pmatrix} \cos\theta & e^{-i\phi}\sin\theta \\ e^{i\phi}\sin\theta & \cos\theta \end{pmatrix}, \tag{3.33}$$

where Ω is the Rabi frequency of the coupling and θ and ϕ are position-dependent parameters.

For example, let us consider a two level atom system on a 2D space, coupled to a laser beam propagating in the x-direction with wave number $k = 2\pi/\lambda$ and frequency ω_L close to the resonance of the transition between the levels (see Fig. 3.4). Then the coupling term of the Hamiltonian reads as [88, 89, 90]:

$$H_{\text{eg}} = \frac{\hbar}{2}\begin{pmatrix} \Delta & \gamma \\ \gamma^* & -\Delta \end{pmatrix}, \tag{3.34}$$

with $\Delta = \omega_L - \omega_S$ and $\gamma = |\gamma(y)|e^{ikx}$ is the spatially depending coupling between the two levels.

Iin term of the eigenstates of the matrix H_{eg}, the wave function reads as:

$$|\psi\rangle = C_1(\mathbf{r},t)|\varphi(\mathbf{r},t)\rangle_1 + C_2(\mathbf{r},t)|\varphi(\mathbf{r},t)\rangle_2, \tag{3.35}$$

where the eigenstates take the form:

$$\begin{aligned} |\varphi(\mathbf{r},t)\rangle_1 &= \begin{pmatrix} \cos(\theta/2) \\ e^{i\phi}\sin(\theta/2) \end{pmatrix}, \\ |\varphi(\mathbf{r},t)\rangle_2 &= \begin{pmatrix} -e^{-i\phi}\sin(\theta/2) \\ \cos(\theta/2) \end{pmatrix}, \end{aligned} \tag{3.36}$$

with eigenvalues $\pm\hbar\Omega/2$ respectively.

The momentum operator in this basis reads as:

$$\begin{aligned}\langle\varphi_j|\mathbf{P}|\psi\rangle &= -i\hbar\langle\varphi_j|\vec{\nabla}|\left(C_1(\mathbf{r},t)|\varphi(\mathbf{r},t)\rangle_1 + C_2(\mathbf{r},t)|\varphi(\mathbf{r},t)\rangle_2\right) = \\ &= \left(-i\hbar\vec{\nabla}\delta_{jl} - \mathbf{A}(\mathbf{r},t)_{jl}\right) C_l(\mathbf{r},t),\end{aligned} \tag{3.37}$$

where $\mathbf{A}(\mathbf{r},t)_{jl} = i\hbar\langle\varphi_j|\vec{\nabla}\varphi_l\rangle$, is the synthetic gauge field. As we will see at Section 9.1, this expression for $\mathbf{A}$ is the definition of the Berry's connection in the space of parameters of the Hamiltonian (3.35).

If the initial state is prepared in one of these two dressed states, namely $|\varphi\rangle_1$ and it evolves adiabatically , then, the state will remain for all the times in such state. The evolution of the state is obtained from the Hamiltonian (3.32), projecting over the subspace $|\varphi\rangle_1$:

$$i\hbar\frac{\partial C_1(\mathbf{r},t)}{\partial t} = \left(\frac{1}{2m}(\mathbf{P}-\mathbf{A})^2 + \tilde{V}\right) C_1(\mathbf{r},t), \tag{3.38}$$

where $\tilde{V}$ is a position dependent potential coming from the change of basis. The vector potential and its magnetic field take the form:

$$\begin{aligned}\mathbf{A}(\mathbf{r}) &= i\hbar\langle\varphi_2|\vec{\nabla}\varphi_1\rangle = \frac{\hbar}{2}(\cos\theta - 1)\nabla\phi, \\ \mathbf{B}(\mathbf{r}) &= \nabla\times\mathbf{A}(\mathbf{r}) = \frac{\hbar}{2}(\nabla\cos\theta)\times\nabla\phi.\end{aligned} \tag{3.39}$$

This scheme of a two-level atom can be efficiently used if the excited state $|e\rangle$ has a very long lifetime, as e.g. for the alkali atoms.

Let us now consider a three level atom with states: $|g_1\rangle, |g_2\rangle, |e\rangle$, such that $|g_1\rangle, |g_2\rangle$ are quasi degenerate states. The Hamiltonian $H_{\rm eg}$ reads as:

$$H_{\rm eg} = \frac{\hbar}{2}\begin{pmatrix} -2\Delta & \gamma_1^* & 0 \\ \gamma_1 & 0 & \gamma_2 \\ 0 & \gamma_2^* & 2\Delta \end{pmatrix}, \tag{3.40}$$

where Δ is the detunning between the Raman resonances γ_i.

When the detuning Δ is negligible, there is a zero energy eigenstate of H_{eg}, the so-called *dark state* D. The other two eigenstates are $|\tilde{e}\rangle_\pm = (|B\rangle \pm |e\rangle)/\sqrt{2}$,

being $|B\rangle$ the *brigth state*:

$$D = \frac{1}{\tilde{\gamma}}(\gamma_1|g_1\rangle - \gamma_2|g_2\rangle),$$
$$B = \frac{1}{\tilde{\gamma}}(\gamma_1^*|g_1\rangle + \gamma_2^*|g_2\rangle), \tag{3.41}$$

with $\tilde{\gamma}$ the normalization factor.

Considering an adiabatic evolution for the *dark state*, the physical state is assumed to remain in such state over the evolution: $|\psi(\mathbf{r},t)\rangle = C_D(\mathbf{r},t)|D\rangle$. The Schrodinger equation reads as:

$$i\hbar\frac{\partial C_D(\mathbf{r},t)}{\partial t} = \left(\frac{1}{2m}(\mathbf{P}-\mathbf{A})^2 + \tilde{V}\right) C_D(\mathbf{r},t), \tag{3.42}$$

where the synthetic vector potential takes the form:

$$\mathbf{A}(\mathbf{r}) = i\hbar\langle D|\vec{\nabla}D\rangle. \tag{3.43}$$

This scheme can be modified to allow the simulation of non-Abelian gauge fields [91, 92, 93], by considering nearly degenerate subspace of dark states $\{|D_1\rangle, |D_2\rangle, ..., |D_N\rangle\}$, such that the physical state can be written as:

$$\psi(\mathbf{r},t)\rangle = \sum_{i=1}^{i=N} C_i(\mathbf{r},t)|D_i\rangle. \tag{3.44}$$

We end this section about geometric potentials by mentioning that these type of schemes have been extended to other systems with atoms with two or more internal degrees of freedom [94, 95].

Artificial gauge field in synthetic dimensions

Recently, a new proposal for generating synthetic gauge field in ultracold atomic systems has been presented by A. Celi *et al* [96]. The remarkable difference with respect to the previous proposals it that it interprets the internal state of the atoms as a *synthetic* dimension of the lattice .

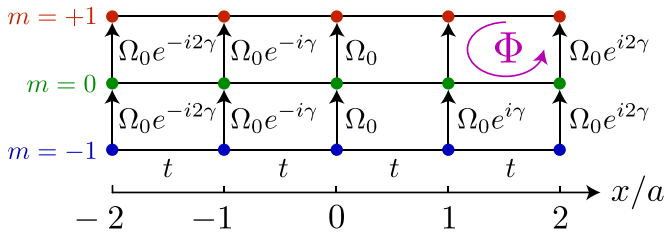

Figure 3.5: A 2D lattice defined by the real $x-$position of the atom and the *synthetic* dimension given by the internal state of the atom (specifically we have considered $F = 1$). If an atom performs a closed loop over an elementary plaquette, it acquires a phase $e^{i\gamma}$, where $\gamma = \frac{k_R a}{\pi}$ and k_R is the recoil energy. Then, the magnetic flux per plaquette is $\Phi = \gamma$. Retreived from [96].

Let us consider a 1D optical lattice with a single species of atom with some magnetic sublevels m_F:

$$m_F = -F, -F+1, ..., 0, 1, 2, ..., F. \tag{3.45}$$

Due to this internal degree of freedom of the atoms, it can be considered that they are placed in a 2D lattice. This lattice contains real space x-dimension and a synthetic y-dimension with $2F + 1$ sites.

Two additional Raman lasers couple the internal states of the atom, producing transitions between the state m_F to m_F+1. This transition provides a recoil momentum k_R, which appears as a phase factor. It depends on the position of the atom in the x axis. Then, a suitable combination of the optical lattice in the real $x-$ direction and the Raman coupling in the $y-$ synthetic direction leads to an effective 2D system under the presence of an uniform and perpendicular magnetic field $\mathbf{B}$. The artificial magnetic flux Φ depends strongly on the recoil momentum:

$$\Phi = \frac{k_R\, a}{\pi}, \tag{3.46}$$

where a the lattice spacing over the x-direction. At Fig. 3.5 there is a pictorial representation of the system.

Thus, this 2D system can exhibit fascinating phenomena like quantum Hall effect and topological phase transitions. The experimental achievement is supported by the fact that it is possible to manipulate systems with large number of internal states (like ^{40}K, with $F = 9/$ which contains 10 magnetic states).

Synthetic gauge fields in shaken optical lattices

Finally we present a new method for generating artificial gauge fields in optical lattice by using periodic lattice shaking techniques [97].

The Hamiltonian of the ultracold gas, which is time-dependent, reads as:

$$\hat{H}(t) = \hat{H}_0 + \sum_i v(t) b_i^\dagger b_i, \tag{3.47}$$

where

$$\hat{H}_0 = -\sum_{\langle i,j \rangle} t_{ij} (b_i^\dagger b_i + \text{H.c.}) + H_{\text{int}}, \tag{3.48}$$

is the usual time-independent Hamiltonian for an atomic gas on an optical lattice, where H_{int} contains on-site interactions between atoms and on-site interactions with an external potential.

It is convenient to transform the Hamiltonian (3.47):

$$\hat{H}(t) \to \hat{H}'(t) = \hat{U}^\dagger \hat{H}(t) \hat{U} - i\hbar \hat{U}^\dagger \frac{d\hat{U}}{dt}, \tag{3.49}$$

by introducing $\hat{U} = e^{i \sum_i \varphi_i(t) \cdot \hat{b}_i^\dagger \hat{b}_i}$ (see [97] for details). The time average of $\hat{H}'(t)$ leads to a new time-independent Hamiltonian which takes the form:

$$\hat{H}_{\text{eff}} = -\sum_{<ij>} t_{ij}^{eff} \hat{b}_i^\dagger \hat{b}_j + H_{\text{int}}, \tag{3.50}$$

where the effective hoppings t_{ij}^{eff} can be either positive or neg1ative. The realization on triangular and hexagonal optical lattices leads to the emergence of rich topological phases [98, 99].

This system can be used for the simulation of non-Abelian gauge fields. The scheme contains a two level atom, nameley $|a\rangle, |b\rangle$, on a 2D lattice with a Raman coupling Ω between the levels and site-dependent energy splitting ΔE_z for these levels. We refer the reader to the original work [97] for the details of the scheme. The Hamiltonian with a periodic driving term $v_i(t)$ is:

$$\hat{H}(t) = -\sum_{<ij>} t_{ij} (\vec{b}_i^\dagger \vec{b}_i + \text{H.c.}) + \sum_i \vec{b}_i^\dagger \left(\Delta E_z \sigma_z + \Omega \sigma_x + v_i(t) \right) \vec{b}_i, \tag{3.51}$$

where $\hat{\vec{b}}^\dagger = (\hat{\vec{b}}_a^\dagger, \hat{\vec{b}}_b^\dagger)$, we consider a sinusoidal driving term $v_i(t) = C_i \sin(\omega t)$ and the Pauli matrices are:

$$\sigma_x = \begin{pmatrix} 0 & 1 \\ 1 & 0 \end{pmatrix} \quad \sigma_z = \begin{pmatrix} 1 & 0 \\ 0 & -1 \end{pmatrix} \tag{3.52}$$

The time average leads to a dynamics governed by:

$$H = -\sum_{\langle i,j\rangle,\sigma,\sigma'} \tilde{t}_{ij} \vec{b}_\sigma^\dagger \, U_{\sigma,\sigma'} \, \vec{b}_{\sigma'}, \tag{3.53}$$

with $\sigma, \sigma' = a, b$ and $U_{\sigma,\sigma'}$ is the 2×2 hopping matrix, which may be unitary matrices by tuning the system properly. Thus, this method allows the simulation of external non-Abelian gauge fields.

3.4 Periodic quantum systems subjected to external gauge fields: the Hofstadter butterfly

We are going to study one of the simplest systems with the action of a gauge field: a 2D non-interacting quantum gas under the presence of an external and perpendicular magnetic field. Despite the simplicity of the system, as we will see, it represents the paradigm of topological phase transition.

The Hamiltonian for a non-interacting quantum gas in the presence of an external gauge field is given by:

$$\hat{H} = -t \sum_{\langle i,j\rangle} (\hat{\vec{\varphi}}_i^\dagger U_{ij} \hat{\vec{\varphi}}_j + \hat{\vec{\varphi}}_j^\dagger U_{ij}^\dagger \hat{\vec{\varphi}}_i), \tag{3.54}$$

which is the Hamiltonian (3.23) for non interacting atoms. The field $\hat{\varphi}_{i,\sigma}^\dagger$ ($\hat{\varphi}_{i,\sigma}$) creates(anihilates) a particle at site i with internal state σ. Then, $\hat{\vec{\varphi}}_i^\dagger = (\hat{\varphi}_{i,1}^\dagger, ..., \hat{\varphi}_{i,N}^\dagger)$.

Any point of the 2D lattice can be labelled by two integers, namely m_1, m_2, such that $\vec{r} = m_1 \vec{e}_x + m_2 \vec{e}_y$. Therefore, the last equation takes the form:

$$\hat{H} = -t \sum_{m_1 m_2} (\hat{\vec{\varphi}}_{m_1+1,m_2}^\dagger U_x^\dagger(m_1, m_2) \hat{\vec{\varphi}}_{m_1,m_2} + \hat{\vec{\varphi}}_{m_1,m_2+1}^\dagger U_y^\dagger(m_1, m_2) \hat{\vec{\varphi}}_{m_1,m_2} + \text{H.c.}). \tag{3.55}$$

Since we consider a non interacting quantum gas, we focus on the state of a one particle:

$$|\psi\rangle = \sum_{m_1,m_2,\sigma} \psi(m_1,m_2,\sigma)\hat{\varphi}^{\dagger}_{m_1,m_2,\sigma}|0\rangle, \tag{3.56}$$

where $|0\rangle$ is the vacuum state: $\hat{\vec{\varphi}}_{m_1,m_2}|0\rangle = 0 \ \ \forall\, m_1, m_2$, and $\psi(m_1,m_2,\sigma)$ the set of complex coefficients conforms the wave function of the state. It fulfils:

$$\sum_{m_1,m_2,\sigma} |\psi(m_1,m_2,\sigma)|^2 = 1. \tag{3.57}$$

The Schrödinger equation for the one particle quantum system reads as:

$$\begin{aligned}
&\sum_{m_1,m_2} \langle m_1,m_2|\hat{H}|m_1',m_2'\rangle\vec{\psi}(m_1',m_2') = E\vec{\psi}(m_1,m_2) \rightarrow \\
&U_x(m_1,m_2)\hat{\vec{\psi}}(m_1+1,m_2) + U_y(m_1,m_2)\hat{\vec{\psi}}(m_1,m_2+1) + \\
&+ U_x^{\dagger}(m_1,m_2)\hat{\vec{\psi}}(m_1-1,m_2) + U_y^{\dagger}(m_1,m_2)\hat{\vec{\psi}}(m_1,m_2-1) = -\frac{E}{t}\vec{\psi}(m_1,m_2),
\end{aligned} \tag{3.58}$$

where $\vec{\psi}(m_1,m_2) = (\psi(m_1,m_2,1),...,\psi(m_1,m_2,N))$.

The usual electromagnetic interaction is given by the U(1) gauge group, i.e. the complex number with modulus one. Then, the hopping matrix is given by:

$$U_{ij} = e^{iqaA_{ij}} \in \mathbb{C}, \tag{3.59}$$

where q is the charge of the particle. Due to the presence of U_{ij}, the particle acquires a phase U_{ij} when it hops from $i \rightarrow j$.

In this particular case of the U(1) gauge group, the internal space of the particle due the gauge symmetry is a 1D space. Then, we omit the vector symbol and the label σ for the wave function: $\vec{\psi} \rightarrow \psi$. Then, the Schrödinger equation (3.58) takes the form:

$$\begin{aligned}
&U_x\psi(m_1+1,m_2) + U_x^{*}\psi(m_1-1,m_2) \\
&+ U_y\psi(m_1,m_2+1) + U_y^{*}\psi(m_1,m_2-1) = -\frac{E}{t}\psi(m_1,m_2).
\end{aligned} \tag{3.60}$$

We consider a homogeneous magnetic field. Then, the vector potential $\mathbf{A}$ is chosen according to the Landau gauge:

$$\mathbf{A} = (0, Bm_1a, 0) \longleftrightarrow \nabla \times \mathbf{A} = \mathbf{B}. \tag{3.61}$$

This choice of the vector potential leads to the following hopping amplitudes:

$$\begin{aligned}(m_1, m_2 \to m_1 + 1, m_2) &\to U_x(m_1, m_2) = e^{iqaA_x} = 1,\\ (m_1, m_2 \to m_1, m_2 + 1) &\to U_y(m_1, m_2) = e^{iqaA_y} = e^{iqB\cdot m_1 a^2}.\end{aligned} \tag{3.62}$$

Therefore, when a particle hops along the closed path of an elementary plaquette, as is represented at Fig. 3.6, it picks up a phase Φ, which is the magnetic flux penetrating the plaquette:

$$\begin{aligned}&\psi(m1, m2) \to \psi'(m1, m2) =\\ &U_y^\dagger(m1, m2+1)U_x^\dagger(m1+1, m2+1)U_y(m1+1, m2)U_x(m1, m2)\ \psi(m1, m2) =\\ &U_y^\dagger(m1, m2+1)U_y(m1+1, m2)\ \psi(m1, m2) = e^{-iqB\cdot m_1 a^2} e^{iqB\cdot(m_1+1)a^2}\ \psi(m1, m2) =\\ &e^{iqBa^2}\ \psi(m1, m2) = e^{iq\Phi}\psi(m1, m2),\end{aligned} \tag{3.63}$$

The product of the hopping operators over the links along a closed path Γ is called *Wilson loop* W_Γ and it is a gauge invariant quantity, as we discussed at Section 2.6:

$$W_\Gamma = \prod_i U_i, \tag{3.64}$$

where U_i is the hooping amplitude on the link $i \to i + 1$. For this case, the particle hopping on a elementary plaquette the Wilson loop corresponds to:

$$\begin{aligned}W_C(m1, m2) = U_y^\dagger(m1, m2+1)U_x^\dagger(m1+1, m2+1)&\\ U_y(m1+1, m2)U_x(m1, m2) = e^{iq\Phi},&\end{aligned} \tag{3.65}$$

which is independent of the position.

Substituting the hopping elements U (3.62), finally the Schrödinger equation can be written as:

$$\begin{aligned}&\psi(m_1+1, m_2) + \psi(m_1-1, m_2)\\ &+ e^{i2\pi\nu\cdot m_1}\psi(m_1, m_2+1) + e^{-i2\pi\nu\cdot m_1}\psi(m_1, m_2-1) = -\frac{E}{t}\psi(m_1, m_2),\end{aligned} \tag{3.66}$$

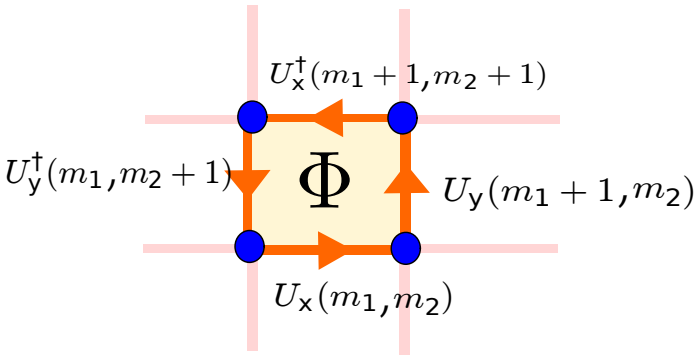

Figure 3.6: Closed path around an elementary plaquette on the 2D lattice. The path encloses a magnetic flux $\Phi = Ba^2$

where $\nu = \frac{\Phi}{2\pi} = \frac{qBa^2}{2\pi}$ and a^2q is the flux quanta per unit cell for a square plaquette of lenght a.

If $\nu = r/s,\ r, s \in \mathbb{Z}$, the Hamiltonian (3.54), which generates the previous Schrodinger equation, with the hopping amplitudes (3.62) is invariant under the space translations:

$$\begin{aligned} T_x : H(m_1, m_2) \to H'(m_1, m_2) = T_x H(m_1, m_2) T_x^\dagger = H(m_1 + s, m_2) = H(m_1, m_2), \\ T_y : H(m_1, m_2) \to H'(m_1, m_2) = T_y H(m_1, m_2) T_y^\dagger = H(m_1, m_2 + 1) = H(m_1, m_2). \end{aligned} \tag{3.67}$$

where the translation vector $\mathbf{T}$ is given by:

$$\mathbf{T} = (T_x, T_y) = (s, 1) = s\vec{e}_x + \vec{e}_y. \tag{3.68}$$

Then, the Bloch theorem (see Eq. (3.9)) can be applied to eigenvalue problem (3.66). The eigenstates of the Hamiltonian $\psi_k^{(\alpha)}(\mathbf{r})$ read as:

$$\psi_k^{(\alpha)}(\mathbf{r}) = u^{(\alpha)}(\mathbf{r}) \cdot e^{i\mathbf{kr}}, \tag{3.69}$$

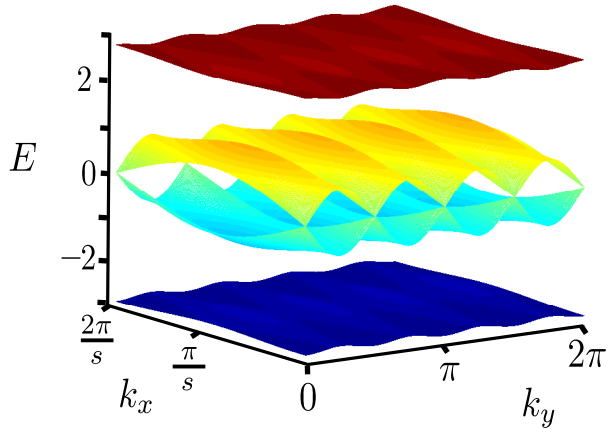

Figure 3.7: Energy Spectrum for a 2D charged particle subjected to a perpendicular magnetic field with $\phi = \frac{1}{4}$. It can be seen the gaps between the upper(lower) band and the next one and the Dirac cones appearing between the central bands.

where $u^{(\alpha)}(\mathbf{r}) = u^{(\alpha)}(\mathbf{r}+\mathbf{T})$ and the $\mathbf{k} = (k_x, k_y)$ is the quasi-momentum, which belongs to the first Brillouin zone:

$$k_x \in \left[-\frac{\pi}{as}, \frac{\pi}{as}\right],$$
$$k_y \in \left[-\frac{\pi}{a}, \frac{\pi}{a}\right]. \tag{3.70}$$

The index α labels the *bands*: each value of momentum k gives different solutions, corresponding to the different *bands*.

Since the periodicity in the y-direction is 1 (see Eq. (3.68)), the system of interest does not depend explicitly on the y coordinate. Therefore, the Schrödinger equation (3.66) takes the form:

$$e^{ik_x}u^{(\alpha)}(n+1) + e^{-ik_x}u^{(\alpha)}(n-1) + 2\cos(2\pi\nu n - ky)u^{(\alpha)}(n) = -\frac{E_\alpha}{t}u^{(\alpha)}(n), \tag{3.71}$$

which is known as Harper's equation [100].

The solution of this equation forms a spectrum composed of s bands which may be separated by gaps depending on the external magnetic field. In Fig. 3.7 it is shown the band structure for $\nu = 1/4$.

The plot of the energy spectrum as a function of the number of quanta of magnetic flux per plaquette, ν, leads to the emergence of a wonderful figure, the *Hofstadter butterfly*, which was first derived by D. Hotstadter [100]. This impressive figure it a self-similar object, it exhibits fractal nature (Figure 3.8). This figure has been extensively studied for the community since it was discovered.

Despite the simplicity of the system considered in this section, it represents a paradigmatic example of non-trivial topological order. It exhibits the so-called *quantum Hall effect*: at very low temperatures it presents a quantized transverse conductivity related to the appearance of edge currents. Thus, the system exhibits some topological invariants, it is a topological insulator.

3.5 The Quantum Hall effect

As we mentioned in the last section, the 2D system under the action of a perpendicular magnetic field represents a paradigm of a novel phase of matter, the

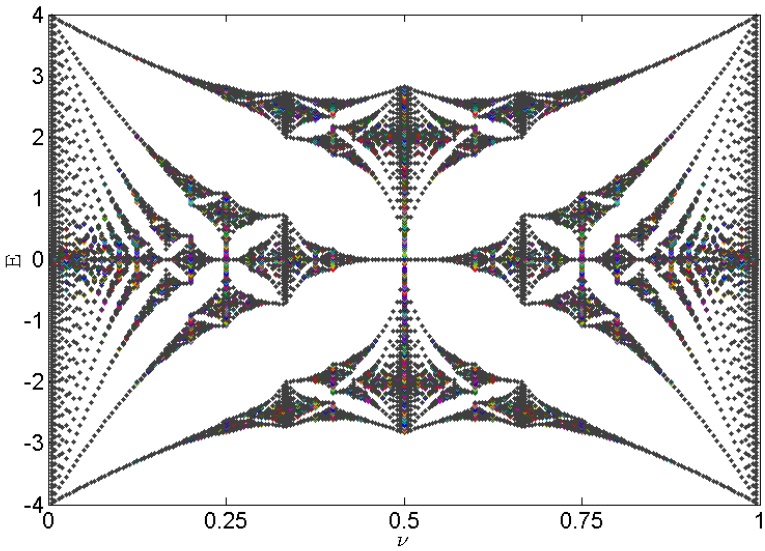

Figure 3.8: Energy spectrum as a function of the magnetic flux per plaquette for the quantum charged particle in a 2D lattice under the action of a constant and perpendicular magnetic field. The fractal figure is known as the *Hofstadter butterfly*.

topological insulator. We are going to treat this phenomenon in this section. We will start with a short introduction to the classical Hall effect, which appears in classical conductors. Next we will consider the quantum Hall system and we will derive their topological properties.

Let us start considering a classical a piece of a 2D conductor material under the action of some electric field E_x, acting in the $x-$ direction. The presence of E_x induces a current in the x-direction: j_x. However, the picture changes drastically when a perpendicular and homogeneous magnetic field $\mathbf{B} = (0, 0, B_z)$ is applied to the conductor. The Lorentz force, qvB causes the carriers to curve their trajectories. This effect produces the accumulation of charges in the edges of the material, and consequently the appearance of a non-zero voltage, V_H (Hall voltage) and a non-zero component of the electric field, E_y, in this y-direction (see Fig. 3.9). In a steady state, the electrical and magnetic forces on the carriers are balanced on the y-direction:

$$E_y = v_x B_z, \tag{3.72}$$

where v_x is the velocity in the x-direction.

Therefore, in such situation, the current $\mathbf{j}$ reads as:

$$\mathbf{j} = \sigma_M \mathbf{E}, \tag{3.73}$$

where $\mathbf{j} = (j_x, j_y)$, $\mathbf{E} = (E_x, E_y)$ and the conductivity σ_M is a matrix given by:

$$\sigma_M = \begin{pmatrix} \sigma_{xx} & \sigma_{xy} \\ \sigma_{xy} & \sigma_{yy} \end{pmatrix}. \tag{3.74}$$

The magnetic field causes the appearance of non-zero off-diagonal terms σ_{xy}. This phenomenon is referred as the *Hall effect*. The Hall conductivity $\sigma_H = \sigma_{xy}$ is the off-diagonal element of the conductivity σ_M. From Eq. (3.72) it turns out that the Hall conductivity is proportional to the inverse of the applied magnetic field:

$$\sigma_H \propto \frac{1}{B_z}. \tag{3.75}$$

However, when the system is cold enough, the quantum regime gets relevant and the behaviour of the Hall conductivity changes drastically. It is no longer inversely proportional to the magnetic field, it presents a series of plateaus for some quantized values [101]:

$$\sigma_H = N \frac{e^2}{h}, \tag{3.76}$$

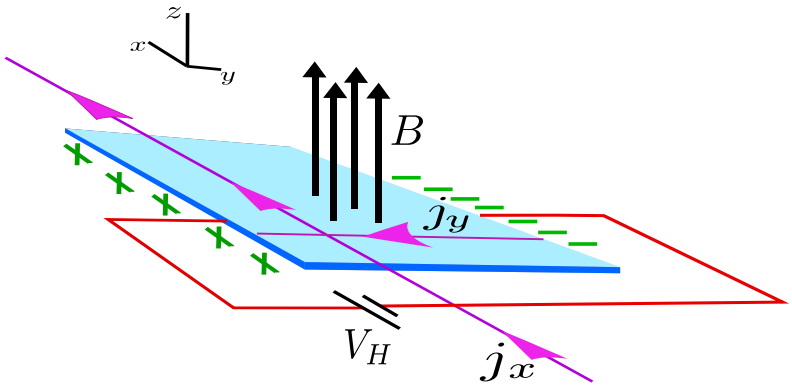

Figure 3.9: A 2D metallic material is placed on a perpendicular magnetic field **B**. The presence of an external field E_x leads to the appearance of current in the $x-$direction, j_x and additionally, another current, j_y in the $y-$direction, due the presence of the magnetic field. This current produces a difference in the electric potential, the *Hall* voltage (V_H), between the edges of the material.

where h is the Planck's constant, e is the electron charge and $N \in \mathbb{Z}$ is an integer number. Thus, the transverse conductivity only depends on fundamental constants of Nature. This is the so-called *integer quantum Hall effect*. In Fig. 3.10 the transverse and longitudinal conductivities are represented for a typical 2D quantum Hall system.

The conductivity can be calculated under the theory developed by R. Kubo, which is based on the linear response of a system under the action of an external perturbation [102], namely h_P. The starting Hamiltonian is given by:

$$\hat{H} = \hat{H}_0 + \hat{h}_P = \hat{H}_0 + \sum_{m_1,m_2} qaE_x \cdot \hat{\tilde{\varphi}}^{\dagger}_{m_1,m_2} \hat{\tilde{\varphi}}_{m_1,m_2}, \tag{3.77}$$

where $\hat{H}_0$ is the Hamiltonian appearing in (3.55), q, and a are the charge of the particle and the lattice spacing, respectively and E_x is the external electric field.

When a small electric field E_x is applied, the system can be studied by

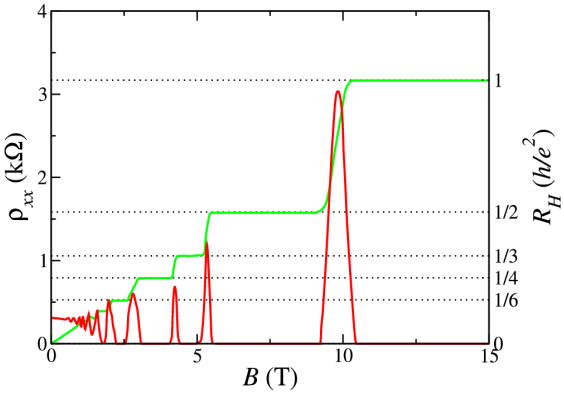

Figure 3.10: Transverse (R_H, green plot) and longitudinal (ρ_{xx}, red plot) resistance for a 2D quantum Hall system as a function of the applied perpendicular magnetic field B. It can be seen the plateaus for R_H at integral multiples of the von Klitzing constant h/e^2. Retreived from http://oer.physics.manchester.ac.uk/AQM2/Notes/Notes-4.4.html

considering perturbation theory. Thus, the conductivity reads as:

$$\sigma_{ij} = \frac{q^2\hbar}{i} \sum_{E_\alpha < E_F < E_\beta} \frac{\langle\alpha|v_j|\beta\rangle\langle\beta|v_i|\alpha\rangle - \langle\alpha|v_i|\beta\rangle\langle\beta|v_j|\alpha\rangle}{(E_\alpha - E_\beta)^2}, \tag{3.78}$$

where v_i is the velocity along the i direction, E_F is the Fermi energy and $|\alpha\rangle, |\beta\rangle$ are the eigenstates of the Hamiltonian $\hat{H}_0$ with energies E_α, E_β respectively.

Since the Harper equation (3.71) reads as:

$$\hat{H}_0(k_x, k_y)u^{(\alpha)} = E_\alpha u^{(\alpha)}, \tag{3.79}$$

the term $\langle\alpha|v_j|\beta\rangle$ of the conductivity can be written as [103]:

$$\langle\alpha|v_j|\beta\rangle = \frac{1}{\hbar}\left\langle u^{(\alpha)}\middle|\frac{\partial\hat{h}(k_x,k_y)}{\partial k_j}\middle|u^{(\beta)}\right\rangle = \frac{1}{\hbar}(E_\alpha - E_\beta)\left\langle u^{(\alpha)}\middle|\frac{\partial u^{(\beta)}}{\partial k_j}\right\rangle \tag{3.80}$$

Then, the conductivity can be expressed as:

$$\begin{aligned}\sigma_{ij} &= \frac{q^2}{i\hbar}\sum_{E_\alpha<E_F<E_\beta}\left[\left\langle u^{(\alpha)}\middle|\frac{\partial u^{(\beta)}}{\partial k_j}\right\rangle\left\langle u^{(\beta)}\middle|\frac{\partial u^{(\alpha)}}{\partial k_i}\right\rangle - \left\langle u^{(\alpha)}\middle|\frac{\partial u^{(\beta)}}{\partial k_i}\right\rangle\left\langle u^{(\beta)}\middle|\frac{\partial u^{(\alpha)}}{\partial k_j}\right\rangle\right] \\ &= \frac{q^2}{i\hbar}\sum_{E_\alpha<E_F}\left[\left\langle\frac{\partial u^{(\alpha)}}{\partial k_j}\middle|\frac{\partial u^{(\alpha)}}{\partial k_i}\right\rangle - \left\langle\frac{\partial u^{(\alpha)}}{\partial k_i}\middle|\frac{\partial u^{(\alpha)}}{\partial k_j}\right\rangle\right],\end{aligned} \tag{3.81}$$

where we stress that the last sum is performed over the occupied states below the Fermi level. Moreover, we have considered the completeness relation:

$$\sum_{E_\alpha<E_F}|u^{(\alpha)}\rangle\langle u^{(\alpha)}| + \sum_{E_\beta>E_F}|u^{(\beta)}\rangle\langle u^{(\beta)}| = \mathbb{I}. \tag{3.82}$$

The sum over the energies below the Fermi energy is carried out for each occupied band of all the possible momenta of the magnetic Brillouin zone. For the considered case, this momentum space is topologically a 2D *torus* $\mathbb{T}^2$: (k_x, k_y), where the ranges of the momenta k_x and k_y are expressed in Eq.(3.70). Then, the points $k_x = 0$ and $k_x = 2\pi/as$ are equivalent (similarly for the points $k_y = 0$ and $k_y = 2\pi$).

Then, the transverse conductivity σ_{xy} is given by:

$$\sigma_{xy} = \sum_\alpha \sigma_{xy}^{(\alpha)} = \sum_\alpha \frac{q^2}{i\hbar}\int_{\mathbb{T}^2} d^2k\left(\left\langle\frac{\partial u^{(\alpha)}}{\partial k_j}\middle|\frac{\partial u^{(\alpha)}}{\partial k_i}\right\rangle - \left\langle\frac{\partial u^{(\alpha)}}{\partial k_i}\middle|\frac{\partial u^{(\alpha)}}{\partial k_j}\right\rangle\right). \tag{3.83}$$

Defining the Berry's connection $\vec{A}^{(\alpha)}(k_x, k_y)$ in the magnetic Brillouin zone as:

$$\vec{A}^{(\alpha)}(k_x, k_y) = \left\langle \frac{\partial u^{(\alpha)}}{\partial k_j} \middle| \frac{\partial u^{(\alpha)}}{\partial k_i} \right\rangle - \left\langle \frac{\partial u^{(\alpha)}}{\partial k_i} \middle| \frac{\partial u^{(\alpha)}}{\partial k_j} \right\rangle = \langle u^{(\alpha)}(k_x, k_y) | \nabla_{\mathbf{k}} | u^{(\alpha)}(k_x, k_y) \rangle. \quad (3.84)$$

The conductivity for filled band α can be expressed as:

$$\sigma_{xy}^{(\alpha)} = \frac{q^2}{h} \frac{1}{2\pi i} \int_{\mathbb{T}^2} d^2k \left(\nabla_{\mathbf{k}} \times \vec{A}^{(\alpha)}(k_x, k_y) \right)_z, \quad (3.85)$$

which is the so-called *Thouless-Kohmoto-Nightingale-Den Nijs formula* or TKNN formula [104, 105].

The, , the total Hall conductivity can be expressed as a sum of topological invariant numbers, the *Chern numbers* (C_α) [104, 106, 107]:

$$\sigma_{xy} = \sum_\alpha \sigma_{xy}^{(\alpha)} = \frac{q^2}{h} \sum_\alpha C_\alpha, \quad (3.86)$$

where:

$$C_\alpha = \frac{1}{2\pi i} \int_{\mathbb{T}^2} d^2k \left(\nabla_{\mathbf{k}} \times \vec{A}^{(\alpha)}(k_x, k_y) \right) = \frac{1}{2\pi i} \int_{\mathbb{T}^2} d^2k \mathcal{F}(k_x, k_y), \quad (3.87)$$

is the Chern number related to the filled band α and we have introduced the Berry's curvature $\mathcal{F}(k_x, k_y)$:

$$\mathcal{F}(k_x, k_y) = \nabla_{\mathbf{k}} \times \vec{A}^{(\alpha)}(k_x, k_y). \quad (3.88)$$

Therefore, we can express the Hall conductivity as:

$$\sigma_{xy} = \sum_\alpha \sigma_{xy}^\alpha = \sum_\alpha \frac{q^2}{h} n^{(\alpha)} = \frac{q^2}{h} n, \quad (3.89)$$

where $n^{(\alpha)} \in \mathbb{Z}$ and $n = \sum_\alpha n^{(\alpha)}$.

For the quantum Hall system considered, the Hilbert space is a manifold parametrized by a 2D Torus $\mathbb{T}^2$. As we discuss in Appendix 9.1, the Chern number results from the non trivial topology of this manifold. Moreover, this is an intimately relation between this feature and the geometric phase [108], which is also discussed in this Appendix.

Chapter 4

Layered Quantum Hall Insulators with Ultracold Atoms

As we have reviewed in last section, in recent years there has been an incresing interest in the study and implementation of quantum simulators of artificial gauge fields in ultracold atomic platforms. These studies open the posibility of the characteritzation of novel states of matter, as the topological insulators. The simplest paradigmatic example of topological transport is the integer quantum Hall effect taking place at low enough temperatures (see Section 3.5)), where the transverse conductivity takes only quantized values. Soon after the topological considerations of two-dimensional insulator phases the theory has been generalized to three dimensions where the transverse conductiviy is a tensor [109, 110]. However, in three dimensions one usually suffers from the collapse of the energy gaps and the system remains an insulator only in special situations. Another generalization of the integer quantum Hall effect to higher degrees of freedom is to stack more layers of more or less independent quantum Hall insulators on top of each other. Since inter-layer tunneling is small well developed gaps remain. A lot of work has been devoted to study the effects of bi- or multi-layer structures on the quantum Hall effect, especially the fractional one [111, 112]. In bilayer graphene the TC plateaus were studied and a new type of IQH effect was found with a zero-level anomaly interpreted by a 2π Berry's phase of the charge carriers [113].

In this chapter, we propose a novel scheme for the realization of synthetic gauge fields in ultracold atomic setups. Particularly we focus in non-Abelian gauge fields, where the difficulty arising from the multicomponent nature of particles sensitive to a non-Abelian gauge field is overcome quite naturally by mapping the gauge index to an external coordinate, thus rendering the realization of a non-Abelian external gauge field experimentally easier. The external coordinate is the position in a perpendicular direction. Depending on whether the extension of the system is finite or infinite in this direction, one can realize compact, or non-compact external gauge groups, respectively. In this chapter we consider the non-compact case. We propose therefore an experimental scheme with single component ultracold atoms in a 3D optical lattice with cubic geometry but anisotropic hoppings to mimic the behavior of a 2D system but with (possibly) infinitely many internal states.

Until now not much interest has been directed towards non-compact gauge groups, which is mainly rooted in that these gauge groups have ill defined invariants, such as Wilson loops. However, as external fields they can induce topological phases with peculiar transport properties. The question is what kind of physics does it yield, and what can be their physical realization? This work answers positively to both questions.

Here we study the effects of the simplest non-compact gauge group, namely the *Heisenberg-Weyl group*, which is generated by two elements, say $\hat{z}$ and $\hat{p}_z$, with the canonical commutation relation:

$$[\hat{z}, \hat{p}_z] = i\mathbb{I}. \tag{4.1}$$

As a consequence of non-compactness this commutator cannot be represented in finite dimensions (one arrives to a contradiction by taking the trace in both sides of the last relation for finite matrices).

We show that despite of the above difficulties this gauge group can be realized relatively simply with today's technology of ultracold fermions and optical lattices by identifying the role of the Heisenberg Weyl group in layered 3-dimensional lattice systems. We provide the phase diagram of the system. We also show that the multilayer structure provides further prospects beyond the zero level anomaly, such as a significant tunability of the positions and strengths of the quantum Hall plateaus. In a possible interferometric application such a strong transverse conductivity can, in principle, enhance the precision of the measurement.

4.1 Lattice formulation of the Heisenberg-Weyl gauge group theory

A 2D non-interacting ultracold fermionic gas coupled to an external gauge field in a sufficiently deep optical lattice is described by the tight binding Hamiltonian (3.54):

$$\hat{H}_{2\mathrm{d}} = t \sum_{m,n,\sigma,\sigma'} \Big(U_x(m,n,\sigma)\, \hat{c}^{\dagger}_{m+1,n,\sigma'} \hat{c}_{m,n,\sigma} + U_y(m,n,\sigma)\, \hat{c}^{\dagger}_{m,n+1,\sigma'} \hat{c}_{m,n,\sigma} + \mathrm{H.c.} \Big), \tag{4.2}$$

where $\hat{c}_{m,n,\sigma}$ ($\hat{c}^{\dagger}_{m,n,\sigma}$) is the fermion annihilation (creation) operator at position $\vec{r} = m\,a\,\vec{e}_x + n\,a\,\vec{e}_y$ (a being the lattice spacing and m, n integer numbers) and σ is the gauge coordinate corresponding to the internal space. The hopping amplitude is given by t.

As we discussed in Chapter 2, the link matrices $U^x(m,n)$ and $U^y(m,n)$ encode the gauge degree of freedom in a lattice. For electromagnetism, the U(1) gauge theory, the hopping matrices are ordinary site dependent phase factors (see Eq.(3.59)). If the gauge group is non-Abelian, but compact they become unitary matrices with finite dimension. Here we choose them to be elements of the Heinsenber-Weyl group, which is non-compact, and it does not have finite dimensional representation. Then, the link matrices become infinite dimensional. Specifically we focus the study on the following choice:

$$\begin{aligned} U_x(m,n) &= e^{i\alpha\,\hat{p}_z}, \\ U_y(m,n) &= e^{2\pi i(\beta\,m + \gamma\,\hat{z})}. \end{aligned} \tag{4.3}$$

The operators $\hat{z}$ and $\hat{p}_z$ obey the commutation relations given in (4.1) The effect of these operators for a given physical state ψ is:

$$\begin{aligned} &\hat{z}\psi(z) = z\psi(z) \rightarrow e^{i\gamma\hat{z}}\psi(z) = e^{i\gamma z}\psi(z), \\ &e^{i\alpha\hat{p}_z}\psi(z) = \psi(z+\alpha). \end{aligned} \tag{4.4}$$

where z labels the internal space of ψ. Then, $\hat{z}$ is a diagonal operator in the z position basis, while $\hat{p}_z$ is the generator of translations in such internal space.

The $x-y$ position dependence of the vector potential has been chosen here similarly to the Landau gauge (see Eq.(3.61)), which in the case of U(1) electrodynamics gives a homogeneous magnetic field responsible for the quantum Hall effect. The numeric parameters α, β, and γ are real numbers, which can be controlled experimentally, and are measuring the flux penetrating each plaquette.

The key idea of our work is to map the gauge coordinate σ to the real external z direction. Let us further assume, that the z direction also supports a sufficiently deep optical lattice with lattice spacing a. So the 2-dimensional problem with infinitely many internal states is mapped to a true 3-dimensional problem, where the position is given by $\vec{r} = m\,a\,\vec{e}_x + n\,a\,\vec{e}_y + \sigma\,a\,\vec{e}_z$. Since a particle can hop only from site to site – even in the z direction, therefore the parameter α, appearing in Eq. (4.4), has to be integer times the lattice spacing.

By considering the simplest choice, $\alpha = a$, then $U^x(m,n)$ becomes the translation operator in the z direction by one lattice site (see (4.3)). Therefore, the tunneling operators in the lattice Hamiltonian (4.2) act as:

$$\begin{aligned} U_x(m,n,\sigma)\hat{c}^\dagger_{m+1,n,\sigma'}\hat{c}_{m,n,\sigma} &= \hat{c}^\dagger_{m+1,n,\sigma}\hat{c}_{m,n,\sigma-1}, \\ U_y(m,n,\sigma)\hat{c}^\dagger_{m,n+1,\sigma'}\hat{c}_{m,n,\sigma} &= e^{2\pi i(\beta\, m+\gamma\,\sigma)}\hat{c}^\dagger_{m,n+1,\sigma}\hat{c}_{m,n,\sigma}. \end{aligned} \tag{4.5}$$

The first expression represents the annihilation of a fermion at site $\tilde{r}_1 = (m,n,\sigma-1)$ and creation of a fermion at site $\tilde{r}_2 = (m+1,n,\sigma)$, where $\tilde{r}$ is a vector with components belonging to the real space $x-y$ together with the internal component σ. The second expression indicates that the hopping in the y-direction is accompanied by a phase factor which depends on the external position x and on the internal one σ

Going back to the mapped real $x-y-z$ space, the process at the previous equation describes a tunnelling process in the xz plane which is special because when the particle tunnels in the x direction by one to the left (right), it has to tunnel one position in the z direction up (down) too. Then, it is convenient to introduce new coordinates in order to characterize this simultaneous hopping in both directions:

$$\begin{aligned} \xi &= \frac{1}{2}(m-\sigma), \\ \eta &= \frac{1}{2}(m+\sigma). \end{aligned} \tag{4.6}$$

Then, the Hamiltonian takes the following form:

$$\hat{H}_{\mathrm{HWG}} = t \sum_{\xi,\eta,n} \left(\hat{c}^{\dagger}_{\xi+1,\eta,n} \hat{c}_{\xi,\eta,n} + e^{i\theta_y}\, \hat{c}^{\dagger}_{\xi,\eta,n+1} \hat{c}_{\xi,\eta,n} + \mathrm{H.c.} \right). \tag{4.7}$$

The phase factor acquired by tunneling along the y-direction reads in the new coordinates as

$$\theta_y = 2\pi\beta'\xi + \pi\gamma'\eta, \tag{4.8}$$

with the definitions $\beta' \equiv \beta - \gamma$, and $\gamma' \equiv \beta + \gamma$.

As there is no tunneling along the η-direction, Eqs. (4.7) and (4.8) describe a system composed by independent 2-dimensional integer quantum Hall systems layered on top of each other.

Each layer behaves similarly, except for η even, ξ takes integer values and for η odd, ξ takes half integer values. The tunneling phase Eq. (4.8) depends also on η (the quantum number indexing the different planes). Refer to Fig. 4.1 a) for illustration.

We study the eigenvalue problem of the Schrödinger equation for the single quantum particle system (see Sec. 3.4):

$$\begin{aligned} &\sum_{\xi',n'} \langle \xi,\eta,n|\hat{H}_{\mathrm{HWG}}|\xi',\eta,n'\rangle \psi(\xi',\eta,n') = E\psi(\xi,\eta,n) \rightarrow \\ &\psi(\xi+1,\eta,n) + \psi(\xi-1,\eta,n) + \\ &+ e^{i\theta_y}\psi(\xi,\eta,n+1) + e^{-i\theta_y}\psi(\xi,\eta,n-1) = -\frac{E}{t}\psi(\xi,\eta,n), \end{aligned} \tag{4.9}$$

where $\psi(\xi,\eta,n)$ is the one particle wave function:

$$|\psi\rangle = \sum_{\xi,\eta,n} \psi(\xi,\eta,n)\hat{c}^{\dagger}_{\xi,\eta,n}|0\rangle, \tag{4.10}$$

and $|0\rangle$ is the vacuum state: $\hat{c}_{\xi,\eta,n}|0\rangle = 0 \;\; \forall\, \xi,\eta,n$.

Each value of η gives an independent Schrödinger equation, whose solution lies in a 2D ξ-n plane:

$$\psi(\xi,\eta,n) \rightarrow \psi_{\eta}(\xi,n). \tag{4.11}$$

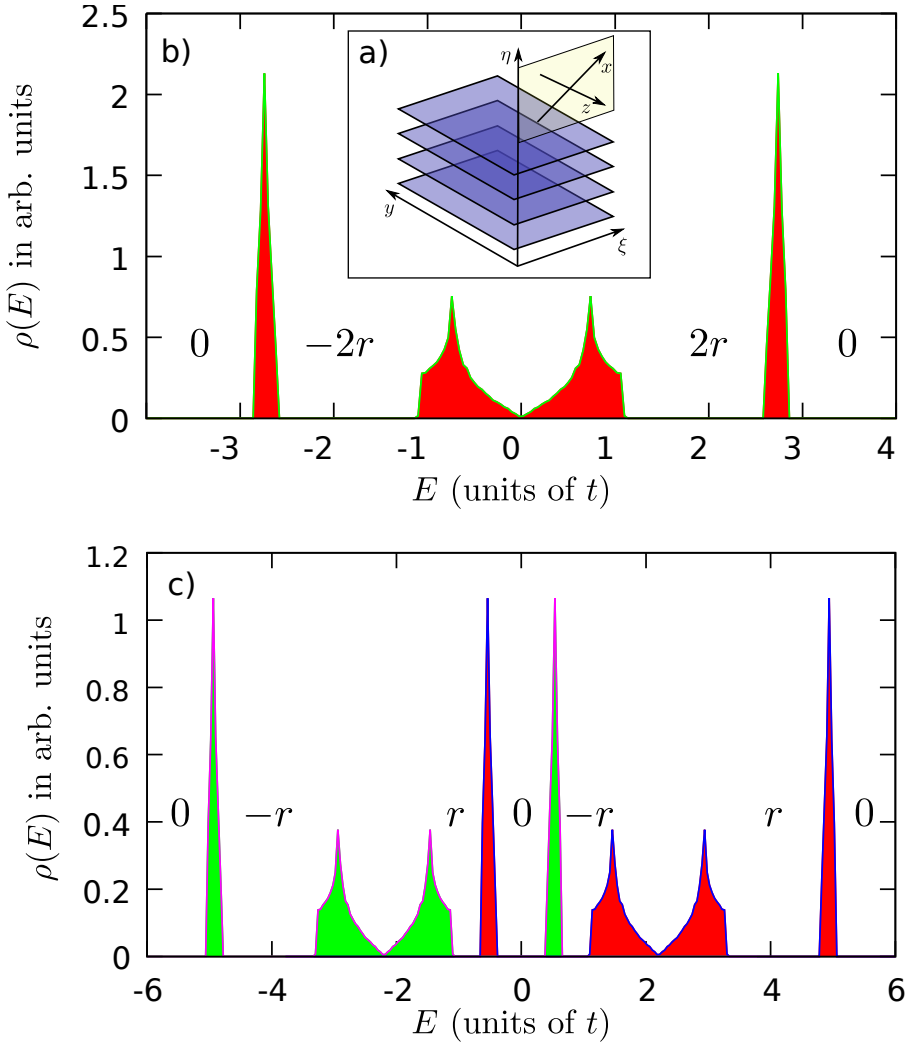

Figure 4.1: a) The schematic illustration of the new coordinates, the system splits into independent quantum Hall layers. b)-c) The density of states for $\beta' = 1/4$ as a function of the energy. In subfigure b) each different η plane contributes equally to the density of states. In c) the value of the staggered potential in Eq. (4.18) is chosen to be $\lambda = 2.2t$. The net transverse conductivitys are shown on the figure for each band gap.

We chose β' as a rational number: $\beta' = p/q$ with p and q co-prime integers. In this case the Hamiltonian is invariant under translations in the ξ coordinate by q lattice positions and under translations int the y-direction by 1 lattice position:

$$\begin{aligned} T_\xi &: H_{\mathrm{HWG}}(\xi,\eta,n) \to H_{\mathrm{HWG}}(\xi+q,\eta,n) = H_{\mathrm{HWG}}(\xi,\eta,n), \\ T_y &: H_{\mathrm{HWG}}(\xi,\eta,n) \to H_{\mathrm{HWG}}(\xi,\eta,n+1) = H_{\mathrm{HWG}}(\xi,\eta,n) \end{aligned} \tag{4.12}$$

Then, we proceed as in Section 3.4, applying the Bloch's theorem:

$$\psi_\eta(\xi,n) \to \psi_\eta^{(r)}(\xi,n) = u_\eta^{(r)}(\xi) e^{i(k_\xi \xi + k_y n)} \tag{4.13}$$

where r is the *band index* and the function $u_\eta^{(r)}$ has the perodicity in the $\xi-$direction: $u_\eta^{(r)}(\xi) = u_\eta^{(r)}(\xi+q)$. Thereby, the Schrödinger equation (4.9) can be written as a Harper equation:

$$e^{ik_\xi \xi} u_\eta^{(r)}(\xi-1) + e^{-ik_\xi \xi} u_\eta^{(r)}(\xi+1) + 2\cos(2\pi\beta'\xi + \pi\gamma'\eta - k_y) u_\eta^{(r)}(\xi) = -\frac{E}{t} u_\eta^{(r)}(\xi). \tag{4.14}$$

Concretely, we consider the case for $\beta' = 1/4$, where we have 4 bands for each layer η, which are the lattice counterparts of the Landau levels of the continuum case. In such case, the Brilluoin zone defines a 2D torus:

$$\mathbb{T}^2 : k_\xi \times k_y \qquad k_\xi \in [0, 2\pi/q], \quad k_y \in [0, 2\pi]. \tag{4.15}$$

We calculate the density of states for this specific value of β' by direct diagonalization and plot in Fig 4.1 b). It can be seen that the central two bands show the features of a Dirac cone like touching.

When the Fermi energy lies inside a band, the system is metallic and has a non-vanishing longitudinal conductivity. In contrast, when the Fermi energy lies inside a gap, the longitudinal conductivity is zero, and quantum Hall effect can take place: the transverse conductivity is integer times the conductivity quantum.

Since the spectrum is independent of the value of η, the effect of layering is just a degeneracy in the spectrum by the number of planes. For these (longitudinally) insulating phases the transverse conductivity of each plane is given the expression given by the TKNN formula (see Eq. (3.85)):

$$\sigma^\eta = \sum_\alpha \sigma^{(\alpha),\eta} = \sum_\alpha C^{(\alpha),\eta} = \frac{1}{2\pi i} \int d^2k \, \mathcal{F}^\eta(k_\xi, k_y), \tag{4.16}$$

where we have considered $h = 1$ and $q = 1$ (which defines unit for the charge of the Heisenberg Weyl group interaction). The sum is performed over all the filled bands. The expression for the *Chern number* $C^{(\alpha),\eta}$ is given at (3.87), and we have introduced the Berry's curvature $\mathcal{F}^{\eta}$ (3.88):

$$\mathcal{F}^{\eta} = \nabla_{\mathbf{k}} \times \vec{A}^{\eta}(k_{\xi}, k_y), \tag{4.17}$$

with the Berry's connection $\vec{A}^{\eta}(k_{\xi}, k_y) = \sum_{r=1}^{N} \langle u^{(r)}_{k_{\xi},k_y} | \nabla_{\mathbf{k}} u^{(r)}_{k_{\xi},k_y} \rangle$ (see Eq. (3.84)).

We have computed the transverse conductivity with the efficient algorithm of Fukui et al [114]. As we showed in the last chapter, the transverse conductivity takes only integer values since it is a topological invariant: the first Chern class of the U(N) principal bundle over the Brillouin-zone torus (k_{ξ}, k_y). Furthermore at every η plane the transverse conductivity can be only 0, 1 or -1, depending on whether the Fermi energy lies outside the band structure (in this case the lattice is either empty or fully filled and the conductivity is zero), or it lies inside a gap between the satellite bands and the central band (for negative energies the transverse conductivity is negative and for positive energies it is positive for our model and choice of parameters). Accordingly, when we add up all of the contributions to the transverse conductivity from each of the planes we get zero if the Fermi energy lies outside of the band structure, or we get $\sigma_{\perp} = \sum_{\eta} \sigma_{\eta} = \pm 2r$, where $2r$ is the number of planes, what we choose to be even. We have also shown in Fig. 4.1 b) and c) the net transverse conductivity of the band gaps.

4.2 Effects of a staggered potential

The above combination rule of the transverse conductivity can be controlled in a striking way by applying a staggered potential of strength λ, added to the Hamiltonian as

$$H_{\lambda} = H_{\mathrm{HWG}} + \lambda \sum_{\xi,\eta,n} (-1)^{\eta} \, c^{\dagger}_{\xi,\eta,n} c_{\xi,\eta,n}, \tag{4.18}$$

which shifts the energy spectrum locally by $\pm\lambda$ for the even/odd planes.

In Fig. 4.1 c) we have plotted the resulting density of states for $\lambda = 2.2t$. Note, that the original degeneracy is partially lifted by the 2λ energy difference of the planes with different lambda parities. One can imagine as we start to increase λ from zero to a finite value that the original 3 bands start to widen and

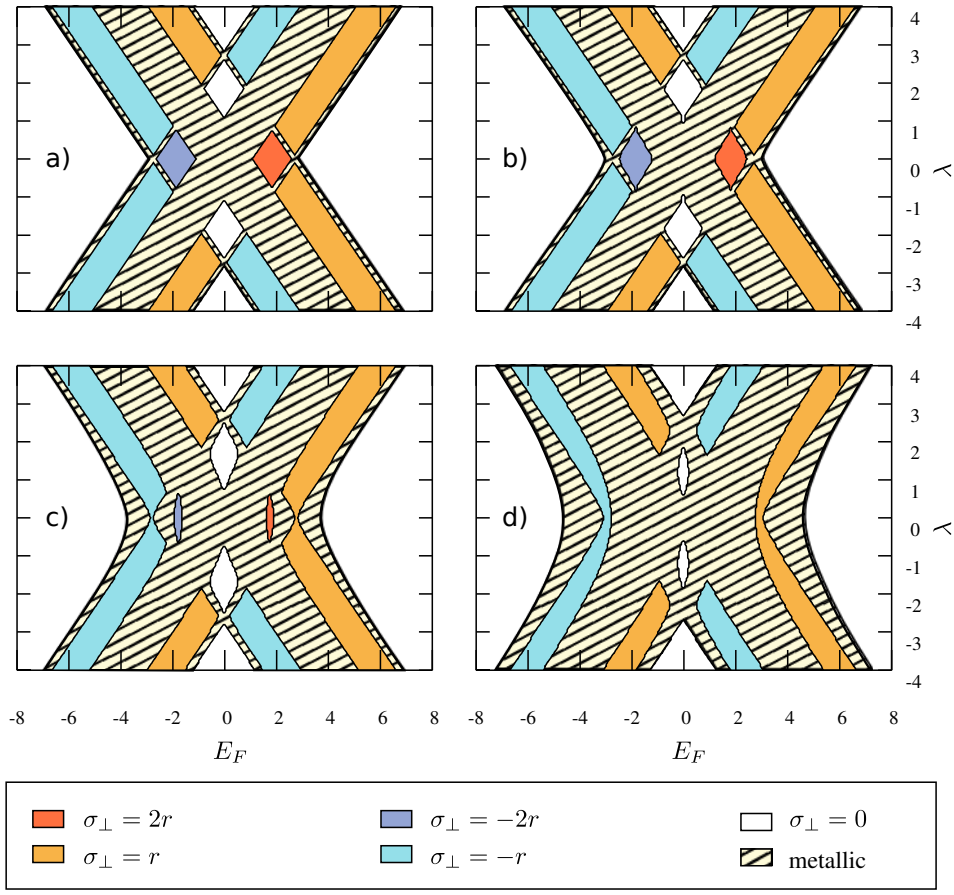

Figure 4.2: The phase diagram of the system in the Fermi energy – staggered potential plane (measured in the hopping strength). Subfigure a) corresponds to the Hamiltonian (4.18). Subfigure b)-d) correspond to Eq. (4.19) with $\epsilon = 0.1$ b), $\epsilon = 0.5$ c), and $\epsilon = 1.0$ d). The flux is taken to be $\beta' = 1/4$. The hatched regions represent areas where either the even or the odd planes are metallic.

then separate, since the one particle energies on the even η planes are getting bigger, while those on the odd η planes are getting smaller.

The phase diagram in the (E_F, λ) plane is plotted in Fig. 4.2 a). One can get a grasp of the structure by imagining that the 3 energy bands of Fig. 4.1 b) get shifted by $\pm\lambda$ providing 3 tilted stripes of metallic behaviour for the even and another 3 stripes (tilted to the other direction) for the odd planes. At the intersections of the stripes all of the planes are metallic at the same time. In the insulating regions, i.e. when the point (E_F, λ) lies outside of the metallic stripes, the net transverse conductivity is the sum of the contributions of the even and odd planes: $\sigma_\perp = \sigma_e + \sigma_o$. With the variation of λ one can achieve that the Fermi energy falls into different band gaps for the even and odd planes, where $\sigma_e \neq \sigma_o$. In the $\beta' = 1/4$ case the gaps are characterized by $\sigma_{e,o} = \{0, -r, +r, 0\}$. Therefore one can have $\sigma_\perp = -2r$, if both set of planes have $\sigma_{e,o} = -r$, and $\sigma_\perp = +2r$ for $\sigma_{e,o} = +r$. We highlight that the zero net transverse conductivity is realized in two ways: either by $\sigma_{e,o} = 0$, or by $\sigma_e = -\sigma_o$. In this latter case the even and odd planes have opposite transverse conductivities, which is similar to the spin quantum Hall effect (for a review see Ref. [115]).

There is an important difference though: in our case the net transverse conductivity is an integral number, not just a Z_2 invariant, the higher is its value the greater is the transverse current. If a quantum phase transition is induced either by the change of the Fermi energy, or by the variation of λ, the transverse conductivity changes at least by half of the number of planes, not just by one conductance quantum.

Another physical picture can be assigned to the insulating regions of the phase diagram based on the bulk-boundary correspondence [116]: by considering the x direction finite, when the Fermi energy is inside a bulk gap with nonzero transverse conductivity, edge states (responsible for the transverse current) traverse the energy spectrum between the two bulk bands surrounding the gap.

In the $\beta' = 1/4$ flux phase one can have a maximum of 1 pair of edge states per plane and the direction of their propagation is determined by the sign of the transverse conductivity. Fig. 4.3 shows a qualitative picture of the possible edge state configurations. In subfigure a) all planes are in the same QHI phase and the transverse currents carried by the edge states add together 'constructively'. Such a situation corresponds to the two diamond shaped regions with $\sigma_\perp = \pm 2r$ of Fig. 4.2 a). In subfigure 4.3 b) every second plane is in a QHI phase while the other half of the planes are either in a metallic or in a normal insulator

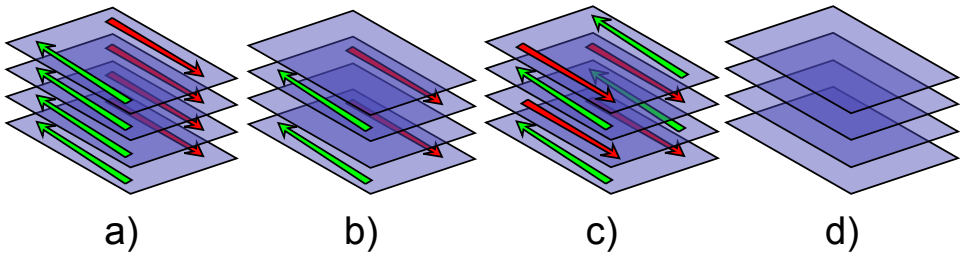

Figure 4.3: The edge states. In situation a) all of the planes are in the same spectral gap, therefore the edge states of the different planes contribute equally to the transverse conductivity; in b) half of the planes is either metallic, totally empty or completely filled thus lacking the edge states, while the other half of the planes have a transverse conductivity of 1; in c) the different parity planes have oppositely propagating edge states; in d) all of the planes are either metallic or trivial insulators, there are no edge states in this case.

phase. Therefore $\sigma_\perp = \pm r$ and the corresponding regions in the phase diagram are those marked out by the integer quantum Hall stripes (except for their intersecting diamond shape regions). The situation in Fig. 4.3 c), where the edge states of the neighbouring planes are counter-propagating, is situated in the intersections of the oppositely transverse conducting integer quantum Hall stripes of Fig. 4.2 a). The net transverse conductivity is zero and an analogy with quantum spin Hall insulators can be established [115].

4.3 Interplane tunneling

In experiments with ultracold atoms in anisotropic 3D lattices it is possible, that the inter-plane tunneling is not exactly zero, and therefore the Heisenberg Weyl group is not realized perfectly. Therefore an analysis of the robustness of the accumulated transverse conductivity is needed.

One introduces tunnelling between the different planes (in a controllable way) by adding an extra term to the Hamiltonian:

$$H_{\lambda,\epsilon} = H_\lambda + \epsilon \sum_{\xi,\eta,n} \left(c^\dagger_{\xi,\eta,n} c_{\xi,\eta+1,n} + \text{H.c.} \right), \tag{4.19}$$

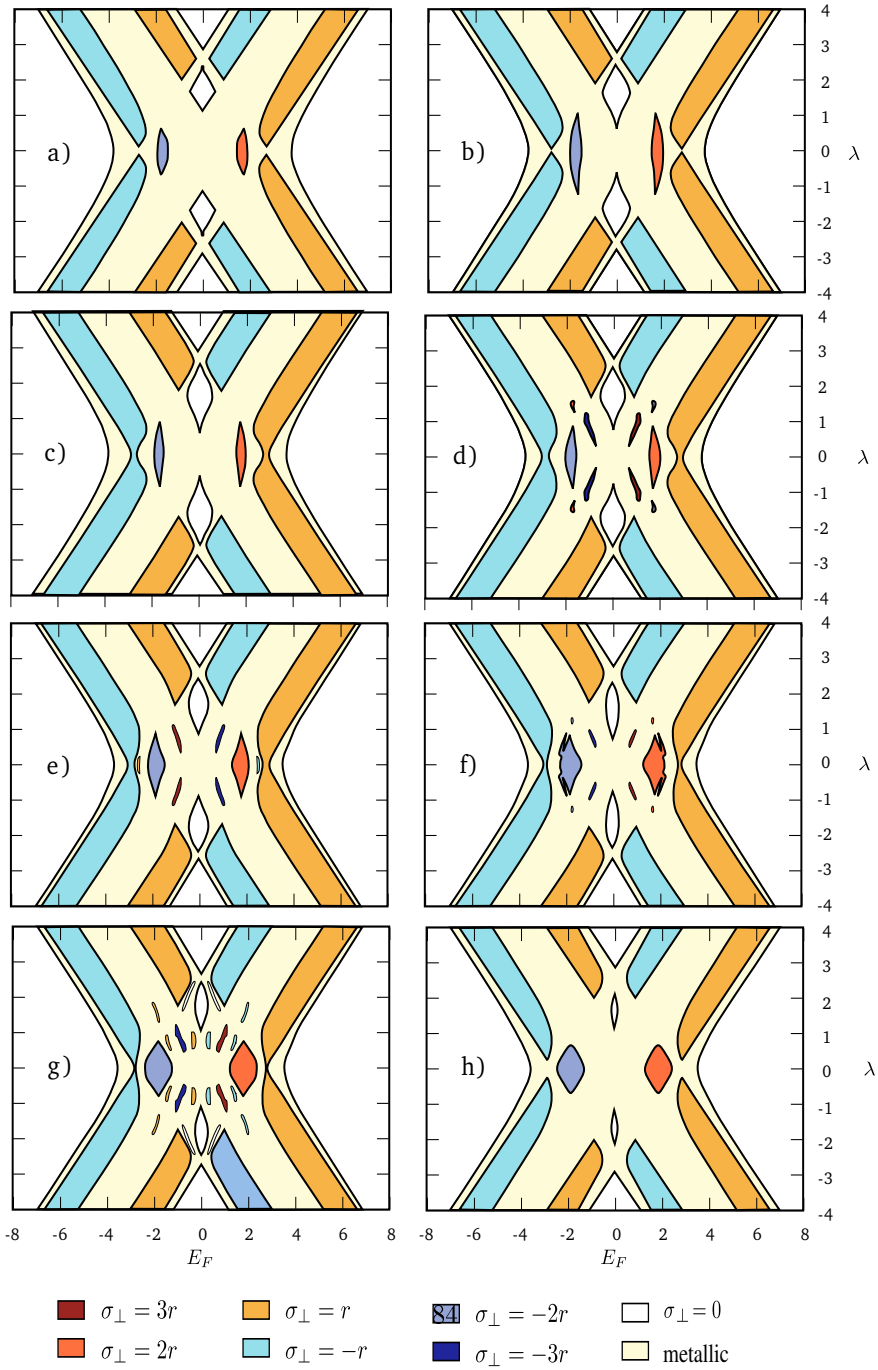

Figure 4.4: The phase diagram for $\epsilon = 0.5$, $\beta' = 1/4$, $\gamma' = p'/q'$, with $q' = 7$ and $p' = 0, 1, 2, 3, 4, 5, 6, 7$ from a) to h).

then η will not be a good quantum number any longer, and consequently σ_η of the individual planes looses its meaning. As an effect of the ϵ strength inter-plane hopping the eigenstates of the different η planes get hybridized and the conducting regions get widened as shown in the phase diagram Fig 4.2 b)-d). However, while ϵ is sufficiently small, the gaps persist and the net $\sigma_\perp$ keeps its significance.

In this case the Brillouin zone is a 3-dimensional torus and one needs to make 2-dimensional slices to get topological invariants [104]. In our case the only nonzero invariant is the one with slicing along a constant k_η value. (For nonzero values of the other components of the conductivity tensor one needs first a gap closing and than a reopening.) As the inter-plane tunneling amplitude is raised the QHI regions shrink and give way to the metallic phase. There is a competition between the staggered potential strength λ and the tunnelling strength ϵ. Therefore the high transverse conductivity QHI regions vanish first (around $\epsilon_c \approx 0.8$) since they are located around $\lambda = 0$.

When $\epsilon \neq 0$ the edge currents are not protected against back-scattering by any discrete symmetry, in contrary to the case of the spin QHIs. If the state of the system is located in the $\sigma_\perp = 0$ islands inside the metallic stripes, corresponding to the alternating transverse edge current setup of Fig. 4.3 c), then inter-plane tunneling causes an effective back scattering, and the originally massless Dirac-like dispersions of the edge states develop mass gaps. The edge states of the other integer quantum Hall regions ($\sigma_\perp \neq 0$) retain their topologically protected nature and the massless touching of their Dirac cones.

So far we have not yet studied the consequences of varying the γ' flux parameter of the vector potential (4.8). While $\epsilon = 0$ the distinct planes are independent and the inclusion of $\gamma' \neq 0$ does not change the transport properties. In Fig. 4.2, the first panel corresponds essentially to uncoupled layers with constant synthetic Abelian magnetic field. This is because the Heisenberg Weyl gauge potential is restricted to $\epsilon = 0$. In contrast, in Fig. 4.4 the full non-Abelian nature of the Heisenberg Weyl group is considerd by setting $\gamma' \neq 0$ together with $\epsilon \neq 0$. The first panel again essentially reduces to the case of constant synthetic Abelian magnetic field, but for the coupled layers. The following panels illustrate then the effects of non-Abelian Heisenberg Weyl gauge fields on the conductivity in coupled layers. This effect consist in appearance of novel insulating islands with transverse conductivities equal to $\pm 3r$ in these new regions, which are bigger then those for $\gamma' = 0$. It constitutes one of the improtant results of this study.

4.4 Experimental realization

The experimental implementation of the Heisenberg Weyl group is straightforward. According to Eq. (4.7) one needs to create a 3-dimensional optical lattice with cubic geometry in 2-dimensions ($\xi - y$ planes) and an AB type layering in the 3rd (η) direction. The gauge potential (4.8) is actually just a phase in this basis, and therefore it can be realized in the usual way [79, 117, 66]. One only needs a staggered potential along the 3rd (η) direction and a control over the tunneling amplitude along this direction. All of these elements are in the reach of current experimental technologies.

The detection of the transverse conductivity and the edge states is a currently running issue. There are different proposals what we are aware of:

- by changing the atomic isotope to a bosonic one, loading them into and finally imaging them in the edge states [118]
- with the help of stimulated Raman scattering one can measure one particle excitations directly [119]
- with the help of Bragg scattering one can directly measure the dynamical structure factor and hence also the single particle excitations [120]
- by a trapping potential which creates a sharp interface, e.g. by controlling the hopping in the y direction and exciting the edge state channel by a focused laser beam [121, 122].

Chapter 5

Gauge fields emerging from time reversal symmetry breaking in optical lattices

In the two previous chapter we have considered the implementation of quantum simulators of external gauge fields in ultracold atomic platforms. The aim of this chapter is to study another, somewhat simpler, proposal with only a single species of ultracold atoms to simulate a 2+1 dimensional U(1) lattice gauge theory with a Chern-Simons term. Our proposal is . The novel features of this new proposal are: i) it is based on the observation that low energy excitations of certain Mott insulators phases can be described by emergent lattice gauge theories [19, 111] ii) it supports the simulation of dynamical gauge theories [111].

The study of Mott insulating states of spin-1/2 systems has a long history in condensed matter physics. The main motivation of these studies lies in their relation to high-T_c superconductivity [19]. Ultracold atoms in optical lattices provides a nice alternative to study Mott insulators and quantum magnetism, since the optical lattice is free of any defects and there is a great liberty in choosing or even tuning the geometry of the lattice even in situ.

In the last decade Mott states of bosonic [60] as well as fermionic [123] atoms have been reached experimentally, however, it still remains a challenge to reach quantum magnetism and detect magnetic correlations. The main reason behind the difficulties is the limitation on cooling, since with present experimen-

tal methods it is hard to access the temperatures at the scale of the magnetic superexchange, i.e. in the range of few nano Kelvins (for recent progress see [124, 125]). Nevertheless, a series of nice experiments were developed to catch quantum [126, 127, 128], or even classical [129] (frustated) magnetism. One possibility is the realization of effective models that can be easier to cool down to sufficiently low temperature. In Ref. [127] tilted Hubbard model was used to mimic an Ising chain, where the empty and double occupied sites represent the spin up and down states, respectively. Another possibility opens by tuning the tunnelling amplitude between the neighbouring lattice sites to create a staggered-dimerized lattice or a quasi-one-dimensional lattice [128]. In these cases the energy scale of the stronger bonds are tuned above the temperature of the cloud, while along the weak bonds the energy is well bellow of it. With this arrangement the system preserves some features of the lower temperature state, and can show weak magnetic order.

High spin Mott insulating states also have been realized experimentally with ytterbium isotopes [130, 131, 132]. Ytterbium just as alkaline-earth atoms have 2 electrons on the outer s-shell, therefore their total electronic angular momentum is zero, and the total hyperfine spin of the atom comes only from the nuclear spin. These atoms interact essentially via s-wave scattering independent of the nuclear spin. As a consequence of the spin independent interaction, alkaline-earth metal systems — or atoms with equivalent electron shell structure — can be described with good accuracy even by extremely high SU(N) symmetric models, where N$= 2S+1$ is given by the nuclear spin S of the atom. Comparing with the usual two-component electron systems, high spin fermionic systems can show novel magnetic behaviour [133, 134, 135, 136]. In the strong atom-atom interaction limit they can provide different multipole orders [137], valence bond solid (VBS) states, spin liquid (SL) states [138, 139, 140, 141, 142], or even chiral spin liquid states with non-trivial topology [140, 141]. SL states lack any kind of long range order, but due to the violation of time reversal invariance, they are stable also at low temperatures. The SU(4) symmetric spin-$3/2$ system as the simplest case after the usual spin-$1/2$ electrons, has been studied intensively in the last few years [138, 139, 143, 144, 145, 146, 147], mostly on square lattice. On mean-field level the ground state is a VBS state with disconnected resonating valence bond plaquettes, but different numerical results for small systems raises the possibility of a bond-antiferromagnetic columnar dimer state [143]. On a honeycomb lattice it was found that the pure SU(4) Heisenberg system realizes a spin-orbital liquid phase [144], while the addition of next nearest neighbor exchange induces collapse to a tetramerized VBS like

state [148].

Specifically we consider a Mott insulator composed of spin-5/2 alkaline earth atoms, such as ^{173}Yb. The study of such systems in square lattices reveals that its mean field ground state is a chiral spin liquid (CSL) [140, 141]. The CSL state violates time reversal symmetry, and is topologically nontrivial and supports chiral edge states on the boundary of the lattice. The low-energy dynamics is described by 6-flavor spinons (as matter fields) interacting with a U(1) gauge field emerging from the antiferromagnetic correlations. The arising U(1) gauge theory is a dynamical Chern-Simons field theory, where the gauge field dynamics is generated by the short distance physics of the underlying fermions [111].

Here we study the spin-5/2 system in a honeycomb lattice. We show that the lowest energy spin liquid ansatz with one particle per site is a CSL. We also identify the following two lowest energy spin liquid states. We show also how the dynamics of the emerging gauge fields is measurable by spin correlation functions.

Further motivation to study spin liquid phases in a honeycomb lattice with ultracold atoms is due to a newly rising interest in related challenging problems, like superconductivity in graphene [149, 150, 151, 152], or other forms of time reversal symmetry breaking that appear for honeycomb and pyrochlore lattices [153, 154].

5.1 Mean field study of the system at T=0

Let us consider a spin-5/2 atomic gas in a deep optical potential. The system can be described with a SU(N) symmetryc Hubbard Hamiltonian:

$$H = -t \sum_{\langle i,j\rangle,\alpha} \left(c^{\dagger}_{i\alpha} c_{j\alpha} + \text{H.c.} \right) + \frac{U}{2} \sum_{i,\alpha,\beta} c^{\dagger}_{i\alpha} c^{\dagger}_{i\beta} c_{i\beta} c_{i\alpha}, \tag{5.1}$$

where $c_{i\alpha}(c^{\dagger}_{i\alpha})$ annihilates (creates) an atom at site i with spin $\alpha \in \{-\frac{5}{2} \dots \frac{5}{2}\}$, t stands for the tunnelling amplitude, and U for the strength of the on-site interaction.

In the strongly repulsive regime, $U \gg t$, the motional (charge) degree of freedom of the fermions gets frozen at low temperatures leading to a Mott

insulator state, and the system can be described by an effective SU(6) spin Hamiltonian [136, 111]. The Néel order is ruled out by energy constraints and the systems exhibits chiral spin liquids states [140]. For 1/6 filling, there is exactly one particle per site. In this case particle tunneling is forbidden due to the very high energy cost of the multiply occupied sites. Only virtual hoping is allowed, and the Hamiltonian (5.1) can be approximated by

$$H_{\text{eff}} = -J \sum_{\langle i,j\rangle,\alpha,\beta} c^{\dagger}_{i\alpha} c_{j\alpha} c^{\dagger}_{j\beta} c_{i\beta}, \tag{5.2}$$

with $J = 2t^2/U > 0$.

This effective Hamiltonian acts in the restricted Hilbert space of 1 atom per site; and therefore, this condition is enforced by the local constraint:

$$\sum_{\alpha} c^{\dagger}_{i\alpha} c_{i\alpha} = 1. \tag{5.3}$$

This constrained Hamiltonian already exhibits gauge invariance, i.e. it is invariant under the following local transformation:

$$c_{i\alpha} \rightarrow c_{i\alpha}\ e^{i\theta_i}. \tag{5.4}$$

We decouple the quartic Hamiltonian (5.2), by introducing a mean field χ_{ij}, which is a C-number defined as:

$$\chi_{ij} \equiv \sum_{\alpha} \langle c^{\dagger}_{i\alpha} c_{j\alpha} \rangle = \chi^{*}_{ji}. \tag{5.5}$$

Then, the mean field effective Hamiltonian takes the form:

$$H_{\text{mf}} = -J \sum_{\langle i,j\rangle} \left[\sum_{\alpha} \left(\chi_{ij} c^{\dagger}_{j\alpha} c_{i\alpha} + \chi_{ji} c^{\dagger}_{i\alpha} c_{j\alpha} \right) - |\chi_{ij}|^2 \right] - \sum_{i} \varphi_i (c^{\dagger}_{i\alpha} c_{i\alpha} - 1), \tag{5.6}$$

where we introduce the fields φ_i as Lagrange multipliers for enforcing the one-particle per site constraint (5.3).

Though the mean-field Hamiltonian (5.6) is already quadratic, one still needs to make further assumptions about the solution in order to obtain a tractable set of equations. We choose a hexagonal unit cell containing 6 lattice sites,

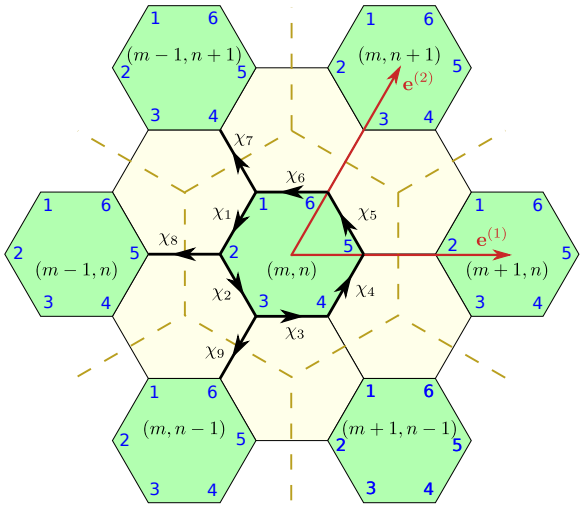

Figure 5.1: Illustration of the unit cell considered here. The unit cell is surrounded by the dashed line and contains 6 sites. The numbers close to the nodes (blue in the color version) label the sublattice index (the sites inside the unit cell), while the (m,n) pair indexes the unit cell itself. There are mean fields inside each unit cell labeled by $\chi_1 \dots \chi_6$ and 3 other independent ones between the neighboring unit cells $\chi_7 \dots \chi_9$. We also show the elementary lattice vectors connecting the neighboring unit cells.

as depicted in Fig. 5.1; such cell respects the original lattice symmetries, and contains as many sites as needed to form a SU(6) singlet.

Then, a site $\mathbf{r}$ of the lattice is indexed by three integers, from which m and n are selecting the unit cell (with a coordinate $\mathbf{r}_{m,n} = m\,\mathbf{e}^{(1)} + n\,\mathbf{e}^{(2)}$ pointing to the center of the cell), and another integer $s \in \{1 \dots 6\}$ selecting the sublattice inside the cell. The elementary lattice vectors $\mathbf{e}^{(1)}$ and $\mathbf{e}^{(2)}$ point from the center of a unit cell to the centers of the two neighboring unit cells as illustrated in Fig. 5.1. The fermion fields $c_{i\alpha}$ are arranged into the 6 component vector:

$$\begin{aligned} c_{i\alpha} &= c_{s,\alpha}(\mathbf{r}_{mn}), \\ \vec{c}_\alpha(\mathbf{r}_{mn}) &= [c_{1,\alpha}(\mathbf{r}_{mn}), c_{2,\alpha}(\mathbf{r}_{mn}), \dots c_{6,\alpha}(\mathbf{r}_{mn})]^T. \end{aligned} \tag{5.7}$$

We use plane wave basis for one particle states:

$$c_{s,\alpha}(\mathbf{r}_{m,n}) = \frac{1}{\sqrt{V}} \sum_{\mathbf{k}} c_{s,\alpha}(\mathbf{k}) e^{i(k_1 m + k_2 n)}, \tag{5.8}$$

where $\mathbf{k} = k_1 \mathbf{f}^{(1)} + k_2 \mathbf{f}^{(2)}$ is the wavenumber in reciprocal space spanned by $\mathbf{f}^{(1)}$ and $\mathbf{f}^{(2)}$. We use the normalization $(\mathbf{f}^{(i)}, \mathbf{e}^{(j)}) = \delta_{ij}$.

With our choice of the unit cell we have 6 independent mean fields inside the cell (m, n) (see Fig. 5.1.): $\chi_1(\mathbf{r}_{mn}) \dots \chi_6(\mathbf{r}_{mn})$ and another 3 connecting the unit cell (m, n) to its 3 neighbors to the left: $\chi_7 \dots \chi_9$:

$$\chi_i(\mathbf{r}_{m,n}) = \frac{1}{V} \sum_{\mathbf{k}} \chi_i(\mathbf{k}) e^{i(k_1 m + k_2 n)}. \tag{5.9}$$

Now, the fields φ corresponding to the Lagrange multipliers can be writeen as:

$$\varphi_i(\mathbf{r}_{m,n}) = \frac{1}{V} \sum_{\mathbf{k}} \varphi_i(\mathbf{k}) e^{i(k_1 m + k_2 n)}, \tag{5.10}$$

Then, the mean field Hamiltonian given at Eq. (5.6) can be written as:

$$H_{\mathrm{mf}} = \sum_{\mathbf{k},\alpha} \vec{c}^{\,\dagger}_\alpha(\mathbf{k}) \cdot M(\mathbf{k}) \cdot \vec{c}_\alpha(\mathbf{k}) + \frac{V}{J} \sum_{i=1}^{9} |\chi_i|^2 + V \sum_{s=1}^{6} \varphi_s, \tag{5.11}$$

where we have redefined the fields as: $F_i \to \frac{1}{J} F_i$, for F being the χ fields and the φ fields.

The matrix $M(\mathbf{k})$ reads as:

$$M(\mathbf{k}) = \begin{pmatrix} \varphi_1 & -\chi_1 & 0 & -\chi_7 e^{-i\gamma_7} & 0 & -\chi_6^* \\ -\chi_1^* & \varphi_2 & -\chi_2 & 0 & -\chi_8 e^{-i\gamma_8} & 0 \\ 0 & -\chi_2^* & \varphi_3 & -\chi_3 & 0 & -\chi_9 e^{-i\gamma_9} \\ -\chi_7^* e^{i\gamma_7} & 0 & -\chi_3^* & \varphi_4 & -\chi_4 & 0 \\ 0 & -\chi_8^* e^{i\gamma_8} & 0 & -\chi_4^* & \varphi_5 & -\chi_5 \\ -\chi_6 & 0 & -\chi_9^* e^{i\gamma_9} & 0 & -\chi_5^* & \varphi_6 \end{pmatrix}, \tag{5.12}$$

where the $\gamma_i = \gamma_i(\mathbf{k})$ are phase factors describing the momentum dependence of the inter unit cell links. They are given in Table 5.1.

The diagonalization of the Hamiltonian (5.11) or analogously, the diagonalization of the $M(\mathbf{k})$ matrix, introduces the eigenvectors of the system:

$$\sum_s M_{s's}(\mathbf{k}) v_s^{(a)}(\mathbf{k}) = \lambda_{\mathbf{k}}^{(a)} v_s^{(a)}(\mathbf{k}). \tag{5.13}$$

After some straightforward algebra and using the self-consistency condition (5.5), one arrives at a set of equations for the mean-field amplitudes and for the local Lagrange multipliers (5.3):

$$\begin{aligned} \bar{\chi}_j &= \frac{6J}{V} \sum_{\mathbf{k},a} e^{i\gamma_j(\mathbf{k})} v_{\beta_j}^{(a)}(\mathbf{k})\, v_{\alpha_j}^{(a)*}(\mathbf{k}), && \text{for } j \in \{1 \dots 9\}, \\ 1 &= \frac{6}{V} \sum_{\mathbf{k},a} v_s^{(a)}(\mathbf{k})\, v_s^{(a)*}(\mathbf{k}), && \text{for } s \in \{1 \dots 6\}. \end{aligned} \tag{5.14}$$

The specific form of the newly introduced indices α_i and β_i are given in Table 5.1 together with the phase factor $\gamma_i(\mathbf{k})$.

This set of equations is highly nonlinear and there are infinitely many solutions which give the same physical wave function of the spin system $\Psi_{\text{spin}}^{\chi_{ij}}$. This wave function is obtained by the Gutzwiller projection, i.e., by restricting the solution to the space with one particle per site:

$$\Psi_{\text{spin}}^{(\chi_{ij})} = \langle 0_c | \prod_i c_i | \Psi_{\text{mean}}^{(\chi_{ij})} \rangle, \tag{5.15}$$

j	α_j	β_j	$\gamma_j(\mathbf{k})$	j	α_j	β_j	$\gamma_j(\mathbf{k})$	j	α_j	β_j	$\gamma_j(\mathbf{k})$
1	2	1	0	4	5	4	0	7	4	1	$k_1 - k_2$
2	3	2	0	5	6	5	0	8	5	2	k_1
3	4	3	0	6	1	6	0	9	6	3	k_2

Table 5.1: The "incoming" and "outgoing" indices α_j and β_j and the phase factor $\gamma_j(\mathbf{k})$ appering at the mean field equations

where $|0_c\rangle$ is the vacuum for the c fermions, i.e. $c_i|0_c\rangle = 0 \ \forall\, c_i$

Under the gauge transformation appering at (5.4), the mean field transforms as:

$$\chi_{ij} \to \chi'_{ij} = e^{i\theta_i}\chi_{ij}e^{-i\theta_j}, \tag{5.16}$$

and the physical only gets a global phase:

$$\Psi^{(\chi_{ij})}_{\text{spin}} \to \Psi'^{(\chi_{ij})}_{\text{spin}} = \Psi^{(\chi'_{ij})}_{\text{spin}} = \langle 0_c|\prod_i c_i|\Psi^{(\chi'_{ij})}_{\text{mean}}\rangle = \quad \langle 0_c|\prod_i c'_i|\Psi^{(\chi_{ij})}_{\text{mean}}\rangle = e^{i\sum_i \theta_i}\Psi^{(\chi_{ij})}_{\text{spin}}. \tag{5.17}$$

Since two different physical wave functions related by the gauge transformation differ by a global phase, they describe the same physical state, i.e. they are physically equivalent.

In order to factor out the gauge freedom in the set of solutions, we distinguish the mean field solutions by the elementary Wilson loops, which are obtained with the product of the χ fields around an elementary plaquette of the lattice. Equivalent solutions exhibit equal Wilson loops, they are, gauge equivalent.

The unit cell consists of three elementary and independent plaquettes. One of them is the plaquette corresponding to the central hexagon of the unit cell, its Wilson loop is:

$$\Pi_1 = \bar{\chi}_1\,\bar{\chi}_2\,\bar{\chi}_3\,\bar{\chi}_4\,\bar{\chi}_5\,\bar{\chi}_6. \tag{5.18}$$

The other two can be chosen from the neighboring plaquettes with the requirement that they have to be independent. One of them can be the one which is between the unit cells (m,n), $(m-1,n)$ and $(m-1,n+1)$, its Wilson loop is:

$$\Pi_2 = \bar{\chi}_7\,\bar{\chi}_3^*\,\bar{\chi}_4^*\,\bar{\chi}_5^*\,\bar{\chi}_8^*\,\bar{\chi}_1^*, \tag{5.19}$$

E	Π_1	Π_2	Π_3
-6.148	$-0.159 - 0.276i$	$-0.159 - 0.276i$	$-0.159 - 0.276i$
-6.148	$-0.159 + 0.276i$	$-0.159 + 0.276i$	$-0.159 + 0.276i$
-6.062	0.460	-0.223	-0.223
-6.062	-0.223	0.460	-0.223
-6.062	-0.223	-0.223	0.460
-6	1	0	0
-6	0	1	0
-6	0	0	1

Table 5.2: Mean-field solutions. The first column represents the energy of the mean-field solution, the other three columns give the Wilson loops of the 3 different plaquettes.

and the third one can be the one between (m, n) and $(m-1, n)$ and $(m, n-1)$, with a Wilson loop:

$$\Pi_3 = \bar{\chi}_8 \, \bar{\chi}_4^* \, \bar{\chi}_5^* \, \bar{\chi}_6^* \, \bar{\chi}_9^* \, \bar{\chi}_2^*. \tag{5.20}$$

The three lowest energy states solutions are showed in Table 5.2. The ground state of the system corresponds to the solution with the lowest energy (first two lines of Table 5.2). It is a CSL liquid, or ΦΦΦ-*flux phase* [140] (or [155] for the analog SU(3) system). All of the χ fields have an equal magnitude:

$$|\chi_1| = |\chi_2| = \ldots = |\chi_9| \approx 0.82651, \tag{5.21}$$

and all of the 3 non-equivalent Wilson loops are equal:

$$\Pi_1 = \Pi_2 = \Pi_3 = |\chi_1|^6 \, e^{i\Phi}, \tag{5.22}$$

where $\Phi = \pm 2\pi/3$. As the phase of the Wilson loop is neither 0 non π, this state exhibits complex fields. The emerging Φ phase can be thought as the flux of a fictitious magnetic field that points up or down perpendicular to the plane of the lattice, it is doubly degenerate. The two degenerate states are related by time reversal symmetry. This phase is symmetric with respect to lattice translations and rotations, but it violates time reversal symmetry — that causes the chiral nature of this spin liquid state.

The next three lines of Table 5.2 show the next phase, whose energy is a bit higher: the *quasi plaquette* or $0\pi\pi$-*flux phase*. In this phase the χ fields inside a central plaquette have higher absolute values than the others: $|\chi_1| = |\chi_2| =$

$\ldots = |\chi_6| > |\chi_7| = |\chi_8| = |\chi_9|$. The flux of the central plaquette is 0, while the flux of the neighboring plaquettes is π. This phase is three times degenerate due to the choice of the central plaquette, which can be any of the three independent elementary plaquettes, i.e. the hexagon of the unit cell, or one of its two independent neighbors. This state is time reversal symmetric, but violates the translation symmetry by one hexagon.

Finally, the three last lines of of Table 5.2 contains the third phase sorted by energy. It is the *plaquette phase*. The χ fields inside a the central plaquette are non zero an equal in magnitude:

$$|\chi_1| = |\chi_2| = \ldots = |\chi_6|, \tag{5.23}$$

with a Wilson loop:

$$\Pi_1 = 1. \tag{5.24}$$

Whereas, the others χ fields conecting different plaquettes are zero: $\chi_7 = \chi_8 = \chi_9 = 0$ and consequently, $\Pi_2 = \Pi_3 = 0$. This phase also contains degeneracy and violates the lattice space translation by one plaquette, but is invariant under time reversal.

All these three phases are showed schematically in Figure 5.5.

In the CSL state, the complex value of the Wilson loops indicates the existence of a penetrating equivalent magnetic flux. This magnetic flux is artificial, it is generated by the configuration of the mean-field solutions. As a consequence, these 2D system can exhibit quantum Hall effect and the corresponding edge states localized in the boundaries. Figure 5.3 depicts the energy spectrum with the bulk bands and the edge states. For 1/6 filling only the lowest bulk band is filled, which is well separated from the next band. We have calculated the Chern number (C) for the system, obtaining a value $C = 6$ for the lowest gap, which is in accordance with the observation that there is one edge state pair per spin component. Then, an elementary flux of $\Phi_0 = \pi/3$ is attached to every spinon (the quasi-particle excitation of the $c^\dagger_{i,\alpha}$ operators). The spinons are not neither bosons non fermions, they follow anyoninc statistics. Each site of the lattice belongs to 3 different plaquettes, effectively every plaquette contains 2 spinons, generating a flux with value $\Phi = 2\Phi_0 = 2\pi/3$, as expected.

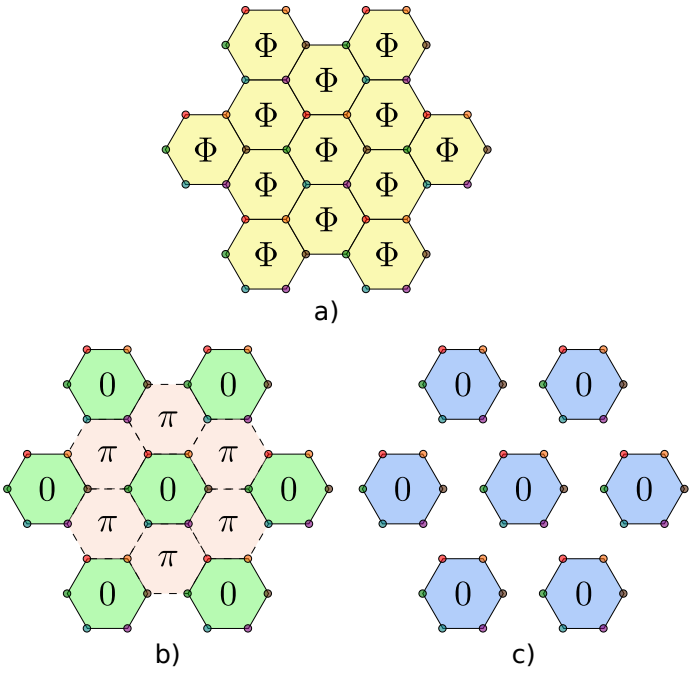

Figure 5.2: Lowest energy mean-field solutions. Subfigure a) illustrates the chiral spin-liquid configuration with all bonds having the same magnitude. Subfigure b) depicts the quasi plaquette phase with real Wilson loops. The dashed line represents a smaller bond value than the solid line. Subfigure c) shows the plaquette phase configuration with only one nonzero Wilson loop per three cells. Links with a zero mean-field value are removed from the figure.

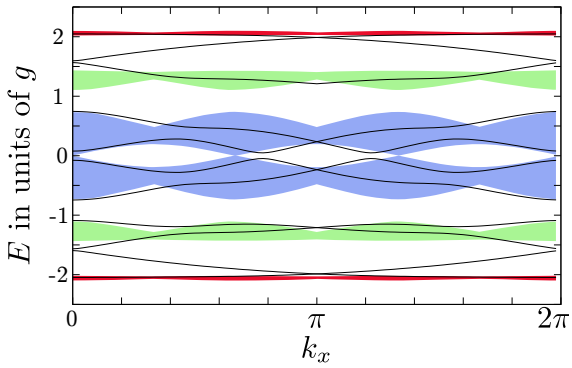

Figure 5.3: The energy spectrum of the system for open boundary conditions in one direction.

5.2 Effective gauge theory

The inclusion of the fluctuations around the mean field configurations has deep consequences in the system we are considering. This point is going to be treated in this section.

There are two types of fluctuations: the amplitude and the phase fluctuations. We are going to consider only the last ones, since the first ones have a finite energy gap [111]. Adding the phase fluctuation a_{ij}, the mean field χ_{ij} takes the form:

$$\chi_{ij} = \chi_{ij}^{\mathrm{mf}}\, e^{ia_{ij}}, \tag{5.25}$$

where χ_{ij}^{mf} is the value of the mean field without fluctuations.

Under the U(1) gauge transformation (5.4), the mean field transforms as:

$$\chi_{ij}^{\mathrm{mf}}\, e^{ia_{ij}} \rightarrow \chi_{ij}^{\mathrm{mf}}\, e^{ia_{ij}+\theta_i-\theta_j}. \tag{5.26}$$

Therefore, the phase field a_{ij} transforms as a gauge field under the action of the U(1) gauge group:

$$a_{ij} \rightarrow a_{ij} + \theta_i - \theta_j. \tag{5.27}$$

The Lagrangian L_{mf} for the system of interested with the fluctuations is given

by:

$$L_{\rm mf} = \sum_{i,\alpha} c^\dagger_{i\alpha}(i\partial_t)c_{i\alpha} - H_{\rm mf} = \sum_{i,\alpha} c^\dagger_{i\alpha}(i\partial_t + \varphi_i)c_{i\alpha} -$$
$$- \sum_{\langle i,j\rangle,\alpha} \left[\chi^{\rm mf}_{ij}\, e^{ia_{ij}} c^\dagger_{j\alpha}c_{i\alpha} + (\chi^{\rm mf}_{ij})^*\, e^{-ia_{ij}} c^\dagger_{i\alpha}c_{j\alpha} - \frac{1}{J}|\chi^{\rm mf}_{ij}|^2\right] - \sum_i \varphi_i, \quad (5.28)$$

where we have considered the Hamiltonian appearing in (5.6) with the fluctuation of the mean fields.

By considering *time-dependent* gauge transformations, the gauge transformations for the fields become:

$$\begin{aligned} &c_j \to c_j e^{i\theta_j}, \\ &a_{ij} \to a_{ij} + \theta_i(t) - \theta_j(t), \\ &\varphi_j \to \varphi_j + \partial_t\theta_j(t). \end{aligned} \quad (5.29)$$

Therefore, the field a_{ij} plays the role of a gauge vector potential, whereas the field φ_j as the scalar potential.

under such transformations, the action $S = \int dtL$ transforms as:

$$S \to S' = S - \sum_i \int dt\partial_t\theta_i(t). \quad (5.30)$$

Then, the action is invariant as long as $\theta_i(-\infty) = \theta_i(+\infty)$. This condition can be relaxed considering a specific family of gauge transformations [156].

The Lagrangian (5.28) describes a non-relativistic matter field on a 2D lattice coupled to a U(1) gauge field a_{ij}, concretely a compact gauge field, the Lagrangian is invariant under $a_{ij} \to a_{ij} + 2\pi$.

But, the dynamical term for the gauge field $S_{\rm EM}$ (see Eq. (2.4)) does not appear in this expression. This is because the gauge field is a constraint in our theory. As we will discuss in detail in the next section, in the *path integral formalism* the effective action $S^{\rm eff}_{\rm EM}$ for the gauge field can be obtained by integrating out the fermionic field in the expression (5.28):

$$e^{iS^{\rm eff}_{\rm EM}(a)} = \int D[\bar{c}, c] e^{i\int dtL_{\rm mf}}. \quad (5.31)$$

By integrating out only the high energy fermionic field, the resulting theory in the continuum considers a fermionic matter field interacting with a dynamical gauge field:

$$\mathcal{L} = -\frac{1}{4g^2}(\mathbf{e}^2 - v\mathbf{b}^2) - \frac{C}{4\pi}\sum_{\mu,\nu,\lambda=0}^{4} \epsilon^{\mu\nu\lambda} a_\mu \partial_\nu a_\lambda + \sum_{\alpha=1}^{6}\left[-ic^\dagger_{l,\alpha}(\partial_t - ia_0)c_{l,\alpha} + \frac{1}{2m_s}\sum_{j=1}^{3} c^\dagger_{l,\alpha}(\partial_j + ia_j)^2 c_{l,\alpha}\right]. \quad (5.32)$$

The low energy spinon excitations are coming from the vicinity of the energy maxima of the valence band, and from the energy minima of the conduction band. Since there are 6 such points, the low-energy dynamics is governed by spinons with 6 flavors interacting with a U(1) gauge field. The speed of sound v is proportional to $1/J \sim U/t^2$.

The first term of the last relation corresponds to usual free Lagrangian density for the U(1) gauge field. The constant g^2 arises from the integration of the spinon fields and is in the order of the spinon gap Δ. The fields $\mathbf{e}$, and $\mathbf{b}$, are the artificial electric and magnetic fields, respectively. They come from the scalar and vector potentials a_0 and $\mathbf{a}$ through the Maxwell equations. These fields are related to their lattice counterpart (5.32) with the relations:

$$\begin{aligned} \varphi_i &= a_0\left(\mathbf{r_i}\right), \\ a_{ij} &= \frac{\mathbf{a}(\mathbf{r_i}) - \mathbf{a}(\mathbf{r_j})}{2}. \end{aligned} \quad (5.33)$$

The second term in (5.32) is the so called *Chern-Simons* term. It breaks parity and time reversal symmetries. It depends only on the topology of the system: it is proportional to the *Chern number* C. This term is non zero ($C = 6$) for the CSL phase (this phase exhibits a non trivial topology), whereas it is zero for the quasi plaquette and the plaquette phases.

Due to this topological term, the propagator of the gauge boson contains a pole [156]:

$$q^2 - g^4\theta^2 = 0, \quad (5.34)$$

where $|\theta| = C/(2\pi)$. Thus, the gauge boson γ is massive for the CSL phase: $m_\gamma = g^2|\theta|$. Consequently, it can only mediate short range interactions between the spinons. Then, the fluctuations of the mean field solution are suppressed by

the mass gap and the mean-field solution is stable [111], as we will discuss in the next sections of the chapter.

Then, the considered ultracold atomic platform in the deep Mott insulator phase may act as a quantum simulator of a U(1) compact lattice gauge theory with dynamical gauge fields.

5.3 Stability analysis: finite temperature consideration

In the first section of the chapter we described the three lowest energy phases for the mean field theory at $T = 0$. Next, we showed the emergence of a gauge theory in the spin liquid phase by considering the phase fluctuations around the mean field configurations. In this section we are going to continue the fluctuation analysis by considering the stability of the mean field phases around the fluctuations. Since we are dealing with a physical system, we expect it to be stable under fluctuations. Moreover, since experiments are always done at finite temperature, in this section we also are going to study the stability of the different phases respect to the finite temperature.

The finite temperature calculation was made for a similar system in Ref. [157] in the high temperature regime, and they managed to describe the metal-insulator transition, but still left open the finite temperature physics far in the Mott insulator regime, where quantum magnetism characterizes the system.

5.3.1 Path integral formulation of SU(N) magnetism

Since we are focussed to discuss the finite temperature properties of the system, we are going to work in the canonical formalism. Then, the partition function of the system at inverse temperature β is evaluated in the imaginary time path-integral formalism [158]:

$$Z(\beta) = \int D[\overline{c}, c] e^{-S[\overline{c},c]} \prod_{i,\tau} \delta \left(\sum_{\alpha} \overline{c}_{i\alpha} c_{i\alpha} - 1 \right). \tag{5.35}$$

The delta functions in the integrand assures the one-particle constraint at every site for every imaginary time $\tau = -it$. We use $\hbar = 1$ units, and $\overline{c}$ (c) are

Grassmann numbers associated to $c^\dagger$ (c).

The action in the imaginary time is given by:

$$S[\bar{c}, c] = \int_0^\beta d\tau \left(\sum_{i,\alpha} \bar{c}_{i\alpha} \partial_\tau c_{i\alpha} + H \right), \tag{5.36}$$

where H is expressed in (5.2). It is quartic in the fermion fields, thus we need to rely on an approximation scheme. According to the pioneering works by Marston and Affleck on the general SU(N) Hubbard models [133], and the more recent analysis of Hermele, Gurarie and Rey on SU(N) symmetric models realized with ultracold atoms [140], we consider only spin liquid states, i.e. where the global SU(6) symmetry is not broken. In this case, with the help of a Hubbard-Stratonovich (HS) transformation [158], new, slowly varying fields are introduced.

$$\begin{aligned} &\exp\left(J \int_0^\beta d\tau \sum_{\langle i,j\rangle,\alpha,\beta} \bar{c}_{i,\alpha} c_{j,\alpha} \bar{c}_{j,\beta} c_{i,\beta} \right) \\ &= \int D[\chi^*, \chi] \exp\left\{ \int_0^\beta d\tau \sum_{\langle i,j\rangle} \left[\sum_\alpha \left(\chi_{ij} \bar{c}_{j,\alpha} c_{i,\alpha} + \chi_{ij}^* \bar{c}_{i,\alpha} c_{j,\alpha} \right) - \frac{1}{J} |\chi_{ij}|^2 \right] \right\}. \end{aligned} \tag{5.37}$$

The Hubbard-Stratonovich field χ_{ij} lives on the links between adjacent sites and are complex, furthermore $\chi_{ij}^* = \chi_{ji}$. Finally, another bosonic field, φ_i, is introduced in order to cast the delta functions also to a Gaussian form by

$$\begin{aligned} &\prod_{i,\tau} \delta\left(\sum_\alpha \bar{c}_{i\alpha} c_{i\alpha} - 1 \right) \\ &\qquad = \int D[\varphi] \exp\left[- \int_0^\beta d\tau \sum_i \varphi_i \left(\sum_\alpha \bar{c}_{i,\alpha} c_{i,\alpha} - 1 \right) \right]. \end{aligned} \tag{5.38}$$

The bosonic field φ_i is purely imaginary for the proper Fourier representation of the delta functions. However, we conceal its imaginary nature, because it is very suggestive in the final form of the action, as playing the role of a scalar

potential for the fermions.

Combining Eqs. (5.2), (5.35), (5.36), (5.37) and (5.38) the partition function takes the form

$$Z(\beta) = \int D[\overline{c}, c, \chi^*, \chi, \varphi] e^{-S_{\rm tot}[\overline{c}, c, \chi^*, \chi, \varphi]}, \tag{5.39}$$

with the total action

$$\begin{aligned} S_{\rm tot}[\overline{c}, c, \chi^*, \chi, \varphi] = \int_0^\beta {\rm d}\tau \Bigg\{ & \sum_{i,\alpha} \overline{c}_{i\alpha}(\partial_\tau - \varphi_i) c_{i\alpha} \\ & + \sum_{\langle i,j \rangle} \left[\sum_\alpha \left(\chi_{ij} \overline{c}_{j\alpha} c_{i\alpha} + {\rm H.c.} \right) - \frac{1}{J} |\chi_{ij}|^2 \right] + \sum_i \varphi_i \Bigg\}. \end{aligned} \tag{5.40}$$

As we already mentioned in section 5.2, the total action (5.40) is also U(1) gauge invariant under the transformations:

$$\chi_{ij} \to \chi_{ij} e^{i(\theta_j - \theta_i)}, \tag{5.41a}$$

$$\varphi_i \to \varphi_i - i\partial_\tau \theta_i. \tag{5.41b}$$

Thus, the phase of χ transforms as a vector potential, and φ transforms as a scalar potential. The theory expressed in (5.40) describes a fermionic matter in a lattice coupled to a U(1) gauge field. Indeed, the integration over the gauge degrees of freedom is the essence of the path-integral formulation of the problem as it renders the expectation values of all non gauge invariant quantities to be zero. Then, the mean value of those operators, which violate the one particle per site constraint, are annulled [159, 160].

As we discussed in the first section, in order to be able to treat the system, we introduce the nontrivial unit cell depicted in Fig. 5.1.

Introducing the plane wave basis for one particle states, the fields can be written as:

$$c_{s,\alpha}(\mathbf{r}_{m,n},\tau) = \frac{1}{\sqrt{V\beta}} \sum_{\mathbf{k},l} c_{s,\alpha}(\mathbf{k}, i\omega_l) e^{i(k_1 m + k_2 n - \omega_l \tau)}, \tag{5.42}$$

$$\chi_i(\mathbf{r}_{m,n},\tau) = \frac{1}{V\beta} \sum_{\mathbf{k},l} \chi_i(\mathbf{k}, i\nu_l) e^{i(k_1 m + k_2 n - \nu_l \tau)},$$

$$\varphi_s(\mathbf{r}_{m,n},\tau) = \frac{1}{V\beta} \sum_{\mathbf{k},l} \varphi_s(\mathbf{k}, i\nu_l) e^{i(k_1 m + k_2 n - \nu_l \tau)},$$

where the Fourier transform has been extended over the *imaginary time* dimension with the help of $\omega_l = (2l+1)\pi/\beta$ and $\nu_l = 2l\pi/\beta$, which are the Matsubara frequencies for fermions and bosons respectively. Moreover, $\mathbf{k} = k_1\mathbf{f}^{(1)} + k_2\mathbf{f}^{(2)}$ is the wavenumber in reciprocal space spanned by $\mathbf{f}^{(1)}$ and $\mathbf{f}^{(2)}$. We use the normalization $(\mathbf{f}^{(i)}, \mathbf{e}^{(j)}) = \delta_{ij}$. Here and from now on, $i = 1 \ldots 9$ indexes the 9 different χ_i fields and $s = 1 \ldots 6$ denotes the sublattice and therefore indexes the φ_s fields.

The $c_{s,\alpha}(\mathbf{r}_{m,n},\tau)$ fermionic field is defined at (5.7). With our choice of the unit cell there are 6 independent HS fields inside the cell (m,n) (see Fig. 5.1.), $\chi_1(\mathbf{r}_{mn}) \ldots \chi_6(\mathbf{r}_{mn})$ and another 3 connecting the unit cell (m,n) to its 3 neighbors to the left, $\chi_7 \ldots \chi_9$ (see first Section). The $\varphi_s(\mathbf{r}_{mn})$ fields lie on the sites (6 per unit cell). They are analogue to the φ fields appearing in (5.10).

The total action Eq. (5.40) in momentum space is evaluated by some straightforward algebra to

$$S_{\mathrm{tot}}[\overline{c}, c, \chi^*, \chi, \varphi] = -\sum_s \varphi_s(\hat{q}=0) + \frac{1}{JV\beta} \sum_{\hat{q},i} |\chi_i(\hat{q})|^2 - \sum_{\hat{k},\hat{q},s,s',\alpha} \overline{c}_{s'\alpha}(\hat{k}+\hat{q}) G^{-1}_{s's}(\hat{k},\hat{q}) c_{s\alpha}(\hat{k}), \tag{5.43}$$

where we have used the shorthand notations $\hat{k} \equiv (\mathbf{k}, i\omega_n)$, and $\hat{q} \equiv (\mathbf{q}, i\nu_m)$. In the sum α is over the spin components of the fermions, while $i = 1 \ldots 9$, and $s, s' = 1 \ldots 6$.

$G^{-1}_{s',s}(\hat{k},\hat{q})$ is the inverse of the fermion propagator, depending on the boson fields. Its explicit form is given by

$$G^{-1}_{s's}(\hat{k},\hat{q}) = i\omega_n \delta_{\mathbf{q},\mathbf{0}} \delta_{m,0} \delta_{s',s} - H_{s's}(\hat{k},\hat{q}), \tag{5.44}$$

and

$$H(\hat{k},\hat{q}) = \frac{-1}{\beta V}\begin{bmatrix} -\varphi_1(\hat{q}) & \chi_1(\hat{q}) & 0 \\ \chi_1^*(-\hat{q}) & -\varphi_2(\hat{q}) & \chi_2(\hat{q}) \\ 0 & \chi_2^*(-\hat{q}) & -\varphi_3(\hat{q}) \\ \chi_7^*(-\hat{q})e^{i\gamma_7(\mathbf{k}+\mathbf{q})} & 0 & \chi_3^*(-\hat{q}) \\ 0 & \chi_8^*(-\hat{q})e^{i\gamma_8(\mathbf{k}+\mathbf{q})} & 0 \\ \chi_6(\hat{q}) & 0 & \chi_9^*(-\hat{q})e^{i\gamma_9(\mathbf{k}+\mathbf{q})} \end{bmatrix}$$

$$\begin{bmatrix} \chi_7(\hat{q})e^{-i\gamma_7(\mathbf{k})} & 0 & \chi_6^*(-\hat{q}) \\ 0 & \chi_8(\hat{q})e^{-i\gamma_8(\mathbf{k})} & 0 \\ \chi_3(\hat{q}) & 0 & \chi_9(\hat{q})e^{-\gamma_9(\mathbf{k})} \\ -\varphi_4(\hat{q}) & \chi_4(\hat{q}) & 0 \\ \chi_4^*(-\hat{q}) & -\varphi_5(\hat{q}) & \chi_5(\hat{q}) \\ 0 & \chi_5^*(-\hat{q}) & -\varphi_6(\hat{q}) \end{bmatrix}, \quad (5.45)$$

where the γ_i phase factors are given in Table 5.1.

All the φ_s and χ_i field depend on the transferred momentum $\mathbf{q}$ and Matsubara frequency ν_m. In the phases, k_1, k_2, q_1 and q_2 denote the respective components of the wavenumbers.

The total action (5.43) is quadratic in the fermionic fields, thus, this field can be integrated out in the functional integral (5.39):

$$Z(\beta) = \int D[\chi^*, \chi, \varphi]\, e^{-S_{\text{eff}}[\chi^*,\chi,\varphi]}, \quad (5.46)$$

where the effective action reads as:

$$S_{\text{eff}}[\chi^*, \chi, \varphi] = -\sum_s \varphi_s(\hat{q}=0) + \frac{1}{JV\beta}\sum_{\hat{k},i} |\chi_i(\hat{k})|^2 - 6\,\text{tr}[\ln(\beta G^{-1})], \quad (5.47)$$

where the trace is a sum over $\hat{k}$ and s and factor 6 comes from the summation over the spin index α.

Equations (5.46) and (5.47) are the main results of the general path integral formulation of SU(N) magnetism for non-classically ordered antiferromagnetic states [133, 141].

The effective action (5.47) is a functional of the slowly varying (both in space and in imaginary time) bosonic fields χ and φ.

The expression $e^{-S_{\text{eff}}}$ acts as a weight function of the field configurations. If this expression was evaluated, all the correlation functions of the fields and of the original fermionic operators could be calculated exactly.

5.3.2 Saddle-point approximation

Derivation of the saddle-point equations

Since the effective action (5.47) is highly non-polynomial in the bosonic field, in order to evaluate the expression (5.46) it is needed to rely on an approximation scheme. We are going to consider the saddle-point evaluation method: we assume that the probability distribution $e^{-S_{\text{eff}}}$ is dominated by the maxima values and their neighbouring are close to a Gaussian functions. Thus, we proceed by expanding the fields χ and φ around the homogeneous saddle-point configurations and by considering the fluctuations around them,

$$\chi_i(\hat{q}) = \beta V \bar{\chi}_i \delta_{\hat{q},0} + \delta\chi_i(\hat{q}), \tag{5.48a}$$

$$\varphi_s(\hat{q}) = \beta V \bar{\varphi}_s \delta_{\hat{q},0} + \delta\varphi_s(\hat{q}). \tag{5.48b}$$

Here and in the following $\delta_{\hat{q},0} = \delta_{\mathbf{q},0}\delta_{m,0}$.

The complex numbers $\bar{\chi}$ and $\bar{\varphi}$ are the homogeneous stationary points: the functional derivative of S_{eff} with respect to $\delta\chi$ and $\delta\varphi$ has to vanish.

$$\left.\frac{\delta S_{\text{eff}}[\delta\chi^*, \delta\chi, \delta\varphi]}{\delta\phi}\right|_{\delta\chi=\delta\chi^*=\delta\varphi=0} = 0, \tag{5.49}$$

where we have introduced a 24 component vector ϕ_μ composed of the fluctuations. The first 18 elements are the complex fields $\delta\chi$ and their complex conjugates, and the last 6 elements are the $\delta\varphi$ fields:

$$\phi_\mu(\hat{q}) = [\delta\chi_i(\hat{q}), \delta\chi_i^*(-\hat{q})), \delta\varphi_s(\hat{q})]_\mu. \tag{5.50}$$

With the decomposition (5.48) of the fields χ and φ, the inverse of the fermionic Green's function (5.44) is split to two parts

$$G^{-1}_{s's}(\hat{k}, \hat{q}) = G^{-1}_{(0)s's}(\hat{k}, \hat{q}) - \Sigma_{s's}(\hat{k}, \hat{q}), \tag{5.51}$$

where the inverse of the saddle-point Green's function, $G_{(0)}^{-1}$, contains only the saddle-point values of the HS fields, while the self-energy, Σ contains the fluctuations of the HS fields (their explicit forms are given below).

With such a separation a systematic expansion around the saddle point can be done in terms of powers of Σ. The effective action (5.47) can be expanded in powers of the fluctuations around the mean field:

$$S_{\text{eff}} = S_0 + S_1 + S_2 + 6\sum_{n=1}^{\infty} \frac{\text{tr}\,(G^0\Sigma)^n}{n}, \tag{5.52a}$$

$$S_0 = -\beta V \sum_s \bar{\varphi}_s + \frac{\beta V}{J}\sum_i |\bar{\chi}_i|^2 - 6\,\text{tr}\log(\beta G_0^{-1}), \tag{5.52b}$$

$$S_1 = -\sum_s \delta\varphi_s(\hat{q}=0) + \frac{1}{J}\sum_i \left[\bar{\chi}_i^*\delta\chi_i(\hat{q}=0) + \text{H.c.}\right], \tag{5.52c}$$

$$S_2 = \frac{1}{J\beta V}\sum_{i,\hat{q}} \delta\chi_i^*(\hat{q})\delta\chi_i(\hat{q}), \tag{5.52d}$$

where S_0, S_1, S_2 contains the fluctuations of the fields with zeroth, first, and second order, respectively, and the logarithm in Eq. (5.47) is expanded in powers of the self-energy Σ as:

$$\begin{aligned}\text{tr}\log(\beta G^{-1}) &= \text{tr}\log\left[\beta(G_{(0)}^{-1} - \Sigma)\right] \\ &= \text{tr}\log\left(\beta G_{(0)}^{-1}\right) + \sum_{n=1}^{\infty}\frac{\text{tr}(G_{(0)}\Sigma)^n}{n}.\end{aligned} \tag{5.53}$$

The evaluation of $\text{tr}(G_{(0)}\Sigma)^n$ via a systematic Feynman diagram method is detailed in Appendix 9.2.

Now the saddle-point equations (5.49) are cast to a more direct form by collecting the first order contributions to the effective action, and therefore

$$\frac{\partial S_1}{\partial\phi_\mu(\hat{q})} + 6\,\text{tr}\left(G_{(0)}\frac{\partial\Sigma}{\partial\phi_\mu(\hat{q})}\right) = 0. \tag{5.54}$$

These equations provide the self consistent equations for the mean-field (i.e. saddle-point) solutions. In order to solve them we need the explicit form of the saddle-point Green's function $G_{(0)}$, and the self-energy Σ.

The saddle-point Green's function is diagonal in momentum space, and in the Matsubara frequencies:

$$G^{-1}_{(0)s's}(\hat{k},\hat{q}) = G^{-1}_{(0)s's}(\hat{k})\delta_{\hat{q},0}, \tag{5.55}$$

with

$$G^{-1}_{(0)s's}(\hat{k}) \equiv G^{-1}_{(0)s's}(\mathbf{k}, i\omega_n) = \left(i\omega_n\delta_{s',s} - H^{(0)}_{s's}(\mathbf{k})\right). \tag{5.56}$$

The mean-field fermion Hamiltonian $H^{(0)}_{s's}(\mathbf{k})\delta_{\hat{q},0}$ is obtained by replacing $\chi_i(\hat{q})$ and $\varphi_s(\hat{q})$ in Eq. (5.45) with $\beta V\bar{\chi}_i\delta_{\hat{q},0}$ and $\beta V\bar{\varphi}_s\delta_{\hat{q},0}$. The $H^{(0)}_{s's}(\mathbf{k})$ Hamiltonian can be easily diagonalized for all $\mathbf{k}$ momentum

$$\sum_s H^{(0)}_{s's}(\mathbf{k})v^{(a)}_s(\mathbf{k}) = \varepsilon^{(a)}_{\mathbf{k}}v^{(a)}_s(\mathbf{k}), \tag{5.57}$$

with eigenvalues $\varepsilon^{(a)}_{\mathbf{k}}$ and eigenvectors $v^{(a)}_s(\mathbf{k})$, where the eigenvalue index is $a \in \{1\ldots 6\}$. With the help of Eqs. (5.56) and (5.57) the saddle-point Green's function is expressed as

$$G_{(0)s's}(\hat{k}) \equiv G_{(0)s's}(\mathbf{k}, i\omega_n) = \sum_a \frac{v^{(a)}_{s'}(\mathbf{k})\, v^{(a)*}_s(\mathbf{k})}{i\omega_n - \varepsilon^{(a)}_{\mathbf{k}}}. \tag{5.58}$$

Note, that the saddle-point Green's function depends on the saddle-point values of the fields, $\bar{\chi}$ and $\bar{\varphi}$, through the eigenvalues and eigenvectors of the matrix $H^{(0)}$.

The self-energy is obtained by replacing $\chi_i(\hat{q})$ and $\varphi_s(\hat{q})$ in Eq. (5.45) with their fluctuations $\delta\chi_i(\hat{q})$ and $\delta\varphi_s(\hat{q})$. It can be compactly written as

$$\begin{aligned}\Sigma_{s's}(\hat{k},\hat{q}) = \frac{-1}{\beta V}\sum_{i=1}^{9}\Big[&\delta_{s',\beta_i}\delta_{s,\alpha_i}e^{-i\gamma_i(\mathbf{k})}\delta\chi_i(\hat{q}) \\ &+ \delta_{s',\alpha_i}\delta_{s,\beta_i}e^{i\gamma_i(\mathbf{k}+\mathbf{q})}\delta\chi^*_i(-\hat{q})\Big] + \frac{1}{\beta V}\sum_{r=1}^{6}\delta_{s'r}\delta_{sr}\delta\varphi(\hat{q}),\end{aligned} \tag{5.59}$$

where the specific form of the indices α_i and β_i together with the phase factor $\gamma_i(\mathbf{k})$ appear in Table 5.1.

Equation (5.54) can be cast to an explicit form now. The first term is easily evaluated with the help of Eq. (5.52c). In the second term the trace is a sum over the wavenumber $\mathbf{k}$, Matsubara frequency ω_n and the sublattice index s. Using the "free" propagator (5.58) and performing the sum for the Matsubara frequencies, one arrives to

$$\mathrm{tr}\left(G_{(0)}\frac{\partial\Sigma}{\partial\phi_\mu(\hat{q})}\right) = \sum_{\hat{k},s,s'} G_{(0)s,s'}(\hat{k})\frac{\partial\Sigma_{s',s}(\hat{k},\hat{q})}{\partial\phi_\mu(\hat{q})}$$
$$= \sum_{\mathbf{k},a,s,s'} \beta\frac{v_s^{(a)}(\mathbf{k})\, v_{s'}^{(a)*}(\mathbf{k})}{1+e^{\beta\varepsilon_{\mathbf{k}}^{(a)}}}\,\frac{\partial\Sigma_{s',s}(\hat{k},\hat{q})}{\partial\phi_\mu(\hat{q})}. \quad (5.60)$$

The derivative of Σ can also be readily evaluated with the help of its compact form Eq. (5.59). After some straightforward algebra one arrives to the explicit form of the self-consistency equations (5.54):

$$\bar{\chi}_j = \frac{6J}{V}\sum_{\mathbf{k},a} e^{i\gamma_j(\mathbf{k})}\frac{v_{\beta_j}^{(a)}(\mathbf{k})\, v_{\alpha_j}^{(a)*}(\mathbf{k})}{1+e^{\beta\varepsilon_{\mathbf{k}}^{(a)}}}, \qquad \text{for } j\in\{1\ldots 9\},$$
$$1 = \frac{6}{V}\sum_{\mathbf{k},a} \frac{v_s^{(a)}(\mathbf{k})\, v_s^{(a)*}(\mathbf{k})}{1+e^{\beta\varepsilon_{\mathbf{k}}^{(a)}}}, \qquad \text{for } s\in\{1\ldots 6\}. \quad (5.61)$$

We observe that these saddle-point equations extensions to finite T of the corresponding ones obtained for the mean field treatment at T=0 (see Eq. (5.14)). Since we are considering the finite temperature case, the unique difference between both sets of equations is the appearance of the occupation number factor or the Fermi-Dirac distribution function:

$$n^{(a)}(\mathbf{k}) = \frac{1}{1+e^{\beta\varepsilon_{\mathbf{k}}^{(a)}}}. \quad (5.62)$$

In the limit $T\to 0$ the previous equations are reduced to the ones given in Eq. (5.14).

It is worth to emphasize that we have used the term “mean field” throughout this section as a synonym for “saddle point”. In the mean-field calculation the χ_{ij} mean fields are the fermion correlators $\chi_{ij} = \sum_\alpha \langle c_{i\alpha}^\dagger c_{j\alpha}\rangle$. Here they

are HS fields and their saddle-point values correspond to the mean fields. The advantage of the path-integral method beyond its transparency is its straightforward application for non-zero temperatures, just as when going beyond the saddle-point approximation as we will see in Sec. (5.3.3).

At finite temperature each solution is characterized by th free energy. The state with the lowest free energy dominates the partition function. The free energy

$$F = -k_B T \log Z(\beta), \tag{5.63}$$

at mean-field level, i.e. by neglecting quantum fluctuations, is given by:

$$F_{\rm mf}(T,V) = \frac{S_0}{\beta} = -V \sum_s \bar{\varphi} + \frac{V}{J} \sum_i |\bar{\chi}|^2 - \frac{6}{\beta} \sum_{\mathbf{k},a} \log\left(1 + e^{-\beta \varepsilon_{\mathbf{k}}^{(a)}}\right), \tag{5.64}$$

where we have performed the sum for the Matsubara frequencies [158]

$$\mathrm{tr}\log(\beta G_0^{-1}) \;=\; \sum_{\mathbf{k},n,a} \log\left(i\beta\omega_n - \beta\epsilon_{\mathbf{k}}^{(a)}\right) \;=\; \sum_{\mathbf{k},a} \log\left(1 + e^{-\beta\epsilon_{\mathbf{k}}^{(a)}}\right). \tag{5.65}$$

In order to describe the possible competition of various configurations we determine the three lowest lying solutions. Their basic properties are discussed in the next subsection.

Finite temperature mean-field solutions

We present the lowest free energy solutions of Eqs. (5.61). As we already mentioned in the first section, there are infinitely many solutions to the coupled equations due to the gauge freedom Eqs. (5.41). From any set of saddle-point solutions we can generate new ones with the same free energy by applying an arbitrary τ independent gauge transformation according to (5.41a). In order to factor out this trivial gauge freedom, we distinguish the saddle-point solutions by the elementary Wilson loops (see Eqs. (5.18), (5.19),(5.20)), i.e. those solutions are considered to be equivalent, whose elementary Wilson loops are equal.

The results at T=0 coincide completely with those analysed at Section 5.1. Even at finite temperatures these three states remain to be the three lowest free energy solutions. The behaviour of the free energy as a function of the temperature is plotted for these three phases in Fig. 5.4. We have found that the free energy of the CSL state remains slightly below the two other states, however,

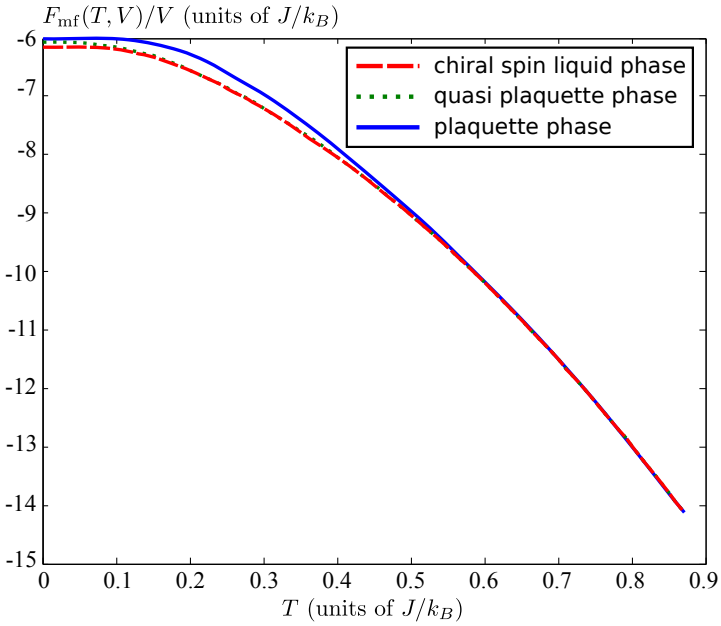

Figure 5.4: The free energy per plaquette $F_{\mathrm{mf}}(T,V)/V$ of the three lowest lying saddle-point solutions.

close to the critical point the free energy curves approach each other with high accuracy. This is in agreement with the behavior of the order parameters.

When the temperature is increased the order parameters, the saddle-point values of the HS fields, get smaller and smaller and eventually vanish at a common critical temperature $T_c \approx 0.83\, J/k_B$. The order parameters vanish with an exponent of $1/2$, characteristic to the mean-field approximation. Above this temperature the paramagnetic Mott phase is stable, and close to T_c a Ginzburg-Landau type analysis, based on this saddle-point expansion, describes the critical behavior. The temperature dependence of $|\chi|$ together with a sketch of the elementary fluxes is plotted in Fig. 5.5.

In the last section we have considered the stationary values of the field (see Eq. (5.54)) in the saddle-point approximation. The effective action Eq. (5.52a) has no first order contribution in the fluctuations. In order to go beyond the

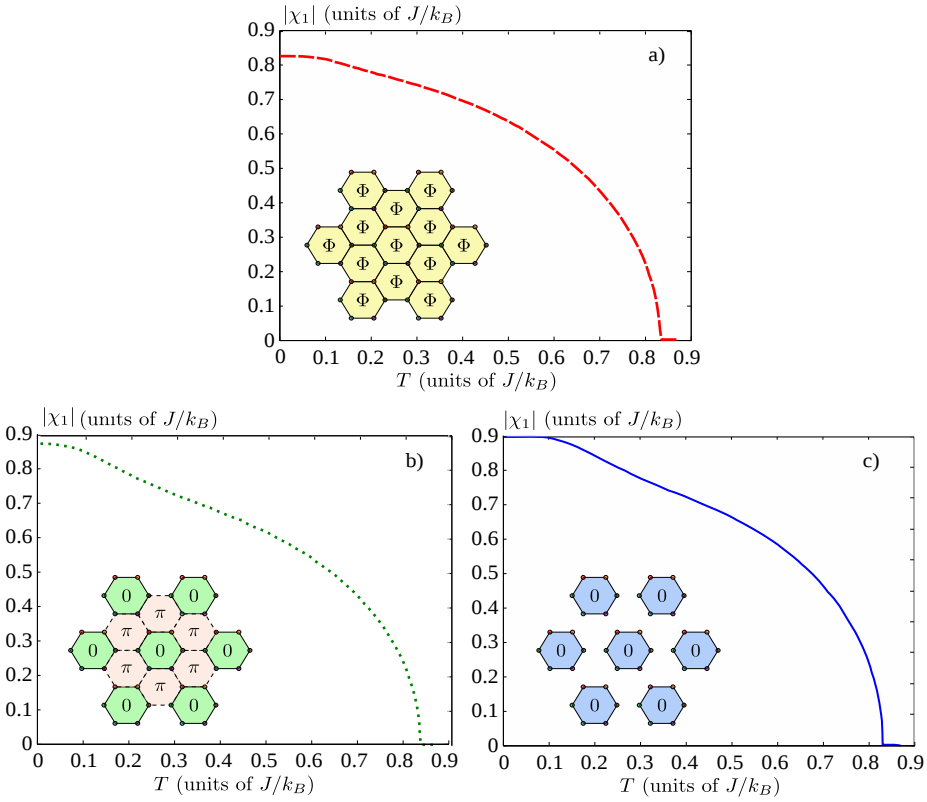

Figure 5.5: The saddle-point solutions for the three lowest free energy spin liquid states. a) The chiral spin liquid state. b) The quasi plaquette state. c) The plaquette state.

saddle-point approximation we consider the leading correction, which is the second order one in the fluctuations. Thus the functional integral becomes a Gaussian integral with the effective action:

$$S_{\text{eff}} \approx S_0 + S_2 + 3\,\text{tr}(G_{(0)}\Sigma)^2. \tag{5.66}$$

The last two terms, which are quadratic in the fluctuations, can be arranged to a convenient matrix form:

$$\begin{aligned} S^{(2)}_{\text{eff}} &= \frac{1}{J\beta V}\sum_{i=1}^{9}\sum_{\hat{q}} \delta\chi_i^*(\hat{q})\delta\chi_i(\hat{q}) + 3\,\text{tr}(G^0\Sigma)^2 \\ &= \frac{1}{2\beta V}\sum_{\mu,\nu=1}^{24}\sum_{\hat{q}} \phi_\mu^*(\hat{q})C_{\mu\nu}(\hat{q})\phi_\nu(\hat{q}). \end{aligned} \tag{5.67a}$$

The $C_{\mu,\nu}$ kernel is the so-called Hessian and provides the curvature of the effective action:

$$C_{\mu\nu}(\hat{q}) = \frac{\partial^2 S_{\text{eff}}}{\partial\phi_\mu^*(\hat{q})\partial\phi_\nu(\hat{q})}. \tag{5.67b}$$

The Hessian is a 24×24 matrix, and depends on the saddle-point values of the fields $\bar{\chi}, \bar{\varphi}$. The derivation and explicit form of $C_{\mu\nu}$ is given in Appendix 9.2.

Throughout the study we have assumed that the weight function $e^{-S_{\text{eff}}}$ in the path integral around the saddle-point configurations takes Gaussian form. In this case the path integral can be evaluated and the partition function is the sum of the Gaussian contributions of the different saddle-points. The first step to test the validity of a specific phase is to check whether the Hessian $C_{\mu\nu}(\hat{q})$ is positive definite at the related configuration [160]. If $C_{\mu\nu}(\hat{q})$ is positive definite, the weight function in the path integral drops when we move a bit farther from the saddle point, so the saddle-point solution is stable. The curvature (5.67b) is complex for nonzero Matsubara frequencies, but the sum of the contributions of the $\pm i\nu_m$ pairs always provides a non-negative curvature, since $C_{\mu\nu}(\mathbf{q}, -i\nu_m) = C^*_{\nu\mu}(\mathbf{q}, i\nu_m)$. Therefore, it is sufficient to check the stability of the phases for $\nu_m = 0$ only.

A minor difficulty still remains. Namely, the scalar potential, introduced in Eq. (5.38) has to be purely imaginary for the representation of the Dirac delta

functions. However, the saddle-point equations provide real solutions for $\bar{\varphi}_s$. Such solutions are physical, and one can interpret the homogeneous and real $\bar{\varphi}$ as the chemical potential of the system. Consequently the functional integral representation (5.38) has to be understood after an analytical continuation $\delta\varphi_s \to i\delta\varphi_s$. Hence in the Hessian the curvature is changed from positive to negative along the 6 directions of the scalar potential. The easiest way to treat the problem is to perform the Gaussian integral over $\delta\varphi_s$, as was done e.g. in Ref [133] to arrive to an effective action only for the $\delta\chi$ fields,

$$S_{\text{eff}}^{(2)'} = \frac{1}{2\beta V} \sum_{k,l=1}^{18} \sum_{\hat{q}} \phi_k^*(\hat{q}) \widetilde{C}_{kl}(\hat{q}) \phi_l(\hat{q}), \tag{5.68}$$

with $\phi_k(\hat{q})$ a vector of 18 elements, obtained from $\phi_\mu(\hat{q})$ by simply dropping the last 6 entries. $\widetilde{C}_{kl}(\hat{q})$ is a 18×18 matrix whose elements are formed from the matrix $C_{\mu\nu}(\hat{q})$. Its final form is also given in Appendix 9.2.

Now we reduced the stability problem to the eigenvalue analysis of the $\tilde{C}_{kl}$ matrix: if all the 18 eigenvalues of $\tilde{C}_{kl}$ for each $\mathbf{q}$ (i.e. in the whole Brillouin zone) are positive, $\tilde{C}_{kl}$ is positive definite, the path integral remains Gaussian, so the saddle-point approximation is reliable.

5.3.3 Stability analysis

We have determined the spectrum of $\tilde{C}_{kl}$ for each of the three low lying states at low temperatures. In Fig. 5.6 we plot the lowest nonzero eigenvalues for the stability matrix $\widetilde{C}_{ij}(\mathbf{q}, 0)$ in the Brillouin zone for the CSL phase a), and for the quasi plaquette phase b). The CSL phase is stable against perturbations, as the lowest nonzero eigenvalue is positive everywhere. Contrary, the lowest nonzero eigenvalue of the curvature of effective action in case of the quasi plaquette phase develops prominent negative values around the Γ point. This phase turns out to be unstable. Note that among the 18 eigenvalues (for every $\mathbf{q}$) of the stability matrix $\widetilde{C}_{ij}(\mathbf{q}, 0)$ we have some flat zero modes corresponding to the local gauge symmetry. Both the CSL and quasi plaquette phases have 6 such flat bands, since 6 of the link variables can be chosen real with the help of gauge fixing.

In the plaquette phase all eigenvalues are constant, because the lattice is formed by the completely disjoint plaquettes and no momentum dependence remains. In this phase three of the links are zero, and we can fix only 5 of the

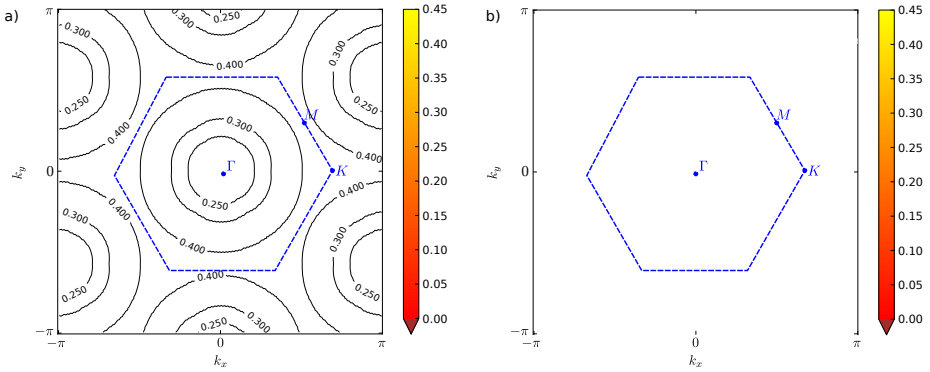

Figure 5.6: The lowest static eigenvalues of the curvature of the effective action in the Brillouin zone at zero temperature for the chiral spin liquid phase a), and for the quasi plaquette phase b).

6 remaining $\bar{\chi}$ links to be real. Correspondingly only 5 flat zero modes remain. All the other (nonzero) eigenvalues are positive, which means that the plaquette phase is stable.

It is worth to emphasize however, that the free energy analysis suggests a strong competition of the quasi plaquette state and the CSL state (see Fig. 5.4). The stability analysis shows that the quasi plaquette state collapses towards the lower free energy solution. The situation is similar to the case when the π-flux state of the SU(2) system on square lattice turns out to be unstable and collapse into the so called "box" state [133, 161]. Accordingly, only the CSL state remains the lowest lying state at least up to $k_{\mathrm{B}}T \sim 0.5J$, where its free energy starts to compare with that of the plaquette state. Above this temperature the two states have practically the same free energy, and with simple cooling it can not be predicted, which phase will stabilize. Nevertheless, the two phases have different symmetries and most importantly different topological properties that may allow to select the demanded state. For example it could happen during cooling and yet in the high temperature phase via imprinting a synthetic external gauge field to generate the nontrivial topology of the CSL state, on the low temperature state the enforced topological property remains even, when the external constraints are switched off.

5.3.4 Experimental observation: the structure factor

Ultracold alkaline earth atoms are produced routinely nowadays. A honeycomb optical lattice can also be created by sophisticated laser configurations [162]. Another, even cleaner experimental implementation would be to use the holographic methods of Greiner *et al.*, or Esslinger *et al.*, where an arbitrary two dimensional lattice potential can be created with the help of an optical imaging system [163, 164]. Detecting the CSL phase, or the emerging dynamical gauge theory is not straightforward, but possible. For example, one can measure nearest neighbor pair correlations [165], but there is only access to $|\chi_{ij}|$. In fact, according to the Elitzur's theorem non gauge invariant quantities, such as χ_{ij}, average to zero [159, 166].

A gauge invariant quantity sensitive to chirality and possible to measure is the phase of a loop, which can be detected directly by measuring 3-spin correlations: $\vec{S}_i \cdot (\vec{S}_j \times \vec{S}_k)$. It's nonzero value witnesses for the chiral nature of the spin liquid phase [167].

Finally, and more importantly, one can measure the spin structure factor in experiments, using for instance spin polarization spectroscopy [168]:

$$S^{zz}(\mathbf{r}, \mathbf{r}'; t) = \langle S^z(\mathbf{r}, t) S^z(\mathbf{r}', 0) \rangle, \tag{5.69}$$

where

$$S^z(\mathbf{r}, t) = S^z(\mathbf{r}_{mns}) = \sum_{\alpha\beta} F^z_{\alpha\beta} c^\dagger_{s\alpha}(\mathbf{r}_{mn}, t) c_{s\beta}(\mathbf{r}_{mn}, t) \tag{5.70}$$

is the z-component of the spin operator of a spin-$5/2$ alkaline earth atom at site $\mathbf{r}_{mns}$, accordingly, $F^z = \mathrm{diag}(5/2, 3/2, 1/2, -1/2, -3/2, -5/2)$ is the z-component of the three SU(2) generators in 6 dimensional representation.

This quantity can be expressed with the help of the four point spinon Green's functions, and in the RPA approximation is given by (in momentum space and Matsubara representation):

$$S^{zz}(\mathbf{q}, i\nu_m) = \frac{35}{2} \frac{1}{V\beta} \sum_{\mathbf{k},a,b} \frac{n(\varepsilon^{(a)}_{\mathbf{k}}) - n(\varepsilon^{(b)}_{\mathbf{k}+\mathbf{q}})}{i\nu_m + \varepsilon^{(a)}_{\mathbf{k}} - \varepsilon^{(b)}_{\mathbf{k}+\mathbf{q}}} \times \\ v^{(a)*}_s(\mathbf{k}) v^{(a)}_{s'}(\mathbf{k}) v^{(b)*}_{s'}(\mathbf{k}+\mathbf{q}) v^{(b)}_s(\mathbf{k}+\mathbf{q}). \tag{5.71}$$

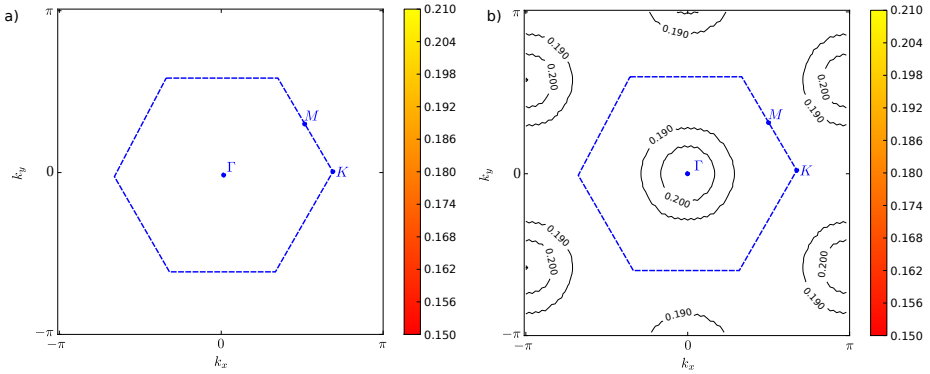

Figure 5.7: (Color online) The static structure factor $\mathcal{S}(\mathbf{q}, 0)$ in the Brillouin zone at zero temperature for the chiral spin liquid phase a), and for the quasi plaquette phase b).

The numeric factor comes from spin summation: $\sum_{\alpha\beta} F^z_{\alpha\beta} F^z_{\beta\alpha} = 35/2$. The fermionic occupation number at finite temperature is given by the Fermi distribution function $n(\varepsilon) = [e^{\beta\varepsilon} + 1]^{-1}$. Here, $\varepsilon_{\mathbf{k}}$ and $v_s(\mathbf{k})$ are the eigenenergies and eigenvectors of $H^{(0)}$, respectively, as they were introduced in Eq. (5.57).

The structure factor $S^{zz}(\mathbf{q}, i\nu_m)$ in Eq. (5.71) is a 6×6 matrix in the sublattice space. In order to take into account the total contribution of the unit cell, one needs to consider its trace:

$$\mathcal{S}(\mathbf{q}, i\nu_m) = \sum_s S^{zz}_{ss}(\mathbf{q}, i\nu_m). \tag{5.72}$$

We plot the static structure factors in Fig. 5.7 of the CSL phase a) and of the quasi plaquette phase b). That of the plaquette phase is completely flat due to its dispersionless spectra, and is not shown. For the other two low lying saddle-point solutions the static structure factors look completely different, both carry unambiguous features to identify them. In the CSL phase the structure factor has a minimum at the center of the Brillouin zone (the Γ point) and it has maxima at the K points. In contrary, in the quasi plaquette phase the structure factor is peaked close to the Γ point and has minima around the edge of the Brillouin zone. Since the experimentally measurable structure factor of the three

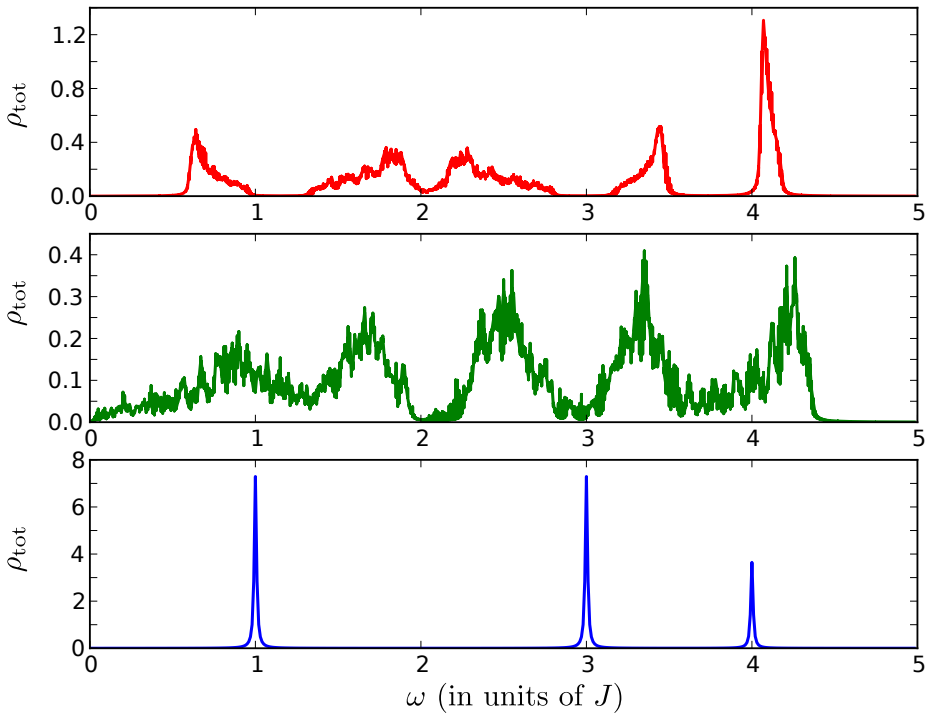

Figure 5.8: The spectral density $\rho_{\rm tot}(\omega)$ at zero temperature of the chiral spin liquid phase a), the quasi plaquette phase b), and the plaquette phase c).

lowest lying saddle-point configurations show completely different behavior, it is a suitable tool to distinguish between them.

By radio-frequency-spectroscopy one can measure the spectral density integrated to the whole lattice. This quantity can also be extracted from the structure factor given by Eq. (5.71). It can be obtained by analytically continuing $S(\mathbf{q}, i\nu_m)$ on the the upper half plane of complex frequencies and through the real axis by setting $i\nu_m \to \omega + i\eta$:

$$\rho_{\rm tot}(\omega) = \sum_{\mathbf{q}} \mathrm{Im}\, \mathcal{S}(\mathbf{q}, \omega + i\eta), \tag{5.73}$$

with η being an infinitesimally small number.

In our calculation we set its value to 10^{-2} (in units of the coupling strength J). We plot the spectral density of the three mean-field solutions in Fig. 5.8. The spectral function of the three different phases looks completely different indicating some characteristic features of the specific phase. While the CSL phase (a), and the plaquette phase (c) are gapped phases, there are no accessible states up to a gap, the quasi plaquette phase (b) is gapless. Furthermore, the plaquette phase is very simple, it contains only 3 delta peaks, also because of the lack of dispersion of the fermion energies. The first two peaks have twice the strength of the third one according to the fermion spectrum that consists of 4 dispersionless flat bands. From these 4 flat bands the lowest and the highest energy bands have only one state for every $\mathbf{q}$ momentum, and between them two doubly degenerate flat bands can be found. At zero temperature the lowest band is occupied and the higher bands are empty. By exciting a fermion to the upper bands the middle two have twice the number of states than the last one.

Chapter 6

The U(1) gauge magnet: phenomenology and digital quantum simulation

The Kogut-Susskind Hamiltonian (2.90) for the U(1) pure gauge theory was originally derived by considering the analogy between the space of configurations for the quantum rigid rotor and the pure quantum gauge theory [55]. It can also be derived from the transfer matrix of the model [169, 53].

In this chapter, we consider an alternative route for the derivation of a lattice gauge theory, the so called *constructive approach*. Using this approach one can interpret different lattice gauge theories known in the literature as *link models or gauge magnets* [170, 171, 172, 173] as a truncated version of the original Kogut-Susskind proposal. We would like to mention that this approach is rooted in the celebrated works by Kitaev about the Toric Code and Quantum Doubles [20] that we follow closely.

A lattice gauge theory is a particular case of a many-body quantum system, where the constituents are arranged on a lattice and the states (and the observables) are invariant under local transformations, which are elements of a given group $\mathcal{G}$. Starting by this operative definition, the basics steps for constructing a gauge invariant Hamiltonian for a lattice system, are:

- the choice of the representation of the gauge group $\mathcal{G}$ that, as we will see,

has immediate consequences on the definition of the Hilbert space of the model.

- the definition of the operators defining the gauge transformations.
- the determination of the set of operators that can be used to build the Hamiltonian, which has to be invariant under gauge transformation.

It is worth to notice that, for a given $\mathcal{G}$, infinitely many gauge invariant theories – and Hamiltonian, can be defined, although many of them may be equivalent under renormalization group flow, i.e., may share the same fixed point and critical properties.

6.1 Constructive approach to lattice gauge theories

In this section we are going to derive the Hamiltonian formulation of a gauge theory, following the constructive prescription. We will focus in Abelian lattice gauge theories, particularly in the simplest one, the $\mathbb{Z}_2$ gauge theory. This is the simplest lattice gauge theory one could construct (apart from the percolation lattice gauge theories of [174]), since there are only two different elements of the group, the first is 1 and the other is e, with the following multiplication table:

	1	e
1	1	e
$e^{-1} = e$	e	1

(6.1)

6.1.1 The Hilbert space

As we showed at Section 2.6, the constituents of the lattice gauge theories are attached to the links l connecting sites x of an oriented lattice $\mathcal{L}$. The orientation of the lattice means that, when addressing a link, one has not only to specify its position but also its orientation (the direction to follow in order to walk along it, i.e., in 2D either from left to right or from up to down or viceversa). Considering the physical picture of the links as currents moving from a site to another, the orientation is the direction of the current (and the gauge condition is the analogue of the conservation of the current at each site).

Each of the constituents attached to the oriented links is described by a vector in a local Hilbert space $\mathcal{V}_l$. If the lattice has N links, the global Hilbert space is defined as the tensor product $\mathcal{H} = \mathcal{V}_l^{\otimes N}$.

We remark that the choice of $\mathcal{V}_l$ is not unique, and this is the first freedom at hand in the construction of lattice gauge theories. In particular, the original formulation by Kogut and Susskind uses as local Hilbert space the group algebra $\mathbb{C}(\mathcal{G})$, so that the space of constituents is the vector space generated by linear combinations of elements of $\mathcal{G}$ with complex coefficients. To each element of the group $\mathcal{G}$, one associates a vector $|g\rangle$, with the property $\langle h|g\rangle = \delta_{g,h}$. Here $\delta_{.,.}$ is the Kronecker delta. Therefore, in the Kogut-Susskind formulation, the dimension of the local Hilbert space is strictly related to the number of elements in the group. Hence, it becomes infinite for continuous groups like $U(1)$. In the simplest case of $\mathbb{Z}_2$, the local Hilbert space is generated by the two orthogonal vectors $|1\rangle$ and $|e\rangle$, and it is isomorphic to $\mathbb{C}^2$. However, as we will show below, *it is perfectly consistent to consider a local Hilbert space, whose dimension does not depend on the number of elements* $\mathcal{G}$.

As an example, the space of constituents of a 2D lattice is sketched in Fig. 6.1. Since we are dealing with an oriented lattice, we also orient the states. Following physical intuition of a links as currents between sites, the change of orientation corresponds to *an inversion* of the currents, which is equivalent to the operation

$$|h\rangle_l \to |h^{-1}\rangle_{-l}. \tag{6.2}$$

It is worth to observe that, for the guiding example of $G = \mathbb{Z}_2$, the orientation plays no role since $e^{-1} = e$ and $1^{-1} = 1$, hence, $|e\rangle_l = |e\rangle_{-l}$ and $|1\rangle_l = |1\rangle_{-l}$.

As we indicated, the choice of the local Hilbert space $\mathcal{V}_l$ is not unique. The only requirement is that $\mathcal{V}_l$ has to be isomorphic to a representation of the symmetry group G. In particular, the choice of $\mathbb{C}(\mathcal{G})$ induces the choice of the regular representation of the group, $R(\mathcal{G})$. The action of an element of $X(g) \in R(\mathcal{G})$ on $|h\rangle$, is defined as

$$X(g)|h\rangle = |(gh)\rangle, \tag{6.3}$$

This means that the matrix representation of $X(g)$ reads

$$X(g) = \sum_{h\in\mathcal{G}} |gh\rangle\langle h|. \tag{6.4}$$

Therefore, in the regular representation the matrices are constructed directly from the multiplication table of the group. In order to get the representation

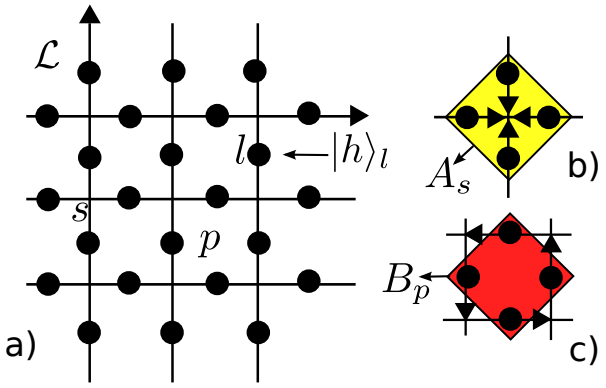

Figure 6.1: a) A lattice gauge theory is many-body system defined on a lattice $\mathcal{L}$. The constituents $|h\rangle_l$ are attached to the links l. The lattice is oriented, meaning that links inherit the standard orientation of the embedding space, depicted in the figure as arrows. When defining operators acting on the states attached to links, one has also to specify an orientation. b) and c) The building blocks of a lattice gauge theories include two sets of four-body operators. b) The one attached to sites s, A_s, which we also refer to as *star* operators, are used to impose the gauge invariance. c) The ones attached to plaquettes p B_p, which we also refer to as *plaquette* operators, describe the dynamics. We define both A_s and B_p by using a customary oriented star and plaquette.

of multiplication by a given element, one substitute the given element in the multiplication with one and all the others with zeros. For the $\mathbb{Z}_2$ case it results:

$$X(1) = \mathbb{I}, \quad X(e) = \sigma_x, \tag{6.5}$$

due to the multiplication table is expressed in (6.1).

When we change the orientation of a link, according to (6.2), we also have to invert the operator that is acting on it,

$$|(gh)\rangle_l \to |(h^{-1}g^{-1})\rangle_{-l} = X_{-l}(h^{-1}g^{-1}h)|h^{-1}\rangle_{-l} = X_{-l}(g)^\dagger |h^{-1}\rangle_{-l} \tag{6.6}$$

where l is an arbitrary oriented link of $\mathcal{L}$ and we have used the fact that, for Abelian groups, $h^{-1}g^{-1}h = g^{-1}$, and, for unitary representations, $X(g^{-1}) = X(g)^\dagger$. The irrelevance of the orientation in the $\mathbb{Z}_2$ case translates to that both $X(1)$ and $X(e)$ are Hermitian.

6.1.2 Gauge invariance and the physical Hilbert space

As we discussed in Section 2.6.2, a generic *gauge transformation* is implemented in the Hilbert space by an unitary operator V acting on the links of the lattice $\mathcal{L}$ (see Eq. (2.87)). This transformation is defined by choosing a group element for each site of the lattice and rotating all the links entering that particular site with the matrices representing the rotation for that particular element. The building blocks of gauge transformations are thus obtained by acting on all links entering a given site with $X(g)$. The operator that induces such rotation is often referred as *star* operator (see (2.87)). In the constructive approach it is convenient to express it as:

$$A_s(g) \equiv \bigotimes_{l \in \{l_i\}_s} X_l(g)\, |h_{l_1}, h_{l_2}, h_{l_3}, h_{l_4}\rangle \to |gh_{l_1}, gh_{l_2}, gh_{l_3}, gh_{l_4}\rangle, \tag{6.7}$$

where s is a generic site of the lattice and $\{l_i\}$, $i = 1, \ldots, 4$, is the set of all the links *entering* s, as depicted on Fig. 6.1 b). In view of (6.2) and (6.6), this operator acting on the links of a lattice oriented in the conventional way (such as in Fig. 6.1a) becomes

$$A_s(g) : |h_{-l_1}, h_{-l_2}, h_{l_3}, h_{l_4}\rangle \to |h_{l_1}^{-1}g^{-1}, h_{l_2}^{-1}g^{-1}, gh_{l_3}, gh_{l_4}\rangle, \tag{6.8}$$

where the links are numbered clockwise starting by the one on the top. In terms of $X(g)$ operators, the above expression is equivalent to:

$$A_s(g) = X^\dagger_{l_1}(g) X^\dagger_{l_2}(g) X_{l_3}(g) X_{l_4}(g). \tag{6.9}$$

Since we are considering local gauge transformations, the choice of the group element g can vary from site to site so it would be more appropriate to use $g(s)$ but in order to simplify the notation we stick to g.

For $G = \mathbb{Z}_2$, we have two possible $A_s(g)$:

$$\begin{aligned} A_s(1) &= \mathbb{I}_{l_1}\mathbb{I}_{l_2}\mathbb{I}_{l_3}\mathbb{I}_{l_4} = \mathbb{I}, \\ A_s(e) &= \sigma^x_{l_1}\sigma^x_{l_2}\sigma^x_{l_3}\sigma^x_{l_4} = (\sigma_x)^{\otimes 4}. \end{aligned} \tag{6.10}$$

Thus, the unique non-trivial operator for $\mathcal{G} = \mathbb{Z}_2$ is $A_s(e)$, which induces spin-flips on all qubits entering the specific site s.

States are invariant under the gauge transformations at site s if they are eigenvectors of the $A_s(g)$ operators with eigenvalue $+1$,

$$A_s(g)|\psi\rangle = |\psi\rangle, \forall g \in \mathcal{G}. \tag{6.11}$$

Since generic gauge transformations are product of local ones, a state is gauge invariant if

$$V[g]|\psi\rangle \equiv \bigotimes_{s\in\mathcal{L}} A_s(g)|\psi\rangle = |\psi\rangle, \forall g \in \mathcal{G}, \tag{6.12}$$

which leads to the definition of the *physical* Hilbert space expressed in (2.89).

For $\mathcal{G} = \mathbb{Z}_2$, the requirement of invariance at a specific site under the action of $A_s(e)$ reduces the 2^4 state of the four links to 8, for a system on a 2D lattice. In order to determine the allowed states, it is better to diagonalize σ^x:

$$\sigma^x = |+\rangle\langle+| - |-\rangle\langle-|. \tag{6.13}$$

In this basis, all those states formed as tensor product of four eigenstates of σ^x with an even number of $|-\rangle$ are eigenstates of $A_s(e)$ with eigenvalue $+1$, and thus gauge-invariant. As we will describe in the following, one can give a nice geometrical interpretation to those states in terms of closed string of $|-\rangle$.

6.1.3 Operators compatible with the requirement of gauge invariance

By definition, the Hamiltonian H has to respect the local symmetry, i.e., commute with all *star* operators $A_s(g(s))$,

$$[H, A_s] = 0, \ \forall A_s. \tag{6.14}$$

Our goal is to build up H as a sum of local terms. To this aim, we introduce a set of operators Z_r, (where r labels the representation of the group) acting on the tensor product of the local Hilbert spaces $\mathcal{V}_l \otimes \mathcal{V}_g$. Again, there is a lot of freedom in defining the local Hilbert spaces $\mathcal{V}_g$, since the only requirement is to support an irreducible representation (irrep) of the gauge group (for a definition of irreducible representation refer to [175]).

When the local Hilbert space is the group algebra, the operators Z_r acquire the following form

$$Z_r = \sum_{h \in \mathcal{G}} R_r(h) \otimes |h\rangle\langle h|, \tag{6.15}$$

where $R_r(h)$ is the matrix representing h in the irreducible representation r of $\mathcal{G}$. Since all irreducible representation of Abelian groups are one dimensional and isomorphic, for Abelian theories we can drop the index r from R_r and think of them as acting only on $\mathcal{V}_l$ since, in this case, $R(h)$ is just a phase.

For the case of $\mathcal{G} = \mathbb{Z}_2$, the only non-trivial choice for Z is:

$$Z = \sigma^z = |1\rangle\langle 1| - |e\rangle\langle e|. \tag{6.16}$$

The relation between Z and $X(g)$ is encoded in the commutation relation

$$[ZX(g) - X(g)Z] = R(g)XZ. \tag{6.17}$$

This immediately suggests a minimal choice to fulfill (6.14). We can, indeed, consider as building blocks for H the product of four Z operators acting on links around elementary plaquettes of the lattice

$$B_p \equiv \bigotimes_{l \in \{l_i\}_p} Z_{l,r}, \tag{6.18}$$

that we generally call *plaquette operator*. Here, $\{l_i\}_p$, $i = 1, \ldots, 4$, is a set of links belonging to the plaquette p and anti-clockwise oriented starting from bottom, as sketched in Fig. 6.1c.

By rewriting B_p for the standard-oriented lattice, as in Fig. 6.1a, we obtain

$$B_p = Z_{l_1,r} Z_{l_2,r} Z^\dagger_{l_3,r} Z^\dagger_{l_4,r}. \tag{6.19}$$

In the elementary case of $G = \mathbb{Z}_2$, the plaquette operator is just $B_p = \sigma^z_{l_1} \sigma^z_{l_2} \sigma^z_{l_3} \sigma^z_{l_4}$.

As a plaquette and a star operator share none or two links, l and l', it is sufficient to verify the relation

$$[Z_l(r) \otimes Z_{l'}(r), X_l(g) \otimes X^\dagger_{l'}(g)] = 0, \tag{6.20}$$

in order to check that B_p and A_s commute. As the above relation is a direct consequence of (6.17) (and that for any representation $R(g^{-1}) = R^{-1}(g)$), the desired result holds:

$$[B_p, A_s(g)] = 0, \quad \forall \{p, s\} \in \mathcal{L}, g \in \mathcal{G}. \tag{6.21}$$

For an Abelian gauge group – the case of interest in this work– any operator $X_l(h)$ commutes with $A_s(g_s)$. Hence, it follows that any hermitian functional of B_p and $X_l(h)$ is a good gauge invariant Hamiltonian for Abelian gauge theories. In particular, we focus on the linear combination

$$H(\theta) = -\cos\theta \sum_p B_p + \sin\theta \sum_l X_l(g) + H.c.\,, \tag{6.22}$$

where p are the elementary plaquettes of the lattice and l are the links. This coincides with the Kogut-Susskind Hamiltonians [176], by indentifying the plaquette term as the *magnetic* term and the star operator term as the *electric* field.

In the specific case of $\mathcal{G} = \mathbb{Z}_2$, it can be written explicitly in terms of Pauli matrices:

$$H(\theta) = -\cos\theta \sum_p \prod_{l \in p} \sigma^z_l + \sin\theta \sum_l \sigma^x_l(g). \tag{6.23}$$

The B_p and X_l operators describe magnetic and electric interactions respectively. They can only have two values, ± 1 for the case of $G = \mathbb{Z}_2$. When $\theta = 0$ there is no electric field in the Hamiltonian and we refer this regime as *plaquette or magnetic regime*, whereas the *electric regime* is refered in the case $\theta = \frac{\pi}{2}$

It is worth noticing that the presence in the Hamiltonian of terms involving four-body interactions is a direct consequence of gauge invariance. There have

been several attempts to obtain a gauge invariant Hamiltonian starting from a model with only first neighbour interactions. For instance, by defining two-body Hamiltonians on a coarse grained lattice [177], one can obtain in some case equivalent Hamiltonians to those with four-body interactions. However, at the moment these type of constructions are restricted to exactly solvable models, and it is unclear how to generalize them to a generic Hamiltonian, as the one we will consider in the following. Thus, in this thesis we stick to the idea that gauge invariance (on square lattices) requires four-body interactions.

6.2 Gauge magnets or link models

The Kogut-Susskind type Hamiltonian (2.90) is obtained from the constructive approach by choosing:

- The local Hilbert space to be the group algebra $\mathbb{C}(\mathcal{G})$.
- The $X(g)$ operators to be obtained by considering the regular representation of the rotation by an element g of group $\mathcal{G}$.
- The Hamiltonian to be constructed using the simplest closed path of the lattice, the plaquettes.

Here, we focus on alternative choices to the first point. The reason is that the $\mathbb{C}(\mathcal{G})$ algebra for a continuous group is infinite dimensional, while the implementation we propose for the simulation of lattice gauge theories with optical lattices can only deal with finite dimensional local Hilbert spaces (see Chapter 6). Therefore, our aim is to construct Abelian lattice gauge theories with the smallest possible local Hilbert space, independently on the number of elements of the group $\mathcal{G}$. This leads to lattice gauge theories that have been called gauge magnets or link models [170, 171, 172, 173] in the literature, whose particular cases are $U(1)$ lattice gauge theories with finite dimensional local Hilbert space.

Let us consider again the (possibly infinite dimensional) local Hilbert space $\mathbb{C}(\mathcal{G})$. A celebrated theorem of group theory, Maschke's theorem, allows us to truncate $\mathbb{C}(\mathcal{G})$ to a finite dimensional Hilbert space, *keeping the gauge symmetric structure*. The theorem states that the regular representation (the one that acts on $\mathbb{C}(\mathcal{G})$) can be written as the direct sum of all possible irreducible representations (with a multiplicity equal to their dimensionality) [175].

As a consequence of this theorem, we are guaranteed that there is a change of basis such that the operators $X(g)$ become block diagonal,

$$X(g) = \oplus_r \sum_{ij} R_r(g)^{i,j} |(r,i)\rangle\langle(r,j)|, \tag{6.24}$$

where we have explicitly written the block structure of $X(g)$ labeled by the r irrep, and the $R_r(g)^{i,j}$ are matrix elements of the irrep r of $g \in \mathcal{G}$, $i,j = 1 \cdots \dim(\mathrm{r})$.

We call the rotation matrix that brings all $X(g)$ to the block diagonal form, $\alpha((r,i),g)$, so that we can express the Z_r operators in the new basis as

$$Z_r = \sum_{(p,i),(q,j)} z_r^{(pi),(qj)} |(p,i)\rangle\langle(q,j)|. \tag{6.25}$$

where

$$z_r^{(pi),(qj)} = \sum_g \alpha((p,i),g) R_r(g) \alpha^{-1}(g,(q,j)). \tag{6.26}$$

We call the new basis with abuse of notation $\{|r\rangle\}$ basis.

In the $\{|r\rangle\}$ basis, we can safely truncate the local Hilbert space of the lattice gauge theories without any effect on the symmetry requirements. Indeed, we just have to include at least one of the diagonal blocks of $X(g)$. However, it could happen that by keeping just one block either $X(g)$ or $Z(r)$ become trivial (that is indeed the case for Abelian theories). For this reason, we need to keep at least two irreps. In this case, the local Hilbert space will have dimension $d = dim(r_1) + \cdots dim(r_n)$, where one can stop at the first n that provides both non-trivial symmetry requirement, and non-trivial dynamics.

In the following, we will provide the specific example of the $U(1)$ gauge magnets, since it is the one we are interested in simulating with optical lattices. In the Appendix 9.3, we provide further examples for generic $\mathbb{Z}_N$ gauge magnets.

6.3 U(1) gauge magnet

For the case of U(1) gauge group, the Hilbert space of the algebra of the group is infinite dimensional. Since this group is Abelian, its irrep. are one-dimensional. Therefore there is basis where all the $X(g)$ are diagonal:

$$R(\alpha) = \begin{pmatrix} 1 & 0 & 0 & 0 & \cdots \\ 0 & e^{i\alpha} & 0 & 0 & \cdots \\ 0 & 0 & e^{i2\alpha} & 0 & \cdots \\ 0 & 0 & 0 & e^{i3\alpha} & \cdots \\ \vdots & \vdots & \vdots & \vdots & \ddots \end{pmatrix}, \tag{6.27}$$

the $X(g)$ are obtained by choosing a phase. In each irrep. a generic element of the group is obtained by multiplying the chosen phases sufficient number of times, except for the first one, r_1, where all the elements are mapped to 1.

For constructing the corresponding gauge magnet one retains at least two arbitrary irreps, $r_1 \oplus r_2$. Since they are one-dimensional, we can work with qubits. We could choose any irreps r_1 and r_2, the simplest choice is to select the trivial irrep, where all the elements are mapped to 1, and the irrep. where a given element $g \in$U(1), distinct than the identity $\mathbb{I}$, is mapped to the phase $e^{i\alpha_g}$: As we are interested in faithful irreps, α_g has to be chosen not commensurable with 2π:

$$\alpha \neq 2\pi \frac{p}{q} \quad p, q \in \mathbb{Z}. \tag{6.28}$$

Then:

$$\forall\ \beta \ \ \exists\ n : R(\beta) = R(n\alpha) = R(\alpha)^n \tag{6.29}$$

Local invariant under a g is sufficient to ensure invariance under any local U(1)-transformation.

We denote the eigenvectors of the $X(g)$s as $|+\rangle$ and $|-\rangle$. This means that the X operators are

$$X(g) = |+\rangle\langle +| + |-\rangle\langle -|e^{i\alpha_g}, \tag{6.30}$$

while the Z operator reads

$$Z = |+\rangle\langle -|. \tag{6.31}$$

This specific model can be mapped (on bipartite lattices) by a unitary transformation to the one studied in [178].

In order to describe the physics of the model, it is important to notice that we can characterize $\mathcal{H}_G$ graphically. In the $|+\rangle$ and $|-\rangle$ basis and with the

standard 2D orientation of Fig. 6.1, the gauge condition (6.11) reads as:

$$A_s|t_{l_1}, t_{l_2}, t_{l_3}, t_{l_4}\rangle = R(-\alpha)_{l_1} R(-\alpha)_{l_2} R(\alpha)_{l_3} R(\alpha)_{l_4} = |t_{l_1}, t_{l_2}, t_{l_3}, t_{l_4}\rangle. \quad (6.32)$$

Then, a given site s the gauge symmetry selects among the 2^4 states of the four links entering s only six possible configurations:

$$|+,+,+,+\rangle, |-,+,-,+\rangle, |+,-,+,-\rangle, |-,-,-,-\rangle, |-,+,+,-\rangle, |+,-,-,+\rangle. \quad (6.33)$$

These are shown in Fig. 6.2.

Similarly to standard lattice gauge theories, we can interpret the U(1)-invariant Hilbert space as the space of closed strings formed by $|-\rangle$ states, onto the vacuum of $|+\rangle$ states. Indeed, as any of the six allowed states contains an even number of $|-\rangle$, at each site of the lattice, for any ingoing $|-\rangle$ there is also the corresponding outgoing one. Hence, the string cannot end on a (bulk) site, i.e. only closed string (or string touching the boundary) are compatible with gauge invariance.

In addition, it is worth to notice that the six allowed configurations do not allow to construct a closed string of finite size (without reaching the boundary). This means that, for lattices with periodic boundary conditions, strings can only close by wrapping around the whole lattice. This implies that their length is at least equal to the lattice size. This is an important difference with respect to standard lattice gauge theories. In standard lattice gauge theories, indeed, closed strings can be of arbitrary length, the shortest being the strings around a single plaquette.

In order to clarify the origin of this discrepancy, one can consider the Kogut-Susskind $\mathbb{Z}_2$ lattice gauge theories introduced in the previous section. There, the group algebra is two-dimensional, that is, the local Hilbert space is still made of qubits. As we have already shown, the gauge condition selects 8 out of the 16 states of the four links entering a given site. It turns out that 6 of them coincide with the one of the $U(1)$ gauge magnet of Fig. 6.2 a), but there are two extra states as shown in Fig. 6.2 b):

$$|-,-,+,+\rangle, |+,+,-,-\rangle. \quad (6.34)$$

These states are, indeed, the ones needed to close a small loop of $|-\rangle$ (for example a single plaquette). In fact, this small difference produces completely different strings patterns, as we can appreciate in Fig. 6.3.

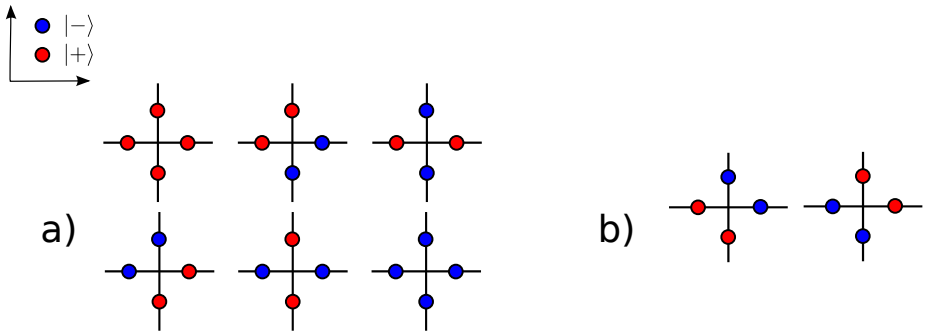

Figure 6.2: **a)** The requirement of gauge invariance of the states using (6.11) selects only 6 out of the total 16 states of the four qubits entering a given site. In the standard 2D orientation, one can visualize the 6 allowed states by coloring in red states $|+\rangle$ and blue $|-\rangle$. **b)** If we consider the standard $\mathbb{Z}_2$ lattice gauge theories the gauge symmetry condition of (6.11) selects 8 out of the 16 states of the four qubits attached to the links entering a given site. They include the same 6 states than those of the U(1) gauge magnet of panel a). The two extra states are represented here, and are those responsible of the existence short closed loops.

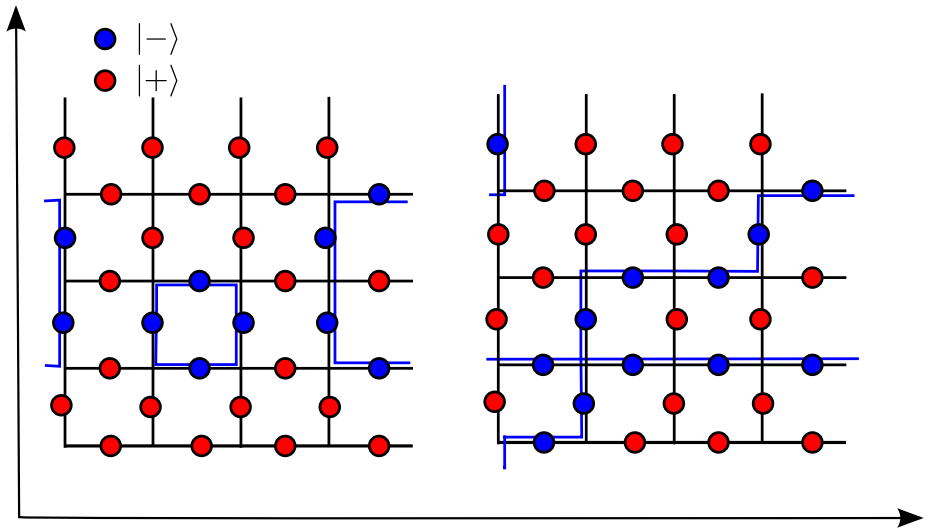

Figure 6.3: Here, we depict a 4x4 lattice with periodic boundary conditions in both directions. Red qubits are in the state $|+\rangle$, while blue qubits are in the state $|-\rangle$. The blue qubits form closed string pattern as required by gauge invariance. On the left, we show a possible gauge invariant state of the standard $\mathbb{Z}_2$ lattice gauge theories. On the right, the same plot is presented for the U(1) gauge magnet. In both cases, the states can be mapped to closed string configurations. There is an important difference between the two cases, however. In $\mathbb{Z}_2$ lattice gauge theories, closed strings can form arbitrary small closed loops. In the U(1) gauge magnet, due to the absence of the states in Fig. 6.2 b), strings are forced to close by wrapping around the whole lattice. This means that their typical length exceeds that of the linear lattice size. Blue lines are drawn as a guide to the eye to recognize the closed string wrapping around the periodic boundaries of the lattice.

6.3.1 Pure gauge theory in the magnetic or plaquette phase: $\theta = 0$

The different string patterns have deep consequences on the physics of the models. Standard lattice gauge theories, indeed, have at least two phases, a confined phase and a deconfined phase. In the confined phase, short closed string abound, while long closed string are very rare and vice-versa in the deconfined phase [179]. In the $U(1)$ gauge magnet, by just noticing the absence of short closed strings, we already have a strong indication that the phase diagram of the model is very different from the one of the standard $U(1)$ lattice gauge theories.

Let us analyse it in details. First, let us consider the dynamics induced by the Hamiltonian (6.22) when $\theta = 0$: plaquette or magnetic phase. Contrary to what happens in standard Abelian lattice gauge theories, for the gauge magnets two plaquettes operator sharing one link are not commuting, i.e., generally:

$$[B_p, B'_p] \neq 0. \tag{6.35}$$

This means that the ground-state is not a simultaneous eigenvector of all the B_p's. However, for the sake of the present discussion we can, as suggested in [178], circumvent this problem on bipartite lattices by considering, first, only half of Hamiltonian, and, afterwards, the effects of the other terms in (6.22). We start with

$$H_0 = -\sum_{p_y} (B_{p_y} + B^\dagger_{p_y}), \tag{6.36}$$

where with p_y we label half of the plaquettes, the ones drawn in yellow in Fig. 6.4. In this way, H_0 only contains operators that do not share any link, and, thus, all commuting.

The model (6.36) is exactly solvable, and we can write its ground-state as the action of a series of projectors onto a given reference state. It is important to notice that the reference state should be i) gauge invariant, and ii) not belonging to the kernel of the various B_p considered.

Indeed, in contrast to what happens for standard lattice gauge theories, the B_p here has only two eigenvalues different from zero, equal to ± 1. It is easy to check that a possible reference state fulfilling these requirements is the one depicted in the central panel of Fig. 6.4, consisting of two strings each of length $L^2/2$ wrapping around the lattice of size $L \times L$ with periodic boundary conditions. We call this reference state $|\psi_0\rangle$.

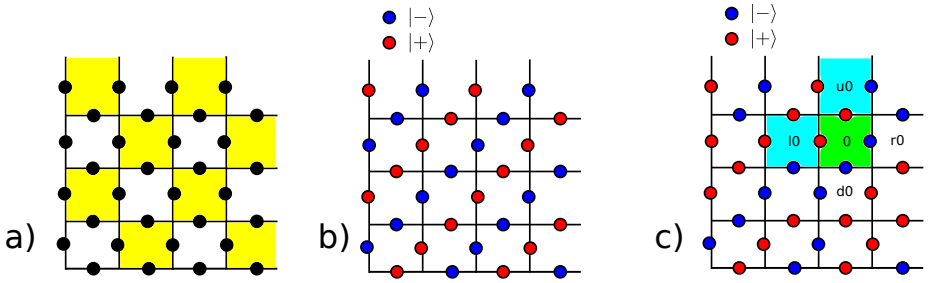

Figure 6.4: **a)** Lattices with an even number of sites and periodic boundary conditions are bipartite. This allow to consider the model with half of the plaquettes (filled in yellow in the figure) turned on. In this way, the different yellow plaquettes do not share any link and the U(1) gauge magnet Hamiltonian is built up of mutually commuting terms. This implies that the ground-state is simultaneous eigenvector of all the terms appearing in the Hamiltonian. **b)** Reference state used to construct the ground-state of the Hamiltonian (6.36) through the action of projectors (6.37). **c)** An example of reference state used to obtain an excitation with gap $\Delta = 2$.

We can define the three different projectors on to the subspace of different eigenvectors of $(B_p + B_p^\dagger)$ as

$$P_p^1 = \frac{1}{2}(B_p + B_p^\dagger)\left(B_p + B_p^\dagger + \mathbb{I}\right), \tag{6.37}$$

$$P_p^{-1} = \frac{1}{2}(B_p + B_p^\dagger)\left(B_p + B_p^\dagger - \mathbb{I}\right), \tag{6.38}$$

$$P_p^0 = -\left(B_p + B_p^\dagger + \mathbb{I}\right)\left(B_p + B_p^\dagger - \mathbb{I}\right), \tag{6.39}$$

so that the ground-state $|\Omega(0)\rangle$ is proportional to

$$|\Omega(0)\rangle \propto \bigotimes_{p_y} P_{p_y}^1 |\psi_0\rangle. \tag{6.40}$$

By construction the above state is not null and minimizes the energy as

$$|\Omega(0)\rangle = \bigotimes_{p_y} |1\rangle_{p_y}, \quad \left(B_{p_y} + B_{p_y}^\dagger\right)|1\rangle_{p_y} = |1\rangle_{p_y}, \forall p_y \in \{\text{yellow plaquettes}\}. \tag{6.41}$$

As, in principle, all the eigenvectors of H_0 can be constructed by applying the projectors (6.37-6.39) on an appropriate gauge invariant state, it follows that there is a gap to the first excited state. Such gap is at least equal to one, corresponding to a state

$$|\Phi(\{0,p'_y\})\rangle = \bigotimes_{p_y \neq p'_y} |1\rangle_{p_y} \otimes |0\rangle_{p'_y}, \quad \left(B_{p'_y} + B^\dagger_{p'_y}\right)|0\rangle_{p'_y} = 0. \tag{6.42}$$

However, it is easy to argue that such a state cannot satisfy the gauge invariance requirement on each of the sites at the vertices of the plaquette p'_y.

Hence, $|\Omega(0)\rangle$ describes a gapped phase with gap 2. The simplest excited state with such energy is

$$|\Phi(\{-1,p'_y\})\rangle = \bigotimes_{p_y \neq p'_y} |1\rangle_{p_y} \otimes |-1\rangle_{p'_y}, \quad \left(B_{p'_y} + B^\dagger_{p'_y}\right)|-1\rangle_{p'_y} = -|-1\rangle_{p'_y}, \tag{6.43}$$

as $|\Phi(\{-1,p'_y\})\rangle \propto \bigotimes_{p_y \neq p'_y} P^1_{p_y} \otimes P^{-1}_{p'_y} |\psi_0\rangle$.

It is worth to notice that first excited states of the form:

$$|\Phi(\{0,p'_y\},\{0,p''_y\})\rangle = \bigotimes_{p_y \neq p'_y, p''_y} |1\rangle_{p_y} \otimes |0\rangle_{p'_y} \otimes |0\rangle_{p''_y}, \tag{6.44}$$

also exist and are gauge invariant, but cannot be obtained just by applying projectors on the reference state $|\psi_0\rangle$ as $P^0_{p_y}|\psi_0\rangle = 0$, $\forall p_y$ in the yellow plaquettes' sublattice. In this case, the procedure is more complex, and it involves a B operator acting on a plaquette of the other sublattice, as illustrated in the right pannel of Fig. 6.4. It is found that

$$|\Phi(\{0,l_0\},\{0,u_0\})\rangle \propto P^0_{d_0} P^0_{r_0} B_0 |\Omega(0)\rangle, \tag{6.45}$$

where d_0, r_0, u_0, l_0 are the plaquettes in the yellow sublattice that surrounds the 0 plaquette of the complementary sublattice.

6.3.2 Plaquette or magnetic regime in presence of static charges

In this simple model, we can compute exactly how the presence of static external charges modifies the ground-state. A static charge ± 1 at site s modifies the

gauge condition (6.11) to

$$A_s(g)|\psi\rangle = \exp(\pm i\alpha_g)|\psi\rangle. \tag{6.46}$$

That is to say, the presence of static charges modifies the allowed string configurations. Open strings are, indeed, allowed if they start and end on the charges. This, clearly, affects the properties of the ground-state of the system.

With two charges ± 1, the ground-state is orthogonal to the one without static charges. This implies that we have to change both the reference state and the set of projectors, in order to construct the new ground-state

$$|\Omega(0)_\pm\rangle \propto \bigotimes_{p_y} \tilde{P}_{p_y}|\psi_{\pm 1}\rangle. \tag{6.47}$$

A simple candidate for $|\psi_{\pm 1}\rangle$ can be obtained by transforming one of the two closed strings of $|-\rangle$ contained in $|\psi_0\rangle$ into an open one. As illustrated in Fig. 6.5 for a 4×4 lattice with periodic boundary condition, this can be done by flipping one or more consecutive $|-\rangle$ (blue) links to (red) $|+\rangle$ links. This creates two static charges of opposite charge at the two ends of the blue string, where modified gauge condition (6.46) holds. Two possible choices of the reference state $\psi_{\pm 1}$, which differ on the position of the static charges, are sketched in Fig. 6.5. The $+1$ static charges are denoted by filled black dots, while -1 ones by empty dots.

Now, the projectors $\tilde{P}_{p_y}$ are determined by the requirement of minimizing the energy while respecting the new gauge condition, which depends only on the position of the ± 1 charges. Since the above defined $|\psi_{\pm 1}\rangle$ differ from $|\psi_0\rangle$ only by few flipped links, located between the two ends of the open string, the projectors $\tilde{P}_{p_y}$ may be distinct from the $P^1_{p_y}$ only for the plaquettes p_y (of the yellow lattice) interested by such flips, $p_y \in \{\text{flipped region}\}$ (pale yellow shaded plaquettes of Fig. 6.5). In fact, as manifestation of orthogonality of the ground-state with back-ground charges to the ground-state without charges, $|\psi_{\pm 1}\rangle$ is annihilated by the projectors (6.37) acting on the plaquettes between the two ends of the open string. Hence, the proper choice of projectors in such a region, which minimizes the energy and does not annihilate the state, is given by the projector of (6.39), $\tilde{P}_{p_y} = P^0_{p_y}$, $\forall p_y \in \{\text{flipped region}\}$.

As a consequence, the ground-state energy of the system with two static charges is higher than the one without the two charges. The energy gap Δ_q is equal to the number of P^0 projectors, i.e., the number of yellow plaquettes that contain flipped links. Up to artifacts of the discretization, such number is

proportional to the number of flipped links itself, n_F, i.e., is proportional to the distance r, in lattice spacing unit, between the charges, $\Delta_q(r) \propto r$. As it can be easily deduced from Fig. 6.5, the exact relation between the gap and the number of flipped links is

$$\Delta_q = n_F - \mathrm{Int}[\frac{n_F}{2}],$$

while the distance between the charge depends on n_F as

$$r = \left|\left(n_F - \mathrm{Int}[\frac{n_F}{2}]\right)(1,0) + \mathrm{Int}[\frac{n_F}{2}](0,1)\right| = \sqrt{n_F^2 + 2\,\mathrm{Int}[\frac{n_F}{2}]^2 - 2\,n_F\,\mathrm{Int}[\frac{n_F}{2}]},$$

where $\mathrm{Int}[x]$ is the integer part of x. The above formula is obtained by taking in account the "zig-zag" behavior the displacement of the charges shows when one additional link is flipped.

These two relations together are the footprint of charge confinement, a phenomenon that the present model shares with many other gauge theories, among them, QCD. This means that the gap scales as

$$\Delta_q(r) = \sigma r, \tag{6.48}$$

where σ is called string tension. In the long distance regime, i.e., $n_F \gg 1$, it follows that $\Delta_q \sim \frac{n_F}{2}$ and $r \sim \frac{n_F}{\sqrt{2}}$, hence, $\Delta_q \sim \frac{r}{\sqrt{2}}$, and the string tension for this model is $\sigma \sim \frac{1}{\sqrt{2}}$.

6.3.3 Gauge magnet in intermediate regimes: $\theta \neq 0$

At this point, we consider the effect of the link term for $\theta \neq 0$. By the Hamiltonian $\cos\theta\, H_0 + \sin\theta \sum_l (X_l(g) + X_l^\dagger(g))$. The last term of the Hamiltonian, $\cos\theta\, H_0 + \sin\theta \sum_l (X_l(g) + X_l^\dagger(g))$ is certainly dominant close to $\theta = \frac{\pi}{2}$. In this phase, the ground-state is the product state

$$|\Omega\left(\frac{\pi}{2}\right)\rangle = \bigotimes_l |-\rangle_l, \tag{6.49}$$

regardless of the α_g we have chosen to represent a generic $U(1)$ element g. Hence, one expects to encounter a phase transition when θ grows from zero to $\frac{\pi}{2}$. We observe that i)

$$H_0|\Omega\left(\frac{\pi}{2}\right)\rangle = 0, \tag{6.50}$$

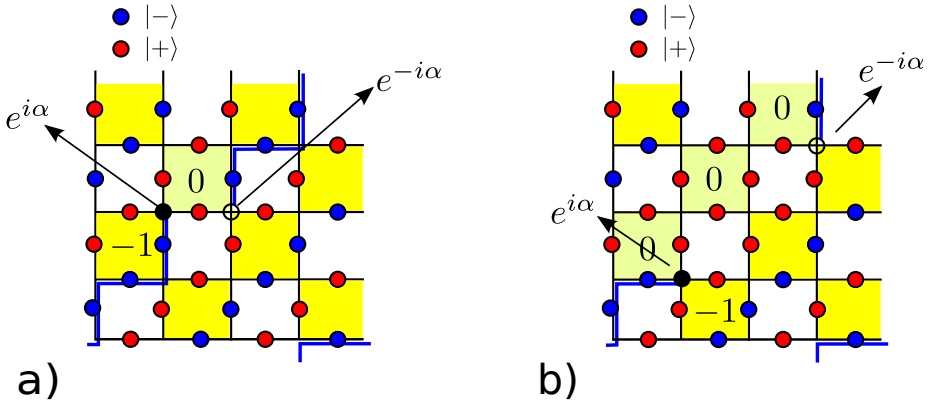

Figure 6.5: The presence of static external charges modifies the ground-state. **a)** Sketch of the reference configuration used to obtain the ground-state with two static first neighbors charges (presented as filled black dots for charge $+1$ and empty dots for charge -1). The blue string os states $|-\rangle$ is broken in between them. The plaquettes states along the broken part of the string are orthogonal to the eigenstates of B_p with eigenvalue 1. These plaquette are filled in with a pale shade of yellow in the drawing while regular plaquettes that contribute -1 to the ground-state energy filled in solid yellow. This implies that the ground-state energy in the presence of static charges increases by an amount proportional to the inter-charge separation, manifestation of charge confinement. **b)** Sketch of the reference state for charges at distance $r = 2\sqrt{2}$. The reference state induces a further pale yellow plaquette with respect to the reference state on the left and has thus higher energy.

i.e., the expectation value of the plaquette part of the Hamiltonian vanishes in the ground-state at $\theta = \frac{\pi}{2}$, and, as well, ii)

$$\sum_{l \in p} (X_l + X_l^\dagger)|1\rangle_p = 4(1 + \cos\alpha_g)|1\rangle_p, \forall p, \tag{6.51}$$

which implies $\sum_l (X_l + X_l^\dagger)|\Omega(0)\rangle = (1 + \cos\alpha_g)L^2|\Omega(0)\rangle$. From i) and ii), it immediately follows that the states $|\Omega(0)\rangle$ and $|\Omega\left(\frac{\pi}{2}\right)\rangle$ are not deformed, but simply shifted in energy, by the change of θ. Hence, the transition between them is a first order phase transition (level crossing), where the expectation value of any (yellow) plaquette operator can be taken as an order parameter, which jumps abruptly from -1 to 0.

Furthermore, the relations (6.50,6.51) allow to compute the critical value of the coupling θ_c simply by equating the energy per plaquette of $|\Omega(0)\rangle$ and $|\Omega\left(\frac{\pi}{2}\right)\rangle$

$$\theta_c : -\cos\theta_c + 4\sin\theta_c(1+\cos\alpha_g) = 8\sin(\theta_c)\cos(\alpha_g), \rightarrow \theta_c = \arctan\left(\frac{1-\cos(\alpha_g)}{4}\right). \tag{6.52}$$

Also in the product state phase, static charges are confined. The minimal configuration containing to two charge excitations of opposite sign, ± 1, is given by the shortest open string of $|+\rangle$-links connecting the charges. These configurations have an energy cost per link that is constant and equal to $2 - 2\cos(\alpha_g)$. Again, the linear behavior of energy gap with the charge distance is a manifestation of the confinement of charges.

Finally, we are ready to study the whole Hamiltonian (6.22). We notice that although the actual shape of ground-state in the plaquette dominated phase $|\Omega(0)\rangle$ is modified, the conditions (6.50-6.51) are not, as the plaquette ground-state has always an equal number of plus and minus links. This implies just a change in the actual value of θ_c, but not in the nature of the phase transition that remains a first order level-crossing phase transition.

Hence, all the properties of the plaquette dominated phase can be studied at $\theta = 0$, as a change of θ only induces a shift in the energy of such state and of the states associated to plaquette excitations.

In order to obtain the full gauge magnet Hamiltonian, we can add the other

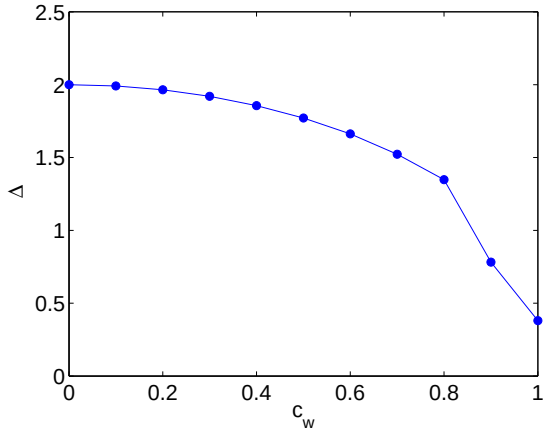

Figure 6.6: Scaling of the gap Δ between the ground-state and the first excited state of the Hamiltonian of (6.53) as a function of the coupling c_w for a 4×4 lattice with periodic boundary conditions in all directions. The gap decreases and eventually saturates to its finite size value. On a infinite lattice the results of [178] predict that it would vanishes at the point at $c_w = 1$.

half of the plaquettes to the Hamiltonian (6.36) adiabatically

$$H_{c_w} = -\sum_{p_y}(B_{p_y} + B_{p_y}^\dagger) - c_w \sum_{p_w}(B_{p_w} + B_{p_w}^\dagger), \tag{6.53}$$

where p_w are the white plaquettes in Fig. 6.4. By varying c_w from 0 to 1 the system is driven to a gapless phase [178]. The dependence of the gap on c_w for the 4×4 lattice is shown in Fig. 6.6. There we appreciate that the gap systematically decreases and eventually saturates to its finite size value.

6.4 Digital quantum simulation of the U(1) gauge magnet

A natural further step in the study of gauge magnets is the implementation of a quantum simulation of such systems with the help of ultracold atoms in optical lattices. It can be done successfully by considering digital ultracold Rydberg

atoms and, specifically, digital quantum simulations. The detailed original proposal was published together with the study of gauge magnet presented in the last section in Ref. [35]. Althought my role in these investigations of implementations was not dominant, in this section I introduce the mentioned work to the reader. We refer to the original work for explicit details of the system.

Rydberg atoms are neutral atoms that can be excited to states close to the continuum spectrum, having very strong dipolar moments. Such dipoles induce long-range interactions that make possible the simultaneous interaction of several atoms together. The basic ideas for digital quantum simulations with Rydberg atoms are described in [180] and involve the presence of ancilla atoms, apart from the ones entering the Hamiltonian of the system to be simulated. These are called "control" Rydberg atoms (see Fig. 6.7 a)). The other atoms, whose interaction should encode the Hamiltonian to be simulated, are generally called "ensemble" Rydberg atoms. They have to be physically arranged following the pattern of the many-body interactions appearing in the desired Hamiltonian. For example, if one is trying to encode four-body interaction of the four atoms around an elementary plaquette of a square lattice, such atoms should be inside the blockade radius of a given control atom, whose dipole moment is used to implement the wanted plaquette interaction among them.

One can carry out simultaneous operations on all the atoms inside the blockade radius of a control atom, operations determined by the state of the control atom itself. This can be achieved through a laser setup involving two- and three-photons transitions. In particular, one can engineer 2D lattices where the ensemble atoms are arranged on the links, while the control atoms are at each site and at the center of each plaquette (see Fig. 6.7 b)); at same time, one can tune the lattice spacing so that all the links belonging to a plaquette and entering a site are simultaneously contained inside the blockade radius of the respective plaquette and site control qubits.

In this setup, one can perform arbitrary time-evolution with the desired (Abelian) lattice gauge theories Hamiltonian, and, in some simple cases, one can also accomplish dissipative quantum simulations to prepare a desired state. This is, for instance, the technique proposed for the preparation of the ground-state of the Toric Code in [181], whose low-energy physics, in the appropriate limit, can be mapped to the $\mathbb{Z}_2$ lattice gauge theories.

In our proposal it is provided a specific proposal to perform a digital quantum simulations with Rydberg atoms of a U(1) lattice gauge theories in two

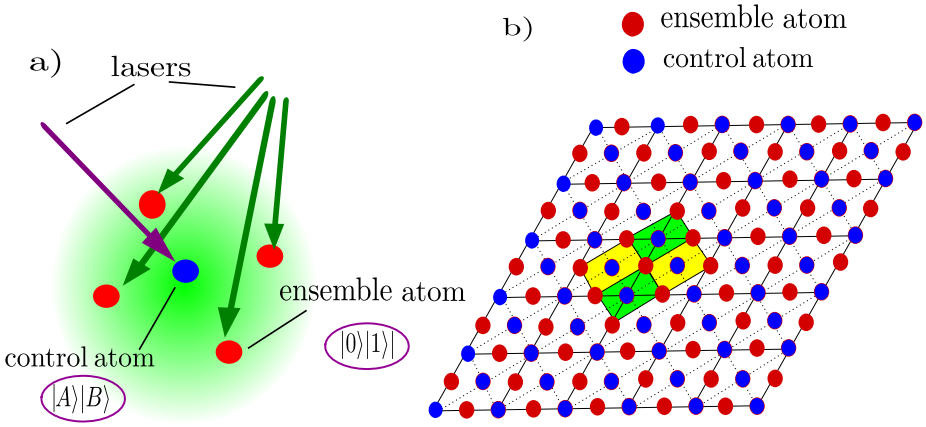

Figure 6.7: a) Schematic of the Rydberg gate. The ensemble atoms, which admit as logical states $|A\rangle$ and $|B\rangle$, are placed sufficiently close to the control atom, whom logic states are $|0\rangle$ and $|1\rangle$, so that the Rydberg interaction, i.e., the dipole interaction in the Rydberg state of the control, is strong (shadow green volume). At the same time, the atoms are sufficiently separated to allow individual single-site addressing by laser pulses. b) Schematic of the simulator. As indicated in the legend, the red dots represent the ensemble atoms, while the blue dots represent the control ones. Between the control atoms, we distinguish the ones at the lattice sites (intersections of continuous lines) and the ones at the center of the plaquettes. The former are needed to impose the gauge condition and interact with the ensemble atoms at the corners of the green squares. The latter control the dynamics of the plaquettes, which involves the ensemble atoms at the corner of the yellows squares. Adapted from [35].

dimensions. Concretely, the authors proposed the quantum simulation of link model or gauge magnet, with the choice of a specific U(1) lattice gauge theories where the constituents are qubits. Such qubits can be represented in terms of atoms with two logical level states, such as the ones available in standard Rydberg setups.

The work contains a specific protocol to prepare the ground-state of the model and perform arbitrary, out of equilibrium, dynamical simulations. As well known, one can extract the excitation spectrum of the model by performing these simulations. In practise, the study can be applied to any system governed by a local Hamiltonian in bipartite lattices. These Hamiltonians can be very complex, strongly interacting, non frustration-free Hamiltonians.

The *experimental sequence* for the preparation of the ground state contains the next steps:

1. Loading of the ultracold atoms in the appropriate square (super)lattice as in Fig. 6.7 b).

2. Preparation of the initial appropriate product state by using dissipation via Rydberg gates (or dissipation combined with single-site manipulation of individual ensemble atoms). As discussed in section 6.3, the matter content of the final desired state to achieve (after the driving, see next point) determines which is the appropriate initial state to start with. The authors proposed as key experimental observables to probe whether the simulator is working properly the absence of spontaneous symmetry breaking and the presence of charge confinement.

3. The second step involves a driven evolution via digital quantum simulations with Rydberg atoms to the final Hamiltonian of gauge magnets. The turning on of the part of the Hamiltonian that has been neglected in the first instance, can be adiabatic or not. Indeed, the efficiency of the ground-state driving can be improved by following the chopped random basis protocol [182, 183]. Moreover, commuting operations can be performed on parallel.

4. Error minimization by enforcing the gauge condition during the driving via dissipation. The two procedures, driving and dissipation, can be applied for alternative intervals of time.

5. Validation of the simulator. Once the ground-state of the system (for the

chosen matter content) has been achieved, it is characterized by measuring correlation functions.

Furthermore, the work also considers how to perform out of equilibrium long-time-evolution of the U(1) gauge magnet with a digital quantum simulations with Rydberg atoms, following the prescription of [181].

This protocol for digital quantum simulation provides a generalization of the techniques described in [184, 185, 186], such to permit to prepare ground-states of Hamiltonians that are not frustration-free.

We end this chapter with a summary of the requirements for the implementation of the simulator for the U(1) guage magnet:

- The first requirement for setting up the experiments is the choice of ultracold atoms suitable for the implementation of the mesoscopic Rydberg gate and for the load in the appropriate optical lattice. In the simplest scenario the authors consider, ensemble and control atoms are of the same atomic species, for instances Rubidium. As a consequence, an ordinary square lattice, obtained by shining the atoms with two pairs of counter-propagating lasers in the X and Y direction, respectively, is sufficient to host all the atoms. If distinct atomic species for ensemble and control are considered, a more complicated superlattice structure has to be employed. In any case, the lattice potential has to be sufficiently high that the free hopping is suppressed (compared with the time scale of the experiment): for simplicity, the atoms are assumed to be in Mott state with just one atom per site.

- The second crucial requirement is single-site addressing, i.e., the capacity of (laser) manipulating the atom in each site individually. Single-site addressing is technically hard, but possible [163] in ultracold atom experiments. It is at the hearth of the functioning of mesoscopic Rydberg gate, see Fig. 6.7 a). Furthermore, due to single-site addressing, the position in the lattice is sufficient by itself to distinguish control atoms from the ensemble ones.

- The third requirement is that the system be sufficiently cold such that the energy scale E associated to the Hamiltonian can be resolved, i.e., $KT < E$ where T is the temperature and K the Boltzmann constant. The energy scale E, roughly speaking the normalization of the plaquette

term (for convenient it has been fixed to 1 in our analysis), is limited by the Trotter approximation to be much less than the inverse of the time Δt in which one unitary step of time evolution is performed. Such time Δt is determined by the number of sequential Rydberg gates N_R needed to engineer the plaquette term evolution, $\Delta t = N_R t_R$, as the further delay due to single-qubit rotations entering the process is negligible compared to the Rydberg gate delay t_R. Hence, it follows $N_R \ll t_R KT$. For state of the art experiments $t_R KT \gtrsim 10^2$, as t_R is about few μs and T is about few tens of nK.

Chapter 7

Splitting a many-body quantum system

The dynamical evolution of an isolated quantum system is governed by a unitary operator and is, consequently, reversible. Therefore, one might think that irreversibility and thermalization should only appear through the system-environment interaction [187]. For a small region inside a large isolated quantum system, a legitimate environment is the system itself. In particular, it is important to understand, under which conditions the large-time out of equilibrium evolution of an isolated system will lead to a thermal state of the small region. Although the decoherence time of most experimental systems is too short for an effective study of that regime, recent advances in cold atomic physics [2] have allowed to experimentally address such situations and have boosted renewed interest in the theoretical understanding of these phenomena [41, 42, 43, 188, 45]. The experiments have been complemented with theoretical insights [189, 190, 40, 191, 192], which have brought about interesting ramifications of the problem, ranging from quantum information and entanglement to the issue of integrability in quantum systems.

In the context of the low energy physics of a many body quantum systems, entanglement has emerged as a privileged tool to characterize quantum phases. In 1D, for example, the scaling of entanglement allows to distinguish between gapped systems and critical systems, and the structure of the entanglement spectrum allows to identify symmetry protected topological phases. Here we try to analyze the effects of the conservation of the entanglement in the out-of-

equilibrium evolution after a quantum quench.

Conserved quantities play a very special role in Physics. In classical mechanics, they allow to define integrable systems as those systems that possess as many conserved quantities as degrees of freedom. In quantum mechanics, this concept is hard to generalize. The expectation value of any operator that commutes with the system Hamiltonian is conserved. In particular, arbitrary powers of the Hamiltonian itself (that in general can define independent operators) are conserved during the out-of equilibrium dynamics. This means that a generic quantum system possesses as many conserved quantities as degrees of freedom, and we still miss a proper definition of integrable quantum systems.

Furthermore, when considering *local equilibration*, the equilibration of a small region inside a large quantum many body system, among all conserved quantities, only few seem to be relevant. For example when a generic quantum many body system locally relaxes, it does it to a thermal state and thus the only *relevant* conserved quantity is the expectation value of the energy. Indeed the Gibbs ensemble (or thermal state) is formally obtained by maximizing the entropy at fixed value of the energy [193, 194, 195]. Exactly solvable systems, can still locally equilibrate, but to more complex ensembles obtained by maximizing the entropy subject to the constraints arising from the conservation of all relevant quantities. It is still unclear in general how to identify the relevant conserved quantities, but in the cases where they are known, the ensembles that describe the equilibrium of small regions are called generalized Gibbs ensembles (GGE) [196, 197].

Is entanglement one of those relevant conserved quantities? In order to understand this we address the non-equilibrium dynamics arising after a *quantum quench* [192]. The system is originally in the ground state of a certain Hamiltonian H_0. One suddenly quenches the Hamiltonian from H_0 to H and observes the subsequent out of equilibrium dynamics. Depending on if H differs from H_0 locally (on few sites) or globally (on the whole system) quenches are called *global* or *local*. In particular, we characterize the quench obtained by *splitting* a critical spin chain into two equal halves. This amounts to turning off at $t = 0$ the interaction between the two half chains. This, together with the fact that the evolution inside each of the two halves is unitary, implies that the original entanglement between them is conserved during the evolution. Thus, the initial correlations between the two halves are expected to survive along the whole evolution.

A similar phenomenon was observed already in the experiments carried out by Gring and coworkers in Vienna [43], where a quasi-1D Bose gas was split into two halves. The two halves were subsequently allowed to evolve inde-

pendently. After a time shorter than the expected equilibration time, many of the observables had relaxed, a phenomenon usually called *prethermalization* [46, 198]. After the prethermalization, the evolution was much slower, and compatible with the effects of the heating of the system due to the residual small interactions with the environment. Nevertheless, the original almost stationary interference pattern between the two halves persisted for large times after the prethermalization time. In a truly isolated system this would have been there forever as a consequence of the initial entanglement between the two halves. A truly isolated quantum system, indeed, conserves the initial entanglement between two systems that are separated and stop interacting. While it is clear, that by splitting the system one initially injects into the system an amount of extra energy that is proportional to the geometry of the splitting (extensive in the Vienna experiment and intensive in the case we consider here) and thus generate the subsequent out-of-equilibrium dynamics, it is not clear what is the role of the conservation of the entanglement in the subsequent equilibration process.

From a quantum information perspective, the key insight is that not only the entanglement is conserved, but also each of the individual eigenvalues of the reduced density matrix of any of the two separated regions is conserved. All together they constitute the entanglement spectrum (ES) [199]. How does this large amount of constraint affect the dynamics?

In order to address this point, we compare the non equilibrium dynamics generated by two similar quenches. We either split a critical spin chain into two halves (we will refer to this situation as to the *split quench*), or we join two critical chains in a larger one (and we will refer to this scenario as to the *join quench*). Both scenarios are local quenches. Initially, in the bulk, in middle of the two regions that are either split or joined, any correlation function of local observables (once appropriately rescaled) is the same in the two cases. Also the post-quench Hamiltonian is the same in the bulk for both quenches. We thus say that the two quenches are in the bulk initially "locally" indistinguishable. They are clearly distinguishable close to the boundaries of the sub-systems. While the split quench conserves the initial correlations between the two halves, the join quench does not since the interaction between the two halves allows to distribute correlations among them along the evolution.

The main result that we present here, is that the out-of-equilibrium dynamics and the subsequent relaxation of the bulk of the two systems are distinguishable, and, thus, the presence/absence of conservation of the entanglement spectrum affects the out of equilibrium dynamics of the system (for related ideas see also Ref. [200]).

7.1 The Splitting Quench

7.1.1 Quenched dynamics and thermalization

Let us consider the ground state $|\phi_0\rangle$ of a certain closed system described by the Hamiltonian H_0. A quench is performed by changing abruptly the Hamiltonian from H_0 to H, in such a way that $|\phi_0\rangle$ ceases to be an eigenstate, and thus undergoes non-trivial unitary evolution

$$|\phi(t)\rangle = \exp(-iHt)|\phi_0\rangle. \tag{7.1}$$

Let us consider a a (small) region of the system, namely A, containing $r \ll N$ spins, described by the reduced density matrix $\rho_A(t) = \mathrm{Tr}_B|\phi(t)\rangle\langle\phi(t)|$, where B is the complement of A. Under certain conditions, the limit $\bar{\rho}_A \equiv \lim_{t\to\infty}\rho_A(t)$ exists, i.e., for large enough times, the region A equilibrates to a stationary state [201, 202, 203, 204]. Typically, a certain amount of time-averaging is necessary in order to remove small fluctuations.

If, at equilibrium, the state of A is well described by a thermal state, it means that, for the equilibration process, the only relevant conserved quantity is the energy E. The thermal state is indeed given by $\bar{\rho}_A \simeq \mathrm{Tr}_B \exp(-\beta H)$, where β is chosen such that $\mathrm{Tr}(H\rho_A)/\mathrm{Tr}(\rho_A) = E$. If the Hamiltonian is known to commute with a larger set of relevant local observables, $\{\langle H_i\rangle\}_{i=1}^K$, the equilibrium state is a generalization of the thermal state, $\bar{\rho}_A \simeq \mathrm{Tr}_B \exp(-\sum_{i=1}^K \beta_i H^i)$ and is called a *Generalized Gibbs ensemble* [197, 205].

7.1.2 The quench protocol

Consider a spin-chain of length N, described by a local homogeneous Hamiltonian with open boundary conditions, H_0, which can be formally decomposed into three terms:

$$H_0 = H_L + H_R + H_{LR}. \tag{7.2}$$

where H_L and H_R act, respectively, on the left and right halves, and H_{LR} represents the term connecting them. We prepare the system in its ground state, $|\Omega_0\rangle$, and proceed to quench the Hamiltonian to

$$H_t \to H = H_L + H_R, \tag{7.3}$$

i.e., we remove the connecting term, H_{LR}. The upper panel of Fig. 7.1 illustrates the procedure.

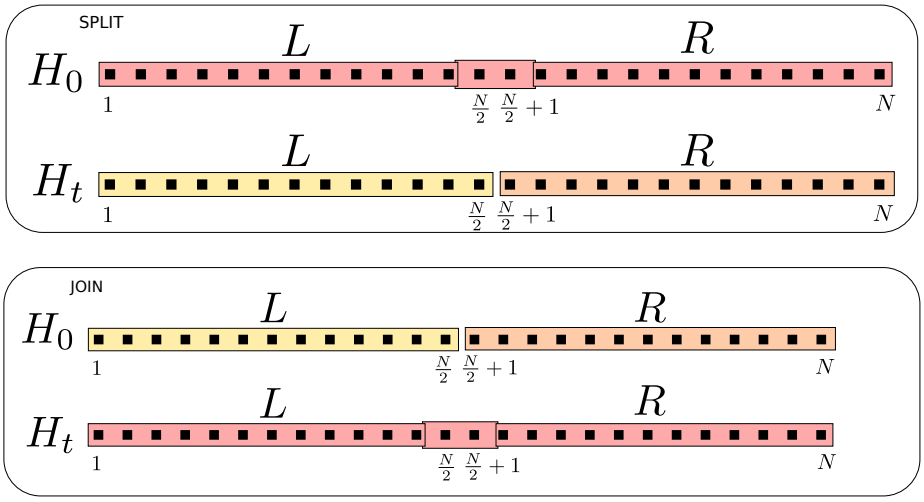

Figure 7.1: Upper panel: *Splitting a spin chain*. After the ground state of a spin-chain of length N has been obtained, the Hamiltonian is quenched by removing the term which connects both halves, effectively splitting them. Lower panel: *Joining two spin chains*. The situation is reversed, the ground states of two separate chains are quenched by adding the missing term in the Hamiltonian which connects them. This provides a reference quench for comparison since the two quenches are locally indistinguishable and only differ by the presence/absence of the conservation of the entanglement spectrum.

The state now evolves as

$$|\phi(t)\rangle = \exp(-iHt)|\Omega_0\rangle. \tag{7.4}$$

The initial state $|\Omega_0\rangle$ has excess energy with respect to the ground state of the new Hamiltonian H, $|\Omega_L\rangle \otimes |\Omega_R\rangle$. This excess energy can be interpreted as the presence at $t = 0$ of a finite density of quasi-particles located at the junction between L and R [206]. If H is a sum of local terms, these quasi-particles will propagate with a finite speed, giving rise to the characteristic light-cone effects observed in local quenches [42]. Of course, if H contains long-range interactions, this behavior can differ [207, 208].

The left half of the system L, at time $t = 0$, is described by a mixed state, obtained by the following reduced density matrix

$$\rho_L(0) = \mathrm{Tr}_R|\Omega_T\rangle\langle\Omega_T|. \tag{7.5}$$

that can be diagonalized as,

$$\rho_L(0) = \sum_{\alpha=1}^{m} \lambda_\alpha |\chi_\alpha\rangle\langle\chi_\alpha|, \tag{7.6}$$

where m is the Schmidt rank, and the orthonormal $\{|\chi_\alpha\rangle\}$ are called Schmidt vectors. The subsequent time evolution of $\rho_L(t)$ will be given by

$$\rho_L(t) = U_L(t)\rho_L(0)U_L^\dagger(t) \tag{7.7}$$

where $U_L(t) = \exp(-iH_L t)$. An immediate consequence is that the spectrum of $\rho_L(t)$, the set of $\{\lambda_k\}_{k=1}^m$, is preserved by the evolution. The Schmidt vectors, nonetheless, evolve in a non-trivial way, describing a time dependent set of orthogonal vectors. At any later time indeed,

$$\rho_L(t) = \sum_{\alpha=1}^{m} \lambda_\alpha |\chi_\alpha(t)\rangle\langle\chi_\alpha(t)|, \tag{7.8}$$

with the same set of $\{\lambda_k\}_{k=1}^m$ than the one in Eq. 7.7. It is customary to describe $\rho_L(0)$ in terms of a certain entanglement Hamiltonian $\mathcal{H}_L$, such that $\rho_L(0) = \exp(-\mathcal{H}_L)$ [199], i.e., as if it were a thermal state at an effective temperature $\beta = 1$. The entanglement spectrum (ES) is defined to be the set of eigenvalues of $\mathcal{H}_L$, $\epsilon_\alpha = -\log(\lambda_\alpha)$. Thus, as a consequence of the conservation of the eigenvalues of ρ_L, the ES between the left and right parts is also conserved.

How does in general change the local equilibration after a quench when the ES is conserved? In order to address this question we can study the equilibration of a generic mixed state constructed from a set of orthogonal vectors $|\phi\rangle_\alpha$ each appearing with probabilities λ_α. We can perform the time evolution for each of the state individually (it is a linear map) and then reconstruct the appropriate mixed state by summing the result with the appropriate probabilities. In the simplest scenario we can assume that each of the vectors $|\phi\rangle_\alpha$ fulfills the necessary conditions for thermalization described in Ref. [203]. Depending on the initial energy of each them E_α, they will locally thermalize to the corresponding temperatures β_α such that $\mathrm{Tr}(H\exp(\beta_\alpha H))/\mathrm{Tr}(\exp(\beta_\alpha H)) = E_\alpha$. If the β_α obtained in this way are not sufficiently close, the final state can not be described by a single temperature. Similarly, if there are more preserved quantities, the final state will not be uniquely determined by their initial expectation values. The final state might, therefore, not be described by a Gibbs (or generalized Gibbs) ensemble. In other words, the system would not locally thermalize in the usual sense but it would equilibrate to an exotic ensemble.

Is this non-thermalization likely to occur for the initial mixed state obtained in the split quench? A generic scaling argument suggests that such temperature mixing is difficult to achieve. Ground states of gapped 1D Hamiltonians fulfill the area law of entanglement [209, 210]. This implies that the number of Schmidt vectors saturates with the system size in the thermodynamic limit. The temperature mixing effect might be more relevant for a critical initial state, for which the number of Schmidt vectors scale as a power law of the system size [211]. Still different Schmidt vectors, typically only differ locally so that their initial energies are very similar. We thus do not expect to observe the temperature (or generalized parameter) mixing in our setting. Still, in the results we present, we will observe some remnants of the fact that the ES is conserved.

In order to clarify the role of the ES-conservation, we will compare the splitting quench with the joining quench of the same spin-chain, as illustrated in the lower panel of Fig. 7.1. In this last case, one first obtains the ground state of H_t in Eq. (7.3) and then quenches the Hamiltonian by adding the connecting term H_{LR}, i.e.: applying H_0. This effectively joins the two independent chains. This case has been addressed both at criticality and away from it using several techniques, which range from conformal field theories (CFT) to free fermions [212, 213, 214].

Since both quenches are locally described by the same Hamiltonian, and the correlation functions of any local operator, in the bulk of the initial states, are indistinguishable, we might expect that the difference between the corresponding out-of-equilibrium evolutions should be negligible far away from the division

between L and R. We will show that this is not the case, and the two quenches produce substantially different states, both globally and —more interestingly— also locally.

7.1.3 The critical Ising chain

As a prototypical example, let us consider the Ising model in transverse field (ITF), a simple integrable one-dimensional spin-chain,

$$H_0 = -J \sum_{i=1}^{N} \left[\sigma_i^x \sigma_{i+1}^x + \lambda \sigma_i^z \right], \tag{7.9}$$

where i ranges over the N sites of a 1D lattice and σ^x and σ^z stand for the Pauli matrices. The model presents two phases: a X-polarized phase for $\lambda < 1$ and a Z-polarized phase for $\lambda > 1$. They are separated by a second-order phase transition at $\lambda_c = 1$, where we will perform all our calculations. The ITF can be rewritten as a free-fermion model via a Jordan-Wigner and a Bogoliubov transformation [215]

$$H_0 = \sum_k \epsilon_k \left(\eta_k^\dagger \eta_k - \frac{1}{2}, \right) \tag{7.10}$$

with $\eta_k^\dagger$ and η_k following the usual anticommutation relations. The model is, therefore, integrable, and all its conserved quantitites can be expressed as a function of the mode occupations n_k [205]:

$$n_k = \langle \Omega_T | \eta_k^\dagger \eta_k | \Omega_T \rangle. \tag{7.11}$$

The low-energy physics of the ITF model close to the phase transition and its out-of-equilibrium dynamics can also be described using CFT [212, 213, 216].

In this work we have studied the two quenches via both free-fermion techniques [217] and the *time evolving block decimation* (TEBD) method, based on matrix product states (MPS) [218, 219]. MPS techniques have the advantage that they can be extended to both interacting models and non-integrable models.

7.2 Numerical results

We first analyse the relation between the Schmidt vectors of the initial state and the eigenvectors of the post quench Hamiltonian H. This gives us the oppor-

tunity to understand better the possible connections between the conservation of the entanglement spectrum and the long-time equilibrium regime. As we have discussed, the distribution of the expectation value of the energy and all relevant conserved quantities taken on the set of the Schmidt vectors are the ultimate quantities that determine if the system equilibrates to a well defined GGE ensemble or not.

We then will proceed to a more traditional characterization of the states resulting from the split quench focusing on two types of properties, global and local. Among the global properties, we will consider the entanglement entropy of different types of blocks and large-distance correlation functions. The local properties are characterized by studying the expectation values of local operators.

The entanglement entropy of a block A, with reduced density matrix ρ_A, is defined as

$$S_A = -\mathrm{tr}\rho_A \log \rho_A. \tag{7.12}$$

We consider both the case in which A is completely contained in one of the two blocks (say L) and when it is shared in between L and R, see Fig. 7.6.

With respect to correlation functions, we will evaluate the two-point correlation function of the order parameter, defined as

$$\begin{aligned} C(r_1, r_2, t) &= \langle\varphi(t)|\sigma_x(r_1)\sigma_x(r_2)|\varphi(t)\rangle \\ &- \langle\varphi(t)|\sigma_x(r_1)|\varphi(t)\rangle\langle\varphi(t)|\sigma_x(r_2)|\varphi(t)\rangle. \end{aligned} \tag{7.13}$$

In particular, we will consider distances $|r_1 - r_2|$ scaling with the size of the system, $|r_2 - r_1| \propto N$, in order to study the thermodynamic limit. Since both the splitting and the joining quenches break the translation invariance explicitly, we will consider separately the cases in which both r_1 and r_2 are on the same side with respect to the splitting point, or when they lie in different sides.

All those properties will be studied as a function of time. We will also focus on the equilibrium regime which emerges after the transient out-of-equilibrium dynamics. Although global properties, as discussed in the introduction, do not equilibrate, in a local quench we can still observe equilibration of an extensive region A that nevertheless should be separated from the boundaries. Indeed, in our simulations, we always observe three different regimes: (i) the static, (ii) the out-of-equilibrium regime and (iii) the equilibration regime, see Fig. 7.2. This fact is well understood by the approximate picture of the radiation of quasi-particles introduced by Cardy and Calabrese [206]. Indeed, through a

local quench, one typically populates all single quasi-particle momentum states with equal probability, which then propagate outwards with finite speed v.

Since our model is described at low energy by a CFT, all pseudo-particles propagate with the same speed at first order in $1/N$. In this work we will not address the corrections to this picture, that i.e. for long times, are responsible for the spread of the pesudo-particles and thus spoil the periodicity of the dynamics.

The out-of-equilibrium evolution of a region A which lies at a distance d from the interface between L and R will start after a time $t_1 \approx d/v$. For earlier times, a *static* regime is observed. Eventually, at a time $t_2 > t_1$ the slowest particles leave the region and the *equilibration* regime begins. Due to the finite size of the chains, if we wait for a large enough time $t_N \gg t_2$, the quasi-particles will bounce back at the boundary and return to the region A, thus making the system depart from equilibration. Thus, we will search for the equilibration regime in the time window $t_2 \gg t \gg t_N$, which depends on the distance from A to the boundaries and the velocities of the different types of quasi-particles. For times $t \gg t_N$ the behavior of the system is plagued with finite-size effects, which we want to avoid since we are interested in the thermodynamic limit. This implies that we can consider at most times of the order of t_N.

When addressing local properties, the static regime is followed by a very fast relaxation which leads to the equilibration regime. This can be readily explained assuming that times t_1 and t_2 coincide.

7.2.1 Schmidt vectors of the initial state

We want to understand the relation between each of the Schmidt vectors and the expectation value of the observables that are conserved during the time evolution. We start with the energy. We arrange the eigenvalues of the reduced density matrix $\rho_L(0)$, $\{\lambda_\alpha\}$, in decreasing order. In this way we can define an effective *energy gap* as

$$\Delta E_L = \langle \chi_2 | H_L | \chi_2 \rangle - \langle \chi_1 | H_L | \chi_1 \rangle. \tag{7.14}$$

We find numerically that ΔE_L decays as a power of the logarithm of the system size, as shown in Fig. 7.3. The appearance of a logarithmic scaling could be related with the results of [220, 221, 222, 223], that establish a mapping between the reduced density matrix of the ITF and the transfer matrix of the corresponding classical model on a cylinder whose radius grows logarithmically with the size of the block.

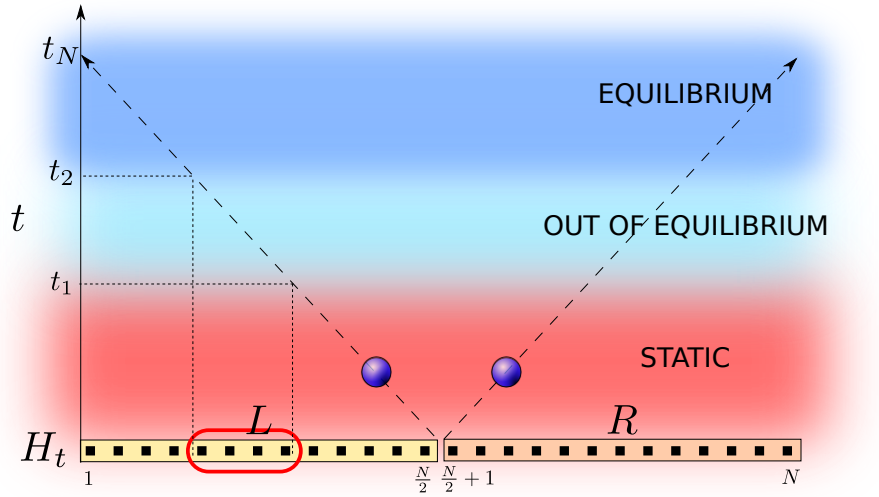

Figure 7.2: *Relevant time scales:* During the out-of-equilibrium evolution which follows the split quench, the region A is characterized by three different regimes as a consequence of the finite speed at which the quasi-particles created at the junction between L and R radiate. A *static* regime, lasting up to time t_1, in which the behavior is almost unchanged. This time t_1 is indeed the time necessary for the fastest quasi-particle to reach the region. After t_1, A experiences an *out-of-equilibrium* regime up to a certain t_2, the time needed by the slowest quasi-particles to travel through A and abandon it. From t_2 up to t_N, we observe *the equilibration* of the region. At t_N, the fastest quasi-particles bounce back from the boundaries so that finite size effects start to play a dominant role.

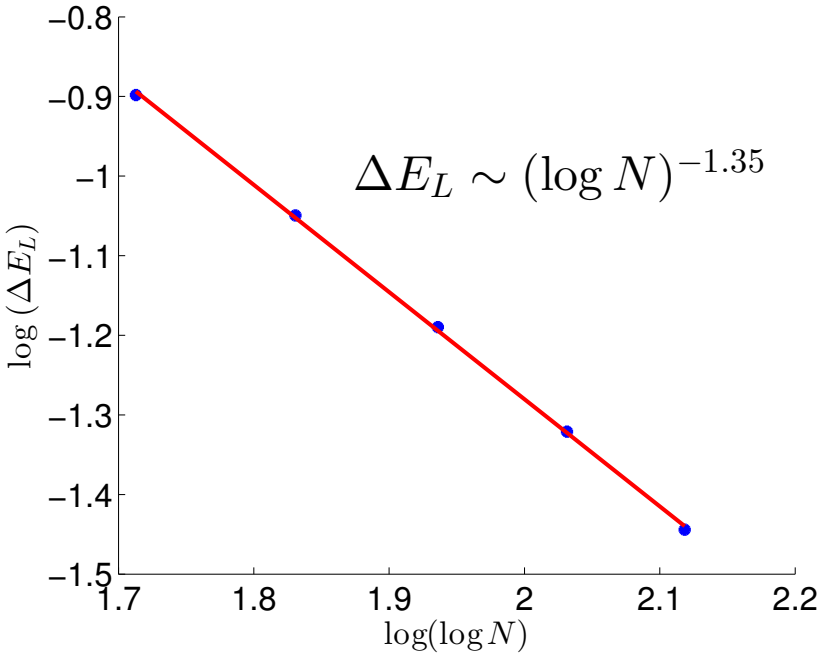

Figure 7.3: Energy gap ΔE_L between the first two Schmidt vectors of the left half of a critical Ising chain as a function of the chain length. The data suggest that the gap closes as a power of the logarithm of the system size.

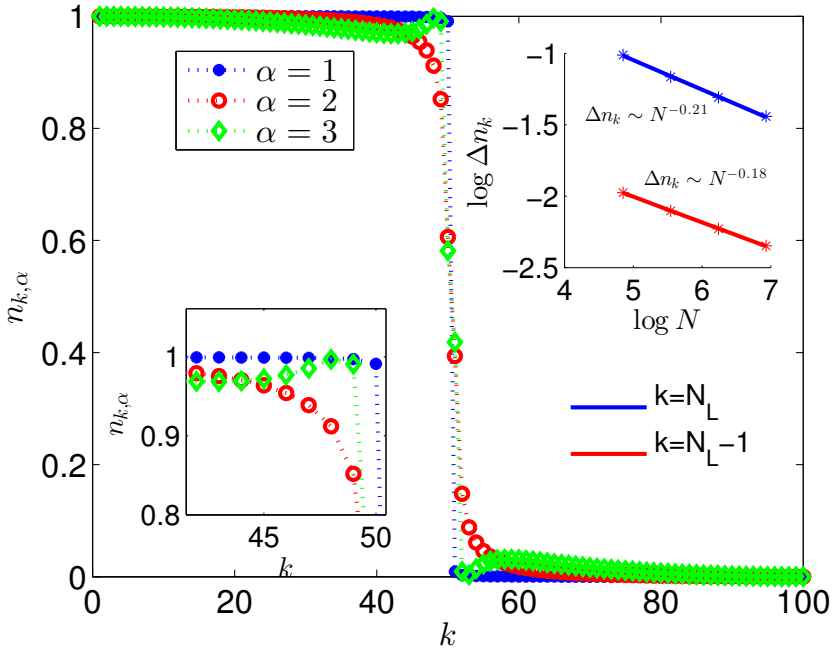

Figure 7.4: Main panel: occupation numbers of the modes of Hamiltonian H_L for the first three Schmidt vectors, for chains with $N = 100$ spins. Left inset: the differences in occupation are more pronounced around the Fermi energy. Right inset: Those differences scale as a power of the system size.

The mode occupations 7.11 for the first three Schmidt vectors are presented in the main panel of Fig. 7.4. They resemble Fermi-Dirac distribution functions at low temperature, and it is possible to identify a certain Fermi level that discriminates between almost fully and almost empty modes. Nonetheless, the occupations near the Fermi level differ considerably among different Schmidt vectors, as shown in the left inset of Fig. 7.4. Those differences decrease slowly as a power law of the system size (see Fig. 7.4, right inset).

The Ising model can be mapped to free fermions and thus all conserved charges are functionally dependent on the mode occupations. Since for each Schmidt vector the mode occupations are different this suggests that this type

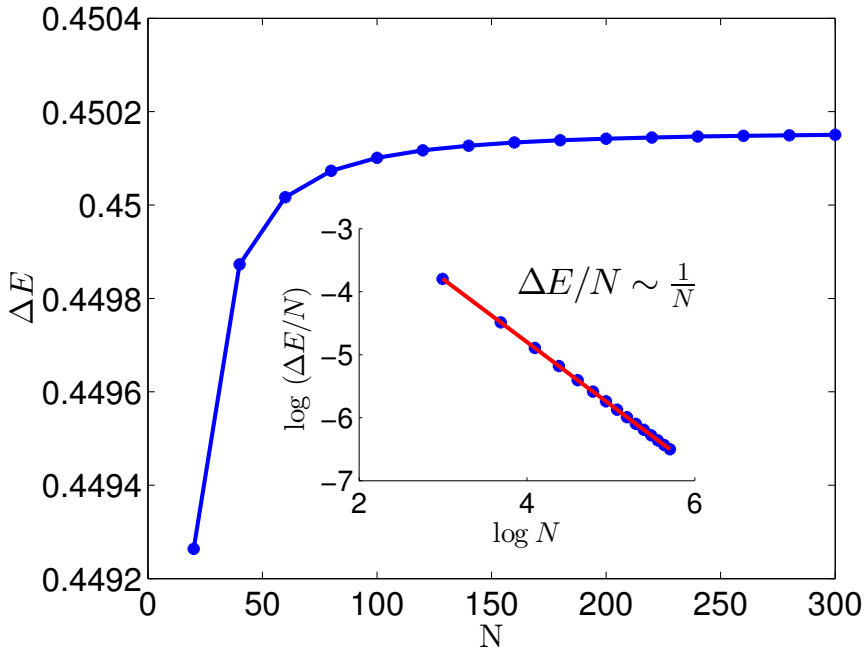

Figure 7.5: Main panel: Energy fluctuations as a function of the system size. We see that local fluctuations (inset) decay to zero as $1/N$, as expected in the case of a local quench.

of quench could provide an example of equilibration to a strongly correlated state that differs both from the Gibbs and the Generalized Gibbs Ensembles (GGE), as opposed to what is expected for standard quenches.

A more careful quantitative analysis, however, shows that this is not the case. Indeed, the fluctuations of the energy in the initial state are not large enough to produce significant effects on the equilibration state. As shown in Fig. 7.5, those fluctuations are independent of the system size, so that in the thermodynamic limit they vanish as $1/N$ (inset).

This is not surprising since, in a local quench, the initial state of the system does not possess enough energy to equilibrate to a thermal (or generalized thermal) state characterized by an extensive scaling of the entanglement entropy of

a region. Indeed, in the initial state of a local quench, the excess energy density with respect to the ground state scales with $1/N$, and thus it is not surprising that also its fluctuations scale as $1/N$. This implies that the equilibrium state of a local quench is very close to a zero temperature state where, for critical systems, the entanglement entropy of a region only grows logarithmically with its size [224, 225, 226, 211, 227]. Still, as we will see in the following, the conservation of the entanglement spectrum has non-trivial consequences both on local and global properties of the system.

7.2.2 Entanglement entropy

The time evolution of the entanglement entropy has been computed analytically in a few selected settings [206, 212, 213, 228, 216], and numerically in many others, local or global quenches, impurities or disorder [214, 229, 229, 230, 231, 232, ?, ?].

In this section we analyze the time evolution of the entanglement entropy of a block A of size $r < N$, as defined in Eq. 7.12, for two different geometrical configurations (see Fig. 7.6), A may have (i) a single active boundary or (ii) two of them. In this second case, the two boundaries may lay on different parts (ii.a) or on the same part (ii.b) of the splitting point.

Fig. 7.7 is devoted to the analysis of entanglement in configuration (i). Let A be formed by the leftmost r sites of a chain with $N = 160$ spins, split into two halves. The upper panel of Fig. 7.7 shows the entanglement entropy $S(r,t)$ as a function of both the size of the block (X-axis, marked r), and time in units of $1/J$ (Y-axis, marked t $(1/J)$). Notice that, since the entanglement Hamiltonian of the left part, $\mathcal{H}_L$, is a constant of motion, $S(N/2,t)$ is preserved during time evolution. At $t = 0$, S_r presents the characteristic shape of a critical system: $S(r,0) = \frac{c}{6}\log\left(\frac{L}{\pi}\sin\left(\frac{\pi l}{L}\right)\right)$ [224, 225, 226, 211, 227]. But for further times, a light-cone develops at the LR interface, and the entanglement entropy only changes when the fastest quasi-particles generated at the quench cross the active boundary of A as a specific case of the cartoon sketched qualitatively in Fig. 7.2.

The lower panel of Fig. 7.7 shows the time evolution of S for blocks of type (i) and different sizes. $S(N/2,t)$ is constant; $S(N/4,t)$, has a single active boundary that lies at the left of the splitting point, and thus it presents a stationary behavior for short times followed by a fast increase when the quasi-particles reach $N/4$; we also analyze $S(2N/3,t)$, whose active boundary lies to the right of the split point. In this case quasi-particles are radiated from within the region and only contribute to an increasing entropy when they leave the

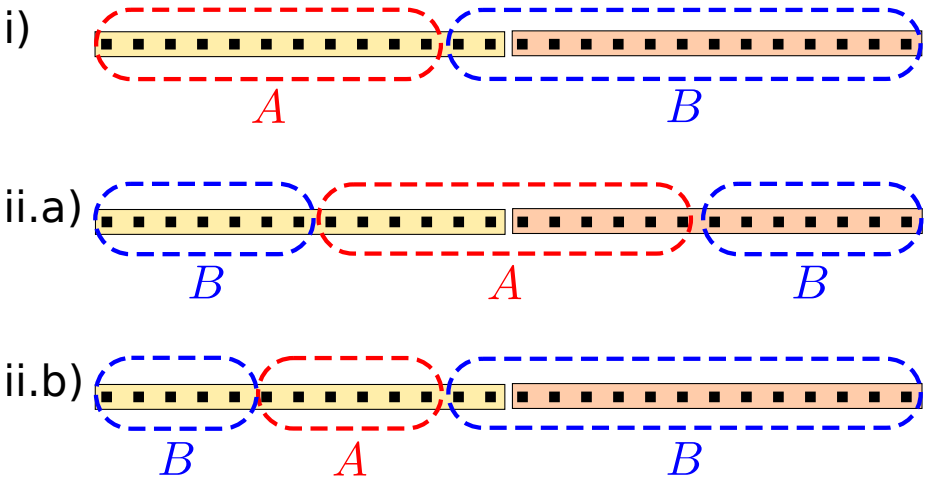

Figure 7.6: The geometrical configuration of block A within the full chain, (i) A has only one active boundary; (ii.a) A has two active boundaries, one in L and the other in R; (ii.b) the two active boundaries are both inside L.

region.

From the space-time diagram of the upper panel of Fig. 7.7 we can extract two projections. A time-like projection $\tilde{S}_T(t)$ is obtained by finding, for each time t, the maximal entropy among all block-sizes, and a space-like projection $\tilde{S}_S(r)$ defined by finding, for each block-size, the maximal entropy achieved along the evolution. After a joining quench, the time-like projection $\tilde{S}_T$ only grows logarithmically with time [213, 229]

$$\tilde{S}_T(t) = \frac{c}{3} \log_2 \left| \frac{N}{\pi} \left(\sin \frac{\pi v t}{N} \right) \right| + \text{const},$$

where $c = \frac{1}{2}$ is the central charge of the critical Ising chain and v is the quasi-particle velocity. The space-like projection, $\tilde{S}_S(r)$ is described by the same equation, just replacing t with r. On the other hand, after a splitting quench, $\tilde{S}_T(t)$ behaves as

$$\tilde{S}_T(t) = \frac{c}{3} \log_2 \left| \frac{N}{\pi} \left(\sin \frac{\pi v t}{N} \right)^{1/2} \right| + \text{const}, \tag{7.15}$$

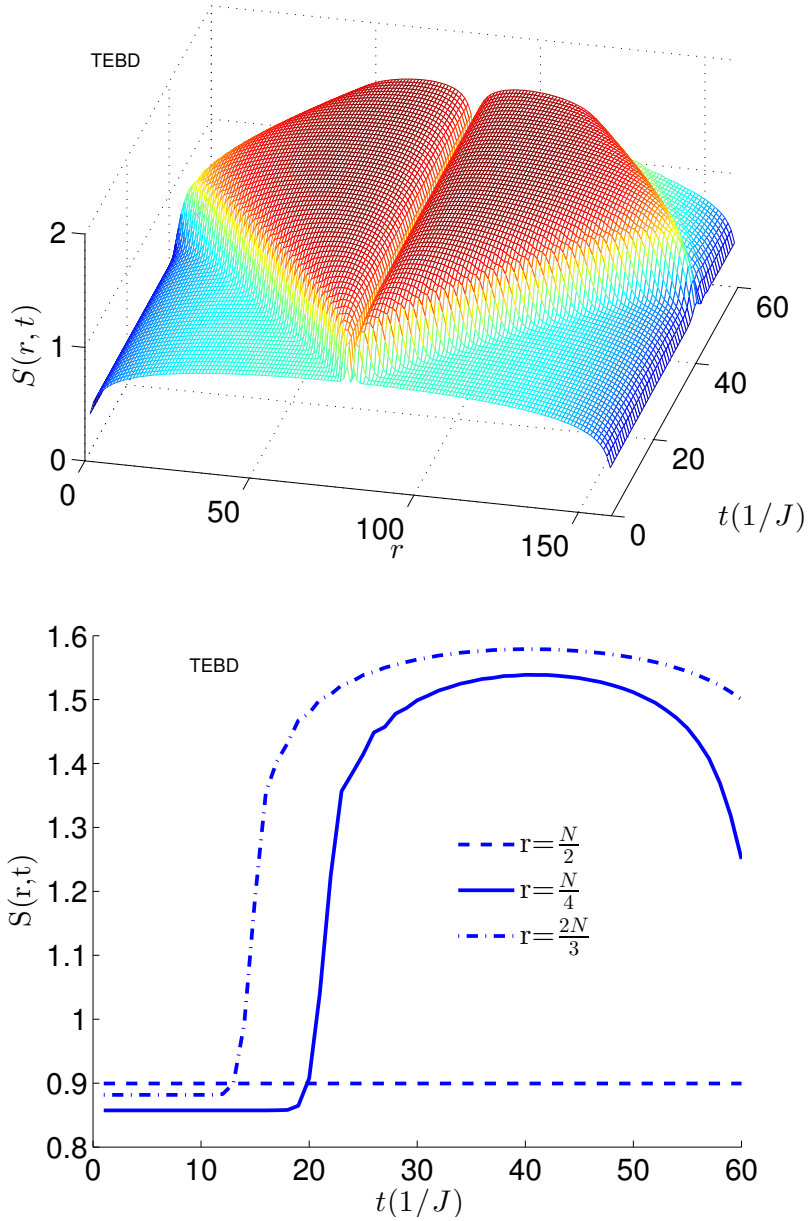

Figure 7.7: *Upper panel:* Time evolution of the entanglement entropy $S(r,t)$ for a chain of $N = 160$ after the splitting. *Lower panel:* Time evolution of $S(r)$ for three different values of r. When $r = N/2$, entropy remains constant. In the other two cases, entropy starts to grow only after the fastest quasi-particles enter (if $r < N/2$) or leave (if $r > N/2$) the block.

where the main difference with the result for the joining quench is the presence of the square root (see upper panel of Fig. 7.8). The space-time projection $\tilde{S}_S(r)$ presents a cusp at $r = N/2$ which is absent in the joining case. Still, for small r, the two cases are difficult to distinguish (see lower panel of Fig. 7.8). The detailed analysis is presented in Appendix 9.4.

The block in configurations (ii) in Fig. 7.6 have two active boundaries. As discussed previously, we distinguish between blocks (ii.a) which overlap with both parts, which we will place centered on the LR interface, and (ii.b), those which lie totally within one part. In Fig. 7.9 we consider two blocks of size $r = 8$, one of them centered on the LR interface (ii.a) and the other at a distance $l = 10$ from it. Notice that the time evolution of the entropy of two blocks presents the three aforementioned stages: static, out-of-equilibrium and equilibrium. In both cases, at large times the entropy converges to a finite value S_{eq}.

In the joining quench the relaxation towards S_{eq} is governed by [214]

$$S(r_0, t) = S_{eq} + \frac{\alpha \, \log(t) + \beta}{t}, \tag{7.16}$$

where the parameters α and β depen on the distance l between the block and the site of the quench.

The insets of Fig. 7.9 unveil a leading behavior of the same type as Eq. 7.16 with superimposed oscillations and faster time scales.

The entanglement spectrum of a block in configuration (i) of Fig. 7.6 presents only the first two out of the three time regimes, static and out-of-equilibrium. This is a consequence of the fact that the block extends up to the extreme of L and the quasi-particles never have space to escape. The Schmidt coefficients of the reduced density matrix of a block increase abruptly when the quasi-particles reach the block, and slower further increase afterwards. During this last regime, the Schmidt coefficients λ_α^r decay as a power of α (see lower panel of Fig. 7.10), pointing to the possibility of approximating the state by keeping only a small number of them, χ. The error of this approximation, which is the usual systematic error of MPS-based techniques, is given by

$$\epsilon = 1 - \sum_{\alpha=1}^{\chi} (\lambda_\alpha^r)^2. \tag{7.17}$$

The lower panel of Fig. 7.10 shows also the Schmidt number χas a function of time required to achieve two possible desired tolerances ϵ. Notice that the

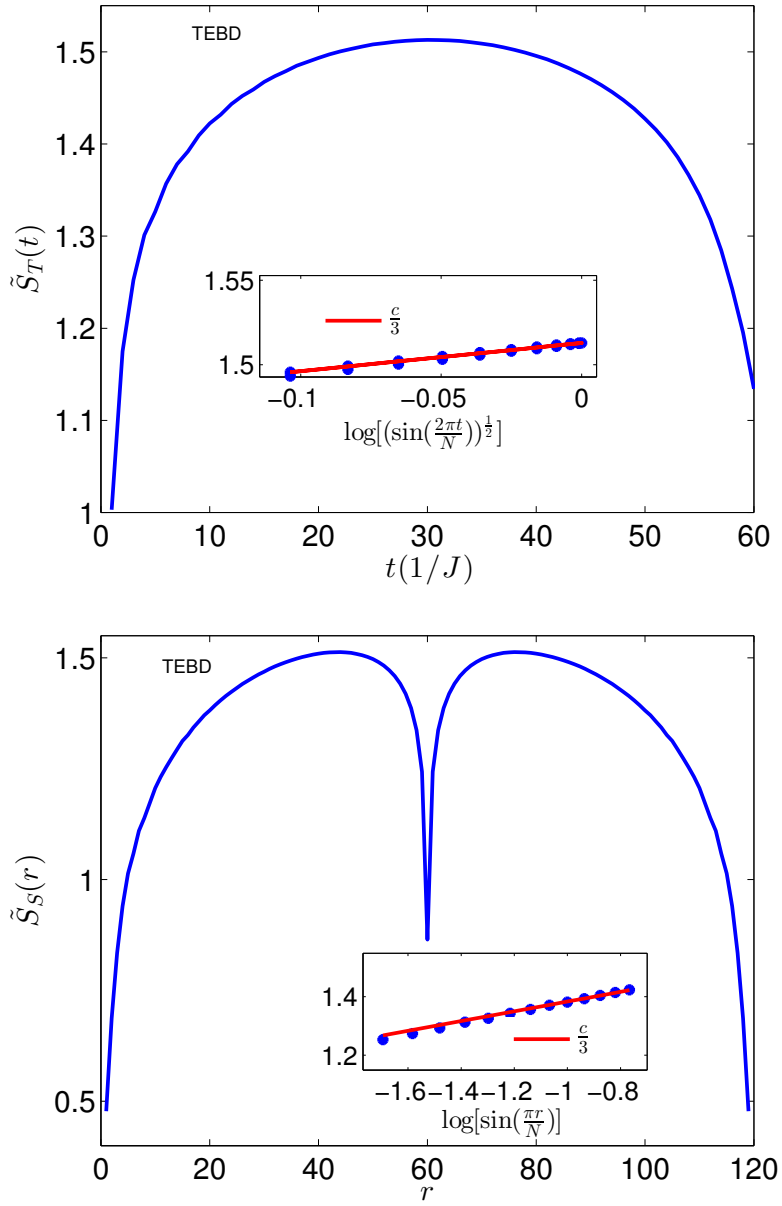

Figure 7.8: *Upper panel:* Time-like projection of the entropy, $\tilde{S}_T(t)$, after a splitting quench. The inset shows that the growth is compatible with a logarithmic growth with a pre-factor close to $\frac{c}{3}$, as in the join quench, but with an extra square root inside the logarithm (see Eq. 7.15). *Lower panel:* Space-like projection, $\tilde{S}_S(r)$. For block sizes very different from $N/2$, it behaves as in the join quench, displaying a logarithmic growth with a pre-factor close to $\frac{c}{3}$.

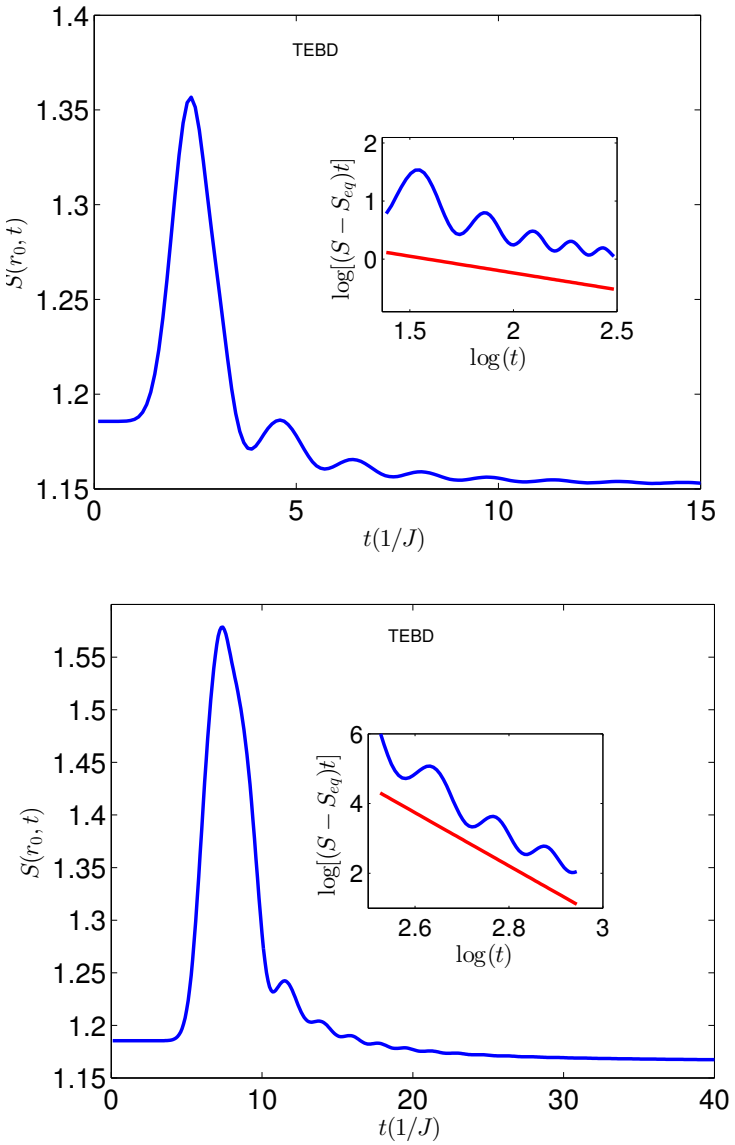

Figure 7.9: *Upper panel:* Time evolution of the entanglement entropy for a block with $r_0 = 8$ sites centered on the LR interface in a spin-chain of $N = 160$ sites. Notice the sudden jump to a maximum value and the slower relaxation towards S_{eq}. *Lower panel:* Same evolution, but for a block with $r_0 = 8$ sites, located at a distance $l = 10$ from the interface. In both cases the insets show that the relaxation behavior is compatible with the one of Eq. 7.16, as in the case of the joining quench, but with faster timescales and super imposed oscillations.

value of χ increases only moderately during the whole time interval, justifying our choice to use the TEBD algorithm [233].

7.2.3 Correlation functions

Let us turn to the time evolution of the two-point correlation functions of the order parameter after splitting the chain, defined in Eq. 7.13, and compare them with the joining case, which has been studied in detail by several authors [212, 234]. As with the entanglement entropy, we will study them in two geometric configurations, shown in Fig. 7.11, when both sites r_1 and r_2 are in different halves of the chain (top panel) and when they lie in the same half (bottom).

In the static regime, since the system is critical, for $|r_2 - r_1| \propto N$, $C(r_1, r_2, t) \propto N^{-2x}$ with $x = 1/8$ (see Fig. 7.14, both panels, for short times).

Let d_1 and d_2 be the distances from both points to the LR interface, $d_{\min} = \min(d_1, d_2)$ and $d_{\max} = \max(d_1, d_2)$. The out-of-equilibrium regime is defined by the condition $d_{\min} < vt < d_{\max}$, i.e.: the time lapse in which the quasi-particles have already reached the closest point and have not yet left the region between the two points. In the time-regime where $d_{\min} < vt \ll d_{\max}$, the CFT predicts that after a joining quench the correlation function will behave as $C \propto d_{\max}^{-2x-1/2}$ [212], independently on whether the points are in the same or different halves. This prediction has been confirmed numerically [234]. Fig. 7.12 shows the results in our case. After the split quench, when the points are in the same half, we also observe $C \propto d_{\max}^{-\alpha}$, but with $\alpha \approx 1/2$ ($\alpha = 0.46(5)$). Generalizing the CFT prediction, we may write this as $C \propto d_{\max}^{-2x-1/4}$. In the case of points in different halves, we do not observe any power law decay in the correlation function, as shown in the lower panel of Fig. 7.12.

We study next a kind of *light-cone regime* by fixing the ratios $\epsilon(t) = \frac{d_{\min}}{vt} < 1$ and $R(t) = \frac{d_{\max}}{vt} > 1$. In the joining quench, the correlation in this regime is described by $C \propto t^{-3x}$ as $t \to \infty$ [234]. Our results for the split quench are shown in Fig. 7.13. We can observe also a power law decay of correlations as in the joining case but when both points are located in the same half of the chain the exponent we extract is 0.46(1) that apparently is not compatible with the joining case. Interestingly, when they lay in different halves, we still observe a polynomial decay of the correlations with t, but with the exponent close 3/4, 0.72(1), that doubles the one observed in the joining case.

Finally, we reach the equilibrium regime. If both points lie on the same half, correlations decay as a power law of the system size, as in the joining quench as shown in the inset of the upper panel of Fig. 7.14. This means that the system

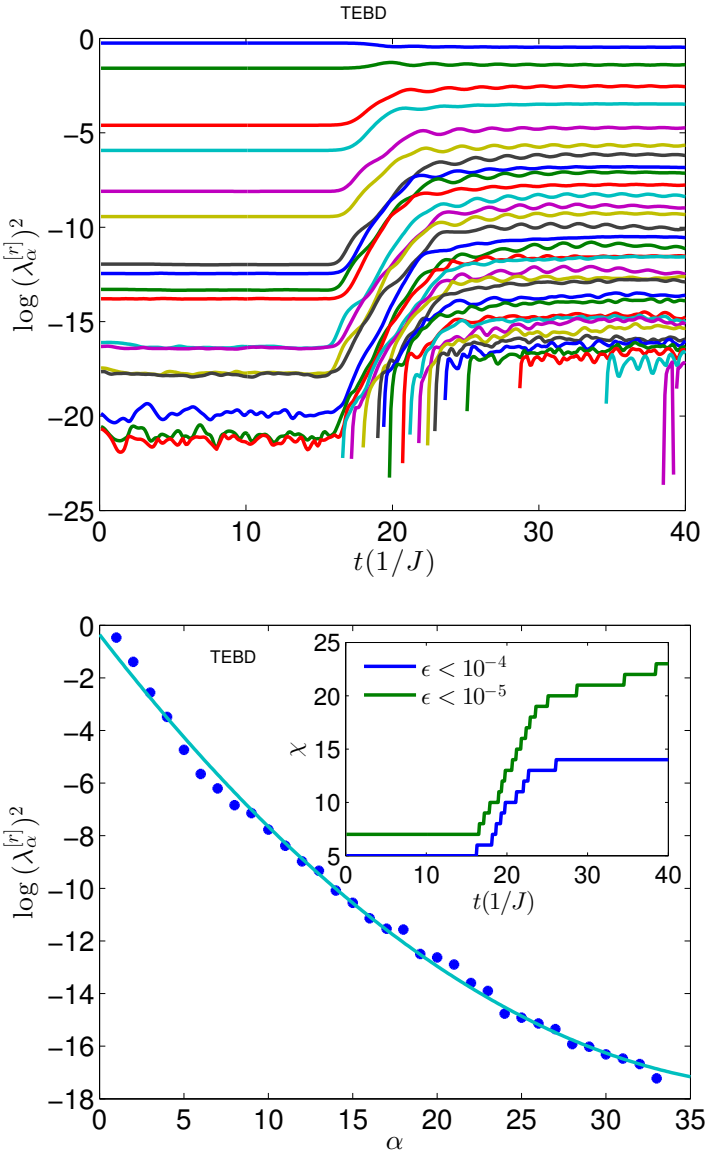

Figure 7.10: *Upper panel:* Time evolution after a split quench of the entanglement spectrum for a block of type (i) with size $N/4$ in a chain of length $N = 140$. Notice that only two time regimes are present: static and out-of equilibrium. *Lower panel:* After the fast increase ($t \lesssim 10$), the entanglement spectrum decays polynomially, showing that the state is neatly approximable with a few Schmidt vectors, χ. Small values of the representation error are obtained with $\chi \approx 20$, as shown in the inset.

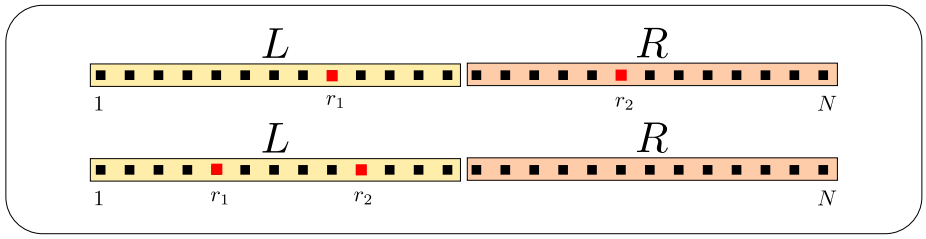

Figure 7.11: *The two-point correlation function of the order parameter,* defined in Eq. 7.13, is studied in two different configurations, when the two sites are on different halves (top) and when they lie on the same half (bottom) of the split chain.

is still critical, with the same critical exponent $x = 1/8$, and has thermalized to a temperature which is very close to zero. If the points are on different halves we still observe power-law behavior but this time we observe anti-correlations that decay with the same critical exponent $x = 1/8$, as shown the inset in the lower panel of Fig. 7.14. See Appendix 9.5 for a detailed explanation of this anti-correlation in terms of quasiparticles coming from the quenched point.

7.2.4 Local properties

As we have seen, the evolution of global quantities after the split quench is very different from the one after a join quench. This is not very surprising, since both quenches are globally very different. Still, we can attempt a local characterization of the equilibrium regime. Since the quenching Hamiltonian are locally identical, and the initial states provide the same correlations functions in the bulk, one might expect similar behaviors in both quenches.

The top panel of Fig. 7.15 shows that, as expected, after splitting or joining, local observables display all three stages, the static, the out-of-equilibrium and the equilibrium stages. The static value of the magnetization depends on the system size as

$$\langle \sigma_z \rangle_0 = \sigma_\infty + \frac{c_z}{N}, \tag{7.18}$$

where both σ_∞ and c_z are known analytically [235]. Let us consider the two cases of a $N = 200$ spin-chain split into two halves and two $N = 100$ chains joined in a single chain. In both cases the static values differ because of the different

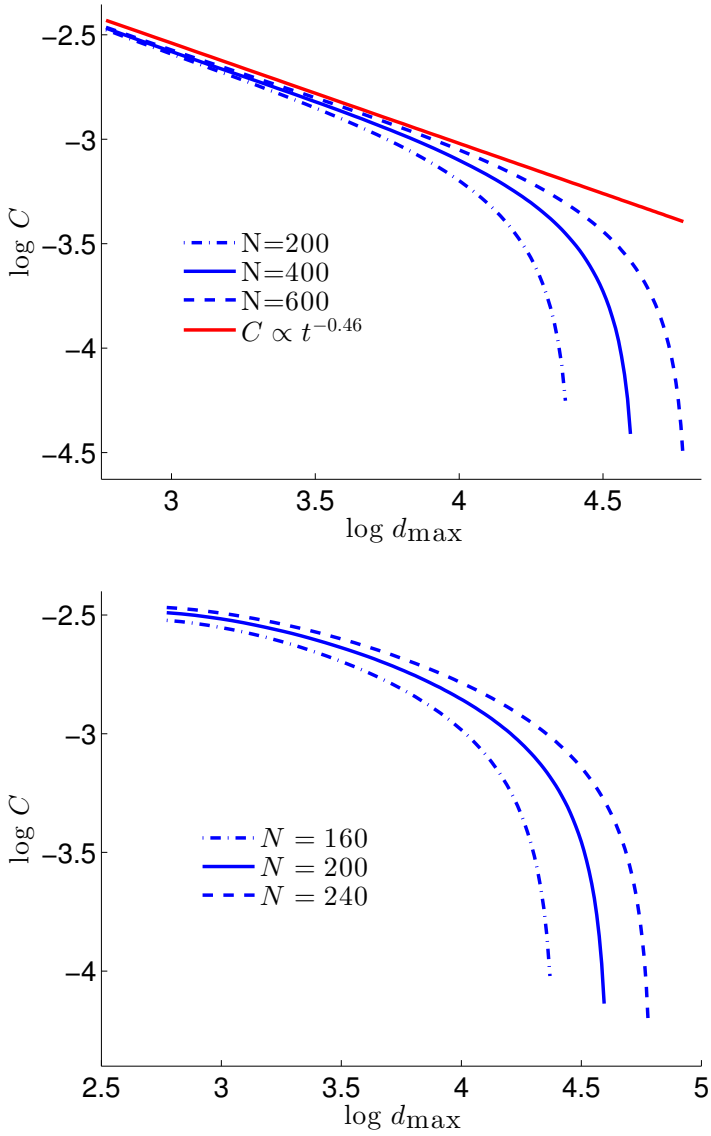

Figure 7.12: *Correlations in the out-of-equilibrium regime.* Both panels show the correlations in the time window $d_{\min} < vt \ll d_{\max}$, as a function of $d_{\max}$. The upper panel considers the case in which both points lie in the same half, showing a power-law decay with $d_{\max}$. The lower panel considers the case in which the two points lie in different halves, showing no power-law behavior. In both cases, we have considered $d_{\min} = 1$, $16 < d_{\max} < N/2$ and $t = 3\ (1/J)$.

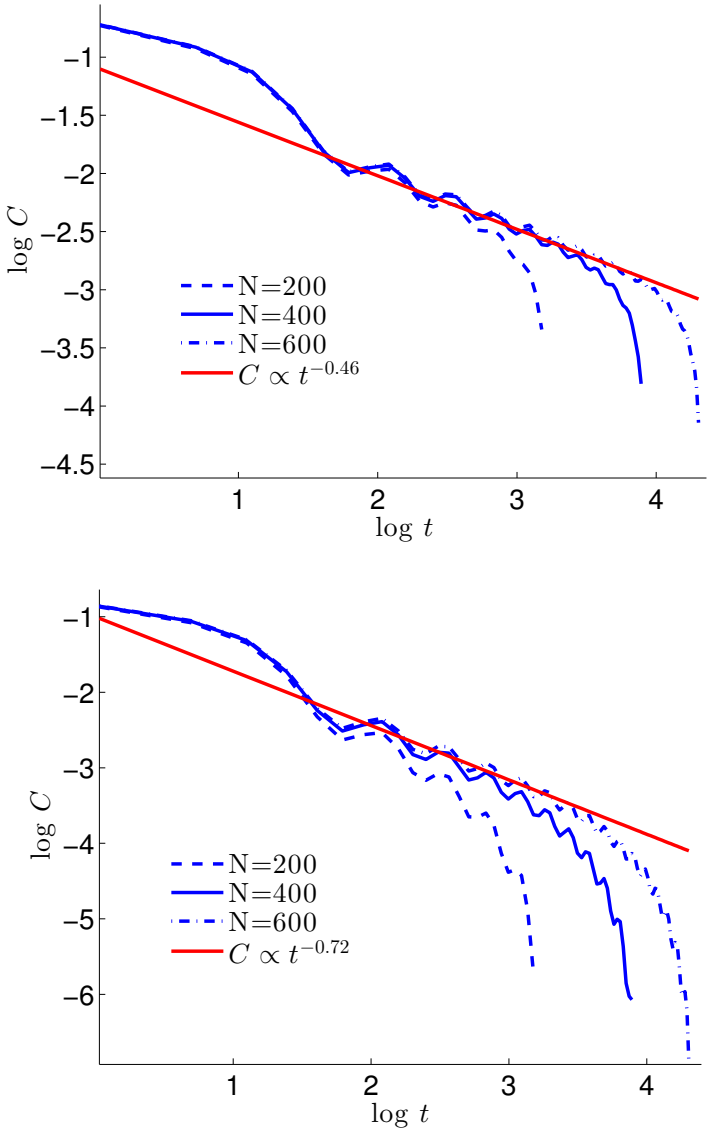

Figure 7.13: *Correlations in the light-cone regime.* We measure the correlations between two points in the regime described in the text as *light-cone*, with $\frac{d_{\min}}{vt} = 1/2$, $\frac{d_{\max}}{vt} = 2$ and $vt < N/2$. Upper panel: if both points are in the same half, correlations decay with time as t^{-3x} with $x = 0.46(1)$. Lower panel: if both points are in different halves, correlations decay with the same law, but $x = 0.72(1)$, close to 3/4.

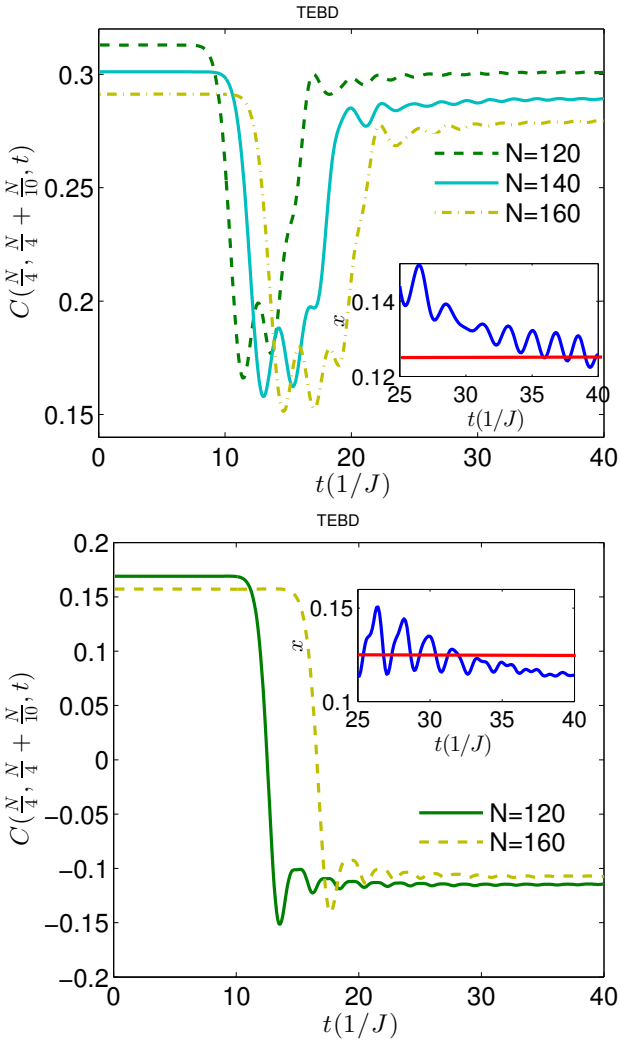

Figure 7.14: *Time-evolution of the correlation functions.* In the upper panel we consider the case when both points are in the same half of the chain. Concretely, we plot $C(N/4, N/4+N/10, t)$ for different chain lengths N. In both the static and equilibrium regime we observe a polynomial decay of the correlation as a function of the system size N. The critical exponent x governing the decay has been monitored as a function of time during the equilibrium regime, showing oscillatory convergence to the static value $1/8$ (see inset). The lower panel shows the time evolution of the correlator when both points lie in different halves, symmetrically placed with respect to the LR interface. Concretely, we plot $C(N/2-N/10, N/2+N/10, t)$. Interestingly, the equilibrium regime leads to anti-correlation between the two half-chains (see Appendix 9.5), whose critical exponent x again converges through some oscillations to $1/8$ (inset).

initial system sizes, with the split value displaying larger magnetization than the join. As expected, both values cross during the out-of-equilibrium phase, and the split equilibrium magnetization is lower than the join equilibrium magnetization. The equilibrium magnetization for the split chain converges to the static value of the two chains that have been joined, while the opposite does not happen, the equilibrium value for the joint chain is not the same as the static value of larger chain before the split. This is a finite-size effect. In the thermodynamic limit, the magnetization is the same before and after the quench in both cases. Still, for finite chains, we can distinguish both quench protocols, since the magnetization approaches the thermodynamic limit from opposite directions.

Indeed, as shown in the bottom panel of Fig. 7.15, the fit to Eq. 7.18 of the finite-size data shows that $\tilde{c}_z^{\text{split}} < 0$ and $\tilde{c}_z^{\text{join}} > 0$, implying that even at a local level the two quench protocols are well distinguishable. The same study is performed for the energy density in Fig. 7.16, where again we see that the quenches are completely distinguishable at a local level.

Finally we can also characterize intermediate quenches, considering a parameter $\tilde{t}$ that modifies the strength of the bond connecting L and R, as $\tilde{t} \cdot H_{LR}$(see Eq. (7.2)) so that the quench is obtained by varying the initial value of $\tilde{t}$. In this way we can either weaken the Hamiltonian bond between L and R by passing from the initial value of $\tilde{t} = 1$ to a quench value of $0 < \tilde{t} < 1$ so to partially split the chain. Alternatively we can quench from the initial $\tilde{t} = 0$ to again any value $0 < \tilde{t} < 1$ so to partially join L and R by switching on a weaker bond between them (weaker than the other present in the chain). The numerical results for such intermediate quenches are shown in Fig. 7.17 where we appreciate that by looking at the sign of the finite size corrections we can distinguish if the chain is being split (even partially) or joined. This last situation is similar to the study of the effects of impurities in critical systems [236].

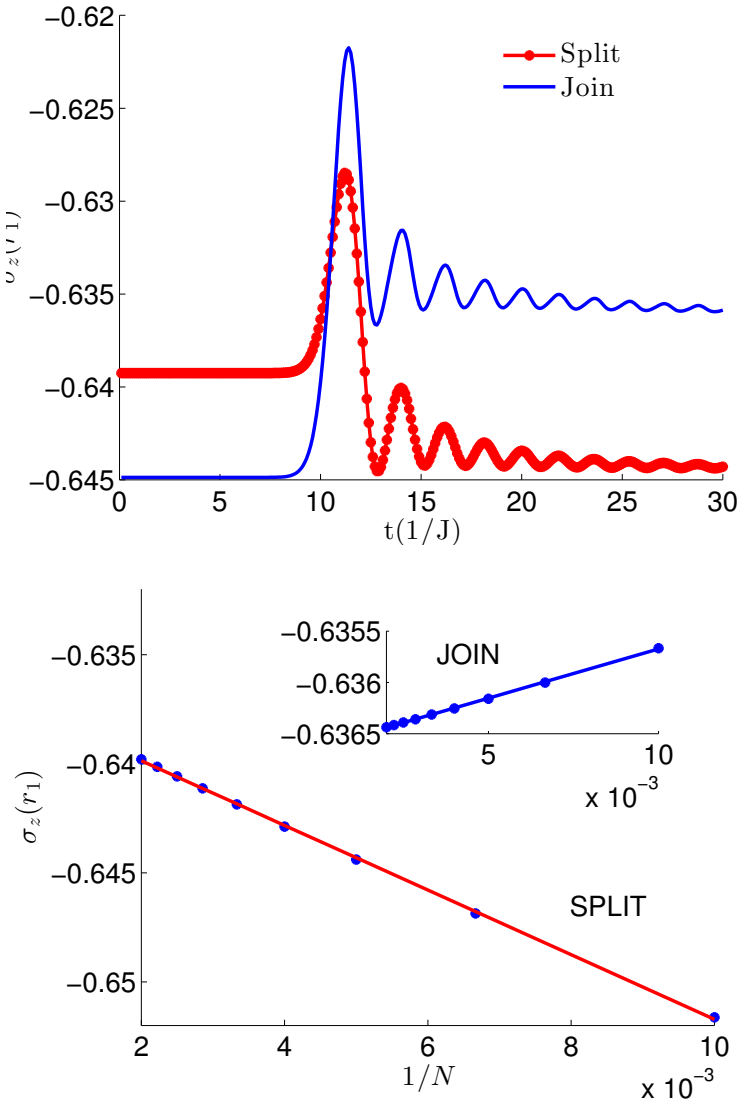

Figure 7.15: *Top:* Time-evolution of the expected magnetization at a site $r = N/2 - N/10$, both after a split quench of an initial chain with $N = 200$, and after a join quench of two initial chains with size 100. During the out-of-equilibrium regime, the join and the split values interchange and finally relax to different equilibrium values. *Bottom:* Scaling analysis shows that in both cases the equilibrium value is well described by Eq. 7.18, but the thermodynamic limit is approached from different directions, $\tilde{c}_z^{\text{split}} < 0$, while $\tilde{c}_z^{\text{join}} > 0$, implying that even at a local level the two quench protocols are well distinguishable.

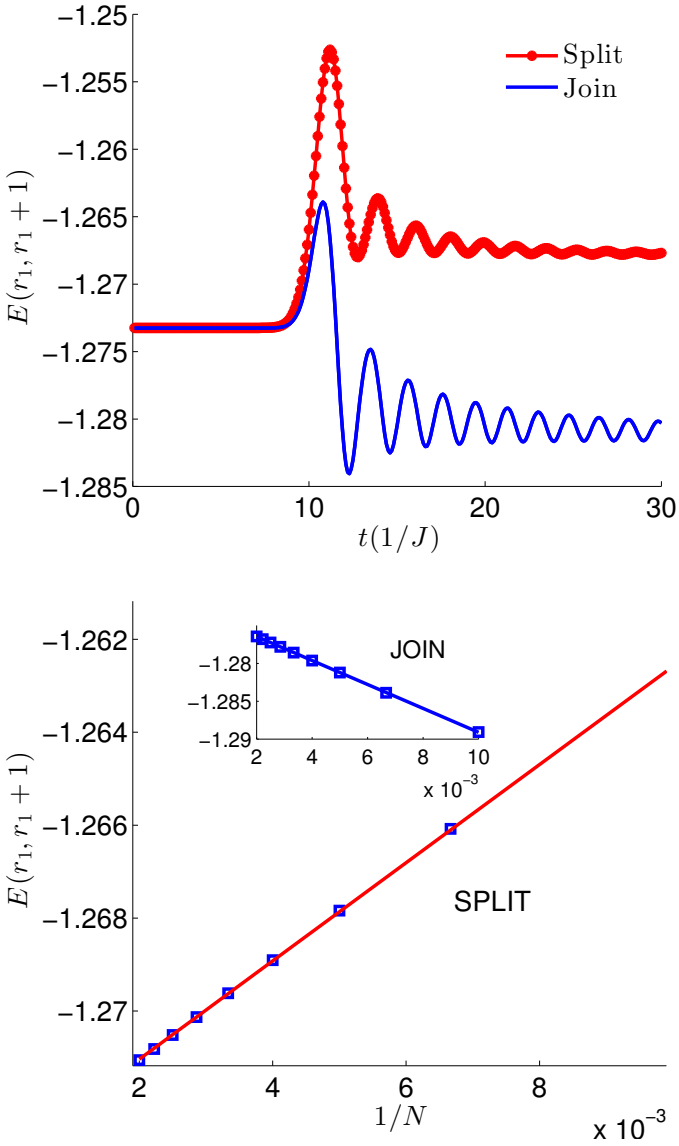

Figure 7.16: *Top:* Time-evolution of the expected energy at link $r_1 = N/2 - N/10$, both after a split quench of an initial chain with $N = 200$, and after a join quench of two initial chains with size 100. They relax to different equilibrium values. *Bottom:* The scaling analysis shows that in both cases the equilibrium value is the same but the thermodynamic limit is approached from different directions, implying that even at a local level the two quench protocols are well distinguishable.

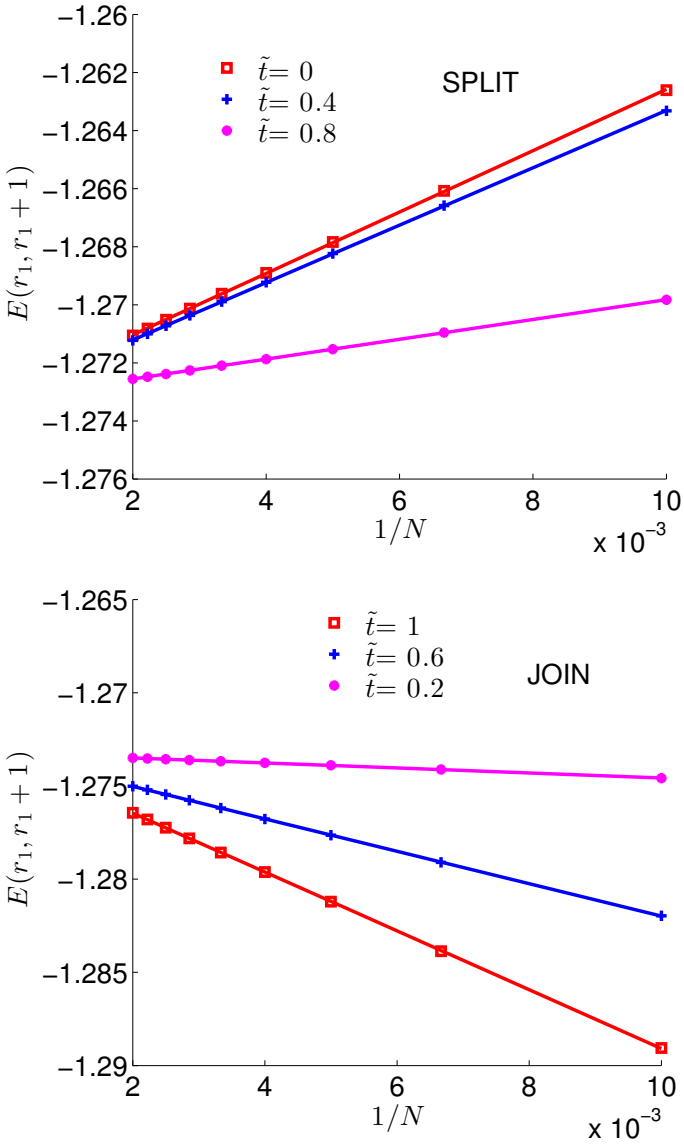

Figure 7.17: Intermediate quenches. The scaling of local observable with respect to the system size are presented in the equilibrium regime after either weakening the Hamiltonian between L and R so to provide a partial split of the two originally joined chains (*upper panel*) and after introducing a weak bond between L and R so to partially join the originally separated chains (*lower panel*). The slope of the finite size effects is in one to one correspondence with the strength of the Hamiltonian bond joining L and R giving the possibility to local discern all the above scenarios. We have considered $r_1 = N/2 - N/10$.

Chapter 8

Conclusions and further investigations

In the present thesis we analysed the realization of different quantum simulations in ultracold atomic platforms in optical lattice. Particularly, we focused on the quantum simulation of lattice gauge theories, considering both analog and digital simulations. We studied quantum systems coupled to either external or dynamical gauge fields and we considered also the quantum simulation of pure gauge theories. Finally, we also analysed the time evolution of a particular strongly correlated quantum many-body system subjected to a sudden quench. The conclusions and further investigations related to these topics are discussed in detail below.

In chapter 4, we considered the quantum simulation of 2D fermions on a lattice under the presence of an external gauge field related to the non-compact Heisenberg-Weyl group. We showed that the quantum simulation of such a system is experimentally realizable by considering layered 3-dimensional Abelian quantum Hall system. Thus, we gave a theoretical proposal for realizing non-Abelian and non-compact gauge groups with ultracold atoms in an optical lattice with phase imprinting techniques only. We considered its advantages in engineering different integer quantum Hall phases by varying the gauge potential and an external staggered potential. Explicitly, we calculated the phase diagram for the Abelian flux of 1/4 per plaquette and related the bulk topological properties to the edge states of open boundary conditions. We also showed that

by varying the other flux parameter one can achieve a non-Abelian character, when the layers are coupled sufficiently strongly. Layered fermion systems are encountered in many corners of condensed matter physics and our motivation was to find new insulating phases with non trivial topologies to get a better understanding on the possible complicated phase diagrams found in such systems. Our analysis opens a viewpoint on such systems, where the layering can be understood as an additional gauge potential on a system with reduced dimensions. Concerning practical points of view, the robustness of the topological quantization of measurable quantities can lead to metronomy standards or to applications in quantum information processing.

Next, in chapter 5, we studied an analog quantum simulation of dynamical gauge fields by considering spin-5/2 alkaline-earth atoms loaded into a 2D hexagonal lattice. In the strongly repulsive regime with a filling of one particle per site, the system is described by an effective nearest-neighbour model of SU(6) spin exchange. We found that the ground state is a chiral spin liquid state with broken time reversal symmetry. We integrated out the high energy spinon fields and arrived to a dynamical U(1) gauge field theory with a Chern-Simons term. This gauge theory describes the spin fluctuations of the system. The gauge field dynamics can be accessed experimentally with the help of spin response measurements. The stability and the finite temperature properties of the three lowest lying states were analysed within the path integral formalism, which is a reformulation of the Gutzwiller projected variational mean-field theory. We found these three phases melt at a common critical temperature in the order of the superexchange interaction. We also studied the stability of the encountered states and showed that the chiral spin liquid state is indeed the stable saddle-point and the quasi plaquette state is unstable against fluctuations with zero momentum. The plaquette state is also stable, though with higher free energy. In experiments cooling the fermions towards quantum degeneracy is a difficult to achieve goal. Combining new experimental methods, as the Pomeranchuk cooling [237] with lattice shaking [97], which can imprint a nontrivial topology to the system, it might be possible to directly cool the SU(6) symmetric Mott insulator into the topologically nontrivial chiral spin liquid state even if its free energy is close to other valence bond solid like phases. The experimentally measurable signatures of the mean-field states, namely the spin-spin correlation function, and its spectral function, of the alkaline earth atoms were considered in this work. This quantities can be key insights for revealing the gauge structure of the different phases.

In chapter 6, we introduced the notion of constructive approach for the lattice gauge theories, which leads to the link models or gauge magnets. As a paradigmatic example, we considered the U(1) gauge magnet, which is a the truncated version of the standard U(1) lattice gauge theory. First of all, we (re)discovered that the simplest plaquette Hamiltonian gives rise to confined phase, as expected, but gapless. Such property distinguishes the gauge magnets from the ordinary U(1) gauge theory in 2+1 (cf. [238]), and it is a consequence of novel gauge condition arising from the different choice of the Hilbert space (such choice, for instance, rules out the existence of short closed-string configurations). The amount of resources needed for the simulation of link models is drastically reduced as the local Hilbert space shrinks from infinity to 2D (qubit). This allows to engineer a digital simulation of gauge magnet in optical lattices based on the developments in Rydberg gates.

How the choice of the group representation affects universal properties like phase diagrams and phase transitions is a fundamental question that raises naturally here and is asking for solutions. Similarly, our constructive approach to gauge magnets allows an infinite class of Hamiltonians built up of local terms to be considered. It is totally unknown, at the moment, whether novel phases and phase transitions are described by such models, and, for instance, whether the Polyakov phase could coexist in the same phase diagram with the gapless phase we encountered in our study. The above questions are especially stimulating as nowadays novel tools in both classical simulation algorithms and in quantum simulation may be designed and employed to find a solution. Furthermore, another interesting line of investigation is the search for analogues of the gauge magnets formulations in 3+1 dimensions and/or for non-Abelian groups. In parallel, the introduction of the coupling to charged matter is very appealing.

Finally, chapter 7 we discussed the time evolution of a critical spin-chain which is quenched by splitting the system in two independent halves. Due to the entanglement in the initial state, each of the two halves is originally in a mixed state. The bipartite entanglement between the halves is conserved during the evolution. We addressed the role of the conservation of the entanglement spectrum by comparing this quench with the one where two independent spin chains are joined together. In the split scenario and in the joining scenario, both the initial state and the Hamiltonian are locally indistinguishable in the bulk of the system away from the partition in two halves. The joining quench however, due to the interaction between the two halves, does not conserve the entanglement spectrum of the bipartition. We showed that the equilibrium states emerging after these two different quenches differ both globally and lo-

cally. This suggests that the conservation of the entanglement spectrum has important consequences on both the out-of-equilibrium evolution of many-body systems and their equilibration regime. As opposed to other scenarios discussed in the literature, the conservation of the entanglement spectrum is not related to integrability of the dynamics, but rather to the specific quench protocol and the basic nature of entanglement. The splitting of a spin chain in two halves is a local quench and as such does not inject enough energy in the system to observe thermalization at any non-zero temperature. In other terms, it can not give rise to an equilibrium state with finite entropy density. We plan to generalize this analysis to global quenches that inject enough energy in the initial state for effective thermalization to take place an thus address which are the effects of the conservation of the entanglement spectrum also in those scenarios.

Chapter 9

Appendix

9.1 Geometric phase

In Chapter 3 we considered a 2D quantum system under the presence of a perpendicular and uniform magnetic field. The Brillouin zone of such a system can be parametrized by a 2D torus. We introduced the Berry's connection and curvature, $\mathcal{A}(k_x, k_y)$ (see Eq. (3.84)) and $\mathcal{F}(k_x, k_y)$ (see Eq. (3.88)) respectively. We found that these fields appear in the calculation of the Hall conductivity. This magnitude is intimately related to some topological invariants of the manifold defined by the Hilbert space.

Let us consider the effect of the next transformation on the eigenvectors $|u^{(\alpha)}\rangle$ of the Harper equation (3.71):

$$|u^{(\alpha)}\rangle \to |u^{(\alpha)}\rangle' = e^{i\theta(k_x,k_y)}|u^{(\alpha)}\rangle. \tag{9.1}$$

Under this transformation, the Berry's connection $\mathcal{A}$ is also changing, while the Berry's curvature $\mathcal{F}$ is invariant:

$$\begin{aligned} &\mathbf{A}^{(\alpha)}(k_x, k_y) \to \mathbf{A}'^{(\alpha)}(k_x, k_y) = \mathbf{A}^{(\alpha)}(k_x, k_y) + i\nabla_{\mathbf{k}}\theta(k_x, k_y), \\ &\mathcal{F}(k_x, k_y) \to \mathcal{F}'(k_x, k_y) = \mathcal{F}(k_x, k_y), \end{aligned} \tag{9.2}$$

The conductivity is *invariant* under such transformation too:

$$\sigma_{xy}^{(\alpha)} \to \sigma_{xy}^{\prime(\alpha)} = \frac{q^2}{h}\frac{1}{2\pi i}\int_{\mathbb{T}^2} d^2k\mathcal{F}'(k_x,k_y) = \frac{q^2}{h}\frac{1}{2\pi i}\int_{\mathbb{T}^2} d^2k\mathcal{F}'(k_x,k_y) = \sigma_{xy}^{(\alpha)}. \quad (9.3)$$

The invariance indicates the freedom in the choice of the Berry's connection $\mathbf{A}^{(\alpha)}(k_x,k_y)$, this vector contains redundant degrees of freedom. This feature is analogous to the *gauge freedom* discussed in the present thesis, as we can identify comparing the expressions (9.1) and (9.2) with the expression appering at Eq. (2.19). The appearance of this gauge symmetry has been studied in the theory of the geometric or Berry's phase in quantum systems.

In 1984, Sir Michael Berry published a paper [108] that a quantum system which performs an adiabatic evolution under a closed loop in its parametric Hilbert space, acquires a phase factor, which is purely geometrical. This geometrica effect is closely related to the change of the orientation of a vector which is parallel transported along a close path on a surface with a non-zero curvature (see Fig. 9.1).

The theory studied in this seminal work establishes a common framework for the study of different systems characterized by the emergence of geometric phases, like the Aharonov-Bohm effect [239], its analogue in a molecular system [240], in different polarization optics phenomena [241], the quantum Hall effect [104],the classical Foucault pendulum and the classical Hannay angle [242].

Let us consider a quantum system $|\psi\rangle$ whose evolution is given by a certain Hamiltonian H which depends on a set of parameters $r_1, r_2, ..r_n$. The time evolution of the system reads as:

$$i\hbar\frac{d}{dt}|\psi\rangle = H(\vec{R}(t))|\psi\rangle, \quad (9.4)$$

where $\vec{R} = (r_1, r_2, ..r_n)$ is the vector composed of the different parameters of H.

At every time t, there is a certain basis $\{|n(\vec{R}(t))\rangle\}$ which diagonalizes the Hamiltonian:

$$H(\vec{R}(t))|n(\vec{R}(t))\rangle = E_n(\vec{R}(t))|n(\vec{R}(t))\rangle. \quad (9.5)$$

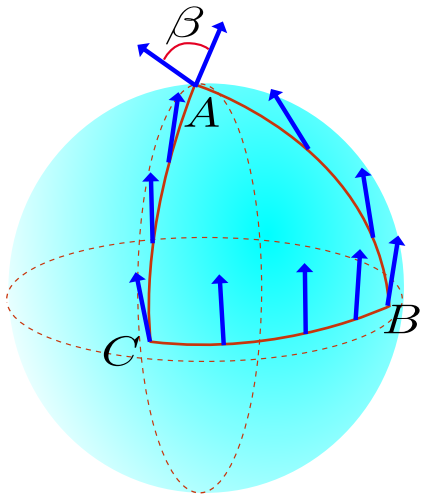

Figure 9.1: A vector is parallel transported along a closed path $A \to B \to C \to A$ on the surface of a sphere. Due to the non-zero curvature of the sphere, the initial vector and the final one differ by an angle β.

Let us consider an adiabatic change of the parameters during the time evolution. Then, if the system initially was the n^{th} eigenstate of the initial Hamiltonian, it will remain during all the evolution in the n^{th} eigenstate of the instantaneous Hamiltonian. Therefore, the state of the system can be written as:

$$|\psi(t)\rangle = e^{i\theta(t)}|n(\vec{R}(t))\rangle, \tag{9.6}$$

with $|\psi(0)\rangle = |n(\vec{R}(0))\rangle$.

To determine $\theta(t)$ we insert (9.6) in the Schrödinger equation (9.4):

$$-i\hbar\left(i\frac{d}{dt}\theta(t)e^{i\theta(t)}|n(\vec{R}(t))\rangle + e^{i\theta(t)}\frac{d}{dt}|n(\vec{R}(t))\rangle\right) = e^{i\theta(t)}E_n(\vec{R}(t))|n(\vec{R}(t))\rangle. \tag{9.7}$$

Multiplying this equation by $\langle n(\vec{R}(t))|e^{i\theta(t)}$ from the left, we end up to:

$$\frac{d}{dt}\theta(t) = -\frac{1}{\hbar}E_n(\vec{R}(t)) + i\left\langle n(\vec{R}(t)\middle|\frac{d}{dt}n(\vec{R}(t))\right\rangle. \tag{9.8}$$

The integration of this equation yields:

$$\theta(T) = -\frac{1}{\hbar}\int_0^T dt\; E_n(\vec{R}(t)) + i\int_{\mathcal{C}} d\vec{R}\;\langle n(\vec{R}(t))|\nabla_{\vec{R}}\, n(\vec{R}(t))\rangle, \tag{9.9}$$

where $\mathcal{C}$ denotes the curve parametrized by $\vec{R}(t)$, with $t \in [0, T]$. For deriving the latter expression we have used the following relation:

$$\left\langle n(\vec{R}(t))\middle|\frac{d}{dt}n(\vec{R}(t))\right\rangle = \frac{d}{dt}\vec{R}(t)\langle n(\vec{R}(t))|\nabla_{\vec{R}}\, n(\vec{R}(t))\rangle; \tag{9.10}$$

Then, the phase factor $\theta(t)$ appearing at (9.6) contains two different terms: the *dynamical phase factor* $\theta_d(t)$, which is the phase accumulated by a system in the state with energy $E(t)$, and the *geometrical phase factor* γ which is a time-independent term, it only depends on the path $\mathcal{C}$ in the parameter space of the Hamiltonian.

$$\begin{aligned}\theta_d(t) &= -\frac{1}{\hbar}\int_0^T dt\; E_n(\vec{R}(t)) \\ \gamma &= i\int_{\mathcal{C}} d\vec{R}\;\langle n(\vec{R}(t))|\nabla_{\vec{R}}\, n(\vec{R}(t))\rangle\end{aligned} \tag{9.11}$$

Defining the Berry's connection:

$$\vec{\mathcal{A}}(R) = -i\langle\psi(\vec{R}(t))|\nabla_{\vec{R}}\,\psi(\vec{R}(t))\rangle, \tag{9.12}$$

the geometric phase (9.11) can be written as:

$$\gamma = -\int_{\mathcal{C}} d\vec{R}\;\vec{A}(R). \tag{9.13}$$

The connection $\mathcal{A}$ acts as a paralell transporter of the vector state $|\psi\rangle$ from a initial point $\vec{R}_0$ to a final one $\vec{R}_T$ along a specific curve $\mathcal{C}$ on the manifold:

$$|\psi(\vec{R}_0)\rangle \to |\psi(\vec{R}_T)\rangle = e^{-i\int_{\mathcal{C}}\vec{\mathcal{A}}\,d\vec{R}}|\psi(\vec{R}_0)\rangle, \tag{9.14}$$

where the curve is parametrized as

$$\begin{aligned}\mathcal{C} &: \mathbb{R} \to \mathcal{M} \\ &t \to \vec{R}(t) \quad t \in [0,T].\end{aligned} \tag{9.15}$$

When the state performs an adiabatic closed path ($\vec{R}_0 = \vec{R}_T$) in the parameter space $\vec{R}$, the geometrical phase reads as:

$$|\psi\rangle \to |\psi\rangle' = \exp\left(-i\oint_{\mathcal{C}}\vec{\mathcal{A}}(R)d\vec{R}\right)|\psi\rangle = \exp\left(-i\int_{S_{\mathcal{C}}}\mathcal{F}\;dS_{\mathcal{C}}\right)|\psi\rangle, \tag{9.16}$$

where the last equation appears applying the Stoke's theorem over the surface $S_{\mathcal{C}}$ closed by the curve $\mathcal{C}$. The new object is the berry's curvature $\mathcal{F}$, first introduced in (3.88)

$$\mathcal{F}_{ij} = \left\langle\frac{\partial\psi}{\partial R_i}\middle|\frac{\partial\psi}{\partial R_j}\right\rangle - \left\langle\frac{\partial\psi}{\partial R_j}\middle|\frac{\partial\psi}{\partial R_i}\right\rangle. \tag{9.17}$$

The TKNN formula (3.85) is expressed in terms of this Berry's connection and the Berry's curvature. Therefore there is an intimately connection between the geometrical phase and the quantum Hall effect.

This relation can be understood in the theory of the *fibre bundles* [107]. Let us consider a quantum system whose evolution is given by Hamiltonian $H(\vec{R})$ (see Eq. (9.4)). The parameter space generated by $\vec{R}$ forms a manifold $\mathcal{M}$. For example, this manifold can be parametrized by a Euclidean space $\mathbb{R}^n$, a D dimensional torus $\mathbb{T}^n$. Since the states $|\psi\rangle$ and $e^{i\phi}|\psi\rangle$ (where α is a global phase)

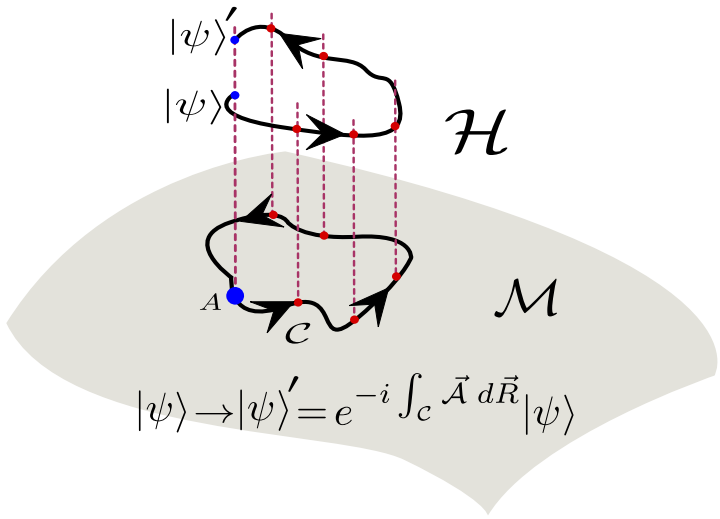

Figure 9.2: A quantum state performs a closed path $\mathcal{C}$ from the starting point A, on the manifold $\mathcal{M}$ given by the configuration space of its Hamiltonian. The starting state $|\psi\rangle$ and the final state $|\psi\rangle'$ do not coincide; they differ by a phase, which is the co-called *geometrical phase*. The values of the phase is given by the parallel transporter of the quantum state along $\mathcal{C}$ by the Berry's connection $\mathcal{A}$

identify the same physical state, both states belong to the same equivalence class. This equivalence class is fully characterized by the U(1) group. Then, the manifold represents the projected Hilbert space. The U(1) group forms a line bundle over each point of the manifold. Both entities, the manifold and the U(1) fibre form the principal fibre bundle $P(\mathcal{M}, U(1))$.

When a quantum state performs a closed path over $\mathcal{M}$, the initial and final states can differ by a phase, which is the geometrical phase (9.13). The phase is obtained by parallel transporting the quantum state over the close path. The parallel transporter is the connection associated to the fibre bundle, which is the Berry's connection expressed as (9.12). In Fig. 9.2 there is a schematic representation of this process.

For a quantum Hall system, the manifold $\mathcal{M}$ is parametrized over a 2D torus $\mathbb{T}^2$ defined by the Brilluoin zone and the fibre bundle is $P(\mathbb{T}^2, U(1))$. This fi-

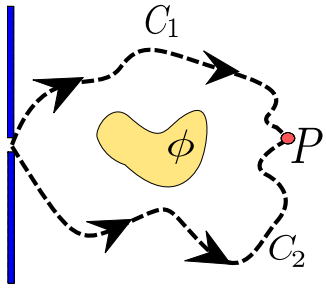

Figure 9.3: An incident beam of charged quantum particles is splitted into two different beams which travel along the curves C_1 and C_2. These two beams finally interfere at point P. The two curves define a closed curve which encloses a certain region (yellow area) with a non-vanishing magnetic flux ϕ. The interference pattern obtained at P depends on the magnetic flux.

bre bundle can be non trivial and, therefore, it represents some non-vanishing topological invariants, which are the *Chern numbers* [107, 103].

The Aharonov-Bohm effect is a manifestation of the geometric phase. It takes place when an incident beam of charged quantum particles is splitted in two different beams which interfere later (see Fig. 9.3). The presence of a non-zero perpendicular magnetic field $\mathbf{B}$ enclosed by the trajectories of the beams affects the interference pattern, even when the quantum particles do not penetrate into the zone with non zero magnetic flux.

The time dependent Schrdinger equation for such a system is:

$$\frac{1}{2m}(-i\hbar\nabla - (q/c)\mathbf{A})\varphi(\vec{r},t) = i\hbar\frac{\partial\varphi(\vec{r},t)}{\partial t}, \tag{9.18}$$

where $\mathbf{A}$ is the vector potential: $\mathbf{B} = \nabla \times \mathbf{A}$.

Let us consider a magnetic field $\mathbf{B}$ which is non zero over a certain surface $\tilde{S}$, and zero outside. The quantum particle travels through two different paths, defined by the curves $\mathcal{C}_1$ and $\mathcal{C}_2$ (see Fig. 9.3). This trajectories are placed in the region where $\mathbf{B}$ vanishes. However, the vector potential $\mathbf{A}$ is not zero along these trajectories. Therefore, the solution for the Eq. (9.18) is given by:

$$\varphi_i(\vec{r},t) = \varphi_0(\vec{r},t)\, e^{\frac{iq}{\hbar c}\int_{\mathcal{C}_i} d\vec{r}\mathbf{A}(\vec{r})}, \tag{9.19}$$

where the label i indicates the different trajectory and $\varphi_0(\vec{r},t)$ is the solution for $\mathbf{A}=0$. This expression is exactly the parallel transport of the state $\varphi_0(\vec{r},t)$ among the closed curve $C=C_1\cup C_2$, on a fibre bundle $\mathcal{P}(\mathcal{M},U(1))$, whose manifold is the 2D-Euclidean space of positions $\mathbb{R}^2$. The Berry's connection coincides with the vector potential: $\vec{\mathcal{A}}=-\frac{q}{\hbar c}\mathbf{A}$. Then, the geometric phase $\tilde{\gamma}_i$ of each trajectory is:

$$\tilde{\gamma}_i=\frac{q}{\hbar c}\int_{\mathcal{C}_i}d\vec{r}\mathbf{A}(\vec{r}). \tag{9.20}$$

The interference pattern at P (see Fig. 9.3) contains a contribution coming from the difference of the geometric phase of the two different trajectories:

$$e^{\frac{iq}{\hbar c}\int_{\mathcal{C}_1}d\vec{r}\mathbf{A}(\vec{r})-\frac{iq}{\hbar c}\int_{\mathcal{C}_2}d\vec{r}\mathbf{A}(\vec{r})}=e^{\frac{iq}{\hbar c}\oint_{\mathcal{C}}d\vec{r}\mathbf{A}(\vec{r})}=e^{i\gamma}. \tag{9.21}$$

Finally, we can write the geometric phase in terms of the magnetic flux ϕ contained in the surface enclosed by the trajectories:

$$\begin{aligned}\gamma=\frac{q}{\hbar c}\oint_{\mathcal{C}}d\vec{r}\mathbf{A}(\vec{r})=\frac{q}{\hbar c}\int_{S_{\mathcal{C}}}d\vec{S}(\nabla\times\mathbf{A}(\vec{r}))=\\ \frac{q}{\hbar c}\int_{\tilde{S}}d\vec{S}(\nabla\times\mathbf{A}(\vec{r}))=\frac{q}{\hbar c}\int_{\tilde{S}}d\vec{S}\,\mathbf{B}=\frac{q\phi}{\hbar c},\end{aligned} \tag{9.22}$$

where $S_{\mathcal{C}}$ is the surface bounded by the closed path $\mathcal{C}$ and $\tilde{S}\subset S$ is the surface with non-vanishing magnetic flux.

Thus, the geometrical phase induces a shift in the interference pattern with respect to the case with zero magnetic flux.

9.2 Feynman rules for the spin liquid phases

In this appendix our goal is to derive the curvature of the effective action and give the explicit form of the stability matrix (5.67b) and the one in Eq. (5.68). To this end we need to evaluate

$$\begin{aligned}\mathrm{tr}(G_0\Sigma)^n=\sum_{\hat{k},\hat{q}_1\ldots\hat{q}_n}\mathrm{tr}\Big[&G_{(0)}(\hat{k})\Sigma(\hat{k}-\hat{q}_1,\hat{q}_1)\\ &\times G_{(0)}(\hat{k}-\hat{q}_1)\Sigma(\hat{k}-\hat{q}_1-\hat{q}_2,\hat{q}_2)\times\ldots\\ &\times G_{(0)}(\hat{k}-\hat{q}_1-\ldots-\hat{q}_{n-1})\Sigma(\hat{k}-\hat{q}_1-\ldots-\hat{q}_n,\hat{q}_n)\Big],\end{aligned} \tag{9.23}$$

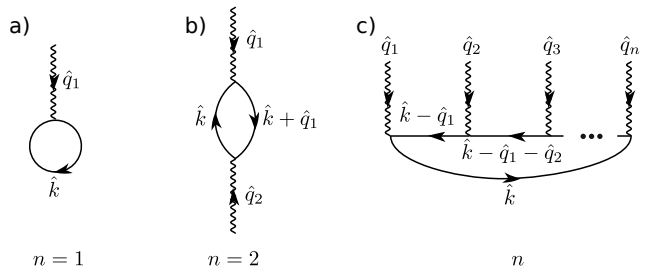

Figure 9.4: Feynman graphs representing the expansion Eq.(9.23). We have plotted the first order a), the second order b) and the nth order c) diagrams. The straight lines represent the free fermion propagator, while the wiggly line is for the Σ vertex. The sum of the incoming momentum has to be zero.

where $\sum_n \hat{q}_n = 0$. In the left hand side of the first line, the trace tr is a sum for momentum, Matsubara frequency and sublattice index. In the right hand side, Tr is understood only in the sublattice indices as the sum is explicitly indicated for the momentum and Matsubara frequencies. Eq.(9.23) is prone to be represented by Feynman diagrams. At a given order (say n) we have exactly n free fermion propagators $G_{(0)}$, represented by straight lines, and also n incoming vertices Σ, represented by wiggly lines. The arrows show the direction of the transfer of momentum. The entire graph is connected and contains a single loop with momentum and Matsubara frequency conservation. For illustration we have shown the first (a), the second (b), and the general, nth order (c) graphs in Fig. 9.4. Note that both $G_{(0)}$ and Σ are matrices in the sublattice index.

For the curvature of the effective action (5.67) we need to evaluate

$$
\begin{aligned}
R_{\mu\nu}(\hat{q}) &\equiv \mathrm{tr}\left[\frac{\partial^2 \left(G_{(0)}\Sigma\right)^2}{\partial\phi^*_\mu(\hat{q})\partial\phi_\nu(\hat{q})}\right] \\
&= \mathrm{tr}\left(G_{(0)}(\hat{k})\frac{\partial\Sigma(\hat{k}+\hat{q},-\hat{q})}{\partial\phi^*_\mu(\hat{q})}G_{(0)}(\hat{k}+\hat{q})\frac{\partial\Sigma(\hat{k},\hat{q})}{\partial\phi_\nu(\hat{q})}\right) \\
&= \sum_{\substack{\mathbf{k},i\omega_n \\ s_1,s_2,s_3,s_4}} G_{(0)s_1,s_2}(\mathbf{k},i\omega_n)G_{(0)s_3,s_4}(\mathbf{k}+\mathbf{q},i\omega_n+i\nu_m) \\
&\qquad \times \frac{\partial\Sigma_{s_2,s_3}(\hat{k}+\hat{q},-\hat{q})}{\partial\phi^*_\mu(\hat{q})}\frac{\partial\Sigma_{s_4,s_1}(\hat{k},\hat{q})}{\partial\phi_\nu(\hat{q})}
\end{aligned}
$$

$$= \sum_{\substack{\mathbf{k},a,b \\ s_1,s_2,s_3,s_4}} \frac{v^{(a)}_{s_1}(\mathbf{k})\, v^{(a)*}_{s_2}(\mathbf{k})\, v^{(b)}_{s_3}(\mathbf{k}+\mathbf{q})\, v^{(b)*}_{s_4}(\mathbf{k}+\mathbf{q})}{i\nu_m + \varepsilon^{(a)}_{\mathbf{k}} - \varepsilon^{(b)}_{\mathbf{k}+\mathbf{q}}}$$

$$\times \left[n(\varepsilon^{(a)}_{\mathbf{k}}) - n(\varepsilon^{(b)}_{\mathbf{k}+\mathbf{q}}) \right] \frac{\partial \Sigma_{s_2,s_3}(\hat{k}+\hat{q},-\hat{q})}{\partial \phi^*_\mu(\hat{q})} \frac{\partial \Sigma_{s_4,s_1}(\hat{k},\hat{q})}{\partial \phi_\nu(\hat{q})}. \quad (9.24)$$

The derivatives of the self-energies are again easily evaluated with the help of Eq. (5.59). Combining Eq. (9.24) with Eqs. (5.67) we arrive to the 24×24 Hessian matrix

$$C_{\mu\nu}(\hat{q}) = 6\, R_{\mu\nu}(\hat{q}) + \frac{1}{J} \sum_{i=1}^{18} \delta_{\mu,i} \delta_{\nu,i}. \quad (9.25)$$

With the help of Eq. (9.24) it can be directly checked that

$$C_{\mu\nu}(\mathbf{q}, i\nu_m) = C^*_{\nu\mu}(\mathbf{q}, -i\nu_m). \quad (9.26)$$

Finally let us construct the Hessian matrix $\widetilde{C}_{kl}(\hat{q})$ appearing in Eq. (5.68) after integrating out the $\delta\varphi$ fields. For a convenient notation let us introduce submatrices of the original 24×24 matrix $C_{\mu\nu}(\hat{q})$, such that

$$C_{\mu\nu}(\hat{q}) = \begin{bmatrix} C_{1,1}(\hat{q}) & C_{1,2}(\hat{q}) & \dots & C_{1,18}(\hat{q}) & W_{1,1}(\hat{q}) & W_{1,2}(\hat{q}) & \dots & W_{1,6}(\hat{q}) \\ & \ddots & & \vdots & \vdots & & & \vdots \\ & & & C_{18,18}(\hat{q}) & W_{18,1}(\hat{q}) & \dots & & W_{18,6}(\hat{q}) \\ & & & & E_{1,1}(\hat{q}) & & \dots & E_{1,6}(\hat{q}) \\ & & & & & \ddots & & \vdots \\ & & & & & & & E_{6,6}(\hat{q}) \end{bmatrix} \quad (9.27)$$

where C_{kl} is a 18×18, W_{ks} is a 18×6 and E_{sr} is a 6×6 matrix. The elements below the diagonal are understood to be filled according to the relation (9.26). With the help of this notation, the path integral over the $\delta\varphi$ fields, in the Gaussian approximation Eq. (5.67) is performed by

$$\int D[\delta\varphi]\, e^{-S^{(2)}_{\text{eff}}[\delta\chi,\delta\chi^*,\delta\varphi]} = \frac{1}{\sqrt{\det E}} e^{-S^{(2)'}_{\text{eff}}[\delta\chi,\delta\chi^*]}, \quad (9.28)$$

with $S^{(2)'}_{\text{eff}}$ given in Eq. (5.68) with the matrix

$$\widetilde{C}_{kl}(\mathbf{q}, i\nu_m) \;=\; C_{kl}(\mathbf{q}, i\nu_m) \;-\; \sum_{r,s=1}^{6} W_{ks}(\mathbf{q}, i\nu_m) E^{-1}_{sr}(\mathbf{q}, i\nu_m) W^{*}_{lr}(\mathbf{q}, -i\nu_m). \tag{9.29}$$

9.3 Quantum link models for $\mathbb{Z}_N$ gauge theories

9.3.1 Gauge group $\mathbb{Z}_2$.

The local Hilbert space

The gauge theory generated by the $\mathbb{Z}_2$ group is the simplest one could imagine (apart from the percolationg lattice gauge theory of [174]). The orientation of the lattice is not important, since there are only two different elements of the group, the first is 1 and the other is e, which has the property that $e^2 = ee^{-1} = 1$. The local Hilbert space with spin 1/2 is the algebra of the group and the representation matrices of the group coincide with the regular representation of the group. The regular representation is defined to be the representation in which the matrices are constructed directly from the multiplication table of the group. In order to get the representation of multiplication by a given element, one substitute the given element in the multiplication with one and all the others with zeros. For the $\mathbb{Z}_2$ case we have the following group multiplication table

	1	e
1	1	e
$e^{-1} = e$	e	1

(9.30)

thus $X(1) = \mathbb{I}$, $X(e) = \sigma^x$. There is an important theorem relating the regular representation with the irreducible representations. This theorem states that the regular representation contains all the irreducible representations a number of time equal to their dimensions [175].

In this case, we have two $A_s(g)$, $A_s(1) = \mathbb{I}$ and $A_s(e) = (\sigma^x)^{\otimes 4}$. Thus the condition (2.89) is projecting out half of the 2^4 states associated to a site.

The gauge invariant Hilbert space

In order to show that the condition (2.89) is neither trivial or empty, and how it can be implemented, we first consider the minimal lattice, made of only one plaquette. This is shown explicitly in Fig. 9.5 v). The gauge invariant Hilbert space is embedded in the $2^4 = 16$ dimensional Hilbert space $\{|l_1 l_2 l_3 l_4\rangle\}$. Due to

the periodic identification of of the links on the plaquette, (2.89) applied for s_1 implies

$$\sigma^x_{l_4} \otimes \sigma^x_{l_1} |l_1 l_4\rangle = |l_1 l_4\rangle. \tag{9.31}$$

Since σ^x has eigenvalues ± 1. We have two possibilities $|l_1 l_4\rangle = |{+}{+}\rangle$, $|l_1 l_4\rangle = |{-}{-}\rangle$, where

$$\sigma^x|+\rangle = |+\rangle,\ \sigma^x|-\rangle = -|-\rangle. \tag{9.32}$$

By iteratively applying all the $A_s(g)$ on subsequent sites, one realizes that there are two allowed states and thus a generic gauge invariant state is a linear combination of them

$$|\phi_+\rangle = |{+}{+}{+}{+}\rangle,\ |\phi_-\rangle = |{-}{-}{-}{-}\rangle. \tag{9.33}$$

This formalize the naive intuition (which has to be modified for finite systems with periodic boundary conditions [243]) that gauge invariant states are related to the elementary plaquettes of the lattice.

The gauge invariant operators

The operators compatible with gauge invariance constraints are either

- product of σ^x on arbitrary links of the lattice
- product of $\sigma^{i\neq x}$ on closed paths

The simplest choice is then $\sigma^z_{l_1} \otimes \sigma^z_{l_2} \otimes \sigma^z_{l_3} \otimes \sigma^z_{l_4}$. Going back to the lattice formed by a single plaquette of Fig. 9.5 v) we define the Hamiltonian

$$H_0 = -B_P = -\sigma^z_{l_1} \otimes \sigma^z_{l_2} \otimes \sigma^z_{l_3} \otimes \sigma^z_{l_4}, \tag{9.34}$$

that is the form that the generic Hamiltonian of (6.22) on the chosen lattice when $\theta = 0$. In this simple example, we see that the ground-state is given by the linear combination

$$|\psi_0^{B_p}\rangle = \frac{1}{\sqrt{2}} \left(|{+}{+}{+}{+}\rangle + |{-}{-}{-}{-}\rangle\right), \tag{9.35}$$

and the first excitation is given by

$$|\psi_1^{B_p}\rangle = \frac{1}{\sqrt{2}} \left(|{+}{+}{+}{+}\rangle - |{-}{-}{-}{-}\rangle\right). \tag{9.36}$$

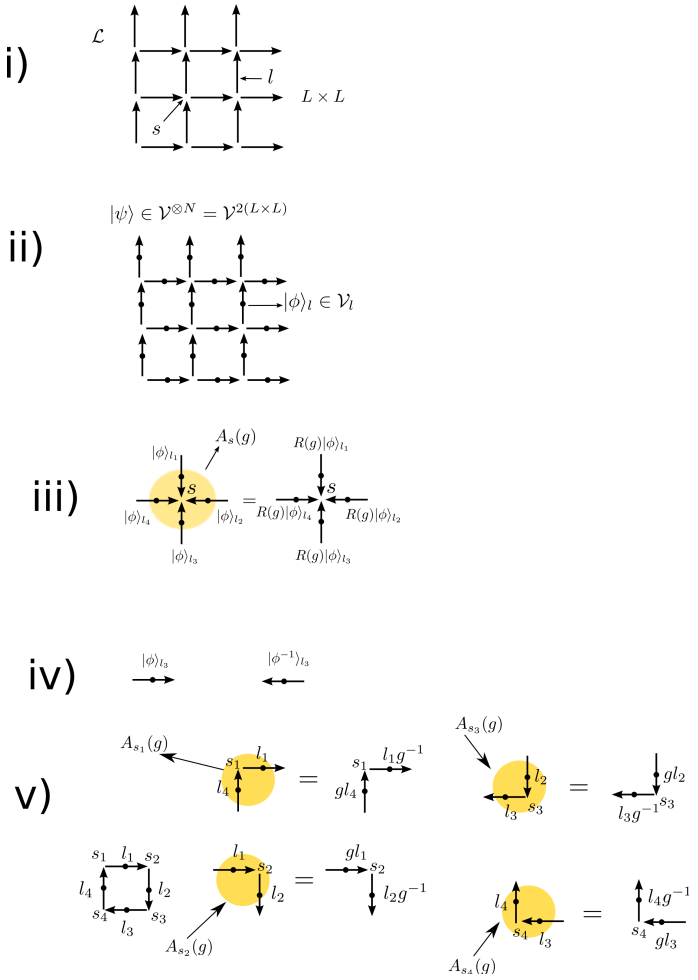

Figure 9.5: i) Example of an oriented lattice $\mathcal{L}$ with L sites s and $N = 2L$ links l. ii) A many-body state of the lattice is obtained by defining a local Hilbert space $\mathcal{V}$ on each of the links. A state of the lattice is then a state of the tensor product $|\psi\rangle \in \mathcal{H}_G = \mathcal{V}^{\otimes N}$. iii) For each site s of the lattice we can define operators $A_s(g)$ acting on the local Hilbert space $\mathcal{H}_G|_s = \mathcal{V}^{\otimes 4}$, where $\mathcal{V}$ is the Hilbert space of a link ending in s. $A_s(g)$ multiplies each link state $|h_{l_i}\rangle_s$ for the $X(g)$ or $X(g^{-1})$ depending on the fact if the link is entering or exiting the particular site. Gauge invariance is the requirement that the state $A_s(g)\bigotimes_i |h_{l_i}\rangle_s\rangle = \bigotimes_i |h_{l_i}\rangle_s\rangle\rangle$.iv) A particular case is obtained when the local Hilbert space $\mathcal{V}$ is chosen to be the group algebra $\mathcal{C}(G)$. In this case, the states are labeled by $|g_{l_i}\rangle_s$ and changing the orientation of the link, corresponds to $|h_{l_i}\rangle_s \to |h^{-1}{}_{l_i}\rangle_s$. v) A simple example of a one plaquette lattice, discussed in the main text, is worked out in details. It consists of four sites, $s_1 \cdots s_4$ and four links $l_1 \cdots l_4$. The four elementary gauge transformations related to the four sites are explicitly introduced.

We also see that the two states are separated by an energy gap (that does not depend on the system size),

$$\Delta_2 = 2. \tag{9.37}$$

On the other hand, if we consider the opposit limit of the Hamiltonian of (6.22) and set $\theta = \pi/2$, we obtain

$$H_{\pi/2} = -\sum_{l_i} \sigma^x_{l_i}, \tag{9.38}$$

which ground-state becomes

$$|\psi_0^{\sigma^x}\rangle = |++++\rangle, \tag{9.39}$$

and which first excited state is

$$|\psi_1^{\sigma^x}\rangle = |----\rangle. \tag{9.40}$$

Already in this simple example we can appreciate that in the two limit considered of (6.22) we are in a gaped phase but the ground-states of the Hamiltonian in (9.38) and (9.34) have different entanglement properties. Indeed, the ground-state of the latter Hamiltonian is a product state, while the one of the former is locally maximally entangled, since the reduced density matrix of a single link is proportional to the identity. This reasoning can be extended to larger systems since both Hamiltonians of (9.38) and (9.34) are fixed point of the RG flow [243]. The general Hamiltonian (6.22) is not in general a fixed point of the RG flow. From the above discussion it is easy to accept the appearence of a phase transition at a given θ_c in between $\theta = 0$ and $\theta = \pi/2$ that separate the domain of attraction of the RG fixed point at $\theta = 0$ usually called the topological-deconfined phase with the one of the RG fixed point at $\theta = \pi/2$ usually called the confined phase.

9.3.2 The case of the group $\mathbb{Z}_3$, prototype for the generic $\mathbb{Z}_N$

The next step of complication is obtained by considering a $\mathbb{Z}_3$. The main difference with respect to the $\mathbb{Z}_2$ theory is that the group algebra of $\mathbb{Z}_3$ has dimension 3 - N for a generic $\mathbb{Z}_N$ - and not all the elements of the group are the inverse of themselves. Hence, the orientation of the lattice plays a central role. From now

on, we will consider two different basis, the group algebra basis $|g\rangle$, and the basis in which the regular representation becomes the direct sum of the irreducible representations $|t\rangle$.

In the $|g\rangle$-basis the $X(g)$s read

$$\begin{array}{c|ccc} & 1 & e_2 = e_1^{-1} & e_1 = e_2^{-1} \\ \hline 1 & 1 & e_2 & e_1 \\ e_1 & e_1 & 1 & e_2 \\ e_2 & e_2 & e_1 & 1 \end{array}, \tag{9.41}$$

$$X(1) = \mathbb{I}, \tag{9.42}$$

$$X(e_1) = \begin{pmatrix} 0 & 0 & 1 \\ 1 & 0 & 0 \\ 0 & 1 & 0 \end{pmatrix}, \tag{9.43}$$

$$X(e_2) = \begin{pmatrix} 0 & 1 & 0 \\ 0 & 0 & 1 \\ 1 & 0 & 0 \end{pmatrix}. \tag{9.44}$$

As done previously for σ^x, we can diagonalize all the X and we pass to the basis $|t_i\rangle\langle t_i|$, $i = 1 \dots 3$. In this basis

$$X(1) = diag\{1, 1, 1\}, \tag{9.45}$$

$$X(e_1) = diag\{1, e^{\frac{4\pi}{3}i}, e^{\frac{2\pi}{3}i}\}, \tag{9.46}$$

$$X(e_2) = diag\{1, e^{\frac{2\pi}{3}i}, e^{\frac{4\pi}{3}i}\}. \tag{9.47}$$

We then can find the gauge invariant states in the $|t\rangle$-basis

$$|t_1,t_1,t_1,t_1\rangle, |t_2,t_2,t_2,t_2\rangle, |t_3,t_3,t_3,t_3\rangle. \tag{9.48}$$

Now, let us focus on the construction of the plaquette of the Hamiltonian, taking properly in account the orientation of the links. In order to do so, we have to specify the form of the Z operator for the group $\mathbb{Z}_3$, which generalizes the σ^z employed for $\mathbb{Z}_2$. In the $|g\rangle$-basis, it is

$$Z = \begin{pmatrix} 1 & 0 & 0 \\ 0 & e^{\frac{2\pi i}{3}} & 0 \\ 0 & 0 & e^{\frac{4\pi}{3}i} \end{pmatrix}. \tag{9.49}$$

It has the following properties

$$ZX(e_1) = e^{\frac{2\pi}{3}i} X(e_1)Z, \quad ZX(e_2) = e^{\frac{4\pi}{3}i} X(e_2)Z. \tag{9.50}$$

If we orient the plaquettes in such a way that they always have one entering and one exiting link for each site (either anti-clockwise or clockwise) the plaquette will meet a gauge transformation on two consecutive links but the orientation is such that the gauge transformation on these links will look like $X(e) \otimes X(e^{-1})$. Since the orientation of the plaquette is different from the orientation of the gauge transformation given in Fig. 9.5 iii) we are multiplying one of the two links for $X(e^{-1})$ instead than $X(e)$. Hence, the only possibility to obtain an operator commuting with all the gauge transformations is to take again a product of Z as

$$[Z \otimes Z, X(e) \otimes X(e^{-1})] = 0, \tag{9.51}$$

accordingly to (9.50). It follows that the correspondent Hamiltonian term, written on the anti-clockwise or clockwise oriented plaquettes (as the one of Fig. 9.5 v)), reads

$$H_P = -\frac{1}{2} \sum_p \left(Z_{l_1} Z_{l_2} Z_{l_3} Z_{l_4} + Z_{l_1}^\dagger Z_{l_2}^\dagger Z_{l_3}^\dagger Z_{l_4}^\dagger \right). \tag{9.52}$$

This is, as expected, the explicit realization of Hamiltonian of (6.22) with $\theta = 0$ for the group $\mathbb{Z}_3$. It is important to notice that now the $l_1 \cdots l_4$ are the links around a given plaquette in the order of Fig. 9.5 v). Once we move back to the standard orientation of the 2D space of Fig. 9.5 ii) we recover the standard form [**?**]

$$H_P = -\frac{1}{2} \sum_p \left(Z_{l_1}^\dagger Z_{l_2}^\dagger Z_{l_3} Z_{l_4} + Z_{l_1} Z_{l_2} Z_{l_3}^\dagger Z_{l_4}^\dagger \right). \tag{9.53}$$

Once the basis is rotated from $|g\rangle$ to $|t\rangle$, the form of the Z operator is determined by (9.50) to be

$$Z : |t_i\rangle \to |t_{i+1}\rangle, \tag{9.54}$$

and

$$Z^\dagger : |t_i\rangle \to |t_i - 1\rangle, \tag{9.55}$$

i.e., $X(e_1) \to Z$, and $Z \to X(e_1)$.

Again we can consider the ground-state of the plaquette operator for a lattice made of a single plaquette as in Fig. 9.5 v). It turns out that

$$Z_{l_1} Z_{l_2} Z_{l_3} Z_{l_4} : |t_i t_i t_i t_i\rangle \to |t_{i+1} t_{i+1} t_{i+1} t_{i+1}\rangle, \tag{9.56}$$

$$Z^\dagger_{l_1} Z^\dagger_{l_2} Z^\dagger_{l_3} Z^\dagger_{l_4} : |t_i t_i t_i t_i\rangle \to |t_{i-1} t_{i-1} t_{i-1} t_{i-1}\rangle. \tag{9.57}$$

It is easy to realize that the eigenvalues of H_P are -1 or $+1/2$ and its ground-state on a single plaquette is given by

$$|\psi_0\rangle = \frac{1}{\sqrt{3}} \sum_i |t_i t_i t_i t_i\rangle. \tag{9.58}$$

Here, again we discover the emergence of gauge invariant plaquette states. Their number is now 3 and clearly coincide with the $|G|$, the cardinality of the group. The plaquette Hamiltonian is still gapped, but the gap, $\Delta_3 = 3/2$ is now smaller than in the $\mathbb{Z}_2$ case. We can again study the opposite limit of (6.22) with $\theta = \pi/2$. There we see that all spins are aligned in the t_1 direction. As before, by passing to larger lattices, we can repeat the same reasoning and we find two different phases. One in which the ground-state in a product state and the other in which it is robustly entangled. It is also known that by increasing the rank of the group a third phase appear. Here, we will not study that phase and refer the interested reader to the literature [244].

9.4 Splitting quench: profile of the entanglement entropy

From the profile for the for the projection of the entanglement entropy $S(r,t)$ in Section 7.2.2, we guess the following expression for such a quantity:

$$\tilde{S}_X(x) = \frac{c}{\alpha_x} \log_2 \left| \frac{N}{\pi} \left(\sin \frac{2\pi x}{T_x} \right)^{\nu_x} \right| + \text{cst}. \tag{9.59}$$

By either choosing $x = r$ or $x = t$ we recover both space and time sections of the entanglement entropy (see Fig. 7.8). In each case T_x has to be chosen accordingly to the definition discussed in the next paragraph.

$$\begin{aligned} x = r &\to \tilde{S}_X(x) = \tilde{S}_S(r) \\ x = t &\to \tilde{S}_X(x) = \tilde{S}_T(t) \end{aligned} \tag{9.60}$$

- **Calculation of the parameter α_x.** This value is extracted through a finite size scaling analysis. By fixing the ratio $\frac{t}{N}$, the dependency of the expression (9.59) on N is given by $\tilde{S}_X(x) = \frac{c}{\alpha_x} \log_2 N + \text{cst}$. Specifically, we have considered chains with $N = 100, 120, 140, 160, 200, 240$.

  For the case of $\tilde{S}_T(t)$ we have considered ratios

$$\frac{t}{N} = \frac{1}{2} \cdot \left(\frac{2}{10}, \frac{3}{10}, \frac{5}{10}, \frac{6}{10} \right), \tag{9.61}$$

  while for $\tilde{S}_S(r)$ we have considered sites $r \ll N/2$ and ratios

$$\frac{t}{N} = \left(\frac{2}{10}, \frac{3}{10}, \frac{4}{10}, \frac{6}{10}, \frac{7}{10} \right). \tag{9.62}$$

  Averaging on the values of α extracted from the various ratios we obtain

$$\begin{aligned} \tilde{S}_T(t) &\to \alpha_T = 2.919\ (41) \\ \tilde{S}_S(r) &\to \alpha_S = 2.947\ (13) \end{aligned} \tag{9.63}$$

  that are both compatible with $\alpha = 3$. In order to cross-check our strategy we have repeated the same procedure for the join quench. In this case we obtain

$$\begin{aligned} \tilde{S}_T(t) &\to \alpha_{join} = 3.012\ (59) \\ \tilde{S}_S(r) &\to \alpha_{join} = 3.042\ (10) \end{aligned} \tag{9.64}$$

  that is in agreement with the available theoretical prediction $\alpha_{join} = 3$ [228, 213, 229].

- **Calculation of the parameter ν_x.**

  At fixed N, $\tilde{S}_X(x)$ depends linearly on $y = \log_2 \left| \left(\sin \frac{2\pi x}{T_x} \right) \right|$. We can thus extract the value of ν_x through a linear fit of $\tilde{S}_X$ as a function of y at a fixed N. We have performed such analysis for several chains of length $N = 100, 120, 140, 160, 200, 240$, obtaining several estimates values of ν_x.

In particular for $\tilde{S}_T(t)$, $T_x = N$, and for each N we have considered the set of times

$$t = \left(\frac{N}{8}, \frac{N}{8} + 1, ..., \frac{N}{2} - \frac{N}{8} \right). \tag{9.65}$$

For $\tilde{S}_S(r)$, $T_x = 2N$ and we have considered $r \ll N/2$:

$$r = \left(\frac{2N}{10}, \frac{2N}{10} + 1, ..., \frac{N}{4} \right) \tag{9.66}$$

Averaging on the values of ν obtained for each N we get

$$\tilde{S}_T(t) \to \nu_T = 0.500\ (14) \tag{9.67}$$

$$\tilde{S}_S(r) \to \nu_S = 1.004\ (5) \tag{9.68}$$

While the first result is un-expected, the second is compatible with what expected in a join quench. By repeating the analysis for the join quench where we expect $\nu_{join} = 1$ [228, 213, 229] we indeed find

$$\begin{aligned} &\tilde{S}_T(t) \to \nu_{join} = 0.975\ (34) \\ &\tilde{S}_S(r) \to \nu_{join} = 1.070\ (10) \end{aligned} \tag{9.69}$$

as expected.

9.5 Splitting quench: two point anti-correlations from a quasi-particle treatment

As we discussed at Section 7.1, our initial state $|\Omega\rangle_0$ has excess energy with respect to the ground state of the new Hamiltonian H, $|\Omega\rangle_L \otimes |\Omega\rangle_R$. This excess of energy, which is located in the junction between the two chains, can be interpreted as a finite density of quasi-particles of H_t [206]. These quasi-particles start to propagate away with a finite speed. This propagation produces the characteristic light-cone-type spreading of the perturbation [42]. The Lieb-Robinson bound [245] for a system described with a Hamiltonian with local operators explains the finite velocity for the propagation of this perturbation.

For the quantum Ising chain in transverse field, the quasi-particles correspond to the free fermions appearing through the diagonalization of H (see Eq. (7.9)). The quasi-particle picture provides successfully results in the analysis

of quantum Ising chains, as the calculation of correlation lengths in chains in thermal equilibrium [246], or the time evolution of the entanglement entropy [247, 248, 249, 250].

In the spliting scenario studied in Chapter 7, the correlation function $C(r_1, r_2, t)$ appearing in (7.13) exhibits a regime with negative sign or *anti-correlation* for points r_1, r_2 located at different halves (see Fig. 7.14). Our goal is to explain this anti-correlated behaviour in terms of quasi-particles propagating from the quench point.

Since $H_0 = H_L + H_R + H_{LR}$, we can write the initial state $|\Omega\rangle_0$, i.e. the ground state of H_0, in terms of the eigenstates $|\Psi_m\rangle$ of H, which is the Hamiltonian responsible of the time evolution:

$$|\Omega\rangle_0 = |\Omega_L\rangle \otimes |\Omega_R\rangle + \sum_{m\neq 0} \frac{\langle \Psi_m | H_{LR} \left(|\Omega_L\rangle \otimes |\Omega_R\rangle \right)}{E_0 - E_m} |\Psi_m\rangle, \tag{9.70}$$

where we have considered first order in perturbation theory, where H_{LR} is the perturbation. Moreover, $H = H_L + H_R$ and $H|\Psi_m\rangle = E_m|\Psi_m\rangle$, where $|\Omega\rangle_L \otimes |\Omega\rangle_R = |\Psi_0\rangle$ is the ground state of H.

Since $H = H_L + H_R$, we can write:

$$\begin{aligned} &H|\Psi_m\rangle = (H_L + H_R)(|\psi\rangle^L_{m1} \otimes |\psi\rangle^R_{m2}) = \\ &H_L|\psi\rangle^L_{m1} \otimes |\psi\rangle^R_{m2} + |\psi\rangle^L_{m1} \otimes H_R|\psi\rangle^R_{m2} = (E^L_{m1} + E^R_{m2})|\psi\rangle^L_{m1} \otimes |\psi\rangle^R_{m2}. \end{aligned} \tag{9.71}$$

H_R and H_L can be diagonalized in terms of free fermions:

$$H_X = \sum_k \epsilon^X_k \eta^{X\dagger}_k \eta^X_k, \quad X = R, L, \tag{9.72}$$

where $\eta^{X\dagger}_k (\eta^X_k)$ is the creation (annihilation) fermionic operator of the k mode.

Since we consider the quasi-particle picture, then we only take into account the states with one k fermion:

$$|\psi\rangle^X_{m1} = \eta^{X\dagger}_k |\Omega_X\rangle \equiv |k_X\rangle. \tag{9.73}$$

Therefore, the expression (9.70) can be written as:

$$|\Omega\rangle_0 = |\Omega\rangle_L \otimes |\Omega\rangle_R - \sum_{k,k'} F(k, k', N/2, N/2+1)|k\rangle \otimes |k'\rangle, \tag{9.74}$$

where:

$$F(k,k',N/2,N/2{+}1) = -\frac{\langle\Psi_m|H_{LR}\left(|\Omega_L\rangle\otimes|\Omega_R\rangle\right)}{E_0-E_m} = \frac{\langle k|\sigma^x_{\frac{N}{2}}|\Omega_L\rangle\langle k'|\sigma^x_{\frac{N}{2}+1}|\Omega_R\rangle}{E_0-(E_k+E_{k'})}, \tag{9.75}$$

with $H_{LR} = -\sigma^x_{\frac{N}{2}}\sigma^x_{\frac{N}{2}+1}$.

The time evolution of $|\Omega\rangle_0$ is given by:

$$|\varphi(t)\rangle = e^{-iHt}|\Omega\rangle_0 = e^{-iE_0t}|\Omega_L\rangle\otimes|\Omega_R\rangle - \sum_{k,k'} e^{-it(E_k+E_{k'})}\cdot F(k,k',N/2,N/2+1)\cdot|k\rangle\otimes|k'\rangle. \tag{9.76}$$

9.5.1 Calculation of the two point correlator

Lets now calculate the two point correlator function (7.13) for points located in different halves. Considering the last expression, the correlator contains four terms:

$$\langle\varphi(t)|\sigma^x_{r_1}\sigma^x_{r_2}|\varphi(t)\rangle = \sum_i^4 P_i \tag{9.77}$$

- First term: P_1

$$P_1 \equiv e^{-iE_0t}e^{iE_0t}(\langle\Omega_L|\otimes\langle\Omega_R|)\sigma^x_{r_1}\sigma^x_{r_1}(|\Omega_L\rangle\otimes|\Omega_R\rangle) = \langle\Omega_L|\sigma^x_{r_1}|\Omega_L\rangle\langle\Omega_R|\sigma^x_{r_1}|\Omega_R\rangle = 0, \tag{9.78}$$

since $\langle\Omega_X|\sigma^x_r|\Omega_X\rangle = 0\ \ \forall\, r,\ X = L,R.$

- Second term: P_2

$$P_2 \equiv \sum_{k_1,k_2,k_3,k_4} F^*(k_1,k_2,N/2,N/2+1)\cdot F(k_3,k_4,N/2,N/2+1)\cdot \cdot D_2\cdot e^{-it[(E_{k_3}+E_{k_4})-(E_{k_1}+E_{k_2})]} = 0, \tag{9.79}$$

where

$$D_2 = (\langle k_1|\otimes\langle k_2|)\sigma^x_{r_1}\sigma^x_{r_1}(|k_3\rangle\otimes|k_4\rangle) = \langle k_1|\sigma^x_{r_1}|k_3\rangle\cdot\langle k_2|\sigma^x_{r_2}|k_4\rangle = 0, \tag{9.80}$$

since $\langle k|\sigma^x_r|k'\rangle = 0\ \ \forall\, r,k,k'.$

- Third and fourth terms: $P_3,\ P_4$

$$P_3 \equiv -e^{-it[-E_0+(E_k+E_{k'})]} \sum_{k,k'} C(k,k',,N/2,N/2+1)\cdot D_3, \tag{9.81}$$

where

$$\begin{aligned} D_3 &= (\langle\Omega_L| \otimes \langle\Omega_R|)\sigma^x_{r_1}\sigma^x_{r_1}(|k\rangle \otimes |k'\rangle) = \langle\Omega_L|\sigma^x_{r_1}|k\rangle\langle\Omega_R|\sigma^x_{r_2}|k'\rangle = \\ &= F(-k,-k',r_1,r_2)\cdot(E_0-(E_k+E_{k'})) = \\ &= F^*(k,k',r_1,r_2)\cdot(E_0-(E_k+E_{k'})). \end{aligned} \tag{9.82}$$

Then

$$P3 = \sum_{k,k'} e^{-it\Delta(k,k')} C(k,k',N/2,N/2+1)\cdot C^*(k,k',r_1,r_2)\cdot\Delta(k,k') \tag{9.83}$$

with the energy gap $\Delta(k,k') = ((E_k+E_{k'})-E_0)$.

The termP_4 is the complex conjugate of the third term, $P_4 = P_3^*$.

Then, the time evolution of the two point correlator can be written as:

$$\begin{aligned} &C(r_1,r_2,t) = P_3 + P_4 = \\ &\sum_{k,k'} 2\cdot\Delta(k,k')\cdot F(k,k',r_1,r_2)\cdot F(k,k',N/2,N/2+1)\cdot\cos(\Delta(k,k')t) \end{aligned} \tag{9.84}$$

where we take into account the fact that F are real functions.

The dependence of the correlator with respect to the number of k modes considered is displayed in Fig. 9.6.

Considering only the first excited k mode, i. e. k_1, the correlation can be written as:

$$C(r_1,r_2,t) \to \frac{g}{\Delta_0}\cos(2\Delta_0 t) \tag{9.85}$$

where $g = \langle\Omega_L|\sigma^x_{r_1}|k_1\rangle\langle\Omega_R|\sigma^x_{r_2}|k_1\rangle\langle k_1|\sigma^x_{\frac{N}{2}}|\Omega_L\rangle\langle k_1|\sigma^x_{\frac{N}{2}+1}|\Omega_R\rangle$ and Δ_0 is the gap between $|k_1\rangle$ and the ground state of half of the chain.

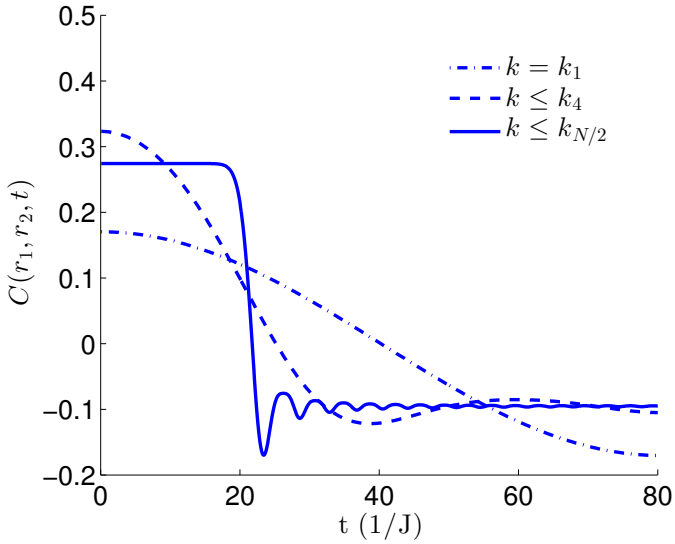

Figure 9.6: Time evolution of two point correlator under the quasi-particle picture for the splitting quench. The consideration of only the first mode,$k = k_1$, (dashed-dotted line) produces an anti-correlation for $t > 40$. The consideration of a higher number of modes leads to the exact anti-correlated result appearing in Fig. 7.14.

Considering that:

$$\Delta_0 \to \frac{\pi}{2L_L} = \frac{\pi}{L}, \tag{9.86}$$

in the limit $L \to \infty$ [251] (L_L is the length of the *left* half of the chain), the correlator behaves as *cosine* a function with period L. Thus, the system exhibits anti-correlations for a certain values of the time t (see dotted-dashed plot in Fig. 9.6. By considerading more k modes, it is recovered the exact anticorrelation behaviour displayed in Fig. 7.14.

Thus, the quasi-particle picture describes succesfully this change of sing of the correlator.

9.6 Free fermions: Jordan-Wigner transformation

The Hilbert space of 1D quantum spin-1/2 systems is isomorphic to the Hilbert space of 1D spinless fermions and 1D hard-core bosons [252, 253].

The transformation from the 1D spin system to a spinless fermion system is obtained trough the celebrated Jordan-Wigner transformation [254]. In this section we will examine such transformation and we will focus in the calculation of some physical magnitudes in the 1D spin system through the Jordan-Wigner transformation.

Let us consider a 1D spin-1/2 system whose Hamiltonian is given in term of the *Pauli matrices*:

$$\sigma^x = \begin{pmatrix} 0 & 1 \\ 1 & 0 \end{pmatrix}, \quad \sigma^y = \begin{pmatrix} 0 & i \\ -i & 0 \end{pmatrix}, \quad \sigma^z = \begin{pmatrix} 1 & 0 \\ 0 & -1 \end{pmatrix}, \tag{9.87}$$

This matrices can be expressed as linear combination of the raising and lowering operators $a^\dagger$, a, defined as:

$$a_j^\dagger = \sigma_j^+ = \frac{1}{2}(\sigma_j^x + i\sigma_j^y) = \begin{pmatrix} 0 & 1 \\ 0 & 0 \end{pmatrix}, \tag{9.88}$$

$$a_j = \sigma_j^- = \frac{1}{2}(\sigma_j^x - i\sigma_j^y) = \begin{pmatrix} 0 & 0 \\ 1 & 0 \end{pmatrix}, \tag{9.89}$$

where the index j labels the site of the 1D spin chain.

One is tempted to use $a_j^\dagger$, a_j as creation and annihilation operators respectively at site j. However, it works only for a system composed of one spin due to these operators are neither fermionic operators non bosonic operators:

$$\begin{aligned} &\{\sigma_j^+, \sigma_j^-\} = \mathbb{I} \\ &[\sigma_i^+, \sigma_j^-] = 0, \ \forall i \neq j. \end{aligned} \tag{9.90}$$

The *truly* fermionic operators $c_j^\dagger, c_j$ are introduced through the Jordan-Wigner transformation [254]:

$$\begin{aligned} c_j &= e^{i\pi \sum_{l<j} \sigma_l^+ \sigma_l^-} \sigma_j^- = \prod_{l<j} (-\sigma_j^z) \sigma_l^-, \\ c_j^\dagger &= \sigma_j^+ e^{-i\pi \sum_{l<j} \sigma_l^+ \sigma_l^-} = \sigma_j^+ \prod_{l<j} (-\sigma_j^z), \end{aligned} \tag{9.91}$$

where we have used the relation:

$$e^{i\pi a_l^\dagger a_l} = -\sigma_l^z. \tag{9.92}$$

Considering that $c_i^\dagger c_i = \sigma_i^+ \sigma_i^-$, the inverse transformations read as:

$$\begin{aligned} \sigma_j^+ &= e^{-i\pi \sum_{l<j} c_l^\dagger c_l} c_j = \prod_{l<j} (-\sigma_j^z) c_j, \\ \sigma_j^- &= c_j^\dagger e^{i\pi \sum_{l<j} c_l^\dagger c_l} = c_j^\dagger \prod_{l<j} (-\sigma_j^z). \end{aligned} \tag{9.93}$$

The c_i operators fulfill the anticommutation rules for fermions:

$$\begin{aligned} &\{c_i, c_j^\dagger\} = \delta_{i,j}, \\ &\{c_i, c_j\} = \{c_i^\dagger, c_j^\dagger\} = 0. \end{aligned} \tag{9.94}$$

Thus, a 1D spin-1/2 can be written in terms of fermionic modes. For instance, let us consider the case of a quantum Ising chain in tranverse field (see Eq. (7.9)). Applying the Jordan-Wigner transformation (9.91), the Hamiltonian (7.9) in terms of the fermionic operators reads as:

$$H/J = \sum_i \left(-c_i^\dagger c_{i+1} - c_i^\dagger c_{i+1}^\dagger + c_i c_{i+1} + c_i c_{i+1}^\dagger + 2\lambda c_i^\dagger c_i - \lambda \right) \tag{9.95}$$

where we have used the relation:

$$\sigma_i^x \sigma_{i+1}^x = (c_i^\dagger - c_i)(c_{i+1}^\dagger + c_{i+1}). \tag{9.96}$$

Therefore, the initial spin system can be mapped to a system of *free* spinless fermions. We remark that the total fermion number $N_f = \sum_i c_i^\dagger c_i$ is not a conserved quantity. Therefore, the *vacuum* state $|\Omega_c\rangle$ of the $c-$fermions:

$$c_i|\Omega_c\rangle = 0 \; \forall \; i, \tag{9.97}$$

is not an eigenstate of the Hamiltonian (9.95).

Let us now diagonalize this free fermion Hamiltonian. First, we consider the fermions in momentum space, i.e. we perform a Fourier transform of the c_i operators:

$$\begin{aligned} c_q &= \frac{1}{\sqrt{N}} \sum_j^N c_j e^{iqr_j}, \\ c_q^\dagger &= \frac{1}{\sqrt{N}} \sum_j^N c_j^\dagger e^{-iqr_j}, \end{aligned} \tag{9.98}$$

with the wave-vector $q = \pi m/(2N)$, where:

$$\begin{aligned} &m = -(N-1), -(N-1)+1, ..., 0, 1, ..., N-1 \;\text{ for } N \text{ even}, \\ &m = -N, -N+1, ..., 0, 1, ..., N \;\text{ for } N \text{ odd}. \end{aligned} \tag{9.99}$$

Then, the Hamiltonian (9.95) reads as:

$$H/J = -\sum_q \left(e^{-iq} c_q^\dagger c_{-q}^\dagger - e^{iq} c_q c_{-q} \right) + \sum_q 2 \left(\lambda - \cos q \right) c_q^\dagger c_q \Big) - N \tag{9.100}$$

The last relation can be written in terms of the positive q modes:

$$H/J = \sum_{q>0} 2i \sin q \left(c_q^\dagger c_{-q}^\dagger - c_{-q} c_q \right) + \sum_q 2 \left((\lambda - \cos q)(c_q^\dagger c_q - c_{-q} c_{-q}^\dagger) \right) =$$
$$2(c_q^\dagger \; c_{-q}) \begin{pmatrix} \lambda - \cos q & i \sin q \\ -i \sin q & -(\lambda - \cos q) \end{pmatrix} \begin{pmatrix} c_q \\ c_{-q}^\dagger \end{pmatrix}, \tag{9.101}$$

where we have dropped out the constant term N. The eigenvalues of the Hamiltonian are:

$$\tilde{\epsilon}_q = \pm\sqrt{(1+\lambda(\lambda-2\cos q))}. \tag{9.102}$$

By employing the Bogoliubov transformation, we can construct a suitable basis of fermionic operators η_q which diagonalize the Hamiltonian:

$$\begin{pmatrix} \eta_q \\ \eta^\dagger_{-q} \end{pmatrix} = U_{\eta,c} \begin{pmatrix} c_q \\ c^\dagger_{-q} \end{pmatrix} = \begin{pmatrix} u_q & iv_q \\ iv_q & u_q \end{pmatrix} \begin{pmatrix} c_q \\ c^\dagger_{-q} \end{pmatrix}, \tag{9.103}$$

where $U_{\eta,c}$ is the matrix for the change of basis and v_q and u_q are real coefficients. Since:

$$\{\eta_q, \eta^\dagger_{q'}\} = \delta_{qq'}, \quad \{\eta_q, \eta_{q'}\} = \{\eta^\dagger_q, \eta^\dagger_{q'}\} = 0, \tag{9.104}$$

the v_q and u_q satify $v_q^2 + u_q^2 = 1$.

Thereby, the Hamiltonian (9.95) in the diagonal form reads as:

$$H/J = \sum_{q>0} \tilde{\epsilon}_q(\eta^\dagger_q\eta_q - \eta_{-q}\eta^\dagger_{-q}) = \sum_{q>0} \epsilon_q(\eta^\dagger_q\eta_q - 1/2), \tag{9.105}$$

where $\epsilon_q = 2\tilde{\epsilon}_q$.

The ground state of the Hamiltonian is the Bogoliubov vacuum $|\Omega\rangle_\eta$:

$$\begin{aligned} &\eta_q|\Omega\rangle_\eta = 0 \ \ \forall q \\ &H|\Omega\rangle_\eta = E_0|\Omega\rangle_\eta, \quad E_0 = -\frac{1}{2}\sum_{q>0}\epsilon_q = -\sum_{q>0}\tilde{\epsilon}_q. \end{aligned} \tag{9.106}$$

9.6.1 Diagonalization of a general fermion quadratic Hamiltonian

Let us consider a general quadratic fermionic Hamiltonian:

$$H = (\vec{c}^\dagger \ \ \vec{c}) \cdot H_{c^\dagger c} \cdot \begin{pmatrix} \vec{c} \\ \vec{c}^\dagger \end{pmatrix} \tag{9.107}$$

where $\vec{c}$ is a N component vector defined as:

$$\vec{c} = [c_1 \ c_2 \ ... \ c_N]^T. \tag{9.108}$$

The matrix $H_{c^\dagger c}$ is hermitian and, due to the anti-commutation relations of the c fermionic modes, it can be written as:

$$H_{c^\dagger c} = \begin{pmatrix} \alpha & \beta \\ -\beta^* & -\alpha^* \end{pmatrix}, \tag{9.109}$$

where α and β are hermitian and antisymmetric matrices respectively:

$$\alpha^\dagger = \alpha,\ \beta = -\beta^T. \tag{9.110}$$

Let us consider a given eigenvector $u = (g\ \ h)^T$ with eigenvalue ω:

$$\begin{aligned} Hu = \omega u \to \begin{pmatrix} \alpha & \beta \\ -\beta^* & -\alpha^* \end{pmatrix} \begin{pmatrix} g \\ h \end{pmatrix} = \omega \begin{pmatrix} g \\ h \end{pmatrix} \to \begin{pmatrix} -\alpha^* & -\beta^* \\ \beta & \alpha \end{pmatrix} \begin{pmatrix} g^* \\ h^* \end{pmatrix} = \\ -\omega \begin{pmatrix} g^* \\ h^* \end{pmatrix} \to \begin{pmatrix} \alpha & \beta \\ -\beta^* & -\alpha^* \end{pmatrix} \begin{pmatrix} h^* \\ g^* \end{pmatrix} = -\omega \begin{pmatrix} h^* \\ g^* \end{pmatrix} \to H\tilde{u} = -\omega\tilde{u}. \end{aligned} \tag{9.111}$$

Then, the eigenvalues of the matrix $H_{c^\dagger c}$ appear in pairs $(\omega, -\omega)$. Thus, we can write:

$$H_{c^\dagger c} = U^\dagger_{c,\eta} \cdot H_{\eta^\dagger \eta} \cdot U_{\eta,c} \tag{9.112}$$

where $H_{\eta^\dagger\eta}$ is the diagonal matrix composed of the all eigenvalues:

$$H_{\eta^\dagger\eta} = \begin{pmatrix} \Sigma & 0_N \\ 0_N & -\Sigma \end{pmatrix}, \tag{9.113}$$

where O_N is the $N \times N$ zero matrix and

$$\Sigma = \begin{pmatrix} \omega_1 & 0 & \cdots & 0 \\ 0 & \omega_2 & \cdots & 0 \\ \vdots & \vdots & \cdots & 0 \\ 0 & 0 & \cdots & \omega_N \end{pmatrix}. \tag{9.114}$$

The change of basis from the $\vec{c}$ fermionic operators to the new ones $\vec{\eta}$, which diagonalize the Hamiltonian, is given by the $U_{\eta,c}$. As we indicate in (9.111), this matrix reads as:

$$U_{\eta,c} = \begin{pmatrix} g & h^* \\ h & g^* \end{pmatrix}. \tag{9.115}$$

Then:

$$\begin{aligned} \vec{\eta} = g\vec{c} + h^*\vec{c}^\dagger \to \eta_k = \sum_i (g_{ki}c_i + h^*_{ki}c^\dagger_i), \\ \vec{\eta}^\dagger = h\vec{c} + g^*\vec{c}^\dagger \to \eta^\dagger_k = \sum_i (h_{ki}c_i + g^*_{ki}c^\dagger_i). \end{aligned} \tag{9.116}$$

The unitarity of the $U_{\eta,c}$ matrix implies:

$$\begin{aligned} gg^\dagger + h^* h^T &= \mathbb{I}, \\ gh^\dagger + h^* g^T &= 0. \end{aligned} \tag{9.117}$$

These relations are equivalent to the fermionic commutation relations for the η operators:

$$\{\eta_k, \eta_{k'}^\dagger\} = \delta_{kk'}, \quad \{\eta_k^\dagger, \eta_{k'}^\dagger\} = \{\eta_k, \eta_{k'}\} = 0 \tag{9.118}$$

The Hamiltonian (9.107) reads as:

$$H = (\vec{c}^\dagger \;\; \vec{c}) \cdot H_{c^\dagger c} \cdot \begin{pmatrix} \vec{c} \\ \vec{c}^\dagger \end{pmatrix} = (\vec{\eta}^\dagger \;\; \vec{\eta}) \cdot H_{\eta^\dagger \eta} \cdot \begin{pmatrix} \vec{\eta} \\ \vec{\eta}^\dagger \end{pmatrix} = (\vec{\eta}^\dagger \;\; \vec{\eta}) \cdot \begin{pmatrix} \Sigma & 0 \\ 0 & -\Sigma \end{pmatrix} \cdot \begin{pmatrix} \vec{\eta} \\ \vec{\eta}^\dagger \end{pmatrix} =$$
$$\sum_{k=1}^{N} \omega_k (\eta_k^\dagger \eta_k - \eta_k \eta_k^\dagger) = \sum_k \epsilon_k (\eta_k^\dagger \eta_k - \frac{1}{2}), \tag{9.119}$$

where $\epsilon_k = 2\omega_k$. As we showed in (9.106), the ground state of the Hamiltonian is the vacuum of the η fermionic operators:

$$\begin{aligned} &\eta_k |\Omega\rangle = 0 \;\; \forall k, \\ &H|\Omega\rangle = E_0 |\Omega\rangle \to E_0 = -\frac{1}{2} \sum_k \epsilon_k = -\sum_k \omega_k \end{aligned} \tag{9.120}$$

In the Schrödinger picture, the time evolution of the η_k operators is given by:

$$-i \frac{d}{dt} \eta_k = [H, \eta_k] = -2\omega_k \eta_k \to \eta_k(t) = e^{-2i\omega_k t} \eta_k \tag{9.121}$$

9.6.2 Correlation matrix

Let us consider a set of operators ϕ_i, which are linear combinations of certain fermionic operators c_j:

$$\phi_i = \sum_j (a_{ij} c_j + b_{ij} c_j^\dagger). \tag{9.122}$$

Applying the Wick's theorem, the expectation value of a product of such operators ϕ_i operators can be obtained through the elementary contractions of pairs of them:

$$\langle \phi_i \phi_2 ... \phi_M \rangle = \mathrm{Pf} \begin{pmatrix} 0 & \langle \phi_1 \phi_2 \rangle & \langle \phi_1 \phi_3 \rangle & \cdots & \langle \phi_1 \phi_M \rangle \\ \langle \phi_1 \phi_2 \rangle & 0 & \langle \phi_2 \phi_3 \rangle & \cdots & \langle \phi_2 \phi_M \rangle \\ \vdots & \vdots & \vdots & \cdots & \vdots \\ \langle \phi_M \phi_1 \rangle & \langle \phi_M \phi_2 \rangle & \langle \phi_M \phi_3 \rangle & \cdots & 0 \end{pmatrix}, \quad (9.123)$$

where, $\langle \phi_i \phi_j \rangle = -\langle \phi_j \phi_i \rangle$.

Then, all the information of the correlation function $\langle \phi_i \phi_2 ... \phi_M \rangle$ is encoded in the set of all the two point correlation functions:

$$\langle C_i C_j \rangle, \;\; C_i \in \{c_1, c_2, ..., c_L, c_1^\dagger, c_2^\dagger, ..., c_L^\dagger\}. \quad (9.124)$$

The set of the two point correlation functions of the c fermionic operators forms the so-called *correlation matrix* $\Gamma_{c^\dagger c}$. This matrix contains all the information of the physical state:

$$\Gamma_{c^\dagger c} = \begin{pmatrix} \langle \vec{c}^\dagger \vec{c} \rangle & \langle \vec{c}^\dagger \vec{c}^\dagger \rangle \\ \langle \vec{c}\, \vec{c} \rangle & \langle \vec{c}\, \vec{c}^\dagger \rangle \end{pmatrix}, \quad (9.125)$$

where

$$\langle \vec{c}^\dagger \vec{c} \rangle = \begin{pmatrix} \langle c_1^\dagger c_1 \rangle & \langle c_1^\dagger c_2 \rangle & \cdots & \langle c_1^\dagger c_N \rangle \\ \langle c_2^\dagger c_1 \rangle & \langle c_2^\dagger c_2 \rangle & \cdots & \langle c_2^\dagger c_N \rangle \\ \vdots & \vdots & \cdots & \vdots \\ \langle c_N^\dagger c_1 \rangle & \langle c_N^\dagger c_2 \rangle & \cdots & \langle c_N^\dagger c_N \rangle \end{pmatrix}, \quad (9.126)$$

and the other sub-matrices appearing in the expression of $\Gamma_{c^\dagger c}$ can be constructed analogously.

The change of basis of the correlation matrix from the c fermionic basis to the c' basis is given by:

$$\Gamma_{c'^\dagger c'} = U_{c'c} \cdot \Gamma_{c^\dagger c} \cdot U_{c'c}^\dagger, \quad (9.127)$$

where $U_{c'c}$ is the unitary matrix for the change of basis.

The time evolution of the correlation matrix is given by:

$$\Gamma_{c^\dagger c}(t, t_0) = \mathcal{U}_{c^\dagger c}^\dagger(t, t_0) \cdot \Gamma_{c^\dagger c}(t_0) \cdot \mathcal{U}_{c^\dagger c}(t, t_0), \quad (9.128)$$

where the time evolution operator reads as:

$$\mathcal{U}_{c^\dagger c}(t,t_0) = e^{-i(t-t_0)2H_{c^\dagger c}} = U^\dagger_{\eta c} \cdot e^{-i(t-t_0)2H_{\eta^\dagger \eta}} \cdot U_{\eta c}, \tag{9.129}$$

where $H_{\eta^\dagger \eta}$ is the diagonal Hamiltonian, in the basis η (see Eq.(9.121)). The factor 2 in the exponential of the last equation comes from the relation given at (9.113).

The correlation matrix for the ground state $|\Omega\rangle$ of a given Hamiltonian H is easily written in the basis η, which diagonalizes such Hamiltonian:

$$\Gamma^\Omega_{\eta^\dagger \eta} = \begin{pmatrix} 0_N & 0_N \\ 0_N & \mathbb{I}_N \end{pmatrix}, \tag{9.130}$$

where $\mathbb{I}_N$ is the $N \times N$ identity matrix.

9.6.3 Expected values of some spin operators

In this section we are going to compute some expected values of spin operators with the help of the fermionic operators resulting from the Jordan-Wigner transformations.

Let us start considering the magnetization in the z-direction. It can be written in terms of the correlation matrix $\Gamma_{c^\dagger c}$ as:

$$m^z_i = \langle \sigma^z_i \rangle = \langle 2c^\dagger_i c_i - 1 \rangle = 2\langle c^\dagger_i c_i \rangle - 1 = 2 \cdot \Gamma_{c^\dagger c}(i,i) - 1, \tag{9.131}$$

where we have considered:

$$\sigma^z = 2\sigma^+\sigma^- - 1 = 2c^\dagger c - 1. \tag{9.132}$$

Specifically for the ground state $|\Omega\rangle$, the correlation matrix $\Gamma^\Omega_{c^\dagger c}$ can be obtained from the expression appearing at (9.130):

$$\Gamma^\Omega_{c^\dagger c} = U^\dagger_{\eta c} \begin{pmatrix} 0_N & 0_N \\ 0_N & \mathbb{I}_N \end{pmatrix} U_{\eta c}, \tag{9.133}$$

where $U_{\eta c}$ is the matrix for the change of basis between the c and the η fermions.

Let us now to compute the two point correlation C^{zz}_{ij} function for the of the σ^z operator:

$$C^{zz}_{ij} \equiv \langle \sigma^z_i \sigma^z_j \rangle = 4\langle c^\dagger_i c_i c^\dagger_j c_j \rangle - 2(\langle c^\dagger_i c_i \rangle + \langle c^\dagger_j c_j \rangle) + 1. \tag{9.134}$$

The first term of the last relation can be expressed using (9.123) as:

$$\langle c_i^\dagger c_i c_j^\dagger c_j\rangle = \mathrm{Pf}\begin{pmatrix} 0 & \langle c_i^\dagger c_i\rangle & \langle c_i^\dagger c_j^\dagger\rangle & \langle c_i^\dagger c_j\rangle \\ \langle c_i c_i^\dagger\rangle & 0 & \langle c_i c_j^\dagger\rangle & \langle c_i c_j\rangle \\ \langle c_j^\dagger c_i^\dagger\rangle & \langle c_j^\dagger c_i\rangle & 0 & \langle c_j^\dagger c_j\rangle \\ \langle c_j c_i^\dagger\rangle & \langle c_j c_i\rangle & \langle c_j c_j^\dagger\rangle & 0 \end{pmatrix} = \\ \langle c_i^\dagger c_j\rangle\langle c_i c_j^\dagger\rangle - \langle c_i^\dagger c_j^\dagger\rangle\langle c_i c_j\rangle + \langle c_i^\dagger c_i\rangle\langle c_j^\dagger c_j\rangle. \quad (9.135)$$

Let us know to consider the two point correlation function C_{ij}^{xx} for the σ^x operator. In term of the c fermions, this spin operator reads as:

$$\sigma_i^x = \prod_{l<i}(-\sigma_l^z)(c_i^\dagger + c_i). \quad (9.136)$$

Therefore, C_{ij}^{xx} can be expressed as:

$$C_{ij}^{xx} \equiv \langle \sigma_i^x \sigma_j^x\rangle = \langle (c_i^\dagger + c_i)\prod_{l=i}^{l-1}(-\sigma_l^z)(c_j^\dagger + c_j)\rangle = \\ \langle (c_i^\dagger + c_i)\prod_{l=i}^{l-1}\Big(-(c_l^\dagger - c_l)(c_l^\dagger + c_l)\Big)(c_j^\dagger + c_j)\rangle, \quad (9.137)$$

where we have considered:

$$\sigma_l^z = 2c_l^\dagger c_l - 1 = (c_l^\dagger - c_l)(c_l^\dagger + c_l) = -(c_l^\dagger + c_l)(c_l^\dagger - c_l) \quad (9.138)$$

With the definitions:

$$A_l = c_l^\dagger + c_l, \\ B_l = c_l^\dagger - c_l, \quad (9.139)$$

and considering $A^2 = 1$, the expression (9.137) can be written as:

$$C_{ij}^{xx} = \langle B_l A_{l+1} B_{l+1} \cdots A_{j-1} B_{j-1} A_j\rangle. \quad (9.140)$$

Due to:

$$\langle A_i A_j\rangle = -\langle B_i B_j\rangle = \delta_{ij}, \quad (9.141)$$

the only non-zero contractions for the expression of C_{ij}^{xx} are given by $\langle A_i B_j \rangle$ and $\langle B_j A_l \rangle$ (the contractions $\langle A_i A_i \rangle$ and $\langle B_i B_i \rangle$ do not appear). Then, the two point correlator reads as:

$$C_{ij}^{xx} = \det \begin{pmatrix} G_{i,i+1} & G_{i,i+1} & \cdots & G_{i,j} \\ G_{i+1,i+1} & G_{i+1,i+1} & \cdots & G_{i+1,j} \\ \vdots & \vdots & \vdots & \vdots \\ G_{j-1,i+1} & G_{j-1,i+2} & \cdots & G_{j-1,j} \end{pmatrix}, \tag{9.142}$$

where

$$G_{m,n} \equiv \langle B_m A_n \rangle = -\langle A_n B_m \rangle. \tag{9.143}$$

For transnational invariant systems:

$$G_{i,i+s} = G_s, \quad G_s = G_{-s}, \tag{9.144}$$

and the correlation can be expressed as:

$$C_{ij}^{xx} = \det \begin{pmatrix} G_1 & G_2 & \cdots & G_r \\ G_0 & G_1 & \cdots & G_{r-1} \\ \vdots & \vdots & \vdots & \vdots \\ G_{r-2} & G_{r-3} & \cdots & G_1 \end{pmatrix}, \tag{9.145}$$

9.6.4 Entanglement entropy

As we discussed in Chapter 7, the density matrix ρ_A of a sub-block A with M sites of a system is obtained tracing B, which is the part of the system that does not belong to A.

This density matrix is the exponential of a certain Hamiltonian $\mathcal{H}$, the so-called *entanglement Hamiltonian*:

$$\rho_A = \mathrm{tr}_B \rho = \mathcal{C} e^{\mathcal{H}}, \tag{9.146}$$

where $\mathcal{C}$ is a constant which ensures the trace of ρ_A to be one.

The entanglement Hamiltonian can be diagonalized in a certain basis with M fermionic modes $\tilde{\eta}$:

$$\mathcal{H} = \sum_{k=1}^{M} \left(\tilde{\epsilon} \tilde{\eta}_k^\dagger \tilde{\eta}_k - \frac{1}{2} \right) \tag{9.147}$$

Since the M fermionic modes are independent, the density matrix ρ_A can be expressed as the direct product of M density matrices $\tilde{\rho}_k$:

$$\rho_A = \mathcal{C}e^{\mathcal{H}} = \mathcal{C}\exp\left(\sum_{k=1}^{M}\tilde{\epsilon}\left(\tilde{\eta}_k^\dagger\tilde{\eta}_k - \frac{1}{2}\right)\right) = \\ \mathcal{C}\prod_{k=1}^{M}\exp\left(\sum_{k=1}^{M}\tilde{\epsilon_k}\left(\tilde{\eta}_k^\dagger\tilde{\eta}_k - \frac{1}{2}\right)\right) = \prod_{k=1}^{M}\tilde{\rho}_k, \quad (9.148)$$

where $\tilde{\rho}_k$ reads as:

$$\tilde{\rho}_k = \mathcal{C}_k\exp\left(\tilde{\epsilon}_k\left(\tilde{\eta}_k^\dagger\tilde{\eta}_k - \frac{1}{2}\right)\right) = \mathcal{C}_k\exp\left(\tilde{\omega}_k\left(\tilde{\eta}_k^\dagger\tilde{\eta}_k - \tilde{\eta}_k\tilde{\eta}_k^\dagger\right)\right) = \\ \frac{1}{e^{-\tilde{\omega}_k} + e^{\tilde{\omega}_k}}\begin{pmatrix} e^{\tilde{\omega}_k} & 0 \\ 0 & e^{-\tilde{\omega}_k}\end{pmatrix} = \frac{1}{1+e^{\tilde{\epsilon}_k}}\begin{pmatrix} e^{\tilde{\epsilon}_k} & 0 \\ 0 & 1\end{pmatrix}, \quad (9.149)$$

with $\tilde{\epsilon}_k = 2\tilde{\omega}_k$.

Thus, the entanglement entropy (7.12) is the *sum* of the entanglement entropies for each independent $\tilde{\eta}_k$ mode:

$$S_A = -\mathrm{tr}\ \rho_A\log\rho_A = \sum_{k=1}^{M}S_k = -\sum_{k=1}^{M}\mathrm{tr}\ \ \tilde{\rho}_k\cdot\log\left(\tilde{\rho}_k\right) = \\ -\sum_{k=1}^{M}\big(p_k\log(p_k) + (1-p_k)\log(1-p_k)\big), \quad (9.150)$$

where:

$$p_k = \frac{1}{1+e^{\tilde{\epsilon}_k}}. \quad (9.151)$$

The correlation matrix $\Gamma^A_{c^\dagger c}$ for the considered block A is fully determined by the density matrix ρ_A:

$$\langle C_iC_j\rangle = \mathrm{tr}(\rho_AC_iC_j), \quad \forall\ C_i, C_j \in \{c_1, c_2, ..., c_M, c_1^\dagger, c_2^\dagger, ..., c_M^\dagger\}, \quad (9.152)$$

where the indices $1, 2, ..., M$ of the c operators label the different sites of the block A. Therefore, there is a fermionic basis $\{\tilde{\eta}_k\}$ which diagonalizes simultaneously the correlation matrix $\Gamma^A_{c^\dagger c}$ and the reduced density matrix ρ_A, which corresponds to the basis that diagonalizes the entanglement Hamiltonian. Moreover, the eigenvalues γ_i of $\Gamma^A_{c^\dagger c}$ coincides with the coeficients p_k appearing at (9.151).

Thus, the entanglement entropy can be computed with the eigenvalues of the correlation matrix through the relation:

$$S_A = -\sum_{k=1}^{M} \left(\gamma_k \log(\gamma_k) + (1-\gamma_k)\log(1-\gamma_k)\right), \tag{9.153}$$

where the correlation matrix in the diagonal form reads as:

$$\Gamma^A_{\tilde{\eta}^\dagger \tilde{\eta}} = \text{diag}[1-\gamma_1, 1-\gamma_2, 1-\gamma_M, \gamma_1, \gamma_2, ..., \gamma_M], \tag{9.154}$$

The relation between the eigenvalues γ_k and the energies $\tilde{\epsilon}_k$ (see Eq.(9.149)) of the entanglement Hamiltonian is given by the expression (9.151):

$$\gamma_k = p_k = \frac{1}{1+e^{\tilde{\epsilon}_k}}, \tag{9.155}$$

9.6.5 Schmidt vectors

As we indicated in Chapter 7, the density matrix of a block A for a certain system can be written as:

$$\rho_A = \sum_i c_i |\phi_i\rangle\langle\phi_i|, \tag{9.156}$$

where c_i and $|\phi_i\rangle$ are the Schmidt coefficients and vectors respectively. If there are at least two non-vanishing Schmidt coefficients, the system is *entangled* with respect to this bipartition and ρ_A describes a *mixed state*.

Let us consider a certain block A of a fermionic system. The eigenvalues of the correlation for such a block (see Eq. (9.154)) define a certain distribution of probability for occupied modes, $p^{\text{F.D.}}_{\mathcal{H}}$. This distribution corresponds to a Fermi-Dirac distribution for the entanglement Hamiltonian at $\beta = 1$:

$$\begin{aligned} p^{\text{F.D.}}_{\mathcal{H}} = \{&p^{\text{F.D.}}_1, p^{\text{F.D.}}_2, ..., p^{\text{F.D.}}_M, ..., p^{\text{F.D.}}_{2M}\} = \\ &\{1-p_1, 1-p_2, ..., 1-p_{M-1}, 1-p_M, p_1, p_2, p_3, ..., p_M\}, \end{aligned} \tag{9.157}$$

where p_i are given in (9.155). The distribution of probability for the empty modes is given by $1 - p^{\text{F.D.}}_{\mathcal{H}}$.

The mixed state ρ_A is characterized completely by $p^{\text{F.D.}}_{\mathcal{H}}$. Each Schmidt vector can be obtained by populating M of these $2M$ modes, considering the constrain that a populated (non-populated) mode $l < M$ implies a non-populated

(populated) mode $M-l$.

The first Schmidt vector corresponds to the most probable state with M modes. It is obtained by populating the last M modes, i.e. from $M+1$ to $2M$. Thus, its correlation matrix in the $\tilde{\eta}$ basis is given by:

$$\Gamma^{A1}_{\tilde{\eta}^\dagger\tilde{\eta}} = \mathrm{diag}[0,0,....,0,1,1,...,1,1]. \tag{9.158}$$

The probability of such state is the first Schmidt coefficient, c_1:

$$c_1 \;=\; \prod_{i=1}^{M}(1-p_i^{\mathrm{F.D.}}) \prod_{j=M+1}^{2M}(p_j^{\mathrm{F.D.}}) \;=\; \prod_{i=1}^{M} p_i \prod_{j=1}^{M} pj \;=\; \left(\prod_{i=1}^{M} p_i\right)^2. \tag{9.159}$$

The second Schmidt vector is the second most probable state according to $p_{\mathcal{H}}^{\mathrm{F.D.}}$. It is obtained by populating the mode M and the modes from $M+1$ to $M-1$:

$$\Gamma^{A2}_{\tilde{\eta}^\dagger\tilde{\eta}} = \mathrm{diag}[0,0,...,1,1,...,1,0]. \tag{9.160}$$

Thus, the second Schmidt coefficient reads as:

$$c_2 = \left(\prod_{i=1}^{M-1}(1-p_i^{\mathrm{F.D.}})\right) p_M^{\mathrm{F.D.}} \left(\prod_{i=M+1}^{2M} p_i^{\mathrm{F.D.}}\right)(1-p_{2M}^{\mathrm{F.D.}}) =$$
$$\left(\prod_{i=1}^{M-1} p_i\right)(1-p_M)\left(\prod_{j=1}^{M-1} p_j\right)(1-p_M) = \left((1-p_M)\prod_{i=1}^{M-1} p_i\right)^2. \tag{9.161}$$

The different Schmidt vectors and coefficients can be obtained applying this procedure.

For instance, let us consider a block with 3 sites. The correlated matrices for the $2^3=8$ Schmidt vectors are given in the $\tilde{\eta}$ basis by:

$$\Gamma^{A1}_{\tilde{\eta}^\dagger\tilde{\eta}} = \mathrm{diag}[0\;\;0\;\;0\;\;1\;\;1\;\;1],$$
$$\Gamma^{A2}_{\tilde{\eta}^\dagger\tilde{\eta}} = \mathrm{diag}[0\;\;0\;\;1\;\;1\;\;1\;\;0],$$
$$\Gamma^{A3}_{\tilde{\eta}^\dagger\tilde{\eta}} = \mathrm{diag}[0\;\;1\;\;0\;\;1\;\;0\;\;1],$$
$$\Gamma^{A4}_{\tilde{\eta}^\dagger\tilde{\eta}} = \mathrm{diag}[1\;\;0\;\;0\;\;0\;\;1\;\;1],$$
$$\Gamma^{A5}_{\tilde{\eta}^\dagger\tilde{\eta}} = \mathrm{diag}[1\;\;1\;\;0\;\;0\;\;0\;\;1],$$

$$\Gamma^{A6}_{\tilde{\eta}^\dagger\tilde{\eta}} = \text{diag}[1\ \ 0\ \ 1\ \ 0\ \ 1\ \ 0],$$
$$\Gamma^{A7}_{\tilde{\eta}^\dagger\tilde{\eta}} = \text{diag}[0\ \ 1\ \ 1\ \ 1\ \ 0\ \ 0],$$
$$\Gamma^{A8}_{\tilde{\eta}^\dagger\tilde{\eta}} = \text{diag}[1\ \ 1\ \ 1\ \ 0\ \ 0\ \ 0]. \tag{9.162}$$

The first state corresponds to the ground state of the entanglement Hamiltonian. The next three state are the states with one particle-hole excitation. The $5^{th}, 6^{th}, 7^{th}$ states contain two particle-hole excitations, whereas the last state corresponds to a state with 3 particle-hole excitations.

9.7 Matrix product states and time evolving block decimation

The dimension of the Hilbert space of a many body quantum system composed of N constituents grows exponentially:

$$\dim(\mathcal{H}) = d^N, \tag{9.163}$$

where d is the internal dimension degree of freedom of each constituent.

Thus, the exact classical computation of these systems are restricted to many-body systems with a few number of constituents. Some numerical methods have been developed for overcoming this feature but they present limitations. For example, the *mean field* techniques do not consider the quantum correlation between the constituents of the many body system and the *quantum Monte Carlo* algorithms present problems in the treatment of fermionic system and frustrated spin models due to the *sign problem*.

Here we summarize a successfully numerical method for classically computing quantum many-body systems based on *tensor networks* (TN) techniques. A TN is a tensor resulting from the product of certain tensors. For instance:

$$T_{ijk} = \sum_{\alpha\beta\nu\sigma\delta} A_{i\alpha\sigma\delta} B_{k\alpha\beta} C_{\alpha\beta\sigma} D_{j\nu\delta}. \tag{9.164}$$

In this example, the 3-rank tensor T_{ijk} is a TN which results from the multiplication of four different tensors, A, B, C, D. TN can be represented pictorially (see sketch in Fig. 9.7 a)).

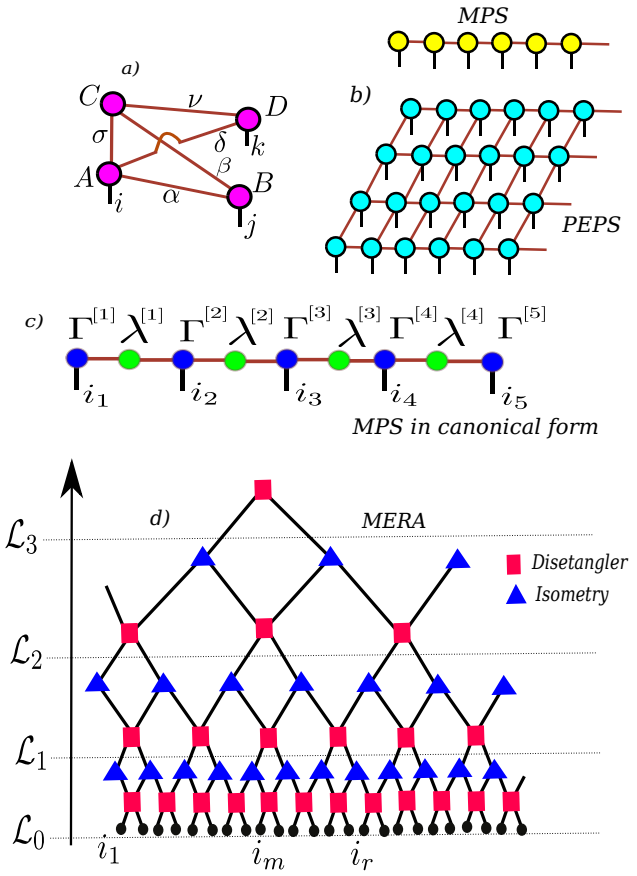

Figure 9.7: a) Pictorical representation of the TN corresponding to the expression (9.164). The tensors are represented by circles and the contraction of indices (multiplcation) by links connecting tensors. The resulting TN contains 3 open indices: i, j, k. *b*) A MPS (up) and its natural generalization to a 2D system, the PEPS (down). *c*) MPS in the canonical form. It contains two types of tensors, the Γ tensors, with physical indices and the λ matrices, without physical indices. *d*) Multiscale Entanglement Renormalization Anzats (MERA) tensor network. It is composed of two different types of tensors: disetanglers and isometries. The indices with black dots are physical indices. The additional dimension $\mathcal{L}$ introduced by the TN corresponds to a real space renormalization flow: each layer $\mathcal{L}_i$, is a renormalization step of the 1D system. This TN captures the physics of the ground state of some 1D critical systems.

9.7.1 Matrix product states

The matrix product states (MPS) [255, 256] is a TN consisting of a 1D array of tensors (see Figure (9.7) (b) and (d)). This TN emerges naturally in successfully numerical studies of different 1D many-body quantum systems, as Density Matrix Renormalization Group [257, 258] and Time Evolving Block Decimation (TEBD) [218, 219, 259]. The latter method will be reviewed in this section.

It turns out that the MPS can efficiently describe slightly entangled quantum many body systems. Low energy states of one dimensional gapped systems described through local Hamiltonians fall into this category, in particular the ground state. One can show that these states fulfil the so called *area law* [260, 261]: the entropy of a subsystem A of a certain systems grows with the boundary between the block A and the rest of the system (see Fig. 9.8 a))

$$S_A \sim \partial A \sim L^{D-1}, \tag{9.165}$$

where D and L are the dimension of the system and the size of the block respectively.

The states which satisfy the are law lie in a small region, $\mathcal{H}_{\text{low}}$, of the full Hilbert space. This region can be successfully explored with the use of MPS. Moreover, it can be proven that the time evolution for a polynomial time in N only explores a exponentially small region of states. Then, the time evolved state of an initial state in $\mathcal{H}_{\text{low}}$, also lies in this region during all the practical evolution [262].

Let us consider a bipartition between blocks A and E of a given quantum state $|\psi\rangle$:

$$|\psi\rangle = \sum_{\nu}^{\chi} |\varphi_\nu^{[A]}\rangle |\varphi_\nu^{[E]}\rangle, \tag{9.166}$$

where $|\varphi_\nu^{[A]}\rangle\}$ and $\{|\varphi_\nu^{[E]}\rangle\}$ are the orthogonal basis of the vectors for the block A and the environment E respectively. They come from the *Schmidt decomposition* (SD) of the bipartition.

If the state $|\psi\rangle$ admits a MPS description (see Fig. 9.7 c)), then:

$$\chi \leq B^2, \tag{9.167}$$

where B is the bond dimension, i.e. the internal dimension of the MPS.

The density matrix ρ_A of the block A is obtained tracing out the environment E:

$$\rho_A = \mathrm{tr}_E(\rho) = \mathrm{tr}_E\left(|\psi\rangle\langle\psi|\right) = \sum_{\alpha} \langle\varphi_\alpha^{[E]}|\left(|\psi\rangle\langle\psi|\right)|\varphi_\alpha^{[E]}\rangle = \sum_{\nu}^{B^2} \tilde{\lambda}_\nu^2 |\varphi_\nu^{[A]}\rangle\langle\varphi_\nu^{[A]}|, \quad (9.168)$$

where $\tilde{\lambda}_\nu^2 = |\langle\varphi_\nu^{[E]}|\varphi_\nu^{[E]}\rangle|^2$. Thus, the rank of ρ_A is bounded by the bond dimension B:

$$\mathrm{rank}(\rho_A) \leq B^2, \quad (9.169)$$

Then, for this 1D system, the entanglement entropy of the block (see Eq.(7.12)) reads as:

$$S = -\mathrm{tr}\rho_A \log \rho_A = -\sum_\alpha \lambda_\alpha \log \lambda_\alpha \leq -B^2(\frac{1}{B^2}) \log \frac{1}{B^2} = 2 \log B, \quad (9.170)$$

which is independent of L, the size of A. It fulfills the *area law*.

Let us now consider a 2D spin system represented by a Projected Entangled Pair Spin (PEPS) [263], which is the natural extension of the MPS for 2D systems (see Fig. 9.7 b)). Proceeding as the last example, the quantum state $|\psi\rangle$ can be written as:

$$|\psi\rangle = \sum_{\nu}^{B^{4L}} |\varphi_\nu^{[A]}\rangle |\varphi_\nu^{[E]}\rangle, \quad (9.171)$$

where A is a rectangular block $L \times L$ of the system and E is the rest of the system and $\{|\varphi_\nu^{[A]}\rangle\}$ ($\{|\varphi_\nu^{[E]}\rangle\}$) are orthogonal basis for the block A and for the environment E respectively (see Fig. 9.8 b)).

The density matrix of the block A reads as:

$$\rho_A = \sum_{\nu}^{B^{4L}} \tilde{\lambda}_\nu^2 |\varphi_\nu^{[A]}\rangle\langle\varphi_\nu^{[A]}|, \quad (9.172)$$

with $\tilde{\lambda}_\nu^2 = |\langle\varphi_\nu^{[E]}|\varphi_\nu^{[E]}\rangle|^2$. Therefore, the rank of ρ_A is bounded by:

$$\mathrm{rank}(\rho_A) \leq B^{4L}, \quad (9.173)$$

In this 2D system, the entanglement entropy for the block is bounded by the perimeter $4L$ of the block:

$$S = -\mathrm{tr}\rho_A \log \rho_A = -\sum_\alpha \lambda_\alpha \log \lambda_\alpha \leq -B^{4L}(\frac{1}{B^{4L}}) \log \frac{1}{B^{4L}} = 4L \log B. \tag{9.174}$$

Thus, the entanglement entropy of the block is proportional to the length of the block in this 2D system.

By inspecting the last relation and (9.170), we conclude that:

- Both the MPS and PEPS tensor networks represent quantum states which fulfil the area law expressed in (9.165).
- Each bond link of the border between the block A and the environment contributes with *log(B)* to the entropy of the block.

Let us consider a many-body quantum state $|\psi\rangle$ composed of N constituents (for instance, a spin chain of length N:

$$|\psi\rangle = \sum_{i_1, i_2, \ldots, 1_N} C_{i_1 i_2 \ \ldots \ 1_N} |i_1 i_2 \ \ldots \ 1_N\rangle, \tag{9.175}$$

where the local basis $\{|i_j\rangle\}$ labels the internal state of each constituent, with dimension d. The coefficients $C_{i_1 i_2 \ \ldots \ 1_N}$ form a N-rank tensor, composed of d^N elements and N opened indices. Our goal is to express this tensor as a MPS.

A general SD of a bipartition in the system leads to express the state as:

$$|\psi\rangle = \sum_{\alpha=1}^{B} \lambda_\alpha |\varphi_\alpha^{[L]}\rangle |\varphi_\alpha^{[R]}\rangle, \tag{9.176}$$

where the diagonal matrix λ contains all the Schmidt coefficients, whereas $|\varphi_\alpha^{[L]}\rangle (|\varphi_\alpha^{[R}\rangle)$ correspond to the left (right) Schmidt vectors, which define two different orthonormal basis.

Let us consider the bipartition for the first spin and the $N-1$ remaining spins. The SD decomposition reads as:

$$|\psi\rangle = \sum_{\alpha=1}^{B_1} \lambda_{\alpha_1}^{[1]} |\varphi_{\alpha_1}^{[1]}\rangle |\varphi_{\alpha_1}^{[2 \ldots N]}\rangle = \sum_{i_1} \sum_{\alpha_1}^{B_1} \Gamma_{i_1 \alpha_1}^{[1]} \lambda_{\alpha_1}^{[1]\alpha_1} |i_1\rangle |\varphi_{\alpha_1}^{[2 \ldots N]}\rangle, \tag{9.177}$$

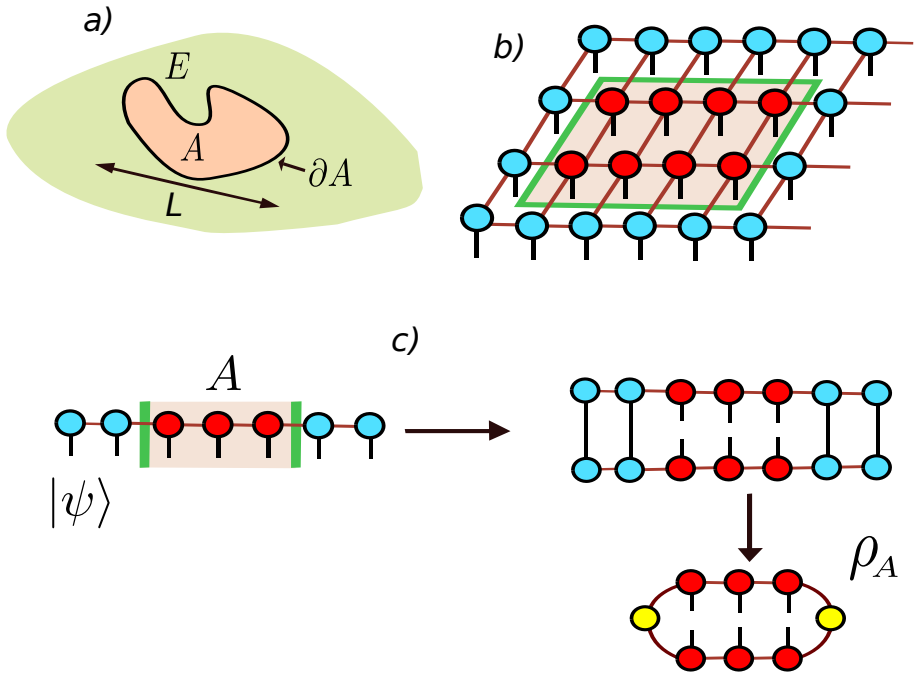

Figure 9.8: *a*) A many body quantum system composed of a block A and the rest of the system or environment E. If the systems fulfils the are law, the entanglement entropy is proportional to the area of the boundary ∂A. *b*) A 2D system represented by a PEPS. Since the boundary is proportional to the number of bonds, this TN satisfies the are law. *ci*) A block A in a 1D system represented by a MPS. This TN also fulfils the area law for the entropy *cii*) ρ_A is obtained by contracting the indices of the environment. *ciii*). The trace of the environment introduces new tensors (yellow tensors) even though the bond between them and the tensors of the block, which determines the rank of ρ_A, remains the same.

where the last expression is obtained by writing the Schmidt vector in the local basis of the site 1: $\Gamma^{[1]\alpha_1}_{i_1}$ is the coefficient of $|\varphi^{[1]}_{\alpha_1}\rangle$ in the $\{|i_1\rangle\}$ basis.

Now, we can continue performing a SD for each vector $|\varphi^{[2...N]}_{\alpha_1}\rangle$ for the bipartition of site 2 and sites 3,4...,N:

$$|\varphi^{[2...N]}_{\alpha_1}\rangle = \sum_{i_2}\sum_{\alpha_2}^{B_2} \Gamma^{[2]\alpha_1}_{i_2\alpha_2}\lambda^{[2]\alpha_2}_{\alpha_2}|i_2\rangle|\varphi^{[3...N]}_{\alpha_2}\rangle, \tag{9.178}$$

where, we have used the local basis $\{|i_2\rangle\}$.

Introducing this expression in the relation (9.177) we obtain:

$$|\psi\rangle = \sum_{i_1}\sum_{\alpha_1,\alpha_2}^{B_1B_2} \Gamma^{[1]}_{i_1\alpha_1}\lambda^{[1]\alpha_1}_{\alpha_1}\Gamma^{[2]\alpha_1}_{i_2\alpha_2}\lambda^{[2]\alpha_2}_{\alpha_2}|i_1\rangle|i_2\rangle|\varphi^{[3...N]}_{\alpha_2}\rangle. \tag{9.179}$$

This procedure can be done for all the sites of the system, leading to a final expression of the quantum state which reads as:

$$|\psi\rangle = \sum_{\substack{i_1 i_2\cdots 1_N \\ \alpha_1,\alpha_2\cdots\alpha_{N-1}}}^{B_1B_2\cdots B_{N-1}} \Gamma^{[1]}_{i_1\alpha_1}\lambda^{[1]\alpha_1}_{\alpha_1}\Gamma^{[2]\alpha_1}_{i_2\alpha_2}\lambda^{[2]\alpha_2}_{\alpha_2}\cdots \Gamma^{[N-2]\alpha_{N-2}}_{i_{N-2}\alpha_{N-1}}\lambda^{[N-1]\alpha_{N-1}}_{\alpha_{N-1}}\Gamma^{[N]\alpha_{N-1}}_{i_N}|i_1\rangle|i_2\rangle|i_3\rangle\cdots|i_{N-1}\rangle|i_N\rangle. \tag{9.180}$$

Thus, the coefficient $C_{i_1 i_2 ... 1_N}$ (see Eq.(9.175)) can be written as a MPS form:

$$C_{i_1 i_2 ... 1_N} = \Gamma^{[1]}_{i_1\alpha_1}\lambda^{[1]\alpha_1}_{\alpha_1}\Gamma^{[2]\alpha_1}_{i_2\alpha_2}\lambda^{[2]\alpha_2}_{\alpha_2}\cdots\Gamma^{[N-2]\alpha_{N-2}}_{i_{N-2}\alpha_{N-1}}\lambda^{[N-1]\alpha_{N-1}}_{\alpha_{N-1}}\Gamma^{[N]\alpha_{N-1}}_{i_N}, \tag{9.181}$$

where it is assumed the summation over the bond indices $\alpha_1, \alpha_2, ..., \alpha_N$.

This is the *canonical form* of the MPS [219, 264] (see Fig. 9.7 *c*). It contains two different types of tensors:

- 3-rank tensors $\Gamma^{[r]\alpha_{r-1}}_{i_r\ \alpha_r}$. They are the coefficients of the Schmidt vectors in the local basis $\{|i\rangle\}$. The label $[r]$ indicates that this tensor can be site-dependent. For a spin system with N sites and open boundary conditions, $\Gamma^{[1]}$ and $\Gamma^{[N]}$ are 2-rank tensors or matrices.
- 2-rank tensors or matrices $\lambda^{[r]\alpha_r}_{\alpha_r}$. This matrices contain the Schmidt coefficients coming from the SD of the bipartition $[1, 2, ..., r]\&[r+1, ..., N]$. They can be r-dependent.

The calculation of an observable O for quantum state expressed as a TN requires the contraction of this tensor (see Fig. 9.9 for the MPS case). This contraction can be done with a finite number of operations $\mathcal{O}(NdB^3)$, which is polynomial both in N and B for the MPS.

Unlike for MPS, the calculation of an observable in a general TN can be a hard problem. For instance, if we consider a PEPS, the natural generalization of a MPS for 2D, it turns out that the contraction of the TN requires a number of operations which grows exponentially with N.

We mention that when the MPS is written in the canonical form, the entanglement entropy of the bipartition $[1, 2, ..., r]\&[r+1, ..., N]$ can be read directly from the $\lambda^{[r]}$ matrices due to they contain all the information of the bipartition of the system at that site:

$$S(r) = -\text{tr}\ \left(\lambda^{[r]}\right)^2 \log\left(\lambda^{[r]}\right)^2. \tag{9.182}$$

9.7.2 Computing of the ground state

In this section we summarize the TEBD method for computing the ground state $|\Omega\rangle$ corresponding to a given Hamiltonian H, in a MPS form.

The procedure consist in to evolve in imaginary time an initial state $|\psi\rangle$. The time evolved state converges to the ground state for a sufficient long time if the initial state the state has a non zero overlap with the ground state:

$$\lim_{\tau\to\infty} \frac{e^{-\tau H}|\psi\rangle}{\||\psi\rangle\|} \to |\Omega\rangle \tag{9.183}$$

This imaginary time evolution can be done in a given number of steps by splitting the total time:

$$e^{-\tau H} = \left(e^{-\delta\tau H}\right)^{\tau/\delta\tau} \equiv U_H(\delta\tau)^{\tau/\delta\tau} \tag{9.184}$$

We write the Hamiltonian as a sum of different elements, which do not necessarily commute. Specifically, we express H as the sum of operators acting on the *odd* links of the spin chain, H_o, and operators acting on the *even* links, H_e:

$$H = \sum_l (H_e^{[l]} + H_o^{[l]}). \tag{9.185}$$

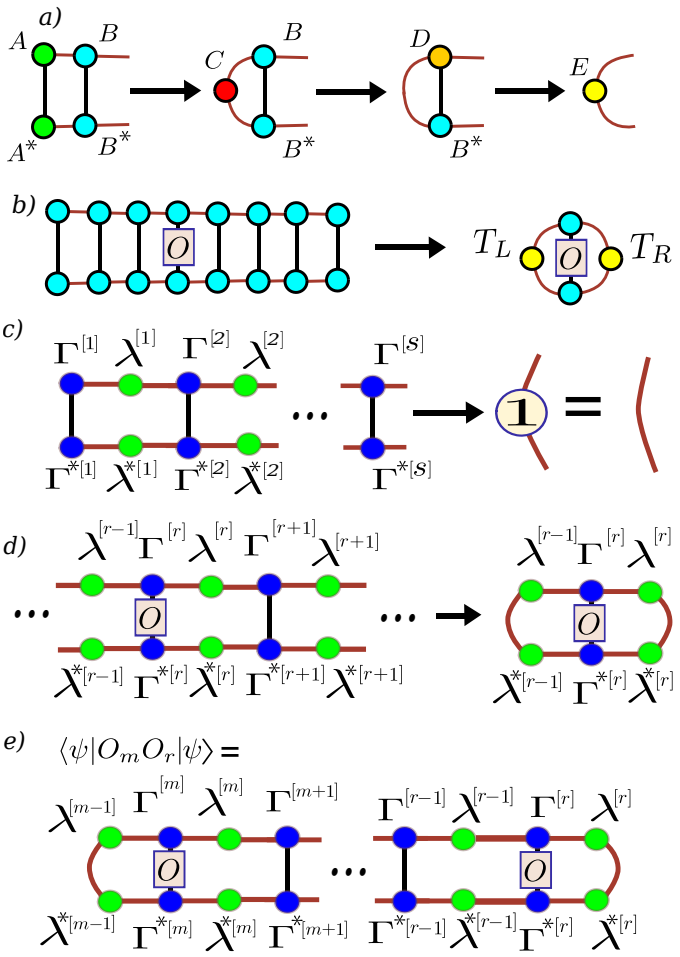

Figure 9.9: *a*) Sequence of basic contractions for a MPS. *b*) Calculation of the expectation value $\langle O \rangle$ for the MPS. The left(right) contractions lead to the appereance of the $T_L(T_R)$ tensors. *c*) The left contraction from site 1 to site s involving $\Gamma^{[1]}, \lambda^{[1]} \cdots \lambda^{[s-1]}\Gamma^{[s]}$ for a MPS in the canonical basis gives the identity tensor. The same result appears in the analogous right contraction. *d*) The expectation value of O takes a simple form in a MPS in canonical form due to the identity tensors appearing in the left/right contractions. *e*) Two sites expectation value $\langle O_m O_r \rangle$ for a MPS in the canonical basis. The contraction of the physical indexes between the sites m and r can not be reduced to identity tensors.

Then, the next relations are fulfilled:

$$[H_e^{[l]}, H_e^{[l']}] = [H_o^{[l]}, H_o^{[l']}] = 0,$$
$$[H_e^{[l]}, H_o^{[l']}] \neq 0, \text{ for some } l, l'. \tag{9.186}$$

Since we consider a family of Hamiltonians that can be written in terms of operators acting at the link l, $H = \sum_l H_{\text{link}}^{[l]}$, the odd and even operators take the form:

$$H_o^{[l]} = H_{\text{link}}^{[l]}, \quad l = 1, 3, 5, ...,$$
$$H_e^{[l]} = H_{\text{link}}^{[l]}, \quad l = 2, 4, 6, ..., \tag{9.187}$$

For instance, for the quantum Ising model in tranverse field (see Eq.(7.9)): $H_{\text{link}}^{[l]} = J(\sigma_l^x \sigma_{l+1}^x + \lambda \sigma_l^z)$.

We introduce the expression (9.185) inside the time evolution operator for small time expressed at (9.184) and we decompose the exponential operator trough a Suzuki-Trotter expansion or decomposition [16]:

$$U_H(\delta\tau) = \exp\left[-\delta\tau H\right] = \exp\left[-\delta\tau \left(\sum_l (H_e^{[l]} + H_o^{[l]})\right)\right] =$$
$$\exp\left[-\frac{\delta\tau}{2}\left(\sum_l (H_o^{[l]})\right)\right] \exp\left[-\delta\tau\left(\sum_l (H_e^{[l]})\right)\right] \exp\left[-\frac{\delta\tau}{2}\left(\sum_l (H_o^{[l]})\right)\right], \tag{9.188}$$

where, specifically we have considered a second order Trotter-Suzuki expansion.

Due to the non-zero commutator appearing at (9.186), this expansion is not exact and it introduces an error in the computation of the ground state. This error can be minimized by considering a higher order in the Suzuki-Trotter expansion.

This last expression can be written as:

$$U_H(\delta\tau) = \prod_{\text{odd}} \widetilde{U}_H^{[l]}(\delta\tau/2) \prod_{\text{even}} \widetilde{U}_H^{[l]}(\delta\tau) \prod_{\text{odd}} \widetilde{U}_H^{[l]}(\delta\tau/2), \tag{9.189}$$

with

$$\widetilde{U}_H^{[l]}(\delta\tau) = e^{-\delta\tau H_{\text{link}}^{[l]}} \tag{9.190}$$

This last operator acts in two sites, l and $l+1$. In the terminology of quantum circuits, it is a *two sites gate*. Then, the imaginary time evolution (9.184) can be viewed as a quantum circuit where the initial state $|\psi\rangle$, which is expressed as a MPS, is transformed by the action of the gate $\widetilde{U}_H^{[l]}$ following the sequence appearing at (9.189). This sequence is repeated $\tau/\delta\tau$ times. The Figure (9.10 a) contains a pictorial representation of this of this process.

Protocol for the computation of the ground state

The basic process in the algorithm for the computation of $|\Omega\rangle$ is the update of the MPS when the gate $\widetilde{U}_H^{[r]}$ is applied:

$$\widetilde{U}_H^{[r]}: \quad \text{MPS} \longrightarrow \text{MPS}'. \tag{9.191}$$

Since $\widetilde{U}_H^{[r]}$ is a two sites operator and we are working in the canonical basis for the MPS, the update of the MPS requires the update of the tensors $\Gamma_{i_r\ \alpha_r}^{[r]\alpha_{r-1}}$, $\Gamma_{i_{r+1}\ \alpha_{r+1}}^{[r+1]\alpha_r}$ and $\lambda_{\alpha_r}^{[r]\alpha_r}$. The rest of the tensors remain invariant.

$$\begin{aligned}\widetilde{U}_H^{[r]}: \quad & \Gamma^{[1]}\lambda^{[1]}\cdots\lambda^{[r-1]}\Gamma^{[r]}\lambda^{[r]}\Gamma^{[r+1]}\lambda^{[r+1]}\cdots\lambda^{[N-1]}\Gamma^{[N]} \longrightarrow \\ & \Gamma^{[1]}\lambda^{[1]}\cdots\lambda^{[r-1]}\widetilde{\Gamma}^{[r]}\tilde{\lambda}^{[r]}\tilde{\Gamma}^{[r+1]}\lambda^{[r+1]}\cdots\lambda^{[N-1]}\Gamma^{[N]},\end{aligned} \tag{9.192}$$

where we have omitted the indices of the tensors of the MPS and the "tilde" symbol indicates the updated tensors.

This update contains a series of operations over the tensor $\Omega_{\nu ij\mu}$, which the tensor of the MPS concerning to the links r and $r+1$:

$$\Omega_{\nu ij\mu} = \sum_{\alpha_1\cdots\alpha_4} \lambda_\nu^{[r-1]\alpha_1}\Gamma_{i\ \alpha_1}^{[r]\alpha_2}\lambda_{\alpha_2}^{[r]\alpha_3}\Gamma_{j\ \alpha_4}^{[r]\alpha_3}\lambda_\mu^{[r+1]\alpha_4}. \tag{9.193}$$

These operation are:

1. Transformation of $\Omega_{\nu ij\mu}$ to $\widetilde{\Omega}_{\nu ij\mu}$ by applying the two sites gate $\widetilde{U}_{H\ ij}^{[r]\ i'j'}$:

$$\widetilde{\Omega}_{\nu ij\mu} = \sum_{\substack{i'j' \\ \alpha_1\cdots\alpha_4}} \Omega_{\nu i'j'\mu}\cdot\widetilde{U}_{H\ ij}^{[r]\ i'j'} = \sum_{\substack{i'j' \\ \alpha_1\cdots\alpha_4}} \lambda_\nu^{[r-1]\alpha_1}\Gamma_{i'\ \alpha_1}^{[r]\alpha_2}\widetilde{U}_{H\ ij}^{[r]\ i'j'}\lambda_{\alpha_2}^{[r]\alpha_3}\Gamma_{j'\ \alpha_4}^{[r]\alpha_3}\lambda_\mu^{[r+1]\alpha_4}. \tag{9.194}$$

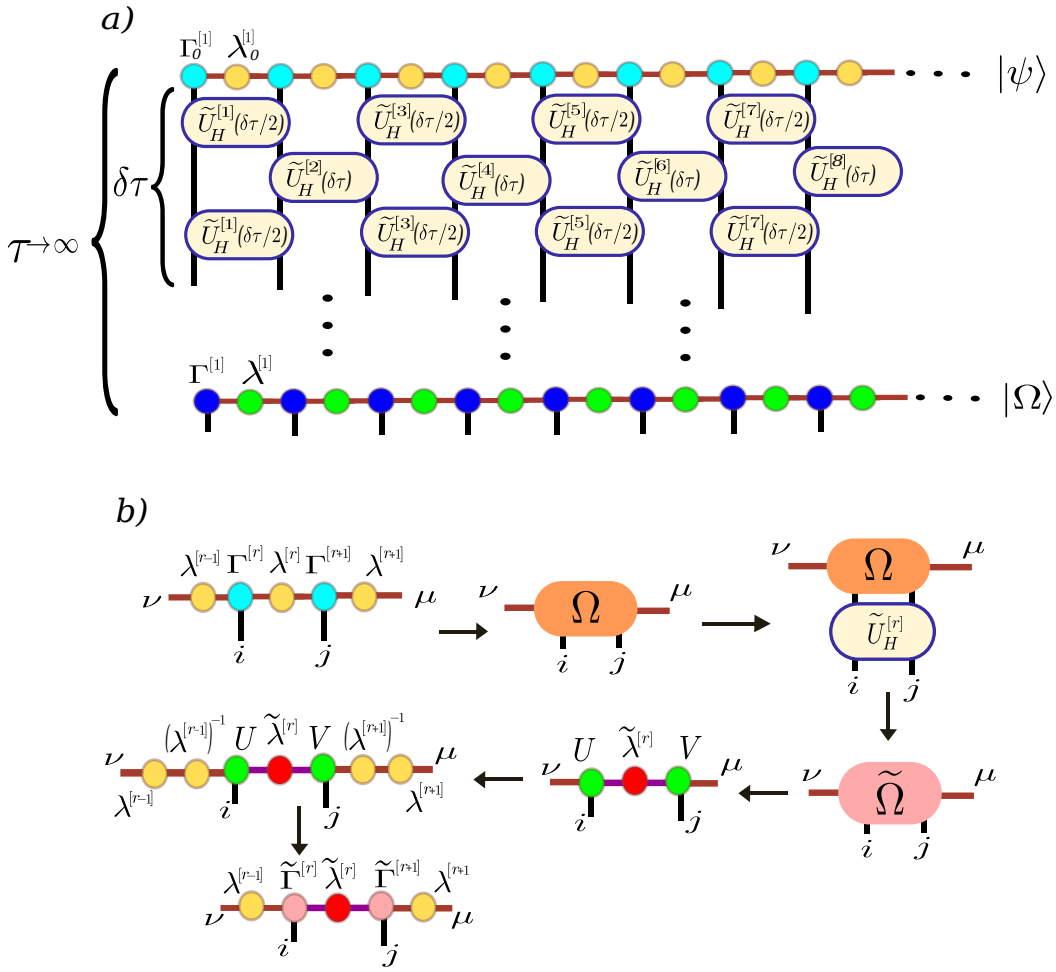

Figure 9.10: *a*) The evolution in imaginary can be viewed as a quantum circuit where an initial quantum state $|\psi\rangle$ is sequentially transformed through a two sites gate $U_H^{[r]}$. The Trotter-Suzuki expansion permits to write the entire evolution as a repetition of a certain sequence acting for $\delta\tau$. *b*) Updating of the MPS when the gate $U_H^{[r]}$ is applied. The SD of the tensor $\Omega(\nu i, j\mu)$ provides the updated matrix $\lambda^{[r]}$. The transformed $\Gamma^{[r]}, \Gamma^{[r+1]}$ are obtained from the Schmidt vectors by the action of $(\lambda^{[r-1]})^{-1}, (\lambda^{[r+1]})^{-1}$ respectively.

2. Schmidt decomposition of the tensor $\widetilde{\Omega}_{\nu i j \mu}$ according to the bipartition $[\nu i][j\mu]$:

$$\widetilde{\Omega}_{\nu i j \mu} = \sum_{\alpha}^{\chi} U^{\alpha}_{\nu\, i} \cdot \widetilde{\lambda}^{[r]\alpha}_{\alpha} \cdot V^{j\ \mu}_{\alpha}, \tag{9.195}$$

where U, V are the Schmidt vectors and $\widetilde{\lambda}^{[r]}$ is the matrix with the Schmidt coefficients, which is the updated $\lambda^{[r]}$. We remark that we only consider a maximum of χ Schmidt coefficients. This truncation is necessary for the practical implementation of the protocol in a classical computer and it introduces an error in the calculation, as we will comment later.

3. Normalization of the state $|\psi\rangle \to \frac{|\psi\rangle}{|||\psi\rangle||}$:

$$\widetilde{\lambda}^{[r]} \to \frac{\widetilde{\lambda}^{[r]}}{\sqrt{\sum_{\alpha}^{\chi} (\widetilde{\lambda}^{[r]\alpha}_{\alpha})^2}}. \tag{9.196}$$

4. Update of the tensor $\Gamma^{[r]}$ and $\Gamma^{[r+1]}$ using the Schmidt vectors appearing in U and V:

$$\widetilde{\Omega} = U\widetilde{\lambda}^{[r]}V = \lambda^{[r-1]}(\lambda^{[r-1]})^{-1}U\widetilde{\lambda}^{[r]}V(\lambda^{[r+1]})^{-1}\lambda^{[r+1]} = \lambda^{[r-1]}\widetilde{\Gamma}^{[r]}\widetilde{\lambda}^{[r]}\widetilde{\Gamma}^{[r+1]}\lambda^{[r+1]}. \tag{9.197}$$

Therefore:

$$\begin{aligned} \widetilde{\Gamma}^{[r]\alpha}_{i\ \beta} &= \sum_{\nu} (\lambda^{[r-1]})^{-1}\big|^{\alpha}_{\nu} \cdot U^{\nu}_{i\ \beta} \\ \widetilde{\Gamma}^{[r+1]\alpha}_{i\ \beta} &= \sum_{\nu} V^{\nu}_{i\ \beta} \cdot (\lambda^{[r+1]})^{-1}\big|^{\alpha}_{\nu}. \end{aligned} \tag{9.198}$$

In Fig. 9.10 b) we can see a pictorial representation of all these different operations for updating the MPS.

Finally let us consider a *one site gate* operator $S^{[r]}$. The action of this type of gates only requires the update of MPS consists on the update of the $\Gamma^{[r]}$ tensor:

$$\widetilde{\Gamma}^{[r]} = S^{[r]} \cdot \Gamma^{[r]} \longrightarrow \widetilde{\Gamma}^{[r]\alpha}_{i\ \beta} = \sum_{j} S^{[r]j}_{i} \Gamma^{[r]\alpha}_{j\ \beta} \tag{9.199}$$

Truncation of the Hilbert subspace

As we saw in the last section, the computation of the ground state requieres the update of the MPS at every loop. This update is given by a SD of the tensor Ω (Fig. 9.10 b)). In this operatio, the rank of the $\widetilde{\lambda}$ matrices can increase:

$$\text{rank}(\widetilde{\lambda}) \leq \max(\nu \cdot i, j \cdot \mu) \tag{9.200}$$

Thus, a practical calculation of the ground state needs an upper value (χ) of the bond dimension of the MPS, such that all the SDÂt's are restricted to this value (see Eq. (9.206)). By doing thies, we are restricting the Hilbert subspace to a sector with can support a maximum of entanglement entropy for a bipartition:

$$S \leq \log(\chi). \tag{9.201}$$

This truncation of the Hilbert subspace introduces an approximation in the computation of the ground state. This approximation is reasonable provided the ground state is a slightly entangled state. As we showed in the last section, this is the case for 1D gapped systems with local interactions, where the Schmidt coefficients decay exponentially [219]:

$$\lambda_l^{[r]} \sim e^{-\mathcal{C}l}, \tag{9.202}$$

where l labels the Schmidt coefficient and $\mathcal{C}$ is a real constant.

In such situation, it is reasonable to consider sufficient large but finite number χ of Schmidt coefficients for encoding all the properties of the ground state. At Fig. 9.11 it is shown the exponential decay (9.202) for a particular realization of the Ising quantum chain in transverse field.

9.7.3 Time evolution in the TEBD formalism

Let us consider the time evolution of a given state $|\psi\rangle$ represented by a MPS:

$$|\psi(t)\rangle = e^{itH}|\psi(0)\rangle. \tag{9.203}$$

Proceeding as in the imaginary time evolution, the time evolution operator can be written as:

$$e^{-itH} = \left(e^{-i\delta tH}\right)^{t/\delta t} \equiv U_H(i\delta t)^{t/\delta t}. \tag{9.204}$$

It takes the same form than the imaginary time evolution operator (9.184), substituting the imaginary time τ per real time it.

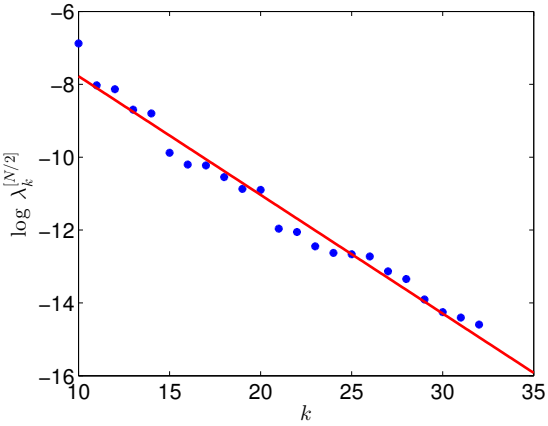

Figure 9.11: Exponential decay of the Schmidt coefficients $\lambda^{[N/2]}$ for the ground state of a quantum Ising: $H = \sum_i (-\sigma_i^x \sigma_{i+1}^x + \sigma_i^z)$, for a chain of total length $N = 100$. The computation of the ground state has been done considering $\chi = 32$.

Thus, the protocol for the real time evolution of the state contains the same structure than the one for the computation of the ground state, by considering that the time evolution is given by an unitary operator and the state is not normalized at every sequence:

1. Update the MPS by applying the gate $\widetilde{U}_{H\ ij}^{[r]\ i'j'}$ (see Eq.(9.193)) :

$$\widetilde{\Omega}_{\nu ij\mu} = \sum_{\substack{i'j' \\ \alpha_1 \cdots \alpha_4}} \Omega_{\nu i'j'\mu} \cdot \widetilde{U}_{H\ ij}^{[r]\ i'j'} = \sum_{\substack{i'j' \\ \alpha_1 \cdots \alpha_4}} \lambda_{\nu}^{[r-1]\alpha_1} \Gamma_{i'\ \alpha_1}^{[r]\alpha_2} \widetilde{U}_{H\ ij}^{[r]\ i'j'} \lambda_{\alpha_2}^{[r]\alpha_3} \Gamma_{j'\ \alpha_4}^{[r]\alpha_3} \lambda_{\mu}^{[r+1]\alpha_4}. \quad (9.205)$$

2. Schmidt decomposition of $\widetilde{\Omega}_{\nu ij\mu}$ according to the bipartition $[\nu i][j\mu]$:

$$\widetilde{\Omega}_{\nu ij\mu} = \sum_{\alpha}^{\chi} U_{\nu\ i}^{\alpha} \cdot \widetilde{\lambda}_{\alpha}^{[r]\alpha} \cdot V_{\alpha}^{j\ \mu}, \quad (9.206)$$

   where U, V contain the Schmidt vectors and $\widetilde{\lambda}^{[r]}$ is the matrix with the Schmidt coefficients and it is the updated $\lambda^{[r]}$. As in the computation of the ground state protocol, we only consider as a maximum χ of the Schmidt coefficients.

3. Update of the tensor $\Gamma^{[r]}$ and $\Gamma^{[r+1]}$ using the tensors U and V:

$$\widetilde{\Omega} = U\widetilde{\lambda}^{[r]}V = \lambda^{[r-1]}(\lambda^{[r-1]})^{-1}U\widetilde{\lambda}^{[r]}V(\lambda^{[r+1]})^{-1}\lambda^{[r+1]} = \lambda^{[r-1]}\widetilde{\Gamma}^{[r]}\widetilde{\lambda}^{[r]}\widetilde{\Gamma}^{[r+1]}\lambda^{[r+1]}. \quad (9.207)$$

   Therefore:

$$\widetilde{\Gamma}_{i\ \beta}^{[r]\alpha} = \sum_{\nu} (\lambda^{[r-1]})^{-1}\big|_{\nu}^{\alpha} \cdot U_{i\ \beta}^{\nu}$$
$$\widetilde{\Gamma}_{i\ \beta}^{[r+1]\alpha} = \sum_{\nu} V_{i\ \beta}^{\nu} \cdot (\lambda^{[r+1]})^{-1}\big|_{\nu}^{\alpha}. \quad (9.208)$$

The truncation to χ Schmidt vectors in the Hilbert subspace (step 2) can introduce an error ε in the norm of the state:

$$\varepsilon(t) = 1 - \sum_{\alpha}^{\chi} (\lambda_{\alpha}^{\alpha}(t))^2. \tag{9.209}$$

Then, the real time evolution considering the truncation of the Hilbert subspace gives accurate results provided that the ε is an small number. This fact depends strongly on the considered system.

In different local perturbation of the ground states in 1D slightly entangled systems, the TEBD method leads to accurate results for real time evolution for medium and long times. As an example, we find the split quench studied in Chapter 7, where the error ε seems to be an small number for medium and long time evolution after the quench (see Fig. 7.10 (inset, lower panel)). We refer the reader to the excellent work carried out by A. Perales and G. Vidal about the topic for different 1D quantum systems. [233]. In contrast, this situation may change drastically for global perturbations of the system, where the bond dimension χ of the MPS can increase a lot even for short times.

Bibliography

[1] S. Stringari and L. Pitaevskii, *Bose-Einstein condensation* (Oxford University Press, 2003).

[2] M. Lewenstein, A. Sanpera, and V. Ahufinger, *Ultracold Atoms in Optical Lattices: Simulating quantum many-body systems* (Oxford University Press, 2012).

[3] I. Bloch, J. Dalibard, and W. Zwerger, Reviews of Modern Physics **80**, 885 (2008).

[4] M. H. Anderson, J. R. Ensher, M. R. Matthews, C. E. Wieman, and E. A. Cornell, Science **269**, 198 (1995).

[5] K. B. Davis *et al.*, Physical Review Letters **75**, 3969 (1995).

[6] C. C. Bradley, C. A. Sackett, and R. G. Hulet, Physical Review Letters **78**, 985 (1997).

[7] A. Eisntein, Sitzungsbericht der Preussischein Akademie der Wissenschaften , 3 (1925).

[8] S. N. Bose, Zeitschrift für Physik **26**, 178 (1924).

[9] D. Jaksch and P. Zoller, Annals of Physics **315**, 52 (2005).

[10] M. Lewenstein *et al.*, Advances in Physics **56**, 243 (2007).

[11] L. Sanchez-Palencia and M. Lewenstein, Nature Physics **6**, 87 (2010).

[12] R. P. Feynman, International journal of theoretical physics **21**, 467 (1982).

[13] I. Buluta and F. Nori, Science **326**, 108 (2009).

[14] M. Georgescu, I. S. Ashhab, and F. Nori, Rev. Mod. Phys. **86**, 153 (2014).

[15] M. A. Nielsen and I. L. Chuang, *Quantum computation and quantum information* (Cambridge university press, 2010).

[16] M. Suzuki, Communications in Mathematical Physics **51**, 183 (1976).

[17] S. Lloyd, Science **273**, 1073 (1996).

[18] A. Y. Kitaev, Russian Mathematical Surveys **52**, 1191 (1997).

[19] P. A. Lee, N. Nagaosa, and X.-G. Wen, Reviews of Modern Physics **78**, 17 (2006).

[20] A. Y. Kitaev, Annals of Physics **303**, 2 (2003).

[21] U.-J. Wiese, Annalen der Physik **525**, 777 (2013).

[22] L. Mazza *et al.*, New Journal of Physics **14**, 015007 (2012).

[23] O. Boada, A. Celi, J. I. Latorre, and M. Lewenstein, Physical Review Letters **108**, 133001 (2012).

[24] H. Büchler, M. Hermele, S. Huber, M. P. Fisher, and P. Zoller, Physical Review Letters **95**, 040402 (2005).

[25] J. I. Cirac, P. Maraner, and J. K. Pachos, Physical Review Letters **105**, 190403 (2010).

[26] E. Zohar and B. Reznik, Physical Review Letters **107**, 275301 (2011).

[27] E. Zohar, J. I. Cirac, and B. Reznik, Physical Review Letters **109**, 125302 (2012).

[28] E. Zohar, J. I. Cirac, and B. Reznik, Physical Review Letters **110**, 055302 (2013).

[29] E. Kapit and E. Mueller, Physical Review A **83**, 033625 (2011).

[30] D. Banerjee *et al.*, Physical Review Letters **109**, 175302 (2012).

[31] E. Zohar, J. I. Cirac, and B. Reznik, Physical Review Letters **110**, 125304 (2013).

[32] E. Zohar, J. I. Cirac, and B. Reznik, Physical Review A **88**, 023617 (2013).

[33] D. Banerjee *et al.*, Physical Review Letters **110**, 125303 (2013).

[34] L. Tagliacozzo, A. Celi, A. Zamora, and M. Lewenstein, Annals of Physics **330**, 160 (2013).

[35] L. Tagliacozzo, A. Celi, P. Orland, M. Mitchell, and M. Lewenstein, Nature communications **4** (2013).

[36] L. Tagliacozzo, A. Celi, and M. Lewenstein, arXiv preprint arXiv:1405.4811 (2014).

[37] E. Rico, T. Pichler, M. Dalmonte, P. Zoller, and S. Montangero, Physical Review Letters **112**, 201601 (2014).

[38] P. Silvi, E. Rico, T. Calarco, and S. Montangero, arXiv preprint arXiv:1404.7439 (2014).

[39] M. Müller, S. Diehl, G. Pupillo, and P. Zoller, Advances In Atomic, Molecular, and Optical Physics **61**, 1 (2012).

[40] M. Rigol, V. Dunjko, and M. Olshanii, Nature **452**, 854 (2008).

[41] T. Kinoshita, T. Wenger, and D. S. Weiss, Nature **440**, 900 (2006).

[42] M. Cheneau *et al.*, Nature **481**, 484 (2012).

[43] M. Gring *et al.*, Science **337**, 1318 (2012).

[44] S. Trotzky *et al.*, Nature Physics **8**, 325 (2012).

[45] T. Langen, R. Geiger, M. Kuhnert, B. Rauer, and J. Schmiedmayer, Nature Physics **9**, 640 (2013).

[46] J. Berges, S. Borsanyi, and C. Wetterich, arXiv preprint hep-ph/0403234 (2004).

[47] V. Rubakov, *Classical theory of gauge fields* (Princeton University Press, 2009).

[48] I. Montvay and G. Münster, *Quantum Fields on a Lattice*Cambridge Monographs on Mathematical Physics (Cambridge University Press, 1997).

[49] P. Ramond and H. Fried, Physics Today **35**, 57 (1982).

[50] E. Noether, Nachrichten von der Gesellschaft der Wissenschaften zu Göttingen, mathematisch-physikalische Klasse **1918**, 235 (1918).

[51] C.-N. Yang and R. L. Mills, Physical review **96**, 191 (1954).

[52] F. J. Dyson, Physical Review **75**, 1736 (1949).

[53] H. J. Rothe*Lattice gauge theories: an introduction* Vol. 74 (World Scientific, 2005).

[54] K. G. Wilson, Physical Review D **10**, 2445 (1974).

[55] J. Kogut and L. Susskind, Physical Review D **11**, 395 (1975).

[56] J. Stark, Nature **92**, 401 (1913).

[57] J. Hubbard, Proceedings of the Royal Society of London. Series A. Mathematical and Physical Sciences **276**, 238 (1963).

[58] D. Jaksch, C. Bruder, J. I. Cirac, C. W. Gardiner, and P. Zoller, Physical Review Letters **81**, 3108 (1998).

[59] M. P. Fisher, P. B. Weichman, G. Grinstein, and D. S. Fisher, Physical Review B **40**, 546 (1989).

[60] M. Greiner, O. Mandel, T. Esslinger, T. W. Hänsch, and I. Bloch, Nature **415**, 39 (2002).

[61] M. Aidelsburger *et al.*, Physical Review Letters **107**, 255301 (2011).

[62] K. Jimenez-Garcia *et al.*, Physical review letters **108**, 225303 (2012).

[63] J. Struck *et al.*, Nature Physics **9**, 738 (2013).

[64] J. Struck *et al.*, Physical review letters **108**, 225304 (2012).

[65] M. Aidelsburger *et al.*, Physical Review Letters **111**, 185301 (2013).

[66] Y.-J. Lin, R. L. Compton, K. Jimenez-Garcia, J. V. Porto, and I. B. Spielman, Nature **462**, 628 (2009).

[67] Y.-J. Lin *et al.*, Physical Review Letters **102**, 130401 (2009).

[68] Y.-J. Lin *et al.*, Nature Physics **7**, 531 (2011).

[69] L. J. LeBlanc *et al.*, Proceedings of the National Academy of Sciences **109**, 10811 (2012).

[70] P. Wang *et al.*, Physical Review Letters **109**, 095301 (2012).

[71] L. W. Cheuk *et al.*, Physical Review Letters **109**, 095302 (2012).

[72] Y.-J. Lin, K. Jimenez-Garcia, and I. Spielman, Nature **471**, 83 (2011).

[73] J.-Y. Zhang *et al.*, Physical review letters **109**, 115301 (2012).

[74] Z. Fu *et al.*, Nature Physics **10**, 110 (2014).

[75] L. Zhang *et al.*, Phys. Rev. A **87**, 011601 (2013).

[76] C. Qu, C. Hamner, M. Gong, C. Zhang, and P. Engels, Physical Review A **88**, 021604 (2013).

[77] L. LeBlanc *et al.*, New Journal of Physics **15**, 073011 (2013).

[78] N. Goldman, G. Juzeliunas, P. Ohberg, and I. B. Spielman, arXiv preprint arXiv:1308.6533 (2013).

[79] D. Jaksch and P. Zoller, New Journal of Physics **5**, 56 (2003).

[80] K. Osterloh, M. Baig, L. Santos, P. Zoller, and M. Lewenstein, Physical Review Letters **95**, 010403 (2005).

[81] N. Goldman *et al.*, Physical Review Letters **103**, 035301 (2009).

[82] N. Goldman, A. Kubasiak, P. Gaspard, and M. Lewenstein, Physical Review A **79**, 023624 (2009).

[83] J. Abo-Shaeer, C. Raman, J. Vogels, and W. Ketterle, Science **292**, 476 (2001).

[84] K. Madison, F. Chevy, W. Wohlleben, and J. Dalibard, Physical Review Letters **84**, 806 (2000).

[85] N. Wilkin, J. Gunn, and R. Smith, Physical Review Letters **80**, 2265 (1998).

[86] N. Wilkin and J. Gunn, Physical Review Letters **84**, 6 (2000).

[87] N. Barberán, M. Lewenstein, K. Osterloh, and D. Dagnino, Physical Review A **73**, 063623 (2006).

[88] J. Dalibard, F. Gerbier, G. Juzeliūnas, and P. Öhberg, Reviews of Modern Physics **83**, 1523 (2011).

[89] R. Dum and M. Olshanii, Physical Review Letters **76**, 1788 (1996).

[90] P. Visser and G. Nienhuis, Physical Review A **57**, 4581 (1998).

[91] J. Ruseckas, G. Juzeliūnas, P. Öhberg, and M. Fleischhauer, Physical Review Letters **95**, 010404 (2005).

[92] G. Juzeliūnas, J. Ruseckas, and J. Dalibard, Physical Review A **81**, 053403 (2010).

[93] A. Jacob, P. Öhberg, G. Juzeliūnas, and L. Santos, Applied Physics B **89**, 439 (2007).

[94] I. Spielman, Physical Review A **79**, 063613 (2009).

[95] K. J. Günter, M. Cheneau, T. Yefsah, S. P. Rath, and J. Dalibard, Physical Review A **79**, 011604 (2009).

[96] A. Celi *et al.*, Phys. Rev. Lett. **112**, 043001 (2014).

[97] P. Hauke *et al.*, Physical Review Letters **109**, 145301 (2012).

[98] A. Eckardt, C. Weiss, and M. Holthaus, Physical Review Letters **95**, 260404 (2005).

[99] H. Lignier *et al.*, Physical Review Letters **99**, 220403 (2007).

[100] D. R. Hofstadter, Physical review B **14**, 2239 (1976).

[101] K. v. Klitzing, G. Dorda, and M. Pepper, Physical Review Letters **45**, 494 (1980).

[102] R. Kubo, Journal of the Physical Society of Japan **12**, 570 (1957).

[103] N. Goldman, *Quantum Transport in Lattices Subjected to External Gauge Fields: The Quantum Hall Effect in Optical Lattices and Quantum Graphs* (VDM Verlag Dr Muller Aktiengesellschaft & Co. KG, 2009).

[104] D. Thouless, M. Kohmoto, M. Nightingale, and M. Den Nijs, Physical Review Letters **49**, 405 (1982).

[105] M. Kohmoto, Annals of Physics **160**, 343 (1985).

[106] R. B. Laughlin, Physical Review B **23**, 5632 (1981).

[107] B. Simon, Physical Review Letters **51**, 2167 (1983).

[108] M. V. Berry, Proceedings of the Royal Society of London. A. Mathematical and Physical Sciences **392**, 45 (1984).

[109] G. Montambaux and M. Kohmoto, Physical Review B **41**, 11417 (1990).

[110] M. Kohmoto, B. I. Halperin, and Y.-S. Wu, Physical Review B **45**, 13488 (1992).

[111] X.-G. Wen, *Quantum field theory of many-body systems: from the origin of sound to an origin of light and electrons* (Oxford University Press Oxford, 2004).

[112] Z. F. Ezawa, *Quantum Hall Effects: Field Theorectical Approach and Related Topics* (World Scientific, 2008).

[113] K. Novoselov *et al.*, Nature Physics **2**, 177 (2006).

[114] T. Fukui, Y. Hatsugai, and H. Suzuki, Journal of the Physical Society of Japan **74**, 1674 (2005).

[115] M. Z. Hasan and C. L. Kane, Reviews of Modern Physics **82**, 3045 (2010).

[116] Y. Hatsugai, Physical Review Letters **71**, 3697 (1993).

[117] F. Gerbier and J. Dalibard, New Journal of Physics **12**, 033007 (2010).

[118] T. D. Stanescu, V. Galitski, and S. D. Sarma, Physical Review A **82**, 013608 (2010).

[119] T.-L. Dao, A. Georges, J. Dalibard, C. Salomon, and I. Carusotto, Physical Review Letters **98**, 240402 (2007).

[120] X.-J. Liu, M. F. Borunda, X. Liu, and J. Sinova, Physical Review Letters **102**, 046402 (2009).

[121] N. Goldman *et al.*, Physical Review Letters **105**, 255302 (2010).

[122] N. Goldman *et al.*, Proceedings of the National Academy of Sciences **110**, 6736 (2013).

[123] R. Jördens, N. Strohmaier, K. Günter, H. Moritz, and T. Esslinger, Nature **455**, 204 (2008).

[124] D. Greif, T. Uehlinger, G. Jotzu, L. Tarruell, and T. Esslinger, Science **340**, 1307 (2013).

[125] R. A. Hart, P. M. Duarte, T.-L. Yang, and R. G. Hulet, Bulletin of the American Physical Society **57** (2012).

[126] R. Jördens *et al.*, Physical Review Letters **104**, 180401 (2010).

[127] J. Simon *et al.*, Nature **472**, 307 (2011).

[128] S. Trotzky, Y.-A. Chen, U. Schnorrberger, P. Cheinet, and I. Bloch, Physical Review Letters **105**, 265303 (2010).

[129] J. Struck *et al.*, Science **333**, 996 (2011).

[130] S. Taie, R. Yamazaki, S. Sugawa, and Y. Takahashi, Nature Physics (2012).

[131] S. Taie *et al.*, Physical Review Letters **105**, 190401 (2010).

[132] B. DeSalvo, M. Yan, P. Mickelson, Y. M. De Escobar, and T. Killian, Physical Review Letters **105**, 030402 (2010).

[133] J. B. Marston and I. Affleck, Physical Review B **39**, 11538 (1989).

[134] C. Wu, Physcs Online Journal **3**, 92 (2010).

[135] D. Wang *et al.*, Phys. Rev. Lett. **112**, 156403 (2014).

[136] A. Gorshkov *et al.*, Nature Physics **6**, 289 (2010).

[137] H.-H. Tu, G.-M. Zhang, and L. Yu, Physical Review B **74**, 174404 (2006).

[138] C. Wu, Modern Physics Letters B **20**, 1707 (2006).

[139] E. Szirmai and M. Lewenstein, Europhysics Letters **93**, 66005 (2011).

[140] M. Hermele, V. Gurarie, and A. M. Rey, Physical Review Letters **103**, 135301 (2009).

[141] M. Hermele and V. Gurarie, Physical Review B **84**, 174441 (2011).

[142] T. C. Lang, Z. Y. Meng, A. Muramatsu, S. Wessel, and F. F. Assaad, Physical Review Letters **111**, 066401 (2013), 1306.3258.

[143] P. Corboz, A. M. Läuchli, K. Penc, M. Troyer, and F. Mila, Physical Review Letters **107**, 215301 (2011).

[144] P. Corboz, M. Lajkó, A. M. Läuchli, K. Penc, and F. Mila, Physical Review X **2**, 041013 (2012).

[145] C. Xu and C. Wu, Physical Review B **77**, 134449 (2008).

[146] H.-H. Hung, Y. Wang, and C. Wu, Physical Review B **84**, 054406 (2011).

[147] Z. Cai, H.-H. Hung, L. Wang, and C. Wu, Physycal Review B **88**, 125108 (2013).

[148] M. Lajkó and K. Penc, Phys. Rev. B **87**, 224428 (2013).

[149] Z. Meng, T. Lang, S. Wessel, F. Assaad, and A. Muramatsu, Nature **464**, 847 (2010).

[150] A. M. Black-Schaffer and S. Doniach, Physical Review B **75**, 134512 (2007).

[151] S. Pathak, V. B. Shenoy, and G. Baskaran, Physical Review B **81**, 085431 (2010).

[152] T. Li, arXiv preprint arXiv:1101.1352 (2011).

[153] Y. Machida, S. Nakatsuji, S. Onoda, T. Tayama, and T. Sakakibara, Nature **463**, 210 (2009).

[154] J. Koch, A. A. Houck, K. Le Hur, and S. Girvin, Physical Review A **82**, 043811 (2010).

[155] P. Corboz, M. Lajkó, K. Penc, F. Mila, and A. M. Läuchli, Physical Review B **87**, 195113 (2013).

[156] E. Fradkin*Field theories of condensed matter systems* Vol. 226 (Addison-Wesley Redwood City, 1991).

[157] K. R. Hazzard, V. Gurarie, M. Hermele, and A. M. Rey, Physical Review A **85**, 041604 (2012).

[158] A. Altland and B. D. Simons, *Condensed matter field theory* (Cambridge University Press, 2010).

[159] G. Baskaran and P. W. Anderson, Physical Review B **37**, 580 (1988).

[160] D. P. Arovas and A. Auerbach, Physical Review B **38**, 316 (1988).

[161] T. Dombre and G. Kotliar, Physical Review B **39**, 855 (1989).

[162] P. Soltan-Panahi *et al.*, Nature Physics **7**, 434 (2011).

[163] W. S. Bakr, J. I. Gillen, A. Peng, S. Fölling, and M. Greiner, Nature **462**, 74 (2009).

[164] B. Zimmermann, T. Mueller, J. Meineke, T. Esslinger, and H. Moritz, New Journal of Physics **13**, 043007 (2011).

[165] D. Greif, L. Tarruell, T. Uehlinger, R. Jördens, and T. Esslinger, Physical Review Letters **106**, 145302 (2011).

[166] S. Elitzur, Physical Review D **12**, 3978 (1975).

[167] X.-G. Wen, F. Wilczek, and A. Zee, Physical Review B **39**, 11413 (1989).

[168] K. Hammerer, A. S. Sørensen, and E. S. Polzik, Reviews of Modern Physics **82**, 1041 (2010).

[169] J. B. Kogut, Reviews of Modern Physics **51**, 659 (1979).

[170] D. Horn, Physics Letters B **100**, 149 (1981).

[171] P. Orland and D. Rohrlich, Nuclear Physics B **338**, 647 (1990).

[172] S. Chandrasekharan and U. Wiese, Nuclear Physics **B**, 455 (1997).

[173] R. Brower, S. Chandrasekharan, and U. Wiese, Physical Review D **60**, 094502 (1999).

[174] F. Gliozzi, S. Lottini, M. Panero, and A. Rago, Nuclear Physics B **719**, 255 (2005).

[175] M. Tinkham, *Group theory and quantum mechanics* (Courier Dover Publications, 2003).

[176] J. Kogut and L. Susskind, Physical Review D **11**, 395 (1975).

[177] S. A. Ocko and B. Yoshida, Physical Review Letters **107**, 250502 (2011).

[178] P. Orland, Nuclear Physics B **372**, 635 (1992).

[179] M. A. Levin and X. Wen, Physical Review B **71**, 045110 (2005).

[180] M. Müller, I. Lesanovsky, H. Weimer, H. P. Büchler, and P. Zoller, Physical Review Letters **102**, 170502 (2009).

[181] H. Weimer, M. Müller, I. Lesanovsky, P. Zoller, and H. P. Büchler, Nature Physics **6**, 382 (2010).

[182] T. Caneva, T. Calarco, and S. Montangero, Physical Review A **84**, 022326 (2011).

[183] P. Doria, T. Calarco, and S. Montangero, Physical Review Letters **106**, 190501 (2011).

[184] F. Verstraete, J. I. Cirac, and M. M. Wolf, Nature Physics **5**, 633 (2009).

[185] S. Diehl *et al.*, Nature Physics **4**, 878 (2008).

[186] B. Kraus *et al.*, Physical Review A **78**, 042307 (2008).

[187] J. von Neumann, Zeitschrift fur Physik **57**, 30 (1929).

[188] S. Trotzky *et al.*, Nature Physics **8**, 325 (2012).

[189] J. Deutsch, Physical Review A **43**, 2046 (1991).

[190] M. Srednicki, Physical Review E **50**, 888 (1994).

[191] M. Rigol, Physical Review Letters **103**, 100403 (2009).

[192] A. Polkovnikov, K. Sengupta, A. Silva, and M. Vengalattore, Reviews of Modern Physics **83**, 863 (2011).

[193] E. Jaynes, Phys. Rev. **106** (1957).

[194] L. D. Landau, L. P. Pitaevskii, and E. M. LifshiÌĂtz, *Statistical physics* (Butterworth-Heinemann, Oxford [etc.], 1980).

[195] R. K. Pathria, *Statistical mechanics* (Butterworth-Heinemann, Oxford; Boston, 1996).

[196] R. Balian, *From Microphysics to Macrophysics: Methods and Applications of Statistical Physics* (Springer, 2007).

[197] M. Rigol, V. Dunjko, V. Yurovsky, and M. Olshanii, Physical Review Letters **98**, 050405 (2007).

[198] M. Kollar, F. A. Wolf, and M. Eckstein, Physical Review B **84**, 054304 (2011).

[199] H. Li and F. D. M. Haldane, Physical Review Letters **101**, 010504 (2008).

[200] M.-C. Chung, A. Iucci, and M. Cazalilla, New Journal of Physics **14**, 075013 (2012).

[201] S. Popescu, A. J. Short, and A. Winter, Nature Physics **2**, 754 (2006).

[202] C. Gogolin, M. P. Müller, and J. Eisert, Physical Review Letters **106**, 040401 (2011).

[203] A. Riera, C. Gogolin, and J. Eisert, Physical Review Letters **108**, 080402 (2012).

[204] L. Masanes, A. J. Roncaglia, and A. Acín, Physical Review E **87**, 032137 (2013).

[205] M. Fagotti and F. H. L. Essler, Physical Review B **87**, 245107 (2013).

[206] P. Calabrese and J. Cardy, Journal of Statistical Mechanics: Theory and Experiment **2005**, P04010 (2005).

[207] P. Hauke and L. Tagliacozzo, Physical Review Letters **111**, 207202 (2013).

[208] J. Schachenmayer, B. P. Lanyon, C. F. Roos, and A. J. Daley, Physical Review X **3**, 031015 (2013).

[209] M. B. Hastings, Journal of Statistical Mechanics: Theory and Experiment **2007**, P08024 (2007).

[210] L. Masanes, Physical Review A **80**, 052104 (2009).

[211] G. Vidal, J. I. Latorre, E. Rico, and A. Kitaev, Physical Review Letters **90**, 227902 (2003).

[212] P. Calabrese and J. Cardy, Physical Review Letters **96**, 136801 (2006).

[213] J.-M. Stéphan and J. Dubail, Journal of Statistical Mechanics: Theory and Experiment **2011**, P08019 (2011).

[214] V. Eisler and I. Peschel, Journal of Statistical Mechanics: Theory and Experiment **2007**, P06005 (2007).

[215] E. Lieb, T. Schultz, and D. Mattis, Reviews of Modern Physics **36**, 856 (1964).

[216] M. Fagotti and P. Calabrese, Physical Review A **78**, 010306 (2008).

[217] G. Torlai, L. Tagliacozzo, and G. De Chiara, arXiv:1311.5509 cond-mat, physics:quant-ph (2013).

[218] G. Vidal, Physical Review Letters **91**, 147902 (2003).

[219] G. Vidal, Physical Review Letters **93**, 040502 (2004).

[220] I. Peschel and T. Truong, Zeitschrift für Physik B Condensed Matter **69**, 385 (1987).

[221] A. M. Lauchli, Report No. 1303.0741, 2013 (unpublished).

[222] G. De Chiara, L. Lepori, M. Lewenstein, and A. Sanpera, Physical Review Letters **109** (2012).

[223] V. Alba, M. Haque, and A. M. Läuchli, Physical Review Letters **108**, 227201 (2012).

[224] C. Holzhey, F. Larsen, and F. Wilczek, Nuclear Physics B **424**, 443 (1994).

[225] C. Callan and F. Wilczek, Physics Letters B **333**, 55 (1994).

[226] M. Srednicki, Physical Review Letters **71**, 666 (1993).

[227] P. Calabrese and J. Cardy, Journal of Statistical Mechanics: Theory and Experiment **2004**, P06002 (2004).

[228] P. Calabrese and J. Cardy, Journal of Statistical Mechanics: Theory and Experiment **2007**, P10004 (2007).

[229] F. Iglói, Z. Szatmári, and Y.-C. Lin, Physical Review B **85**, 094417 (2012).

[230] V. Eisler, D. Karevski, T. Platini, and I. Peschel, Journal of Statistical Mechanics: Theory and Experiment **2008**, P01023 (2008).

[231] A. M. Läuchli and C. Kollath, Journal of Statistical Mechanics: Theory and Experiment **2008**, P05018 (2008).

[232] M. Collura and P. Calabrese, Journal of Physics A: Mathematical and Theoretical **46**, 175001 (2013).

[233] Á. Perales and G. Vidal, Physical Review A **78**, 042337 (2008).

[234] U. Divakaran, F. Iglói, and H. Rieger, Journal of Statistical Mechanics: Theory and Experiment **2011**, P10027 (2011).

[235] T. W. Burkhardt and I. Guim, Journal of Physics A: Mathematical and General **18**, L33 (1985).

[236] V. Eisler and I. Peschel, Journal of Statistical Mechanics: Theory and Experiment **2014**, P04005 (2014).

[237] R. C. Richardson, Reviews of Modern Physics **69**, 683 (1997).

[238] A. M. Polyakov, Physics Letters B **59**, 82 (1975).

[239] Y. Aharonov and D. Bohm, Physical Review **115**, 485 (1959).

[240] C. A. Mead and D. G. Truhlar, The Journal of Chemical Physics **70**, 2284 (1979).

[241] S. Pancharatnam, Generalized theory of interference, and its applications, in *Proceedings of the Indian Academy of Sciences-Section A* Vol. 44, pp. 247–262, Springer, 1956.

[242] J. Hannay, Journal of Physics A: Mathematical and General **18**, 221 (1985).

[243] L. Tagliacozzo and G. Vidal, Physical Review B **83**, 115127 (2011).

[244] D. Horn, M. Weinstein, and S. Yankielowicz, Physical Review D **19**, 3715 (1979).

[245] E. H. Lieb and D. W. Robinson, Communications in Mathematical Physics **28**, 251 (1972).

[246] S. Sachdev and A. Young, Physical Review Letters **78**, 2220 (1997).

[247] P. Calabrese and J. Cardy, Physical Review Letters **96**, 136801 (2006).

[248] D. Rossini, S. Suzuki, G. Mussardo, G. E. Santoro, and A. Silva, Physical Review B **82**, 144302 (2010).

[249] J.-M. Stéphan and J. Dubail, Journal of Statistical Mechanics: Theory and Experiment **2011**, P08019 (2011).

[250] H. Rieger and F. Iglói, Physical Review B **84**, 165117 (2011).

[251] T. W. Burkhardt and I. Guim, Journal of Physics A: Mathematical and General **18**, L33 (1985).

[252] S. Sachdev, *Quantum phase transitions* (Wiley Online Library, 2007).

[253] S. Suzuki, J.-i. Inoue, and B. K. Chakrabarti, *Quantum Ising phases and transitions in transverse Ising models* (Springer, 2013).

[254] P. Jordan and E. P. Wigner, über das paulische äquivalenzverbot, in *The Collected Works of Eugene Paul Wigner*, pp. 109–129, Springer, 1993.

[255] M. Fannes, B. Nachtergaele, and R. F. Werner, Communications in Mathematical Physics **144**, 443 (1992).

[256] A. Klümper, A. Schadschneider, and J. Zittartz, Europhysics Letters **24**, 293 (1993).

[257] S. R. White *et al.*, Physical Review Letters **69**, 2863 (1992).

[258] S. R. White, Physical Review B **48**, 10345 (1993).

[259] G. Vidal, arXiv preprint cond-mat/0605597 (2006).

[260] M. B. Hastings, Journal of Statistical Mechanics: Theory and Experiment **2007**, P08024 (2007).

[261] M. M. Wolf, F. Verstraete, M. B. Hastings, and J. I. Cirac, Physical Review Letters **100**, 070502 (2008).

[262] D. Poulin, A. Qarry, R. Somma, and F. Verstraete, Physical Review Letters **106**, 170501 (2011).

[263] F. Verstraete and J. I. Cirac, arXiv preprint cond-mat/0407066 (2004).

[264] R. Orus and G. Vidal, Physical Review B **78**, 155117 (2008).